Virtual-MIMO Systems with Compress-and-Forward Cooperation

Jing Jiang

A thesis submitted for the degree of Doctor of Philosophy.
The University of Edinburgh.
August 2011

Abstract

Multiple-input multiple-output (MIMO) systems have recently emerged as one of the most significant wireless techniques, as they can greatly improve the channel capacity and link reliability of wireless communications. These benefits have encouraged extensive research on a virtual MIMO system where the transmitter has multiple antennas and each of the receivers has a single antenna. Single-antenna receivers can work together to form a virtual antenna array and reap some performance benefits of MIMO systems. The idea of receiver-side local cooperation is attractive for wireless networks since a wireless receiver may not have multiple antennas due to size and cost limitations.

In this thesis we investigate a virtual-MIMO wireless system using the receiver-side cooperation with the compress-and-forward (CF) protocol. Firstly, to perform CF at the relay, we propose to use standard source coding techniques, based on the analysis of its expected rate bound and the tightness of the bound. We state upper bounds on the system error probabilities over block fading channels. With sufficient source coding rates, the cooperation of the receivers enables the virtual-MIMO system to achieve almost ideal MIMO performance. A comparison of ideal and non-ideal conference links within the receiver group is also investigated. Considering the short-range communication and using a channel-aware adaptive CF scheme, the impact of the non-ideal cooperation link is too slight to impair the system performance significantly.

It is also evident that the practicality of CF cooperation will be greatly enhanced if a efficient source coding technique can be used at the relay. It is even more desirable that CF cooperation should not be unduly sensitive to carrier frequency offsets (CFOs). Thus this thesis then presents a practical study of these two issues. Codebook designs of the Voronoi VQ and the tree-structure vector quantization (TSVQ) to enable CF cooperation at the relay are firstly described. A comparison in terms of the codebook design complexity and encoding complexity is presented. It is shown that the TSVQ is much simpler to design and operate, and can achieve a favourable performance-complexity tradeoff. We then demonstrate that CFO can lead to significant performance degradation for the virtual MIMO system. To overcome it, it is proposed to maintain clock synchronization and jointly estimate the CFO between the relay and the destination. This approach is shown to provide a significant performance improvement.

Finally, we extend the study to the minimum mean square error (MMSE) detection, as it has a lower complexity compared to maximum likelihood (ML) detection. A closed-form upper bound for the system error probability is derived, based on which we prove that the smallest singular value of the cooperative channel matrix determines the system error performance. Accordingly, an adaptive modulation and cooperation scheme is proposed, which uses the smallest singular value as the threshold strategy. Depending on the instantaneous channel conditions, the system could therefore adapt to choose a suitable modulation type for transmission and an appropriate quantization rate to perform CF cooperation. The adaptive modulation and cooperation scheme not only enables the system to achieve comparable performance to the case with fixed quantization rates, but also eliminates unnecessary complexity for quantization operations and conference link communication.

Declaration of originality

I hereby declare that the research recorded in this thesis and the thesis itself was composed and originated entirely by myself in the School of Engineering at The University of Edinburgh.

Jing JIANG

Acknowledgements

First of all, I would like to express my heartily profound thanks, gratitude and appreciation to my supervisor Dr. John S. Thompson for his insightful technical and editorial advice, suggestions, and discussions, leading me to the strict scientific research world. His immense knowledge, great help and encouragement have been so invaluable during my Ph.D. study, and were a real support to complete this thesis. I have learned a lot from him, and working together with him is the most precious experience of my life.

I would also like to sincerely thank my associate supervisors Prof. Norbert Goertz and Prof. Peter M. Grant for their constructive comments and helpful discussions. Prof. Norbert Goertz has given me loads of practical advice on source coding techniques during the early stages of this work. Prof. Peter M. Grant has been so patient and helpful in sharing with me his extensive technical knowledge, and providing me a broad view of recent communication systems.

Many thanks will be given to the current and former colleagues who create a harmonious academic environment at the Institute for Digital Communications (IDCOM), and also to all my friends, especially Dr. Chaoran Du and Miss Ying Hou, for their continuous help and friendships.

A very special thank to my husband Dr. Hongjian Sun for his continuous love, daily encouragement, and unconditional support since 2001. I am so lucky that we completed our B.Eng., M.Sc., and Ph.D. studies together during last ten years. I also want to express my deepest gratitude to my parents Guifu Jiang and Jianxin Sun for their boundless care and strong backing in last 27 years. Thank you so much for your never-ending encouragement and comfort, especially during those tough times.

Finally, I would like to acknowledge the support from the UK/China Scholarships for Excellence programme in funding my Ph.D. study.

Contents

List of figures

List of tables

Acronyms and abbreviations

ACK	Acknowledgement
AF	Amplify-and-forward
AMI	Average mutual information
AWGN	Additive white Gaussian noise
BC	Broadcast Channel
BICM	Bit-interleaved coded modulation
BER	Bit error ratio
BLER	Block error ratio
BIOS	Binary-input output-symmetric
CF	Compress-and-forward
CSI	Channel state information
CDF	Cumulative distribution function
CFO	Carrier frequency offset
DF	Decode-and-forward
DPC	Dirty paper coding
EM	Expectation-maximization
EP	Equal power
FEC	Forward error correction
GA	Gaussian approximation
HSPA	High speed packet access
ISI	Inter-symbol interference
LLR	Log-likelihood ratio
LBG	Linde-Buzo-Gray algorithm
LTE	Long term evolution
MAC	Multiple access channel
MIMO	Multiple-input multiple-output
MISO	Multiple-input single-output
MMSE	Minimum mean square error

MRC	Maximum ratio combining
MSE	Mean square error
ML	Maximum-likelihood
NACK	Negative acknowledgement
PSK	Phase-shift keying
PEP	Pairwise error probability
PDF	Probability density function
QAM	Quadrature modulation
RX	Receiver
SNR	Signal-to-noise ratio
SINR	Signal to interference and nosie ratio
SISO	Single-input single-output
SIC	Successive interference cancelation
STBC	Space-time block coding
TSVQ	Tree-structure vector quantization
TX	Transmitter
TDD	Time-division duplex
UB	Upper bound
UBs	Upper bounds
VBLAST	Vertical-Bell laboratories layered space-time
VQ	Vector quantization
WF	Water-filling
WZ	Wyner-Ziv
ZF	Zero-forcing

Nomenclature

A_d	Sum of bit errors (i.e. information error weight) for error events of distance d
$\boldsymbol{B}$	Diagonal matrix which removes the bias from the MMSE estimates
c^{λ}	λth coded bit ($\forall \lambda = 1, ..., mN_t$)
C	Capacity of the conference link (which is also used to denote the quantization rate, i.e. $C = R_c$, in Chapter 4 and Chapter 5)
C'	Data rate of the non-ideal link
C_i	Quantization rate for the ith stage of TSVQ
C_{ave}	Average quantization rate
C_{BC}	Capacity of the multiple-antenna broadcast channel
C_{CF}	Throughput of the virtual-MIMO system with CF cooperation
C_{MIMO}	Capacity of the MIMO system
$C_{\text{MIMO-EP}}$	Capacity of the MIMO system when equal power is located
$C_{\text{MIMO-WF}}$	Capacity of the MIMO system when water-filling algorithm is used
$C_{\text{MIMO-E}}$	Ergodic capacity of the MIMO system
$C_{\text{MIMO-q}}$	$q\%$ outage capacity of the MIMO system
C_{MAC}	Capacity of the multiple access channel
d_{free}	Minimum free Hamming distance
$\boldsymbol{e}$	Residual inter-symbol interference after the MMSE filter
E_s	Total transmitted power
$E_{s,i}$	Transmitted power during time slot i ($i \in [1, 2]$)
E_{si}	Transmitted power at the ith transmitter ($i \in [1, 2]$)
E_b	Transmitted power per bit
E_r	Relay transmitted power per bit
f_{dn}	Frequency offsets at the destination
f_{rn}	Frequency offsets at the relay
f_{rdn}	Frequency difference between the relay and the destination
$\tilde{f}$	Estimated frequency offsets
h_{in}	ith channel coefficient in the nth block fading channel matrix

h_{rdn}	Channel coefficient from the relay to the destination
h_{sr}	Channel coefficient from the source to the relay
h_{sd}	Channel coefficient from the source to the destination
$\boldsymbol{H}_n$	nth block fading channel matrix
$\widetilde{\boldsymbol{H}}_n$	Scaled channel matrix corresponding to the nth channel matrix
I_c	Channel information rate
k	k-th transmit stream
K_{rd}	Rician factor on the link between the relay and the destination
l	l-th symbol period
L	Number of symbol periods for one channel block
m	Number of bits mapped onto one complex data symbol
M	Number of points in a modulation constellation
n	n-th fading block
N	Number of fading channel blocks
N_0	Noise spectral density
N_t	Number of transmitter antennas
N_r	Number of receiver antennas
P_b	Bit error ratio
P_{block}	Block error ratio
P_{out}	Outage probability
P_{th}	Threshold of the CDF of the smallest singular value
Q_t	Number of training vectors
$\boldsymbol{Q}_s$	Covariance matrix of the transmitted signals
R_{AF}	Achievable rate of the classical relay system using AF protocol
R_b	Rate of a linear binary convolutional encoder
R_c	Quantization rate (i.e. source coding rate)
R_{CF}	Achievable rate of the classical relay system using CF protocol
R_{DF}	Achievable rate of the classical relay system using DF protocol
R_E	End-to-end spectral efficiency
R_{Shannon}	Achievable system sum rate when source coding techniques are used
R_{MIMO}	Sum rate of the MIMO system
R_{MISO}	Sum rate of the MISO system

R_{NC}	Sum rate of direct transmission
R_{WZ}	Achievable system sum rate when WZ coding is used
$\hat{s}$	Saddle point
SNR	Signal-to-noise ratio
S_q	Encoding region associated with the code vector v_q
t	A random variable which selects either Gray-labelling mapping or its complement with probability 1/2
t_s	Symbol interval
T_c	Computational time for one distortion value
T_d	Computational time for comparing two distortion values
T_{LBG}	Computational time for the LBG algorithm
$T_{\text{d,Voronoi}}$	Computational time for the Voronoi VQ
$T_{\text{d,TSVQ}}$	Computational time for TSVQ
$T_{\text{s,Voronoi}}$	Search time for one symbol of the Voronoi VQ
$T_{\text{s,TSVQ}}$	Search time for one symbol of TSVQ
$\boldsymbol{u}_{nl}$	$N_t \times 1$ channel estimation vector
$\boldsymbol{v}$	Colored Gaussian noise vector after the MMSE filter
v_q	Codevector in the encoding region
$\boldsymbol{w}_{nl}$	lth noise vector on the nth channel
w_{cnl}	Compression noise corresponding to y_{rnl}
$w_{i'nl}$	lth noise sample on the nth channel received from the i'th receiver
$\tilde{w}_{1nl}$	Scaled noise sample corresponding to w_{1nl}
$\boldsymbol{W}$	MMSE filtering operation
$\boldsymbol{x}_{nl}$	lth M-ary symbol vector transmitted on the nth channel
$x_{i'nl}$	lth M-ary symbol transmitted on the nth channel from the i'th antenna
$x_{i'}$	Transmitted symbol from the i'th antenna
$\tilde{x}_k$	Nearest neighbour to x_k
$\boldsymbol{y}_{nl}$	Signal vector at the destination after receiving y'_{rnl}
$\tilde{\boldsymbol{y}}_{nl}$	Scaled Signal vector at the destination corresponding to $\boldsymbol{y}_{nl}$
y_{dnl}	Received signal at the destination for the lth symbol period on the nth channel
y_j	Received signal at the jth antenna
y_{rnl}	Received at the relay for the lth symbol period on the nth channel

y'_{rnl}	Compressed version of the received signal y_{rnl} after quantization at the relay
y^c_{rnl}	Noise-free constellation of the received signals
y^u_{dnl}	Received signal at the destination corresponding to $\boldsymbol{u}_{nl}$
y^u_{rnl}	Received signal at the relay corresponding to $\boldsymbol{u}_{nl}$
$\boldsymbol{z}$	Signal vector after the MMSE filter
$\mathcal{H}$	Fading envelope with $\mathcal{H} = (\boldsymbol{H}_1, ..., \boldsymbol{H}_N)$
σ^2_{cn}	Compression noise variance corresponding to the nth channel block
σ^2_{wzn}	Compression noise variance when WZ coding is used for the nth channel block
θ_n	Phase difference between the relay and the destination
δ	Gain factor of the AF protocol
λ	Bit position in the transmitted symbol's binary label
λ_{th}	Threshold of $\lambda_{\text{min}}(\widetilde{\boldsymbol{H}})$
λ_{16QAM}	Threshold of $\lambda_{\text{min}}(\boldsymbol{H})$ for 16QAM modulation
λ_{64QAM}	Threshold of $\lambda_{\text{min}}(\boldsymbol{H})$ for 64QAM modulation
Δ_n	Synchronization error between the relay and destination
μ	Mapping labelling rule
ϵ	Outage probability of the non-ideal cooperation link
ξ	Threshold of the BER upper bound
ρ_k	Instantaneous received SINR for the kth stream
$\rho_{\min}$	Smallest SINR, $\rho_{\min} = \min\{\rho_k\}(k \in [1, N_t])$
η_n	Degradation factor corresponding to the nth channel block
$\mathcal{X}$	Constellation of a modulation
$\mathcal{X}^{\lambda}_b$	Subset of the hypersymbol constellation where the λth bit is equal to b
$\mathcal{X}^{\lambda,k}_b$	Subset within the kth transmit constellation where the λth bit is equal to b
$\boldsymbol{\Psi}$	Covariance matrix
$\arg[\cdot]$	Angle operation
$\mathcal{CN}(\cdot,\cdot)$	Circularly symmetric complex Gaussian distribution
$\exp(\cdot)$	Exponential function
$\mathrm{E}[\cdot]$	Expected value operator
$\mathrm{H}(\cdot)$	Entropy operation
int.^{-1}	Deinterleaver
$I(\cdot)$	Mutual information

$K_{\mathcal{L}}(\cdot)$	Cumulant generating function of $\mathcal{L}(\cdot)$
$\mathcal{L}(\cdot)$	Log-likelihood ratio
$p(\cdot)$	Probability density function
$P_d(\cdot)$	Pairwise error probability
$\Pr(x)$	Probability of event x occurring
$Q(\cdot)$	Q-function
$Q_1(\cdot,\cdot)$	First-order Marcum Q function
$\mathrm{Re}\{\cdot\}$	Real part operation
$\lambda_{\min}(\cdot)$	Smallest singular value
$\lambda_{\max}(\cdot)$	Largest singular value
$\widetilde{\{\cdot\}}$	Scale operation
$\lvert\cdot\rvert$	Magnitude of a scaler
$\lVert\cdot\rVert$	Magnitude of a vector
$\{\cdot\}^*$	Complex conjugate operation
$\{\cdot\}^T$	Matrix transpose operation
$\{\cdot\}^\dagger$	Matrix conjugate transpose operation
$\#\mathcal{X}$	Cardinality of $\mathcal{X}$

Chapter 1
Introduction

This thesis is devoted to virtual-MIMO systems taking advantage of compress-and-forward cooperation. In this introductory chapter, Section 1.1 introduces the origin and motivation of this work. Then the objectives and main contributions of this thesis are summarized in Section 1.2. Finally, Section 1.3 presents an overview of the organisation of the remaining chapters.

1.1 Introduction and Motivation

Wireless communications is the fastest-growing segment in the communications industry and has captured the attention and imagination of the public [2]. Cellular systems have experienced exponential growth over the last decades and this growth continues worldwide. In addition, wireless local area networks currently replace wired networks in many homes, businesses and public areas. Moreover, many new applications exploit wireless communications, such as intelligent transport systems, smart homes and smart grid, and self-organising networks. Wireless communications has rapidly and successfully become an essential part of everyday life, and has influenced many aspects of the world.

Multiple-input multiple-output (MIMO) systems, where both the transmitter and receiver use multiple antennas, were introduced toward the end of the 20th century, and have recently emerged as one of the most significant wireless techniques. The use of multiple antennas can provide diversity gain to combat channel fading caused by multi-path effects, as several replicas of the signal are transmitted over independently fading channels [3]. With high probability, at least one or more of these channels will not be in a deep fade at any given instant. The error performance at the receiver can be significantly improved. Moreover, MIMO systems can offer a spatial multiplexing gain, which results in a linear (in the number of transmit-receive antenna pairs) increase in the capacity without extra power or bandwidth consumption. These advantages are largely responsible for the success of MIMO techniques which have been adopted into various current wireless communications standards.

However, performance improvements using MIMO technology come at the cost of requiring the antennas on a MIMO device to have sufficient spacing for uncorrelated fading [4]. If the antenna spacing reduces, i.e. independent fading cannot be obtained for each pair of antennas, the efficiency will be degraded, resulting in lower MIMO capacity. Moreover, implementing MIMO technology usually requires higher hardware processing and energy consumption costs, which is a critical constraint for a typical wireless product. Some handsets and nodes in a wireless sensor network may not be able to support multiple transmit antennas.

These benefits and limitations of MIMO systems have encouraged extensive research on a virtual MIMO system where the transmitter has multiple antennas and each of the receivers has a single antenna [5], as shown in Figure 1.1. In a broadcast channel scenario, i.e coordination is allowed among the transmit antennas but not among the receive nodes [6,7], the sum capacity of such a system can be achieved through perfect channel state information (CSI) at the transmitter for the wireless link to each receiver. However, because of the limitation on the feedback channel, it is not always possible to obtain perfect CSI or even partial CSI at the transmitter in realistic wireless systems. When the transmitter does not have perfect CSI, which is a common scenario in practical situations, single-antenna receivers can work together to form a virtual antenna array and reap some performance benefits of MIMO systems [8]. The idea of receiver-side local cooperation is attractive for wireless networks since it can overcome the problem we mentioned above that a wireless receiver may not have multiple antennas due to size, cost or hardware limitations.

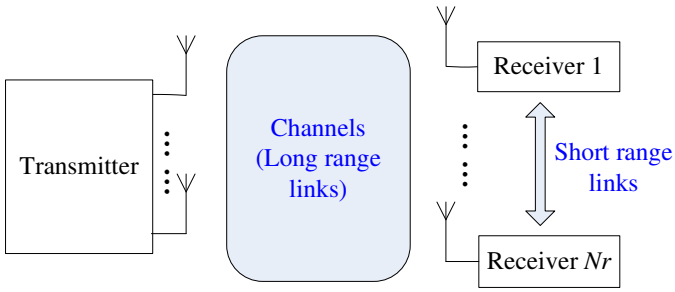

Figure 1.1: *Schematic representation of a virtual-MIMO wireless system with one multiple-antenna transmitter and N_r single-antenna receivers.*

For example, suppose a customer carries some mobile terminals that include a single-antenna 3GPP enabled user device and one or more simple relay devices. Since the distance between the devices is general much shorter than that from the base station, the devices could cooperate

through their short-range Wi-Fi, Bluetooth, or Ultra-Wideband communications links. With such cooperation, the customer could expect traditional MIMO benefits as if the single-antenna user device had multiple antennas. Note that receiver-side communication used for cooperation is realized via an orthogonal channel and allows much higher transmission rate and frequency reuse compared to the long-distance transmitter-to-receiver communication.

Motivated by the above practical scenario, we consider a cooperative virtual-MIMO system in this thesis, with one remote multi-antenna transmitter sending information to several closely spaced single-antenna receivers. As for the cooperation protocol, since the relays get closer to the destination in our scenario, Chapter 2 will show that, compared to amplify-and-forward (AF) and decode-and-forward (DF), the compress-and-forward (CF) protocol provides superior performance [9] [10] and therefore serves as the best candidate for this system. Thus, virtual-MIMO systems taking advantage of CF cooperation is the subject of this thesis.

1.2 Objectives and Contributions

1.2.1 Objectives

The objective of the work presented in this thesis is to study the performance of CF cooperation in virtual-MIMO systems. It aims to determine a practical source coding technique to perform CF at the relay, and seek sufficient source coding rates which could enable the virtual-MIMO system to achieve almost ideal MIMO performance. Codebook design algorithms and the associated complexity should be taken into account. The next part of the work is to investigate the performance degradation of the virtual MIMO system caused by different oscillator frequencies at the source, relay and destination, and how to overcome it. Finally, this work also aims to design a practical adaptive modulation and cooperation scheme, so that the system could adapt its modulation type to the prevailing channel conditions and choose the minimum possible quantization rate.

1.2.2 Key Contributions

The main contributions of this thesis are summarized as follows:

- A cooperative virtual-MIMO system using two transmit antennas that implements bit-interleaved coded modulation (BICM) transmission and CF cooperation among two re-

ceiving nodes is presented. To perform CF cooperation, we propose that rather than the Wyner-Ziv coding (which takes advantage of the dependence between the signals at the relay and the destination), a standard source coding technique should be used for practical considerations at the relay. The nature of the system with a multi-antenna transmitter will reduce the benefit from the Wyner-Ziv coding, based on the analysis of its expected rate bound and the tightness of the bound. The system throughput expression and upper bounds on the system error probabilities over block fading channels are derived. With sufficient source coding rates, the cooperation of the receivers enables the virtual-MIMO system to achieve almost ideal MIMO performance. This material has been submitted to the IET Communications for publication [11].

- To perform source coding, we consider two codebook design algorithms, Voronoi VQ and tree-structure vector quantization (TSVQ). Their codebook design complexities and encoding complexities are investigated. Results show that the TSVQ approach we designed is much simpler for encoding and more computationally efficient than the complicated Voronoi VQ. The material has been published in the IEEE GLOBECOM 2010 Workshop on Heterogeneous, Multi-hop, Wireless and Mobile Networks [12].

- Effects of carrier frequency offsets (CFOs) are investigated. It is demonstrated that CFO could lead to drastic performance degradation for the 2×2 virtual MIMO system. A scheme which maintains clock synchronization and jointly estimates CFO between the relay and the destination, is proposed to overcome the limitations of separate CFO estimation at the relay and destination. Results show that the proposed scheme provides a significant performance improvement. This material together with the codebook design issues have been submitted to the IEEE Transactions on Vehicular Technology for publication [13].

- The expression to upper bound the system bit error ratio (BER) is obtained in closed form, when minimum mean square error (MMSE) detection is used at the destination. It is shown that the smallest singular value of the cooperative channel matrix dominates the system BER. Accordingly, an adaptive modulation and cooperation scheme is proposed, adopting the smallest singular value as the threshold strategy. The system could therefore adapt its modulation type to the prevailing channel conditions and choose the minimum possible quantization rate. It is shown that the proposed scheme eliminates unnecessary complexity, and enables the system to achieve comparable performance to the case with

fixed quantization rates. The results was published in part at the 2nd UK-India-IDRC International Workshop on Cognitive Wireless Systems [14]. A detailed presentation will appear in the IEEE Transactions on Vehicular Technology [15].

1.3 Organisation of the Thesis

The remainder of the thesis is organized as follows:

Chapter 2

This chapter presents the general principles and background knowledge related to the topic of this thesis. It starts with an introduction to the MIMO system model, followed by a brief review of the benefits from using multiple antennas and a study of MIMO channel capacities. Then a cooperative communication system is introduced as a practical alternative to the MIMO system. A review of several cooperation protocols and schemes is provided. This is then followed by a brief study of virtual-MIMO system where virtual antenna arrays are created at both ends of the communication.

Chapter 3

This chapter first specifies the system model of the practical virtual-MIMO system that implements BICM transmission and CF cooperation. A comparison of the standard source coding and Wyner-Ziv coding technique is investigated. Then the system throughput expression and upper bounds on the system error probabilities over block fading channels are derived. Finally, a comparison of ideal and non-ideal conference links within the receiver group is analysed.

Chapter 4

This chapter presents a practical analysis of codebook design and frequency offset estimation in the virtual-MIMO system. Firstly, codebook designs of the Voronoi VQ and the TSVQ to enable CF cooperation at the relay are described, followed by a comparison in terms of the codebook design complexity and encoding complexity. Next, the effects of CFO in the system are illustrated. A clock synchronization and joint CFO estimation scheme is then proposed to overcome these effects.

Chapter 5

This chapter extends the study of the system to the MMSE detection, as it has low complexity and allows good performance when combined with BICM techniques. A closed-form upper

bound for the system BER is then derived, based on which the smallest singular value of the cooperative channel matrix is proved to determine the system error performance. Accordingly, an adaptive modulation and cooperation scheme is proposed, following which the performance of the adaptive scheme is studied.

Chapter 6

This chapter concludes the whole thesis and states several possible directions for future research.

Chapter 2
Background

In this chapter, we provide a basic background for the thesis. We will start our introduction from some fundamental principles of multiple-input multiple-output (MIMO) systems. The MIMO system model will firstly be described, followed by an introduction to the benefits from using multiple antennas at the transmitter and receiver. A study of MIMO channel capacities when the channel is known or unknown to the transmitter will be illustrated. This study will also be carried out for both deterministic and random channels. We shall then introduce a co-operative communication system as a practical alternative to the MIMO system. A review of the work done by the research community in the emerging field of cooperative communications will be provided, including several cooperation protocols and schemes. We shall compare these protocols in terms of their achievable rates. This will then be followed by a brief study of virtual-MIMO system where virtual antenna arrays are created at both ends of the communication. The content of this chapter thus includes three main parts, MIMO wireless systems, cooperative communications, and virtual-MIMO systems. This chapter will provide the reader with a basic background of the current state of the art and will be frequently referred to in the rest of the thesis.

2.1 MIMO Wireless Systems

Communication in wireless networks is impaired by channel fading and interference. With the increasing use of wireless local area networks and next generation mobile systems, the requirements for data rate and quality of service have never been so high. These requirements call for new techniques to enhance the communication performance. The use of multiple antennas at the transmitter and receiver in wireless systems, known as the multiple-input multiple-output (MIMO) technique (see Figure 2.1), has been shown to provide significant improvements in terms of both higher channel capacity and better link reliability. In this section, we will firstly introduce fading channels and then investigate the MIMO system model. This will be followed

by a discussion of the benefits of MIMO technology and a study of MIMO channel capacity results.

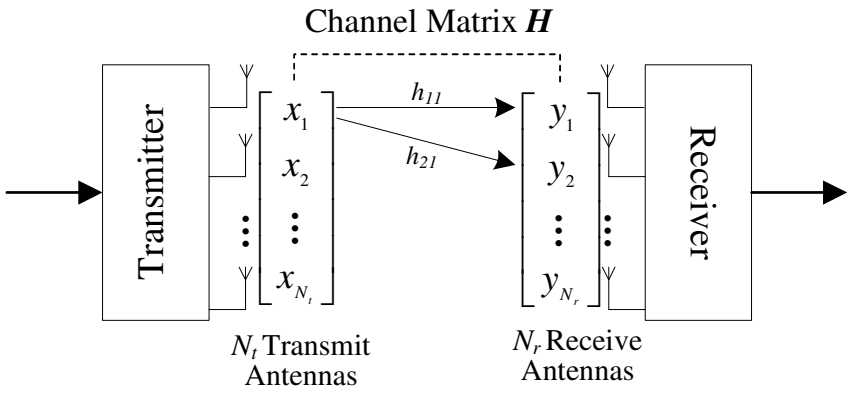

Figure 2.1: *Schematic representation of a MIMO wireless system with N_t transmit and N_r receive antennas. The scalar x_i ($i \in N_t$) refers to the transmitted signal, y_j ($j \in N_r$) refers to the received signal, and h_{ji} denotes the channel coefficient.*

2.1.1 Wireless Fading Channels

Compared with wired communications, wireless transmission is impaired by the fading phenomenon. The transmitted signal power decays with increasing distance and varies randomly due to large objects (such as buildings and hills) in the environment. These two effects, normally referred to as path loss and shadowing, form a large-scale fading. In addition, the signal amplitudes and phases also suffer from small-scale fading which is caused by the constructive and destructive interference of the multiple signal paths between the transmitter and receiver. Large-scale fading is more relevant to issues such as cell-site planning. Small-scale fading is more related to reliable and efficient communication systems design [16]. Thus, in this thesis, we only consider the effect of small-scale fading.

Small-scale fading is normally frequency dependent. An important characteristic for small-scale fading is the channel coherence bandwidth B_c. If B_c is larger than the bandwidth of the transmitted signal, the channel fading is referred to as frequency-flat. All frequency components of the signal experience the same magnitude of fading. On the other hand, if B_c is smaller than the bandwidth of the signal, the signal is said to undergo frequency-selective fading. Different frequency components of the signal therefore experience decorrelated fading [17]. By using some signal processing techniques, such as Orthogonal Frequency Division Multiplexing

(OFDM) [18], a frequency-selective fading channel can be converted to a frequency-flat fading channel. Therefore, we focus on frequency-flat fading channels in this thesis.

2.1.2 MIMO System Model

We focus on a point-to-point communication model, where the transmitter is equipped with N_t antennas and the receiver has N_r antennas, as shown in Figure 2.1. We restrict our discussion to the case where the channel is frequency-flat fading (narrowband assumption). A common channel model in MIMO wireless communications is the block Rayleigh fading model, where the channel matrix entries are constant during each block, but independently Rayleigh distributed on different blocks.

The input-output relation of the $N_t \times N_r$ MIMO channel (as shown in Figure 2.1) is given by,

$$\boldsymbol{y} = \boldsymbol{H}\boldsymbol{x} + \boldsymbol{w}, \tag{2.1}$$

where $\boldsymbol{y} = [y_1 \ y_2 \ ... \ y_{N_r}]^T$ is the $N_r \times 1$ receive signal vector. $\boldsymbol{x} = [x_1 \ x_2 \ ... \ x_{N_t}]^T$ is the $N_t \times 1$ transmit signal vector, where x_i is the ith component, transmitted from antenna i. The channel matrix $\boldsymbol{H}$ is a $N_r \times N_t$ complex matrix,

$$\boldsymbol{H} = \begin{bmatrix} h_{11} & h_{12} & \cdots & h_{1N_t} \\ h_{21} & h_{22} & \cdots & h_{2N_t} \\ \vdots & \vdots & \ddots & \vdots \\ h_{N_r1} & h_{N_r2} & \cdots & h_{N_rN_t} \end{bmatrix}, \tag{2.2}$$

where the component h_{ji} is the fading coefficient from the ith transmit antenna to the jth receive antenna. The elements of $\boldsymbol{H}$ can be deterministic or random. If the channel elements are random, normalization will be applied, so that $\mathrm{E}[|h_{ji}|^2] = 1$, where $|\cdot|$ denotes magnitude and $\mathrm{E}[\cdot]$ denotes the expected value function.

We assume that the channel state information (CSI) is known at the receiver. The channel matrix at the receiver can be obtained by sending a training sequence. If the transmitter is required to know this channel, typically we need to communicate this training information to the transmitter via a feedback channel. For example, when the channels are reciprocal, such as in time-division duplex (TDD) systems, the outgoing and incoming channels are symmetric. In this case, training-based schemes can be used to allow the transmitter to estimate the CSI [19].

When the CSI is known at the transmitter, an optimal energy allocation algorithm will be used to assign various levels of transmitted power to the transmitting antennas. However, it should be noted that the feedback requirements are not only affected by the channel fading states, but also grow with the number of transmit and receive antennas [20]. Because of the limitation on the feedback channel, it is not always possible to obtain CSI at the transmitter in realistic wireless systems. If the channel knowledge is unknown at the transmitter, we assume that the signals transmitted from each antenna have equal powers of E_s/N_t, where E_s is the total transmitted power.

The noise at the receiver is another $N_r \times 1$ vector, denoted by $\boldsymbol{w}$, and $\boldsymbol{w} = [w_1\ w_2\ ...\ w_{N_r}]^T$. The noise components w_j are assumed to be zero mean circularly symmetrical complex Gaussian variables: $w_j \sim \mathcal{CN}(0, N_0)$. If we assume that the total received power per antenna equals the total transmitted power (which implies we ignore signal attenuation, antenna gains, and etc.), the SNR at each receive antenna can be written as SNR $= E_s/N_0$.

2.1.3 Benefits of MIMO Technology

Compared to traditional single-input single-output (SISO) systems, MIMO systems can offer array gain, diversity gain, and multiplexing gain [3]. We briefly review each of these benefits in the following considering a MIMO wireless system with N_t transmit and N_r receive antennas, as shown in Figure 2.1.

2.1.3.1 Array Gain

Array gain is the average increase in received signal-to-noise ratio (SNR), which is achieved due to the coherent combining effect of multiple antennas at the receiver or transmitter or both. If the channel is known to the multiple-antenna transmitter, the transmitter will weight the transmission depending on the channel coefficients, leading to coherent combining at the receiver through the action of the channel. The array gain in this case is called transmitter array gain. Alternately, if CSI is unknown at the transmitter but known at the multiple-antenna receiver, the receiver can suitably weight the incoming signals so that they coherently add up at the output (combining), thereby enhancing the signal, which is called receiver array gain [21]. Extracting transmitter/receiver array gain requires channel coefficients known at the transmitter/receiver, and depends on the number of transmit/receive antennas.

2.1.3.2 Diversity Gain

Diversity is a powerful technique to combat channel fading caused by multi-path effects. Without adequate diversity, the transmit power will have to be higher or the communication range smaller to protect the information signal against channel fading. The basic idea behind diversity is that if several replicas of the signal are transmitted over independently fading channels, then with high probability at least one or more of these channels will not be in a deep fade at any given instant [22]. If the number of diversity branches increases, this probability will increase.

In wireless communications systems, there are three types of diversity: time diversity, frequency diversity, and spatial diversity. Time/frequency diversity is effective when the channel fading is time/frequency selective, and can be exploited by spreading the information over a time/frequency span that is larger than the coherence time/bandwidth of the channel. Compared to time/frequency diversity, spatial diversity is particularly attractive since the diversity gain can be achieved without additional expenditure of time or frequency resources.

Under the subheading of spatial diversity, we can also categorize it into transmit diversity and receive diversity, based on whether diversity is applied on the transmitter or the receiver side. Maximum ratio combining (MRC) is a frequently used scheme in receivers to obtain receive diversity gain. As to transmit diversity, generally it requires complete channel information at the transmitter. But with the advent of space-time coding schemes (as shown in Figure 2.2), such as the Alamouti scheme, implementing transmit diversity without knowledge of the channel becomes possible. We briefly review the Alamouti scheme [23] (considering a $N_t = N_r = 2$ antennas case) in the following, as it exploits both transmit and receive diversity for MIMO systems, and will be referred to in the rest of the thesis.

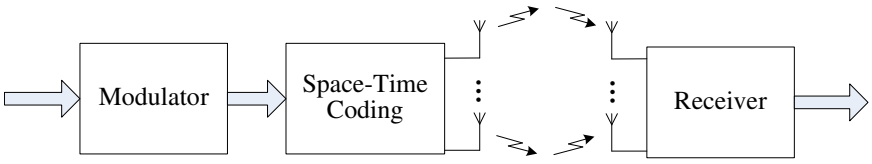

Figure 2.2: *Schematic representation of space-time coding*

Alamouti Space-Time Code

The scheme outlined by Alamouti is shown in Figure 2.3. The information bits are first mapped onto complex data symbols via a M-ary modulation scheme. The encoder then takes two

modulated symbols x_1 and x_2 in one encoding operation and has the coding matrix,

$$S = \begin{bmatrix} x_1 & -x_2^* \\ x_2 & x_1^* \end{bmatrix}. \tag{2.3}$$

The first column of (2.3) represents the first transmission period: the first antenna transmits

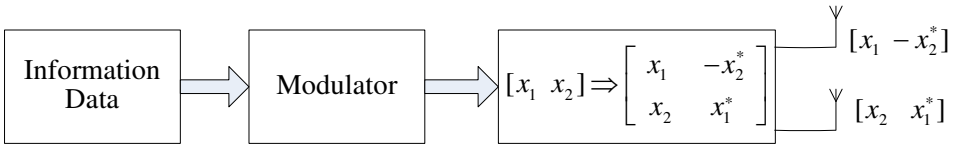

Figure 2.3: *A block diagram of the Alamouti space-time encoder with $N_t = 2$.*

x_1 and the second antenna transmits x_2. During the second transmission period, $-x_2^*$ and x_1^* are transmitted at the two antennas, where $\{\cdot\}^*$ denotes the complex conjugate operation. The transmissions in the Alamouti scheme are orthogonal, i.e. the inner product of the two sequences $[x_1 \ -x_2^*]$ and $[x_2 \ x_1^*]$ is zero. That is, the receiver antenna observes two completely orthogonal streams, which implies a transmit diversity of two. The received signals are given by,

$$\begin{aligned} y_{11} &= h_{11}x_1 + h_{12}x_2 + w_{11} \\ y_{12} &= -h_{11}x_2^* + h_{12}x_1^* + w_{12} \\ y_{21} &= h_{21}x_1 + h_{22}x_2 + w_{21} \\ y_{22} &= -h_{21}x_2^* + h_{22}x_1^* + w_{22}. \end{aligned} \tag{2.4}$$

The scalars y_{jl} and w_{jl} refers to the received signal and the noise sample, respectively, at the jth antenna for the lth transmission period. The combiner in [23] builds the following two signals:

$$\begin{aligned} \hat{x}_1 &= (h_{11}^* y_{11} + h_{12} y_{12}^* + h_{21}^* y_{21} + h_{22} y_{22}^*)/(|h_{11}|^2 + |h_{12}|^2 + |h_{21}|^2 + |h_{22}|^2) \\ &= x_1 + \frac{h_{11}^* w_{11} + h_{12} w_{12}^* + h_{21}^* w_{21} + h_{22} w_{22}^*}{|h_{11}|^2 + |h_{12}|^2 + |h_{21}|^2 + |h_{22}|^2}, \\ \hat{x}_2 &= (h_{12}^* y_{11} - h_{11} y_{12}^* + h_{22}^* y_{21} - h_{21} y_{22}^*)/(|h_{11}|^2 + |h_{12}|^2 + |h_{21}|^2 + |h_{22}|^2) \\ &= x_2 + \frac{h_{12}^* w_{11} - h_{11} w_{12}^* + h_{22}^* w_{21} - h_{21} w_{22}^*}{|h_{11}|^2 + |h_{12}|^2 + |h_{21}|^2 + |h_{22}|^2}. \end{aligned} \tag{2.5}$$

These combined signals are then sent to the maximum likelihood (ML) decoder. We use

$d^2(a,b)$ to denote the squared Euclidean distance between signals a and b, which is calculated by $d^2(a,b) = (a-b)(a^*-b^*)$. To detect x_1, the decision criteria is given by [23]: choose x_i if, and only if,

$$d^2(\hat{x}_1, x_i) \leq d^2(\hat{x}_1, x_k) \ \ \forall i \neq k, \tag{2.6}$$

where phase-shift keying (PSK) modulation (with equal energy constellation) is considered. Similarly, to detect x_2, the decision criteria is: choose x_i if, and only if,

$$d^2(\hat{x}_2, x_i) \leq d^2(\hat{x}_2, x_k) \ \ \forall i \neq k. \tag{2.7}$$

Comparing the detection results with the original signals, we obtain the system bit error ratio. It is obvious that, the ML decodings for x_1 and x_2 is very simple and only based on linear processing. ML decoders provide a full receive diversity gain of N_r at the receiver. The Alamouti scheme therefore exploits the full diversity gain $N_t \times N_r$ given by the transmit and receive antennas. When we consider a system with 2 transmit antennas and N_r receive antennas, a full diversity gain of $2N_r$ will be obtained, without channel knowledge at the transmitter [23]. Further, for any number of transmit antennas, a theory of generalized orthogonal designs to construct space-time block codes was introduced in [24].

In the high SNR regime, a scheme is said to have a diversity gain d, if the average error probability decays according to $1/\text{SNR}^d$ [25]. Consider a MIMO system with N_t transmit antennas and N_r receive antennas, and assume all the channels fade independently. Then a full diversity order of $N_t N_r$ can be achieved, which means at high SNR the average error probability decays like $\text{SNR}^{-N_t N_r}$, in contrast to SNR^{-1} (i.e. diversity order 1) for SISO systems.

Figure 2.4 shows the bit error ratio (BER) performance of a SISO system, a 2×1 MISO (multiple-input single-output) system, and a 2×2 MIMO system. For multiple antenna cases, we use the Alamouti scheme to realize spatial diversity gain. In the Alamouti scheme, the signal power from each transmit antenna is half of the total transmit power needed for the single-antenna system without diversity. We can see that the BER performance of the MISO system decays much faster ($\text{BER} \propto \text{SNR}^{-2}$) than that of the SISO system. With the number of antennas increasing at the receiver, receive diversity is obtained in the MIMO system.

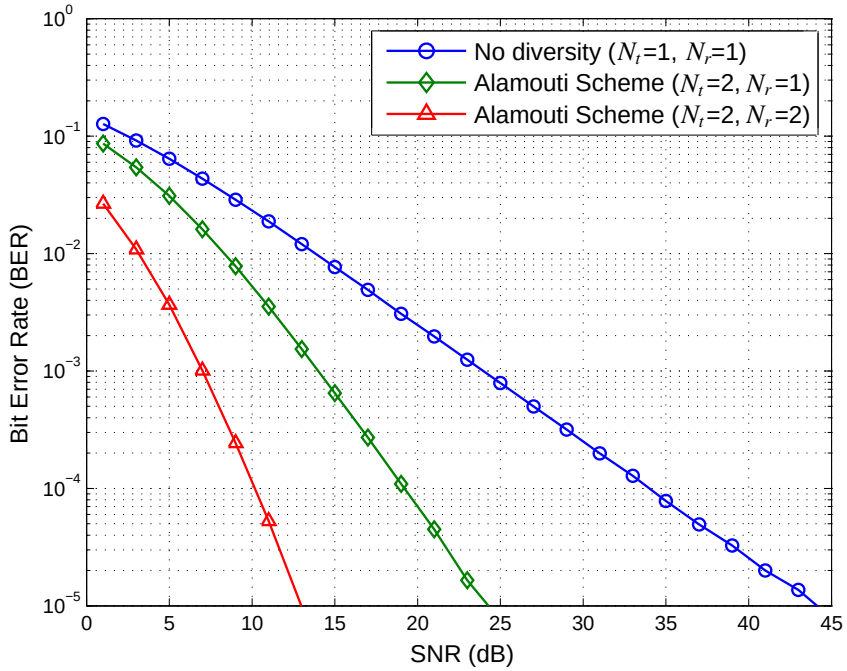

Figure 2.4: *BER performance for Alamouti scheme in MIMO systems, compared to the SISO case. (Flat Rayleigh fading channel and BPSK modulation are used.)*

2.1.3.3 Multiplexing Gain

While spatial diversity gain can be achieved when multiple antennas are present at either the transmitter or the receiver, spatial multiplexing gain requires multiple antennas at both the transmit and receive sides [26]. Spatial multiplexing offers a linear (in the number of transmit-receive antenna pairs) or min (N_t,N_r) increase in the capacity for the same bandwidth and with no additional power expenditure [21]. Consider the case of $N_t = N_r = 2$, the maximal spatial multiplexing gain which can be achieved is 2, without extra power or bandwidth consumption.

The basic principle of spatial multiplexing (without considering precoding techniques) is illustrated in Figure 2.5. The signal bit stream to be transmitted is demultiplexed into N separate parallel sub-streams which are then modulated and transmitted simultaneously from the antennas using the same frequency band. Each receive antenna observes a superposition of the transmitted signal sub-streams, and the detector recovers these individual sub-streams and combines them to recover the original bit stream. Various detector architectures, such as ML, zero-forcing (ZF), minimum mean-squared error (MMSE), and successive interference cancellation (SIC) detector etc., can be used to realize the spatial multiplexing gain. Since the transmitted

sub-streams are completely different from each other, i.e. they carry totally different data, the system has no transmit diversity. But it provides receive diversity, as the receiver has knowledge of the channel. Therefore, spatial multiplexing increases the capacity proportionally with the number of transmit-receive antenna pairs.

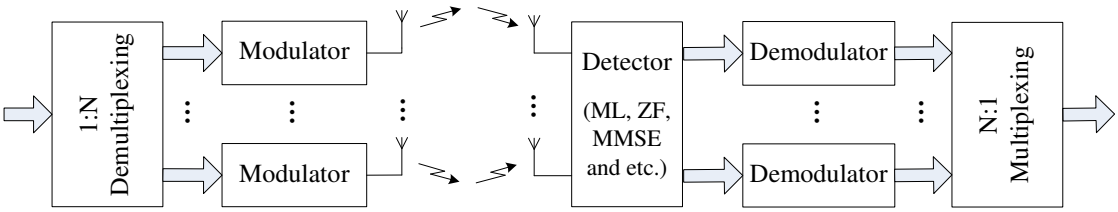

Figure 2.5: *Schematic representation of spatial multiplexing.*

2.1.4 MIMO System Capacity

In Section 2.1.3, we stated that MIMO systems can offer substantial improvements over conventional SISO systems through analysing the principles of diversity and spatial multiplexing. In this section, we explore the absolute gains offered by MIMO in terms of system capacity.

The system capacity is defined as the maximum possible transmission rate for which arbitrarily small error probability can be achieved [16]. Let $\boldsymbol{Q}_s$ denote the covariance matrix of $\boldsymbol{x}$, then the capacity of the system described by (2.1) is given by [27],

$$C_{\mathrm{MIMO}} = \max_{\mathrm{tr}(\boldsymbol{Q}_s)\leq \mathrm{E_s}} \log_2 \left[\det\left(\boldsymbol{I}_{N_r} + \boldsymbol{H}\frac{\boldsymbol{Q}_s}{N_0}\boldsymbol{H}^{\dagger}\right)\right] \quad \mathrm{bits/s/Hz}, \tag{2.8}$$

where $\boldsymbol{H}^{\dagger}$ denotes the conjugate transpose of $\boldsymbol{H}$. Here, $\mathrm{tr}(\boldsymbol{Q}_s) \leq E_s$ holds to provide a global power constraint. With either knowledge of $\boldsymbol{H}$ known or unknown at the transmitter, the optimal form of $\boldsymbol{Q}_s$ will be discussed later.

The capacity C_{MIMO} in (2.8) is also called error-free spectral efficiency or data rate per unit bandwidth that can be sustained reliably over the MIMO link. Thus, if our bandwidth is W_b Hz, the maximum achievable data rate over this bandwidth using MIMO techniques is $W_b C_{\mathrm{MIMO}}$ bit/s [28].

We now give a brief overview of exact capacity results, categorized into the two main scenarios,

where the channel is either known or unknown at the transmitter. Under the subheading of the channel unknown to the transmitter, we can also break down the analysis into deterministic channels and random channels.

2.1.4.1 Channel Unknown to the Transmitter

If the channel is unknown to the transmitter, the entries of the vector $\boldsymbol{x}$ should be statistically independent. Telatar [27] showed that,

$$\boldsymbol{Q}_s = \frac{E_s}{N_0 N_t} \boldsymbol{I}_{N_t}, \tag{2.9}$$

is optimal for i.i.d. Rayleigh fading. That is, the power is equally divided among the transmit antennas. The capacity in such a case is given by (from (2.8)),

$$C_{\mathrm{MIMO-EP}} = \log_2 \left[\det \left(\boldsymbol{I}_{N_r} + \frac{E_s}{N_0 N_t} \boldsymbol{H}\boldsymbol{H}^{\dagger} \right) \right] \quad \mathrm{bits/s/Hz}, \tag{2.10}$$

The capacity can be rewritten in terms of the eigenvalues:

$$C_{\mathrm{MIMO-EP}} = \sum_{i=1}^{\min(N_t,\, N_r)} \log_2 \left(1 + \frac{E_s}{N_0 N_t} \lambda_i \right) \quad \mathrm{bits/s/Hz}, \tag{2.11}$$

where λ_1, λ_2, ..., $\lambda_{\min(N_t,N_r)}$ are the nonzero eigenvalues of $\boldsymbol{W}_H$, and

$$\boldsymbol{W}_H = \boldsymbol{H}\boldsymbol{H}^{\dagger}. \tag{2.12}$$

This formulation can be easily obtained from the direct use of eigenvalue properties [29]. Equation (2.11) expresses the capacity of the MIMO channel as a sum of the capacities of $\min(N_t, N_r)$ equivalent parallel SISO channels, each having a power gain of λ_i (i = 1, 2, ... , $\min(N_t, N_r)$) and transmit power E_s/N_t.

2.1.4.2 Channel Known to the Transmitter

It is possible by some means, to learn the CSI at the transmitter. Typically, CSI needs to be obtained at the receiver and sent back to the transmitter over a reliable feedback channel. When CSI is known at the transmitter (and at the receiver), then $\boldsymbol{H}$ is known in (2.8) and we optimize

the capacity over choices of $\boldsymbol{Q}_s$ subject to the power constraint $\text{tr}(\boldsymbol{Q}_s) \leq E_s$. The optimal $\text{tr}(\boldsymbol{Q}_s)$ in such an event is well known [27, 30] and is called a water-filling (WF) solution, by assigning various levels of transmitted power to various transmitting antennas. This power is assigned on the basis that the higher the channel gain, the more power it allocated and vice versa. This is an optimal energy allocation algorithm.

The resulting capacity is given by,

$$C_{\text{MIMO}-\text{WF}} = \sum_{i=1}^{\min(N_t,\, N_r)} \log_2 (\beta\lambda_i)^+ \quad \text{bits/s/Hz}, \tag{2.13}$$

where is β chosen to satisfy

$$\frac{E_s}{N_0} = \sum_{i=1}^{\min(N_t,\, N_r)} (\beta - \lambda_i)^+, \tag{2.14}$$

and "+" denotes taking only those terms which are positive. The scalar β is a complicated nonlinear function of λ_1, λ_2, ..., $\lambda_{\min(N_t,N_r)}$. $C_{\text{MIMO}-\text{WF}}$ can be simulated using (2.13) and (2.14) for any given $\boldsymbol{W}_H$, so that the optimal capacity can be computed numerically [29].

2.1.4.3 Deterministic Channels

If we assume the CSI is unknown to the transmitter but known to the receiver, we can also break the capacity analysis down into two cases: deterministic channels and random channels. We begin with fundamental results of deterministic channels which compare SISO, MISO, SIMO (single-input multiple-output), and MIMO capacities.

SISO Channel Capacity

The formula of Shannon capacity for a deterministic memoryless 1×1 SISO system is given by,

$$C_{\text{SISO}} = \log_2 \left(1 + \frac{E_s}{N_0}|h|^2\right) \quad \text{bits/s/Hz}, \tag{2.15}$$

where h is the complex coefficient of a fixed wireless channel or that of a particular realization of a random channel [16].

SIMO Channel Capacity

Deploying N_r antennas at the receiver, we have a SIMO system. In this case the channel matrix in (2.10) is a column matrix, i.e. $\boldsymbol{H} = [h_1 \ h_2 ... h_{N_r}]^T$, where h_i is the channel coefficient for the ith receive antenna. Now $\boldsymbol{H}\boldsymbol{H}^\dagger = \sum_{i=1}^{N_r} |h_i|^2$ and $N_t = 1$. From (2.10), we obtain,

$$C_{\mathrm{SIMO}} = \log_2 \left(1 + \frac{E_s}{N_0} \sum_{i=1}^{N_r} |h_i|^2 \right) \quad \mathrm{bits/s/Hz}, \tag{2.16}$$

It is obvious that, increasing the value of N_r only results in a logarithmic increase in average capacity.

MISO Channel Capacity

When we consider transmit diversity, we have a MISO system with N_t transmit antennas. Here we use h_i to denote the channel coefficient from the ith transmit antenna. Since $N_t > N_r$, the channel matrix is represented by the row matrix $\boldsymbol{H} = [h_1 \ h_2 ... h_{N_t}]$. As $\boldsymbol{H}\boldsymbol{H}^\dagger = \sum_{i=1}^{N_t} |h_i|^2$, from (2.10), we obtain the channel capacity [21],

$$C_{\mathrm{MISO}} = \log_2 \left(1 + \frac{E_s}{N_0 N_t} \sum_{i=1}^{N_t} |h_i|^2 \right) \quad \mathrm{bits/s/Hz}. \tag{2.17}$$

The normalization, i.e. $E_s/(N_0 N_t)$ shows the absence of array gain in this case (compared to the SIMO case where the channel energy can be combined coherently). Again, note that the capacity increases logarithmic with N_t.

MIMO Channel Capacity

Now, we consider the use of diversity at both transmitter and receiver, which gives rise to the MIMO system. The capacity is given by $C_{\mathrm{MIMO-EP}}$ in (2.10) and in (2.11). The subscript in (2.10) and (2.11) means that both results are based on N_t equal power (EP) uncorrelated sources. It has been established that [27], the capacity of the MIMO channels grows linearly with $\min(N_t, \ N_r)$, rather than logarithmic increase with N_t as in (2.17). Recall from section 2.1.3.3, the spatial multiplexing gain measures the rate at which the capacity increases. The maximal spatial multiplexing gain which can be achieved by a MIMO system is therefore $\min(N_t, \ N_r)$.

2.1.4.4 Random Channels

We have until now discussed MIMO capacity when the channel is deterministic. We now consider the case when $\boldsymbol{H}$ is chosen randomly: we assume an ergodic block fading channel model where the channel remains constant over a block of symbols, and changes independently across blocks. The average SNR at each receive antenna is given by E_s/N_0, as $\mathrm{E}[|h_{ji}|^2]=1$.

Ergodic Capacity

If the transmitted symbols span an infinite number of independently fading blocks, the Shannon capacity, also known as ergodic capacity, is the ensemble average of the information rate over the distribution of the elements of the channel matrix $\boldsymbol{H}$ [28]. Based on (2.11) the ergodic capacity is expressed as,

$$C_{\mathrm{MIMO-E}} = \mathrm{E}\left[\sum_{i=1}^{\min(N_t,\, N_r)} \log_2\left(1+\frac{E_s}{N_0 N_t}\lambda_i\right)\right] \quad \mathrm{bits/s/Hz}, \tag{2.18}$$

The expectation operator applies in this case because the channel is random. Figure 2.6 depicts the ergodic capacity of several MIMO configurations as a function of E_s/N_0. As expected, at the same SNR, the ergodic capacity increases with N_t and N_r increasing. The capacity also becomes larger as SNR increases. We note that the ergodic capacity of a 1×2 SIMO channel is greater than the ergodic capacity of a 2×1 MISO channel. This is because MISO channels do not offer array gain, in the absence of CSI at the transmitter.

Outage Capacity

In applications where the transmitted symbols span a single block only, the Shannon capacity is zero. This is because, no matter how small the rate at which we wish to communicate, there is always a nonzero probability that the given channel realization will not support this rate [3]. For example, suppose the target transmission rate is R bits/s/Hz. If the channel realization $\boldsymbol{H}$ is such $\log_2\left[\det\left(\boldsymbol{I}_{N_r}+\frac{E_s}{N_0 N_t}\boldsymbol{H}\boldsymbol{H}^{\dagger}\right)\right] < R$, then whatever code that is used by the transmitter, the decoding error probability cannot be made arbitrarily small [16]. Thus, the capacity of the channel in the strict sense is zero. An alternative performance measure is the outage capacity.

We define the $q\%$ outage capacity $C_{\mathrm{MIMO-q}}$ as the information rate I_c that is guaranteed for

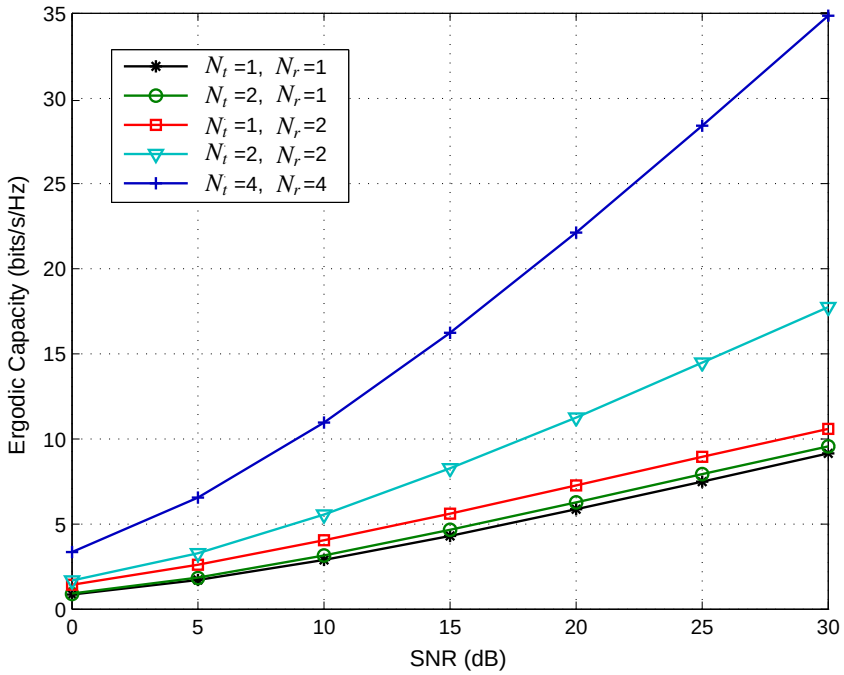

Figure 2.6: *Ergodic capacity for different MIMO antenna configurations. (Rayleigh fading channels are considered.)*

$(100 - q)\%$ of the channel realizations,

$$\Pr(I_c \leq C_{\mathrm{MIMO-q}}) = q\%. \tag{2.19}$$

Figure 2.7 shows the 10% outage capacity for several MIMO configurations as a function of E_s/N_0. As in the case of ergodic capacity, we can see that the outage capacity increases with E_s/N_0 and that MIMO channels provide significant improvements in outage capacity.

The outage probability for a target transmission rate R is the probability that the mutual information I_c falls below that rate R, i.e., $P_{out} = P(I_c \leq R)$.

2.2 Cooperative Communications

As we discussed in Section 2.1, MIMO systems have recently emerged as one of the most significant wireless techniques, as they can greatly improve the channel capacity and link reliability of wireless communications. However, these improvements come at the cost of requiring the antennas on a MIMO device to have sufficient spacing for uncorrelated fading [4]. If the

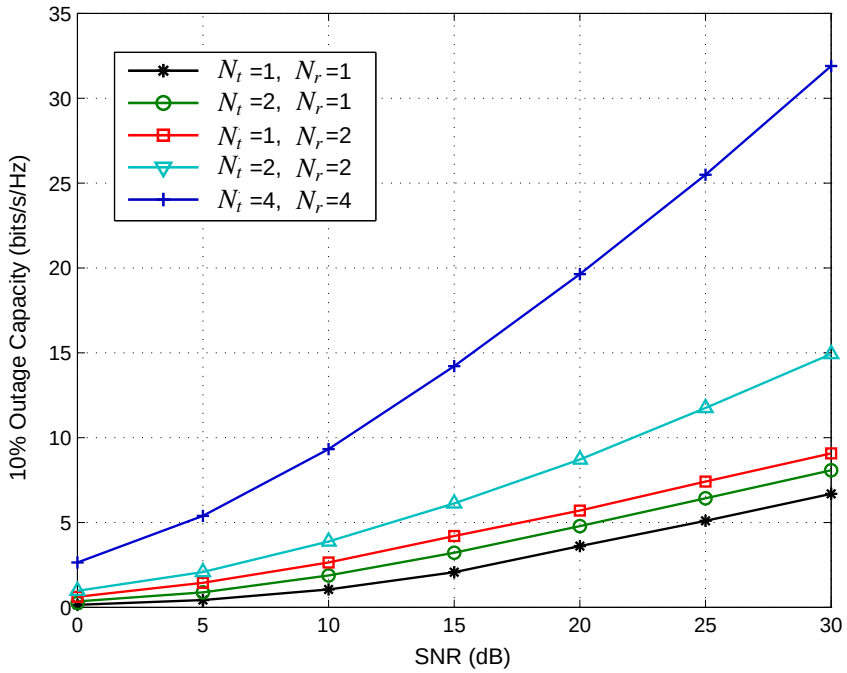

Figure 2.7: *10% outage capacity for different MIMO configurations.(Rayleigh fading channels are considered.)*

antenna spacing reduces, i.e. independent fading cannot be obtained for each pair of antennas, the efficiency will be degraded, resulting in lower MIMO capacity. Moreover, implementing MIMO technology usually results in higher hardware processing costs, which is a critical constraint for a typical wireless product. Some handsets and nodes in a wireless sensor network may not be able to support multiple transmit antennas [31]. Cooperative communication is a practical alternative to a MIMO system when the size, cost, or hardware complexity of the wireless device is limited, which allows single-antenna nodes in a multi-user scenario to share their messages [32].

The advantages of MIMO systems have been presented in Section 2.1; similar to MIMO, cooperative communication could generate diversity, but in a new and interesting way. For an explanation of the basic ideas, we refer to Figure 2.8, which shows two mobile users communicating with a base station. Each user has only one antenna and thus cannot individually generate receive diversity. However, due to the inherently broadcast nature of wireless communications at the base station, it may be possible for one user to receive the information intended for another user, in which case it can help to forward some version of the received information

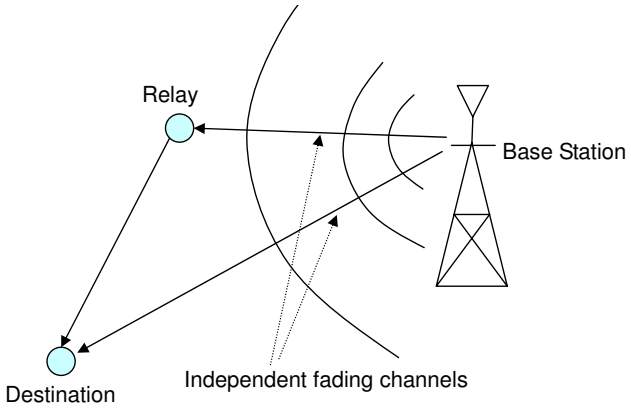

Figure 2.8: *Cooperative communications.*

to the destination. Because the fading channels to the two users are statistically independent, this could generate receive diversity.

Because of diversity, the channel's achievable rates increase, as the negative effects of shadowing and small scale fading can be effectively combated. Furthermore, due to cooperation diversity, the error probabilities at the destination will be reduced. Cooperation among different users is therefore a good way to improve wireless network reliability and capacity [33] [34].

In this section, we will firstly outline some cooperation configurations and operation types. This will be followed by an investigation of typical cooperation protocols and a comparison of their achievable rates. Some relaying schemes will then be presented.

2.2.1 Configurations and Operation Types

The basic ideas behind cooperative communications can be traced back to the ground breaking work of Cover and El Gamal on the information theoretic analysis of the relay channel [35]. A classical relay channel is a three terminal network consisting of a source (S), a relay (R), and a destination (D) [36], as shown in Figure 2.9(a). It was assumed that all nodes operate in the same band. From the viewpoint of the source, the system becomes to a point to multiple-point channel, which is often called a broadcast channel (BC). And from the viewpoint of the destination, it represents a multiple-point to point channel which behaves like the so-called multiple access channel (MAC) [37].

Cooperative communication is not limited to the classical relay channel, this concept can be

extended to larger network architectures. Figure 2.9 depicts various relaying configurations that arise in wireless networks, such as the parallel relay channel in Figure 2.9(b), the virtual MIMO channel in Figure 2.9(c), and the two-way relay channel in Figure 2.9(d). The two-way relay channel is modelled as two source nodes exchanging information with the help of a relay. The virtual MIMO channel will be investigated in detail in Section 2.4.

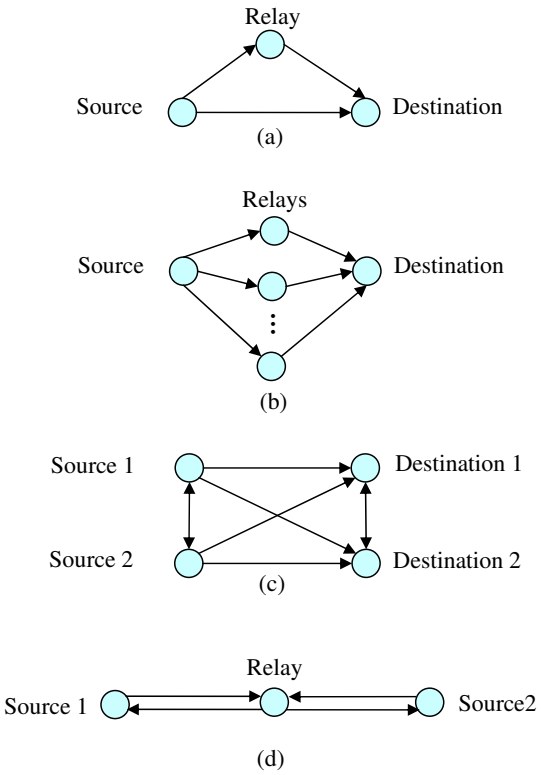

Figure 2.9: *Cooperation architectures: (a) classical relay channel, (b) parallel relay channel, (c) virtual MIMO channel, (d) two-way relay channel.*

The relay operation types are summarized in Table 2.1. For type I, the source terminal communicates with the relay and destination terminals during the first time slot. In the second time slot, both the relay and source terminals communicate with the destination terminal. Type I realizes maximum degrees of broadcasting and receive collision. For type II, only the relay terminal communicates with the destination terminal in the second time slot. This type realizes a maximum degree of broadcasting and exhibits no receive collision. As to the third type, the destination terminal chooses not to receive the direct signal during the first time slot. Types I, II and III were proposed in [38], [39] and [40], respectively. A performance comparison among the three types can be found in [38]. Note that, while the signal transmitted to the relay and

destination terminals over the two time slots is the same under type II, types I and III can potentially convey different signals to the relay and destination terminals. This fact can be exploited in practice in the context of space-time code design [38].

As operation types II and III are essentially derivatives of type I, we focus on Type I for analysing the classical (three-terminal) relay channel. When the virtual-MIMO channel (as shown in Figure 2.9 (c)) is considered, we will then move to operation type II (where Destination 1 serves as the relay), as it is more relevant to compare with the corresponding MIMO system.

Time Slot / Type	I	II	III
1	S $\rightarrow$ R, D	S $\rightarrow$ R, D	S $\rightarrow$ R
2	S $\rightarrow$ D, R $\rightarrow$ D	R $\rightarrow$ D	S $\rightarrow$ D, R $\rightarrow$ D

Table 2.1: *Three Different Time-division Based Relay Types. (Note S, R, and, D stand for the source, relay, and destination terminals respectively. $A \rightarrow B$ signifies communication between terminal A and B.)*

2.2.2 Equivalent Channel Model

We start with the classical relay channel in Figure 2.9(a), and the cooperative operation Type I in Table 2.1.

For direct transmission, our baseline for comparison, we model the channel as,

$$y_d = h_{sd}x_s + w_d. \tag{2.20}$$

Compared to the MIMO channel model (2.1), we use the subscripts s, r, and d, to classify the transmitted (or received) symbols at the source, relay and destination, respectively. The channel coefficient is denoted by h_{ij}, where $i \in s, r$ and $j \in r, d$. We restrict our discussion to the case that CSI is known to (i.e. accurately measured by) the appropriate receivers, but unknown to the transmitters. The noise is denoted by w_j ($j \in r, d$), and $w_j \sim \mathcal{CN}(0, N_0)$. Without loss of generality, the noise power N_0 is normalized to unity.

We now consider the transmission into two slots for cooperative communications. During the

first time slot, we assume $x_{s,1}$ as the source transmitted signal, and obtain,

$$y_r = h_{sr}x_{s,1} + w_r, \tag{2.21}$$

$$y_{d,1} = h_{sd}x_{s,1} + w_d, \tag{2.22}$$

where y_r and $y_{d,1}$ are the received signals at the relay and destination during the first time slot, respectively. For the second time slot, we model the received signal as,

$$y_{d,2} = h_{sd}x_{s,2} + h_{rd}x_r + w_d, \tag{2.23}$$

where $x_{s,2}$ and x_r are the source and the relay transmitted signals over the second time slot.

2.2.3 Cooperation Protocols (DF, AF, and CF)

In this part, we will describe three typical cooperative transmission protocols that can be utilized in the network of Figure 2.9. These protocols determine what the individual relay should do after receiving the signal, employ different types of processing at each relay terminal. We allow the relay to amplify its received signal subject to its power constraint, or to decode, re-encode and re-transmit the message, or to forward a quantized and compressed version of the message employing a source coding method. We refer to these three options as amplify-and-forward (AF), decode-and-forward (DF), and compress-and-forward (CF), respectively [9]. It should be noted that the simplest compress-and-forward protocol is amplify-and-forward, in which the relay simply amplifies the signal before forwarding.

Amplify-and-Forward

Under amplify-and-forward, the relay receives a noisy version of the signal transmitted by the source. As the name implies, the relay then amplifies and retransmits this noisy version,

$$x_r = \delta y_r. \tag{2.24}$$

To remain within its power constraint, an amplifying relay must use a gain factor δ.

$$\delta = \sqrt{\frac{E_r}{|h_{sr}|^2 E_{s,1} + N_0}}, \tag{2.25}$$

where $E_{s,1}$ is the source power during the first time slot, defined as $E_{s,1} = \mathrm{E}[|x_{s,1}|^2]$; E_r is the relay power with $E_r = \mathrm{E}[|x_r|^2]$.

The destination terminal receives a superposition of the relay transmission and the source transmission during the second time slot. Then the received signals at the destination over the two time slots are given by,

$$\begin{aligned} y_{d,1} &= h_{sd} x_{s,1} + w_d, \\ y_{d,2} &= h_{sd} x_{s,2} + h_{rd} h_{sr} \delta \; x_{s,1} + \widehat{w}_d, \end{aligned} \tag{2.26}$$

where the effective noise term $\widehat{w}_d \sim \mathcal{CN}(0, N_0')$, and

$$N_0' = N_0 + N_0 |h_{rd}|^2 \delta^2. \tag{2.27}$$

Although noise is amplified by cooperation, the destination receives two independently faded versions of the signal and can make better decisions for the transmitted symbols than the direct transmission [41].

Decode-and-Forward

For the decode-and-forward protocol, during the first time slot, the signal received at the relay terminal is given by (2.21). The relay now demodulates, decodes, re-encodes and retransmits the signal,

$$x_r = \widehat{x}_{s,1}, \tag{2.28}$$

where $\widehat{x}_{s,1}$ denotes the relay's estimate of $x_{s,1}$. Assume that the signal is decoded correctly (i.e. $\widehat{x}_{s,1} = x_{s,1}$) and retransmitted at the relay. Then we obtain the received signals at the destination over the two time slots,

$$\begin{aligned} y_{d,1} &= h_{sd} x_{s,1} + w_d, \\ y_{d,2} &= h_{sd} x_{s,2} + h_{rd} x_{s,1} + w_d. \end{aligned} \tag{2.29}$$

But it is possible that detection by the relay is unsuccessful, in which case cooperation could be detrimental to the eventual detection at the destination terminal. To avoid the problem of error propagation, Laneman *et al.* [39] proposed an adaptive relaying scheme where the relay only transmits when it successfully decodes the transmitted data.

Compress-and-Forward

The compress and forward protocol has the relay forwarding a quantized and compressed version of the received signal. The relay node can employ standard quantization, or some source coding technique, when compressing the signal.

According to Proposition 1 in [42], suppose that receiver 1 and 2 receives the i.i.d. circular complex Gaussian signals y_1 and y_2, and y_1 is compressed with a rate R_C and forwarded to receiver 2, then this system is equivalent to a system where receiver 2 has two antennas that receive the signals,

$$\begin{bmatrix} y_1 + w_c \\ y_2 \end{bmatrix}, \tag{2.30}$$

where w_c is i.i.d. circular Gaussian noise, which is independent of y_1 and y_2, called the compression noise. If the relay node employs Wyner-Ziv (WZ) Coding [43], one of the source coding techniques, to compress the signal, compression noise w_c has the power,

$$\sigma_{wz}^2 = \frac{\mathrm{E}[|y_1|^2]\mathrm{E}[|y_2|^2] - |\mathrm{E}[y_2 y_1^*]|^2}{(2^{R_C} - 1)\mathrm{E}[|y_2|^2]}. \tag{2.31}$$

Here, we consider the same assumption as above, the final signal received at the destination during the second time slot is,

$$y_{d,2} = h_{sd} x_{s,2} + h_{rd} x_{s,1} + w_c + w_d. \tag{2.32}$$

Specifically, we implement the WZ coding technique at the relay, and assume that the noise power N_0 is normalized to unity. Then we have,

$$\sigma_{wz}^2 = \frac{|h_{sr}|^2 E_{s,1} + |h_{sd}|^2 E_{s,1} + 1}{(2^{R_C} - 1)(|h_{sd}|^2 E_{s,1} + 1)}, \tag{2.33}$$

If the channel coefficient between the relay and the destination is denoted by h_{rd}, R_C will be given by,

$$R_C = \log_2 \left(1 + \frac{|h_{rd}|^2 E_r}{1 + |h_{sd}|^2 E_{s,2}} \right). \tag{2.34}$$

Note that, besides the WZ coding technique, the relay can also employ a standard source coding technique when compressing the signal, at the cost of a slightly lower achievable rate in theory. We have published one paper [44], where a practical CF cooperation using standard source

coding at the relay was proposed for a three-terminal classical relay network. It is shown that standard source coding is much simpler for the CF protocol and also performs well in practical scenarios. The framework of the relay receiver and two practical source coding algorithms are also analysed in [44].

Compared to AF, the CF protocol can provide better performance, but it is a little more complicated as the relay needs to quantize the signal before forwarding. Moreover, the DF protocol outperforms CF when the relay is closer to the source. On the other hand, the CF protocol provides higher rates when the relay is closer to the destination [9] [10]. Simulation results confirming these trends will be presented later in this section.

2.2.4 Rates Comparison of Cooperation Protocols

In this subsection, the achievable rates of three cooperation protocols will be compared. We use the channel model described in Section 2.2.2, where classical relay model is considered, as Figure 2.10 shows. We assume the channels experience independent Rayleigh fading, and suppose that the source node transmits with power $E_{s,1}$ during time slot 1, and with power $E_{s,2}$ during the second time slot, and $E_{s,1} = E_{s,2} = 0.5E_s$. The relay node transmits with power E_r. Also, the noise power N_0 is normalized to unity.

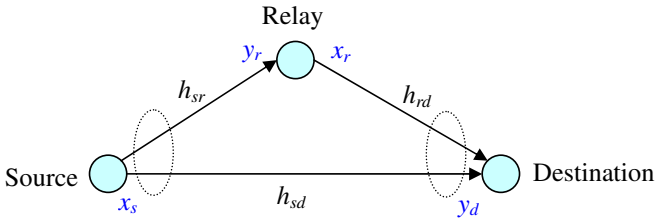

Figure 2.10: *A time-division one-relay network.*

The capacity of the general relay channel was studied in [45]. The relay channel combines a broadcast channel (from the source to the relay and destination) and a multiple-access channel (from the source and relay to the destination). Consider the case where the relay decodes the received signal during time slot I, re-encode it and transmit during time slot II. Using the Theorem 15.7.1 in [45], we get the following achievable rate for the DF protocol,

$$R_{\text{DF}} = \min\{R_{\text{DF1}}, R_{\text{DF2}}\} \leq \min\{I(x_s; y_r y_d | x_r), I(x_s, x_r; y_d)\}, \tag{2.35}$$

where $I(\cdot)$ means mutual information. The first term $I(x_s; y_r, y_d|x_r)$ upper bounds the maximum rate of information transferred from the source to the relay and destination given the condition of x_r, which is the mutual information from the region of the broadcast channel. The second term $I(x_s, x_r; y_d)$ bounds the mutual information between the senders and the destination, from the perspective of the multiple-access channel. Thus we have [9, 10],

$$\begin{aligned} R_{\text{DF1}} &= I(x_s; y_r, y_d|x_r) \\ &= \frac{1}{2}\log_2\left(1+|h_{sr}|^2E_{s,1}\right)+\frac{1}{2}\log_2\left(1+|h_{sd}|^2E_{s,2}\right), \qquad (2.36) \\ R_{\text{DF2}} &= I(x_s, x_r; y_d) \\ &= \frac{1}{2}\log_2\left(1+|h_{sd}|^2E_{s,1}\right)+\frac{1}{2}\log_2\left(1+|h_{sd}|^2E_{s,2}+|h_{rd}|^2E_r\right). \qquad (2.37) \end{aligned}$$

Two time slots are considered in both R_{DF1} and R_{DF2}. Inserting (2.36) and (2.37) in (2.35), the achievable rate for the DF protocol is obtained.

Instead of using the DF protocol, an alternative method is to let the relay forward a quantized and compressed version of the received signal. The following equation gives the achievable CF rate.

$$R_{\text{CF}} = \frac{1}{2}\log_2\left(1+|h_{sd}|^2E_{s,1}+\frac{|h_{sr}|^2E_{s,1}}{1+\sigma_{wz}^2}\right)+\frac{1}{2}\log_2\left(1+|h_{sd}|^2E_{s,2}\right), \qquad (2.38)$$

where the WZ coding technique is assumed at the relay and σ_{wz}^2 is the power of the compression noise defined in (2.33). When we consider the compression rate R_C given in (2.34), we have,

$$\sigma_{wz}^2 = \frac{|h_{sr}|^2E_{s,1}+|h_{sd}|^2E_{s,1}+1}{\frac{|h_{rd}|^2E_r}{1+|h_{sd}|^2E_{s,2}}(|h_{sd}|^2E_{s,1}+1)}. \qquad (2.39)$$

Inserting (2.39) in (2.38), we get the achievable rate of the classical relay system using CF protocol.

The AF protocol is a special case of CF, in which case the relay only amplifies the signal before forwarding. According to (2.26) and (2.27), the achievable rate for AF protocol can be obtained as,

$$R_{\text{AF}} = \frac{1}{2}\log_2\left(1+|h_{sd}|^2E_{s,1}+\frac{|h_{sr}|^2|h_{rd}|^2E_r}{|h_{rd}|^2E_r+|h_{sr}|^2E_{s,1}+1}\right)+\frac{1}{2}\log_2\left(1+|h_{sd}|^2E_{s,2}\right) \qquad (2.40)$$

We also give the rate of direct transmission for reference, considering two time slots,

$$R_{\mathrm{NC}} = \frac{1}{2}\log_2\left(1+|h_{sd}|^2 E_{s,1}\right) + \frac{1}{2}\log_2\left(1+|h_{sd}|^2 E_{s,2}\right) \tag{2.41}$$

Numerical Results

Assume that the power $E_s = E_r = 5.0$ dB, for reference the noise level is 0.0 dB. The channels experience Rayleigh fading with $E[|h_{sd}|^2] = E[|h_{rd}|^2] = 0.0$ dB, and various values of $E[|h_{sr}|^2]$. Then we obtain the simulation results for the achievable rates of typical protocols R_{DF}, R_{AF}, and R_{CF}, and the rate of direct transmission R_{NC}, shown in Figure 2.11. It can be seen that, if $|h_{sr}|^2 < |h_{sd}|^2$, the DF protocol will not work effectively, and only the AF and CF protocols should be used. The CF protocol can be used for all channels and always provides a rate gain over the direct transmission. But as $|h_{sr}|^2$ becomes larger compared to $|h_{sd}|^2$, the DF rate will eventually become larger than the CF rate. It means that the DF protocol outperforms the CF protocol when the relay gets closer to the source.

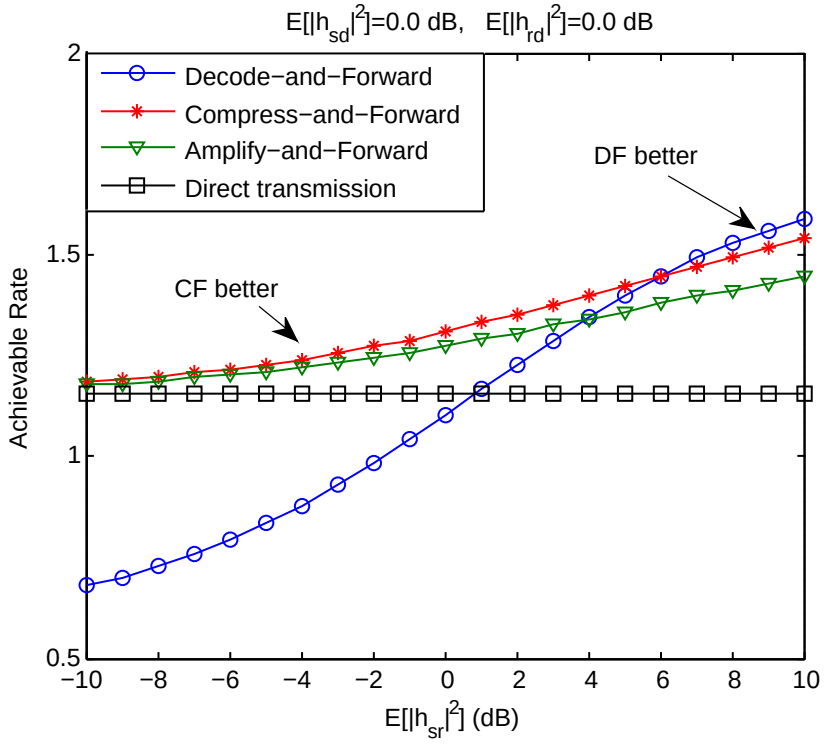

Figure 2.11: *Achievable rates for time-division relay channels, with $E_s = E_r = 5.0$ dB and Rayleigh fading channels.*

2.2.5 Cooperation Schemes

The above Sections 2.2.3 and 2.2.4 show three typical cooperation protocols, which are related to the behavior of individual relays, i.e. what each relay terminal should do after receiving signals. Now, we will briefly illustrate how to deal with the case when several relays exist in the wireless network. Three kinds of cooperation schemes will be presented, which are a fixed relaying scheme, selection relaying scheme and opportunistic relaying scheme.

Fixed Relaying

For fixed relaying, the relays are allowed to decode-and-forward, amplify-and-forward, or compress-and-forward the received signals, and the relays are always active. It means that the relay terminals must take part in the cooperation no matter what the channel gains to the source and destination are.

As discussed in Section 2.2.4, fixed DF relaying is limited by the channel gain between the source and relay. Laneman et al. [39] thus proposed a selection relaying scheme to overcome the shortcoming of fixed relaying.

Selection Relaying

The selection relaying scheme is proposed in [39], and then extended in [41] for a distributed network. The basic idea behind this scheme is that, if the fading coefficients are known to the appropriate receivers, the relays can adapt their transmission behaviors according to the measured values of channel coefficients. A certain threshold is thus needed. The transmissions during the second time slot are performed only by a subset $\mathcal{D}$ of K relays which satisfy:

$$|h_{sk}|^2 \geqslant (2^{2R_E-1})N_0/E_s \tag{2.42}$$

where R_E is the pre-defined end-to-end spectral efficiency in bits/s/Hz. The decoding process at the relay k which satisfies equation (2.42) is assumed to be successful, i.e. no outage event happens during the first time slot.

Thus if the measured channel coefficient between the source and relay falls below the threshold, the relay terminal will not take part in the cooperation, as the first relay shown in Figure 2.12. Otherwise, the relay forwards the received signal to achieve diversity gain, as the left other

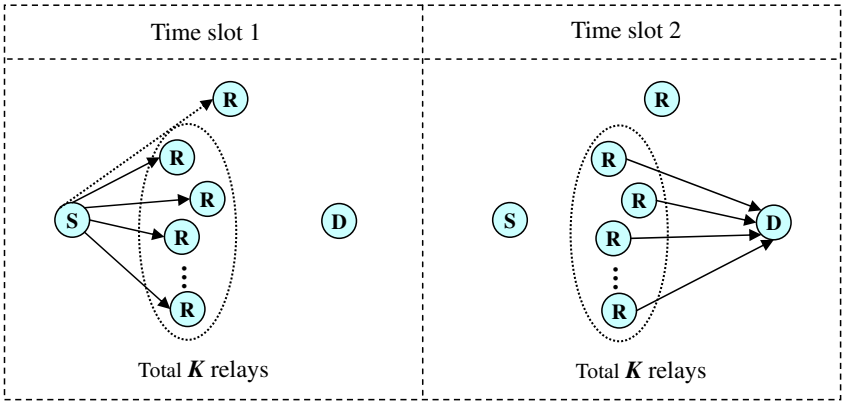

Figure 2.12: *Schematic representation of the selection relaying scheme. (S, R, and, D stand for the source, relay, and destination terminals respectively.)*

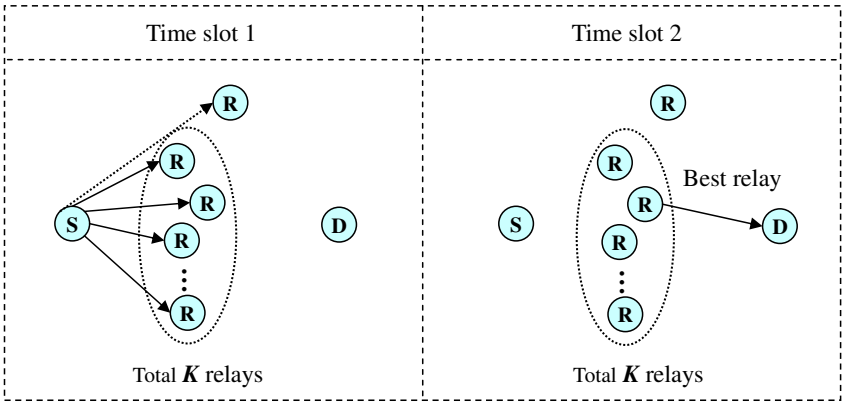

Figure 2.13: *Schematic representation of the opportunistic relaying scheme. (S, R, and, D stand for the source, relay, and destination terminals respectively.)*

relay shown in Figure 2.12.

Opportunistic Relaying

The opportunistic relaying scheme proposed by Bletsas [46, 47] is a best-single-relay-selection scheme. The best relay is selected from the subset $\mathcal{D}$ defined in (2.42). Then only the best relay is used for cooperation, as shown in Figure 2.13. The motivation is based on an aggregate power constraint. If we obtain the best relay, the relay will use the total relay power without sharing with other relays or causing interference to other users.

For an opportunistic relaying scheme using the DF protocol, the best relay is chosen to maxi-

mize the instantaneous channel gain between the relay k and destination for all $k \in \mathcal{D}$ [47]. For the case of AF, the best relay is selected to maximize the mutual information, i.e. to minimize the outage probability [46]. It is shown that opportunistic relaying (with either DF or AF) is not only simple, but also obtains a full cooperative diversity gain. It reveals that cooperation offers diversity benefits even when cooperative relays choose not to transmit but rather choose to cooperatively listen [47].

A detailed comparison between the three cooperation schemes in terms of channel capacity and outage probability can be found in [39, 41, 46, 47].

2.3 Basic Review of Virtual-MIMO Systems

Recall from Section 2.2.1, the virtual-MIMO channel is a particular relaying configuration of cooperative communications, where the neighbour single-antenna terminals contribute their antennas and work together to form a virtual antenna array. When virtual antenna arrays are created at both ends of the communication, the system may expect some traditional MIMO benefits, so called as a virtual-MIMO system. A schematic diagram represents the virtual-MIMO system is illustrated in Figure 2.14 (which is an extension of Figure 2.9(c)).

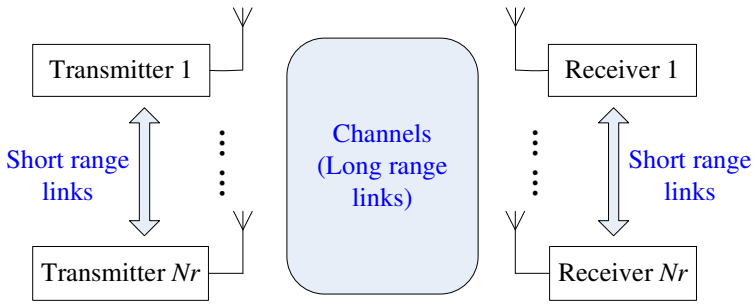

Figure 2.14: *Schematic representation of a virtual-MIMO wireless system with N_t transmitters and N_r receivers.*

To demonstrate the benefits from cooperation in the virtual-MIMO systems, we start with a simple configuration with two single-antenna transmitters and two single-antenna receivers. This kind of virtual-MIMO system was proposed and analyzed in [5, 48]. In this section, the system model of the two-transmitter two-receiver virtual-MIMO configuration will firstly be described, followed by possible cooperations in this system and their performance evaluations.

2.3.1 System Model

Consider an ad hoc network with two clustered transmitters and two clustered receivers as shown in Figure 2.15. The terminals within a cluster are assumed to be close together, but the distance between the transmitter and receiver clusters is large. The data channel gains are denoted by $h_1, ..., h_4$. Let $[x_1, x_2]^T$ denote the transmit signals and $[y_1, y_2]^T$ denote the received signals. $E_{s1} \triangleq E[|x_1|^2]$ and $E_{s2} \triangleq E[|x_2|^2]$ denote the transmission powers and we assume $E_{s1} + E_{s2} = E_s$. In accordance with the above sections, the noise at each receiver is assumed to follow $\mathcal{CN}(0, N_0)$.

There are three orthogonal communication channels: the long-range data channel between the transmitter and receiver clusters, the cooperation channel between the transmitters, and the cooperation channel between the receivers. Suppose that the cooperation is operated by way of a conference link with capacity C, at both the transmitter cluster and receiver cluster, as shown in Figure 2.15.

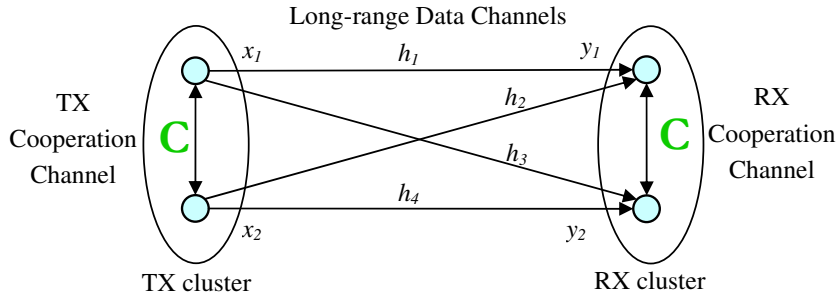

Figure 2.15: *System model of a virtual-MIMO system with two clustered transmitters and two clustered receivers. (TX and RX stand for the transmitter and receiver, respectively.)*

If there is neither transmitter nor receiver cooperation, Transmitter 1 wishes to send information to Receiver 1, and likewise Transmitter 2 to Receiver 2. The system will be a Gaussian interference channel under strong interference, and the noncooperative sum capacity is [5, 42, 49]:

$$R_{\mathrm{NC}} = \min\left\{\log_2\left(1 + |h_1|^2\frac{E_{s1}}{N_0} + |h_2|^2\frac{E_{s2}}{N_0}), \log_2(1 + |h_3|^2\frac{E_{s1}}{N_0} + |h_4|^2\frac{E_{s2}}{N_0}\right)\right\}. \quad (2.43)$$

The capacity improvement from cooperation will be investigated in the following.

2.3.2 Capacity Gain from Cooperation

For the virtual-MIMO system we described in Section 2.3.1, there exist three types of cooperation, transmitter-side cooperation, receiver-side cooperation, and transmitter-and-receiver cooperation:

Transmitter-side Cooperation: If the transmitters were allowed to jointly encode their messages, the channel would be a multiple-antenna BC (i.e. a multiple-antenna point to multiple-point channel), for which dirty paper coding (DPC) is capacity-achieving. Motivated by this, [48] proposed a strategy where the two transmitters first fully exchange their intended signals over the orthogonal cooperation channel, followed by the transmitters jointly encoding both signals using the DPC technique. Here the DPC technique refers to methods for pre-subtraction of known interference at the multiple-antenna transmitter. It requires CSI for the wireless link to each receiver is known perfectly at the transmitter. Tomlinson-Harashima precoding can be used as a DPC method [50]. The capacity achieved by DPC can be equal to the multiple-antenna BC capacity (with a two-antenna transmitter) C_{BC}, but is also limited by the conference link capacity C between the two transmitters. Thus the cooperation sum rate is,

$$R_{\text{TX}} = \min(C, C_{\text{BC}}), \tag{2.44}$$

where C_{BC} denotes the two-antenna BC capacity. As demonstrated in [5, 37], C_{BC} is given by the sum capacity of its dual multiple access channel, and we have:

$$C_{\text{BC}} = \log_2 \left[\det \left(\boldsymbol{I} + [h_1 \; h_2]^\dagger \frac{E_s}{2N_0} [h_1 \; h_2] + [h_3 \; h_4]^\dagger \frac{E_s}{2N_0} [h_3 \; h_4] \right) \right], \tag{2.45}$$

where C_{BC} has been maximised at $E_{s1} = E_{s2} = E_s/2$, as it is symmetric in E_{s1}, E_{s2}.

Receiver-side Cooperation: Assuming non-cooperating transmitters, we consider receiver-side cooperation in the virtual-MIMO system here. It has been shown in Section 2.2.4 that, compared to AF and DF, the CF protocol provides superior performance and therefore serves as the best candidate for such receiver-side cooperation. Suppose Receiver 1 employs CF to send a compressed version of its own observation to the Receiver 2 through the orthogonal cooperation channel. When using the WZ coding technique, the compression noise variance is given by (2.31) on page 25, where R_c needs to be replaced by C. Thus Receiver 2 has a noisy version of Receiver 1's signal, the network is equiva-

lent to a multiple-antenna MAC (i.e. a multiple-point to multiple-antenna point channel). Therefore, when the compression noise is small enough, the sum rate of the receiver-side cooperation R_{RX} can approach the capacity of the multiple-antenna MAC (with a two-antenna receiver) C_{MAC}, that is $R_{\text{RX}} \rightarrow C_{\text{MAC}}$. As demonstrated in [5, 42], the upper bound of R_{RX}, i.e. C_{MAC}, is given by:

$$C_{\text{MAC}} = \log_2 \left[\det \left(\boldsymbol{I} + [h_1 \ h_3]^T \frac{E_s}{2N_0} ([h_1 \ h_3]^T)^\dagger + [h_2 \ h_4]^T \frac{E_s}{2N_0} ([h_2 \ h_4]^T)^\dagger \right) \right], \quad (2.46)$$

where C_{MAC} has also been maximised at $E_{s1} = E_{s2} = E_s/2$.

Transmitter-and-receiver Cooperation: The cooperation methods described above can be combined, i.e. the transmitters exchange their messages and then perform DPC, while the receivers cooperate using the CF protocol. This strategy could exploit both transmit and receive cooperation diversity, but the system sum rate R_{TXRX} can also be limited by the capacity C on the orthogonal cooperation channels. When C is high, the virtual-MIMO system with transmitter-and-receiver cooperation could approach the ideal MIMO performance (from equation (2.8)):

$$C_{\text{MIMO}} = \max_{\text{tr}(\boldsymbol{Q}_s) \leq \text{E}_s} \log_2 \left[\det \left(\boldsymbol{I} + \boldsymbol{H} \frac{\boldsymbol{Q}_s}{N_0} \boldsymbol{H}^\dagger \right) \right]. \quad (2.47)$$

We refer the reader to [5] for detailed analysis of R_{TX}, R_{RX}, and R_{TXRX}.

It has been shown in [5, 48] that, for a weak cooperation channel (i.e. when capacity C is very small), the sum rates of both the transmitter-side cooperation and transmitter-and-receiver cooperation are impaired. This is due to the fact that each transmitter decodes the signal of the other, which will become the limiting factor on performance. On the other hand, receiver-side cooperation always performs better than or as well as noncooperative transmission. When C is large, the sum rates of transmitter-side cooperation and receiver-side cooperation approach the the two-antenna BC capacity and MAC capacity, i.e. $R_{\text{TX}} \rightarrow C_{\text{BC}}$ and $R_{\text{RX}} \rightarrow C_{\text{MAC}}$. Note that as a duality exists between the uplink and downlink, we have $C_{\text{BC}} = C_{\text{MAC}}$. As C increases further, R_{TX} and R_{RX} are bounded by C_{BC} and C_{MAC}, but the rate of transmitter-and-receiver cooperation continues to improve and approaches the MIMO channel capacity C_{MIMO}.

It should be noted that, both the transmitter-side cooperation and transmitter-and-receiver cooperation need to use the DPC technique. Even though DPC is capacity-achieving, it requires CSI to be fully known to the transmitters. A reliable feedback channel is thus needed to com-

municate this information. But in realistic wireless systems, because of the limitation on the feedback channel, it is not always possible to obtain perfect CSI or even partial CSI at the transmitters. When CSI is unknown to the transmitters, the optimal power assigned for the two transmitters will be $E_{s1} = E_{s2} = E_s/2$, and C_{MIMO} thus decreases to C_{MAC} and C_{BC} [5]. In this case, receiver-side cooperation is a good way for achieving close to MIMO performance [7, 8]. This is the subject of this thesis.

2.4 Conclusions

This chapter provided some background on the point-to-point MIMO system and cooperative communications. In the first part, the principles of diversity and spatial multiplexing in MIMO systems were analyzed. It was followed by the study of MIMO channel capacities for the two cases when the channel is known and when it is unknown to the transmitter. It was shown that, MIMO systems can provide significant improvements over the conventional SISO case, in terms of both higher channel capacity and better link reliability.

In the second part, cooperative communication was introduced as a practical alternative to MIMO systems, when the transmitter or receiver may not be able to support multiple antennas. Typical cooperation protocols, i.e. DF, AF, and CF, and their rates comparison were illustrated. It was shown that the achievable rate of DF is higher when the relay is close to the source, but CF outperforms DF when the relay gets closer to the destination. Several cooperation schemes related to the behavior of several relays in a wireless network were also studied.

Finally, a brief review of the virtual-MIMO system was given. Transmitter-side and/or receiver-side cooperation schemes were analyzed. Receiver-side cooperation was shown as a good way for achieving almost MIMO performance, when the CSI is unknown to the transmitters.

The virtual-MIMO system using receiver-side CF cooperation is the subject of this thesis. We will assess the system performance in Chapter 3, and present an efficient source coding technique at the relay in Chapter 4. The effects of carrier frequency offsets and how to overcome them will also be illustrated. A singular value-based adaptive modulation and cooperation scheme will be proposed in Chapter 5 to improve the whole system performance.

Chapter 3
Performance Assessment of Virtual-MIMO Systems with Compress-and-Forward Cooperation

In this chapter, a cooperative virtual-MIMO system using two transmit antennas that implements bit-interleaved coded modulation (BICM) transmission and compress-and-forward (CF) relay cooperation among two receiving nodes is presented. To perform CF cooperation, we propose to use standard source coding techniques for virtual MIMO detection, based on the analysis of its expected rate bound and the tightness of the bound. Since the relay and the destination are closely spaced, we firstly assume an error-free conference link between them, to focus on investigating the achievable gain from the CF cooperation. Then the system throughput expression and upper bounds on the system error probabilities over block fading channels are derived. Results show that the relay enables the proposed cooperative virtual-MIMO system to achieve almost ideal MIMO performance with low source coding rates. Furthermore, when we consider a non-ideal cooperation link for practical considerations, a channel-aware adaptive CF scheme is proposed, so that the relay could always adapt its source coding rate to meet the data rate on the non-ideal link. Because of the short-range communication and the proposed scheme, the impact of the non-ideal link is too slight to impair the system performance significantly.

To concentrate on the system performance assessment, this chapter only considers an optimal vector quantization (VQ), i.e. the Voronoi VQ, at the relay. An alternative VQ will be proposed in Chapter 4, so that the complexity of codebook design will be reduced.

The remainder of this chapter is organized as follows. Section 3.1 introduce the background and motivation of this chapter. Section 3.2 specifies the system model. We analyze the CF cooperation with source coding techniques in Section 3.3, and derive the system throughput and the upper bounds on the system error ratios in Section 3.4. The impact of a non-ideal cooperation link is studied in Section 3.5. Section 3.6 shows the simulation results, and Section 3.7 concludes the chapter.

3.1 Introduction

As mentioned in Chapter 2, multiple-input multiple-output (MIMO) systems have recently emerged as one of the most significant wireless techniques, as it can greatly improve spectral efficiency, channel capacity and link reliability of wireless communications [29] [51]. These benefits have encouraged extensive research on a virtual MIMO system where the transmitter has multiple antennas and each of the receivers has a single antenna [5, 52]. Results in [53] suggest that the virtual MIMO technique can provide significant energy efficiency, even with fading coherence time and channel estimation overheads taken into account.

In a broadcast channel scenario of the virtual MIMO system, coordination is allowed among the transmit antennas but not among the receive nodes, see e.g. [6, 37, 54]. While the above works suggest that the sum capacity of the virtual MIMO system can be achieved by dirty paper coding at the transmitter and the capacity increases linearly with the number of transmit antennas, they all rely on the assumption that channel state information (CSI) for the wireless link to each receiver is known perfectly at the transmitter. However, CSI needs to be obtained at the receiver and sent back to the transmitter over a reliable feedback channel. The feedback requirements are not only affected by the channel fading states, but also growing with the number of transmit and receive antennas [20]. Because of the limitation on the feedback channel, it is not always possible to obtain perfect CSI or even partial CSI in realistic wireless systems.

When the transmitter does not have CSI in the virtual-MIMO system, receiver-side local cooperation is a good way for achieving capacity gains [7, 8], as shown in Figure 3.1. Single-antenna nodes, which may not be able to use multiple antennas due to size and cost limitations, can work together to form a virtual antenna array. For example, suppose a customer carries some mobile terminals that include a single-antenna 3GPP enabled user device and one or more simple relay devices. Since the distance between the devices is general much shorter than that from the base station, the devices could cooperate through their short-range Wi-Fi, Bluetooth, or Ultra-Wideband communications links. With such cooperation, the customer could expect traditional MIMO benefits as if single-antenna user device had multiple antennas. Note that receiver-side communication used for cooperation is realized via an orthogonal channel and allows much higher transmission rate and frequency reuse compared to the long-distance transmitter-to-receiver communication.

Motivated by the above practical scenario, we consider a cooperative virtual-MIMO system in

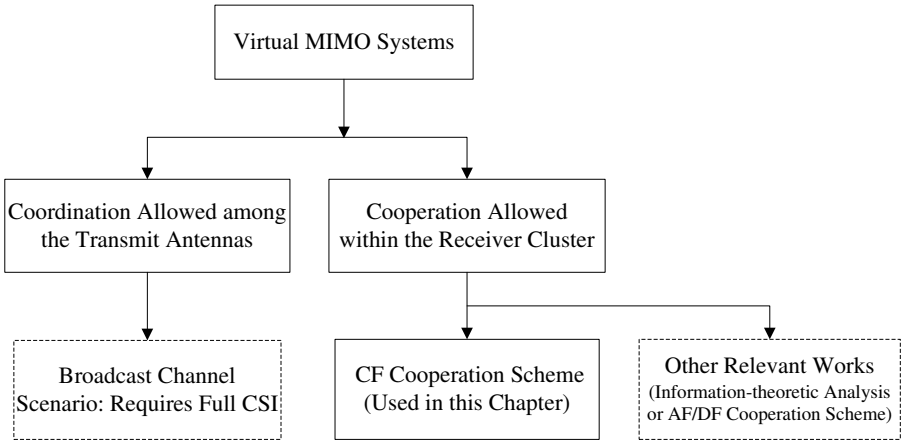

Figure 3.1: *Background of Virtual MIMO Systems.*

this chapter, with one remote multi-antenna transmitter sending information to several closely spaced single-antenna receivers. As for the cooperation protocol, since the relays get closer to the destination in our scenario, it has been shown in Chapter 2 that, compared to amplify-and-forward (AF) and decode-and-forward (DF), the compress-and-forward (CF) protocol provides superior performance [9] [10] and therefore serves as the best candidate for this system. Furthermore, we implement the bit-interleaved coded modulation (BICM) technique [55] to provide forward error correction (FEC). BICM separates the aspects of coding and modulation by bit-interleaving, so that a symbol error at the decoder does not cause consecutive error bits in the codeword, which improves system performance. Note that the virtual-MIMO system studied here is not limited to BICM, other FEC coding schemes, such as Turbo coding or LDPC coding, could also be employed according to different application requirements.

In recent years, research in CF cooperation has mainly focused on the classical three terminal relay channel, such as [7, 9, 10, 56–58]. The capacity performance of a scenario where the relay is very close to the destination is investigated in [56, 57]. The cooperation in [7, 58] is realized by way of an error-free conference link between the relay and the destination. Ng et al. [58] also compares the one-shot cooperation with a two-round iterative conference scheme. An extension of the classical CF cooperation to a virtual-MIMO system was introduced in [5], where an achievable cooperative capacity was analysed theoretically. One relevant work [59] describes a virtual-MIMO scheme, but focuses on relay node selection. Its channel model explicitly includes noise due to the AF process. Two recent papers, [60] and [61], consider a virtual-MIMO channel with partial cooperation among users. However, a simple AF protocol is considered,

and the transmitter needs partial CSI to perform beamforming, which may be an impractical requirement for the single-antenna receiver. This chapter deals with a practical virtual-MIMO system with BICM transmission and CF cooperation. To the best of our knowledge, this is the first attempt to investigate the effect of the CF cooperation using standard source coding at the relay, which could enable the virtual-MIMO system to achieve almost MIMO performance. Although the principle could be applied to any virtual-MIMO configuration, we start with a simple configuration with a two-antenna transmitter and two single-antenna receivers, to demonstrate the achievable performance improvements and sensitivities.

We now summarize the main contributions of this chapter: Firstly, we present a practical virtual-MIMO relay system that implements BICM transmission. The short range links within the receiver group enable CF cooperation. Next, to perform CF cooperation at the relay, we propose that, a standard source coding technique should be used rather than Wyner-Ziv coding for practical considerations. The nature of the system with a multi-antenna transmitter will reduce the benefit from the Wyner-Ziv coding, based on the analysis of its expected rate bound and the tightness of the bound. Moreover, we state the system throughput expression and upper bounds on the system error probabilities over block fading channels. With sufficient source coding rates, the cooperation of the receivers enables the virtual-MIMO system to achieve almost ideal MIMO performance. Finally, a comparison of ideal and non-ideal conference links within the receiver group is investigated. It is shown that, considering the short-range communication and using a channel-aware adaptive CF scheme, the impact of the non-ideal cooperation link is too slight to impair the system performance significantly.

3.2 System Model

A cooperative virtual-MIMO network is considered, with one remote N_t-antenna transmitter sending information to N_r closely spaced single-antenna receivers. To focus on the performance and practical implementation of the CF cooperation, we simplify the system to the $N_t = N_r = 2$ antennas case, as shown in Figure 3.2. Further performance improvements are expected for the case of more cooperating terminals equipped with larger numbers of antennas. BICM, which introduces a spatial and temporal bit interleaver into the transmitter, is employed here to provide forward error correction and improve system performance. At the transmitter, a rate-R_b linear binary convolutional encoder is considered. The coded bits are then interleaved through an ideal random bit interleaver (int.), which rearranges the coded bits using a random

permutation. In each stream after the demultiplexer (or demux), groups of m bits are mapped onto complex data symbols via Gray-labeled $2^m = M$-ary quadrature modulation (QAM) or phase-shift keying (PSK) whose signal constellation is $\mathcal{X}$. The transmission rate is $N_t m R_b$ bits per channel use. Finally the transmitter sends the modulated data symbols through N_t antennas simultaneously.

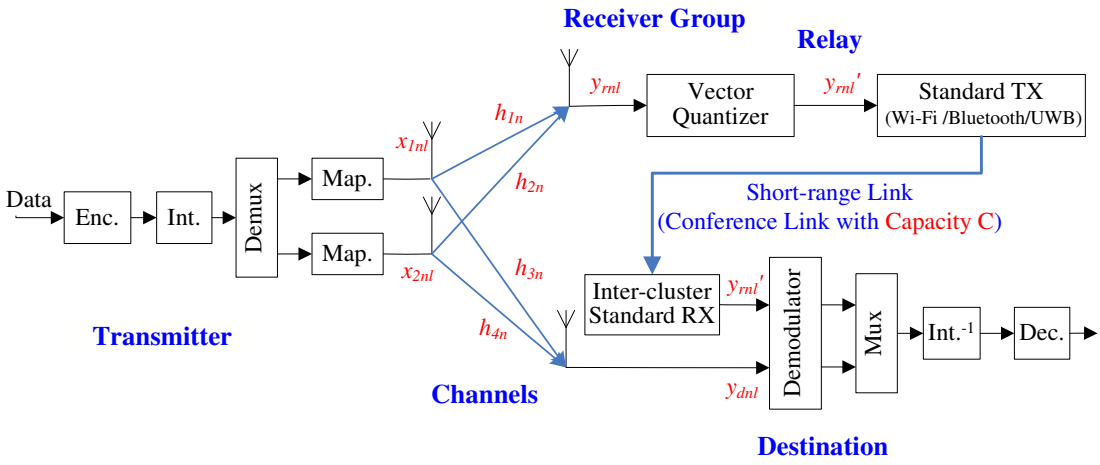

Figure 3.2: *System model of the cooperative virtual-MIMO system. (TX and RX stand for the transmitter and receiver, respectively, $N_t = 2$, $N_r = 2$.)*

Since the transmitter is far away from the receiver group, we assume the channels between them are block fading, which is practical and particularly relevant in wireless communications situations [62]. Thus a block fading channel model with N fading blocks is assumed here, with each block having length L symbol periods. Fading is flat and constant on each block, but independently Rayleigh distributed on different blocks. When we consider a single symbol period l for the nth channel, the channel model is given by,

$$\begin{bmatrix} y_{rnl} \\ y_{dnl} \end{bmatrix} = \boldsymbol{H}_n \boldsymbol{x}_{nl} + \boldsymbol{w}_{nl}, \text{ with } \boldsymbol{H}_n = \begin{bmatrix} h_{1n} & h_{2n} \\ h_{3n} & h_{4n} \end{bmatrix}, \tag{3.1}$$

where $\boldsymbol{H}_n$ denotes the nth block fading channel matrix, with each $h_{in}(i \in [1, ..., 4])$ is independent and identically distributed (i.i.d.). We also define the vector $\boldsymbol{x}_{nl} = [x_{1n1}, x_{2nl}]^{\mathrm{T}}$, where $x_{i'nl}(i' \in [1, 2])$ presents the lth M-ary symbol transmitted on the nth channel from the i'th antenna. The noise vector $\boldsymbol{w}_{nl} = [w_{1n1}, w_{2nl}]^{\mathrm{T}}$, with components $w_{i'nl} \sim \mathcal{CN}(0, N_0)$. The scalars y_{rnl} and y_{dnl} are the received signals at the relay and the destination. Note that the index notation (inl) is used to emphasize the block fading nature of the virtual-MIMO channel. Moreover,

without loss of generality, we assume normalized Rayleigh fading, so that $\mathrm{E}[|h_{in}|^2]=1$, where $|\cdot|$ denotes magnitude and $\mathrm{E}[\cdot]$ denotes the expected value function. The average transmitted power per modulation symbol is $\mathrm{E}[|x_{i'nl}|^2] = E_s/N_t$. We normalize the total transmitted power E_s to unity, and the corresponding power per bit is $E_b = E_s/(mR_b)$. Then the average signal-to-noise ratio (SNR) will be SNR=$1/N_0$. We assume that perfect CSI is available at the receivers only.

There exist two clustered receivers, the destination and the helping relay. As the receivers are closely spaced, it is reasonable to expect that the communication between the two receivers is much better and more stable than that between the transmitter and receivers. It is highly likely that we could achieve high channel capacity with high reliability on this short range link. Hence as also considered in [7], [63] and [58], we assume the two receivers cooperate by way of an error-free conference link, with capacity C, as shown in Figure 3.2. We consider one-shot conference cooperation [58], [64], which requires the destination to decode the signal sent over the conference link. The CF protocol is chosen here, so that a compressed version of the signals, denoted by y'_{rnl}, will be passed to a standard transmitter and sent over the cooperation or conference link , as will be illustrated and detailed in Section 3.3.

The destination is assumed to be equipped with a receiver which observes signals y_{dnl} from the transmitter, and an intra-cluster receiver which observes signals from the relay, written as y'_{rnl} because of the error-free conference link, as shown in Figure 3.2. We denote the received signals at the destination as $\boldsymbol{y}_{nl} = [y'_{rnl} \;\; y_{dnl}]^{\mathrm{T}}$. Next the destination performs joint maximum-likelihood (ML) demodulation of the signal $\boldsymbol{y}_{nl}$, and computes the log-likelihood ratio (LLR) for each coded bit. The two path LLRs are combined into one output stream by the multiplexer, and then reordered into their original positions by the deinterleaver (int.$^{-1}$). Finally, the decoder accepts the LLRs of all coded bits and employs a soft-input Viterbi algorithm to decode the signals. Thus, with help from the relay, the single-antenna destination receives two path signals. Although the compressed signal y'_{rnl} includes some compression noise, a good quality compression process will allow the destination to use y'_{rnl} for MIMO decoding.

3.3 Compress-and-Forward Cooperation

This virtual-MIMO operation is performed by the receiver-side cooperation on the conference link. In order to avoid interfering with the data from the transmitter, the conference link is

realized via an orthogonal channel to the transmitter array. That is, two different frequency bands are used for transmitting and receiving signals at the relay. Compared with the long range data channel $\boldsymbol{H}_n$, the orthogonal conference link is much shorter-range and could be reused many times for short hops in the coverage area of the long range link. Thus cooperation will not affect the overall system throughput. The relay may help the virtual-MIMO system to achieve almost ideal MIMO performance.

As to cooperation protocols, the Alamouti space-time block coding (STBC) based DF scheme [65] could be implemented, with two signals x_{1nl} and x_{2nl} transmitted in one symbol period, and $-x^*_{2nl}$ and x^*_{1nl} originated from x_{1nl} and x_{2nl}, sent in the next symbol period. But the spectral efficiency of the Alamouti DF scheme is only one-half of that with CF or AF protocols, causing a drastic performance degradation, as will shown in section 3.6. Further, because AF requires the relay to amplify its received signal and also the noise, an AF-relayed packet may become too noisy to be used. The CF protocol, which provides better performance when the relay is closer to the destination [42], is the best candidate and thus implemented in this virtual-MIMO system.

3.3.1 Receiver-side Cooperation Using CF protocol

To perform CF cooperation, a standard source coding technique is employed for practical considerations. That is, the relay is equipped with a vector quantizer (VQ). The key tasks of the relay thus include constructing a good codebook and quantizing the received signals. We assume a fixed quantization rate (i.e. source coding rate), denoted by R_c bits/sample. Since the two receivers cooperate by way of an error-free conference link, unless otherwise stated, the link capacity C is assumed to be equal to the fixed source coding rate R_c.

The codebook design at the relay is based on the desired codebook size which equals 2^C and requires knowledge of the noise-free constellation. Besides signal symbols, some control information such as the modulation type is also transmitted on control channels in practice. Then the relay could construct the noise-free constellation of the received signals, i.e. the constellation of $h_{1n}x_{1nl}+h_{2n}x_{2nl}$. The codebook design based on this constellation will be simple and efficient. Further, Voronoi VQ [66] is employed at the relay to design the codebook, as it has the advantage that the codebook is optimal in the sense of minimising average distortion. To implement this VQ, the LBG algorithm which performs an iterative design of the codebook, is used [44]. A detailed explanation of the Voronoi VQ will be provided in Section 4.3.1.1.

After the Voronoi VQ, a compressed version of the signal y'_{rnl} will be passed into a standard transmitter and transmitted over the conference link. In [63] and [67], it is demonstrated that, if $y'_{rnl}|y_{rnl}$ is assigned a Gaussian distribution, adding to y_{rnl} a Gaussian compression noise could model y'_{rnl}. In our system where the transmitter has multiple antennas with QAM or PSK modulation and slow Rayleigh fading channels are considered, the distribution of y_{rnl} is complex. Also, Voronoi VQ is employed to quantize y_{rnl}. It is reasonable to expect that nearly Gaussian codebooks and Gaussian quantization are obtained at the relay. Thus we model the compression noise as an i.i.d. complex Gaussian noise,

$$y'_{rnl} = y_{rnl} + w_{cnl}, \tag{3.2}$$

where w_{cnl} is the compression noise, which is assumed to be independent of y_{rnl}, with variance σ^2_{cn}, i.e. $w_{cnl} \sim \mathcal{CN}(0, \sigma^2_{cn})$. After each block of the compressed signal y'_{rnl}, the relay also sends the value of σ^2_{cn} over the conference link. With knowledge of σ^2_{cn}, and assuming w_{cnl} is i.i.d. complex Gaussian noise, the destination scales y'_{rnl} so that y'_{rnl} and y_{dnl} have the same power of additive Gaussian noise [5]. Then this system is equivalent to a system where destination has two antennas that receive the signals:

$$\tilde{\boldsymbol{y}}_{nl} = \left[\tilde{y}'_{rnl} \;\; y_{dnl}\right]^{\mathrm{T}} = \widetilde{\boldsymbol{H}}_n \boldsymbol{x}_{nl} + \left[\tilde{w}_{1nl} \;\; w_{2nl}\right]^{\mathrm{T}}, \tag{3.3}$$

$$\text{with} \quad \widetilde{\boldsymbol{H}}_n \triangleq \begin{bmatrix} \sqrt{\eta_n} h_{1n} & \sqrt{\eta_n} h_{2n} \\ h_{3n} & h_{4n} \end{bmatrix}, \; \eta_n \triangleq \frac{N_0}{N_0 + \sigma^2_{cn}}, \tag{3.4}$$

where $\tilde{w}_{1nl} \sim$ i.i.d. $\mathcal{CN}(0, N_0)$, η_n is the degradation factor due to the compression noise, and $\tilde{y}'_{rnl} = \sqrt{\eta_n} y'_{rnl}$. The LLR for each coded bit c^λ at the destination will be calculated as,

$$\mathcal{L}(c^\lambda|\tilde{\boldsymbol{y}}_{nl}, \widetilde{\boldsymbol{H}}_n) = \ln \frac{\Pr\{c^\lambda = 1|\tilde{\boldsymbol{y}}_{nl}, \widetilde{\boldsymbol{H}}_n\}}{\Pr\{c^\lambda = 0|\tilde{\boldsymbol{y}}_{nl}, \widetilde{\boldsymbol{H}}_n\}} = \ln \frac{\sum_{\tilde{\boldsymbol{x}} \in \mathcal{X}_1^\lambda} p\{\tilde{\boldsymbol{y}}_{nl}|\tilde{\boldsymbol{x}}, \widetilde{\boldsymbol{H}}_n\}}{\sum_{\tilde{\boldsymbol{x}} \in \mathcal{X}_0^\lambda} p\{\tilde{\boldsymbol{y}}_{nl}|\tilde{\boldsymbol{x}}, \widetilde{\boldsymbol{H}}_n\}}, \tag{3.5}$$

where $\lambda \in \{1, ..., mN_t\}$, and $p\{\tilde{\boldsymbol{y}}_{nl}|\tilde{\boldsymbol{x}}, \widetilde{\boldsymbol{H}}_n\}$ is the conditional probability density function (PDF):

$$p\{\tilde{\boldsymbol{y}}_{nl}|\tilde{\boldsymbol{x}}, \widetilde{\boldsymbol{H}}_n\} = \frac{1}{(\pi N_0)^{N_r}} \exp\left(-\frac{\|\tilde{\boldsymbol{y}}_{nl} - \widetilde{\boldsymbol{H}}_n \tilde{\boldsymbol{x}}\|^2}{N_0}\right), \tag{3.6}$$

where $\|\cdot\|$ denotes magnitude of a vector. The notation $\mathcal{X}_b^\lambda = \{\tilde{\boldsymbol{x}} : c^\lambda = b\}$ is the subset of the hypersymbol constellation where the λth bit is equal to b. The scaled channel matrix $\widetilde{\boldsymbol{H}}_n$ will help the destination to mitigate the effects of the compression noise.

3.3.2 Standard Source Coding VS. Wyner-Ziv coding

To perform CF cooperation, a standard source coding technique is employed for practical considerations. From Shannon's rate-distortion theory (Sec. 10, [45]), now we lower bound the variance of the compression noise:

Proposition 3.1: We denote the lower bound of σ_{cn}^2 by $\bar{\sigma}_{cn}^2$. From Shannon's rate-distortion theory, we obtain:

$$\bar{\sigma}_{cn}^2 = \frac{\mathrm{E}[|y_{rnl}|^2]}{2^C - 1} = \frac{N_0 + \frac{1}{2}|h_{1n}|^2 + \frac{1}{2}|h_{2n}|^2}{2^C - 1}. \tag{3.7}$$

The proof is presented in Appendix A. The lower bound $\bar{\sigma}_{cn}^2$ helps us to upper bound the achievable sum rate of this cooperative system as:

$$\bar{R}_{\text{Shannon}} = \log\ \det\left[\boldsymbol{I} + \widetilde{\boldsymbol{H}}_{cn}\left(\frac{\text{SNR}}{2}\boldsymbol{I}\right)\widetilde{\boldsymbol{H}}_{cn}^{\dagger}\right], \tag{3.8}$$

$$\text{with } \widetilde{\boldsymbol{H}}_{cn} \triangleq \begin{bmatrix} \sqrt{\frac{N_0}{N_0+\bar{\sigma}_{cn}^2}}h_{1n} & \sqrt{\frac{N_0}{N_0+\bar{\sigma}_{cn}^2}}h_{2n} \\ h_{3n} & h_{4n} \end{bmatrix}. \tag{3.9}$$

Here, $\boldsymbol{H}^{\dagger}$ denotes the conjugate transpose of $\boldsymbol{H}$.

Compared with Wyner-Ziv (WZ) coding, why do we choose a standard source coding technique for the CF protocol? Using WZ coding, the lower bound of the compression noise variance $\bar{\sigma}_{wzn}^2$ has been discussed in [42] and [63]. It is shown that, under the assumption that $y'_{rnl}|y_{rnl}$ is Gaussian distributed, the compression noise with WZ coding can also be modelled as i.i.d. circular Gaussian noise, with the lower bound on the power [42]:

$$\begin{aligned} \bar{\sigma}_{wzn}^2 &= \frac{\mathrm{E}[|y_{rnl}|^2]\mathrm{E}[|y_{dnl}|^2] - |\mathrm{E}[y_{rnl}y_{dnl}^*]|^2}{(2^C-1)\mathrm{E}[|y_{dnl}|^2]} \\ &= \frac{\left(\frac{|h_{1n}|^2}{2} + \frac{|h_{2n}|^2}{2} + N_0\right)\left(\frac{|h_{3n}|^2}{2} + \frac{|h_{4n}|^2}{2} + N_0\right) - \left|\frac{h_{1n}h_{3n}^*}{2} + \frac{h_{2n}h_{4n}^*}{2}\right|^2}{(2^C-1)\left(\frac{|h_{3n}|^2}{2} + \frac{|h_{4n}|^2}{2} + N_0\right)}, \end{aligned} \tag{3.10}$$

where y_{dnl}^* denotes the complex conjugate of y_{dnl}. A more general modelling of y'_{rnl} for WZ coding can be found in [63]. For consistency with equation (3.2), we assume that adding to y_{rnl} a Gaussian compression noise, is reasonable and preferable to do this performance comparison.

The upper bound of the achievable sum rate of the system using WZ coding is given by,

$$\bar{R}_{\text{WZ}} = \log\det\left[\boldsymbol{I} + \widetilde{\boldsymbol{H}}_{wzn}\left(\frac{\text{SNR}}{2}\boldsymbol{I}\right)\widetilde{\boldsymbol{H}}_{wzn}^{\dagger}\right], \tag{3.11}$$

$$\text{with } \widetilde{\boldsymbol{H}}_{wzn} \triangleq \begin{bmatrix} \sqrt{\frac{N_0}{N_0+\bar{\sigma}_{wzn}^2}}h_{1n} & \sqrt{\frac{N_0}{N_0+\bar{\sigma}_{wzn}^2}}h_{2n} \\ h_{3n} & h_{4n} \end{bmatrix}. \tag{3.12}$$

The only difference between the two achievable rates $\bar{R}_{\text{Shannon}}$ and $\bar{R}_{\text{WZ}}$ is due to the compression noise variance. A comparison of the noise powers under different SNR assumptions for $N_t = N_r = 2$ is shown in Figure 3.3.

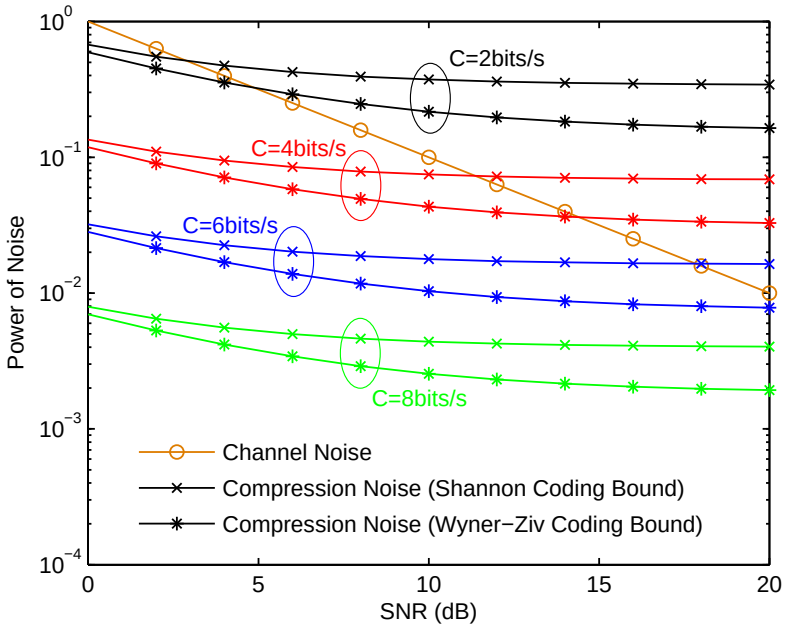

Figure 3.3: *Power comparison of the compression noises under various coding rate assumptions.*

As the conference link capacity C increases, the variance bound of the compression noise, whether using standard source coding or WZ coding technique, is expected to become smaller. For a specific C, there exists a small performance gap between the two noise variance bounds $\bar{\sigma}_{cn}^2$ and $\bar{\sigma}_{wzn}^2$, that is the WZ coding technique performs a little better than the standard coding technique [68]. But the performance gaps are too small to impair significantly the achievable rates, as shown in Figure 3.4. The sum rate of the corresponding MIMO system, as if the

receivers were connected via a wire, is given here for comparison,

$$R_{\text{MIMO}} = \log\det\left[\boldsymbol{I} + \boldsymbol{H}_n\left(\frac{\text{SNR}}{2}\boldsymbol{I}\right)\boldsymbol{H}_n^{\dagger}\right]. \tag{3.13}$$

The achievable sum rates are also compared to the performance of the corresponding MISO system where the relay is silent,

$$R_{\text{MISO}} = \log\left(1 + |h_{3n}|^2\text{SNR}/2 + |h_{4n}|^2\text{SNR}/2\right). \tag{3.14}$$

It can be seen that, WZ coding provides a similar expected rate bound to the standard source coding technique at low SNR (e.g. SNR= 0 dB), and could support a slightly higher achievable rate bound at high SNR (e.g. SNR= 20 dB). Until now, the comparison between WZ coding and standard source coding is based on their performance upper bounds. These bounds give some indication that there is not a huge performance advantage from WZ coding. Given this small performance benefit, and considering the complexity of the WZ coding in practice, standard source coding may attract more practical interest for virtual MIMO systems.

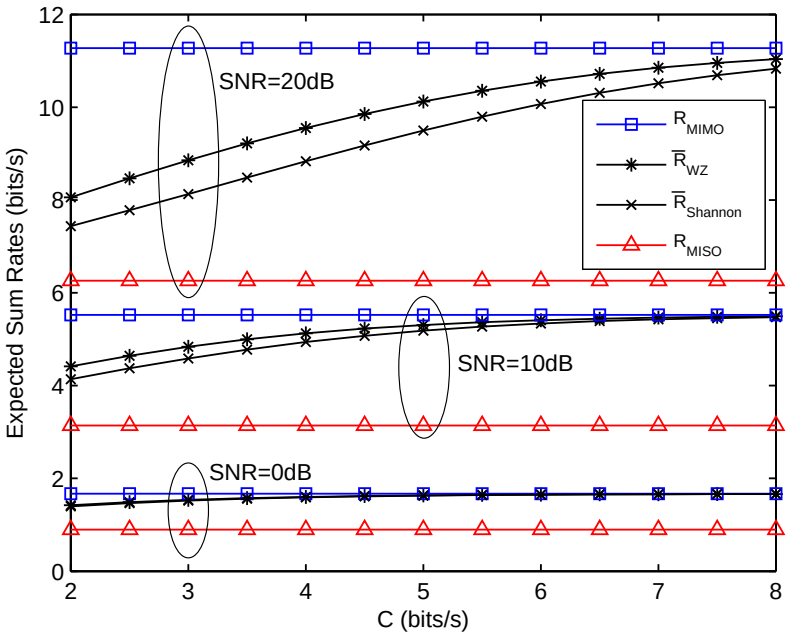

Figure 3.4: *Sum rates comparison among MIMO, MISO and virtual-MIMO systems under different SNR assumptions.*

We will now clarify the tightness of these upper bounds from an implementation perspective. It

is known that, the benefit of WZ coding is due to the assumption that the relay can compress y_{rnl} by treating y_{dnl} as the side information [10] [42]. It takes advantage of the dependence between the signals at the relay and the destination. However, our virtual-MIMO system with two antennas at the transmitter means that the signals received at the relay and the destination, i.e. y_{rnl} and y_{dnl}, are not highly correlated (Chapter 2, [69]). The low correlation will diminish the benefit from exploiting side information significantly. Hence it is quite hard for the WZ coding to approach its performance upper bound in a practical virtual-MIMO system where multiple transmit antennas are considered. As for the standard source coding technique, we employ Voronoi VQ which has the feature that the codebook is optimal in the sense of minimising average distortion. Efficient VQ enables the theoretical performance bound $\bar{R}_{\text{Shannon}}$ to be approached in practice. As shown in Figure 3.4, with C and hence R_c increasing, the bound $\bar{R}_{\text{Shannon}}$ is increasing and achieves R_{MIMO}. It is reasonable to expect that the standard source coding technique performs well in practice and can help the cooperative system to achieve almost ideal MIMO performance. Thus, since the standard source coding technique is much simpler to perform, and has a only slightly degraded rate bound which can be approached closely in practical scenarios, we choose to implement it at the relay.

3.4 System Performance Assessment

In this section, we present the throughput expressions for our cooperative virtual-MIMO system with BICM transmission and ML decoding over block fading channels. Upper bounds on the bit and block error probabilities of this system are derived as well.

3.4.1 System Throughput Analysis

Now we compute the throughput of the virtual MIMO-BICM system with ideal interleaving. To do it, we adopt the parallel-channel model in [55] to model ideal interleaving, which consists of a set of m parallel independent and memoryless binary input channels connected to the encoder output by a random switch (i.e. each channel corresponds to a position in the label of the signals of $\mathcal{X}$). For a specific $\boldsymbol{H}_n$, the conditional average mutual information (AMI) for each bit level is obtained by averaging the mutual information with respect to the switch position of the parallel channels. According to [55] and [70], with perfect CSI at the receiver, the conditional AMI for

the λth bit level is then given by,

$$\begin{aligned} I(c^{\lambda};\tilde{\boldsymbol{y}}_{nl}|\widetilde{\boldsymbol{H}}_n) &= \mathrm{H}(c^{\lambda}) - \mathrm{H}(c^{\lambda}|\tilde{\boldsymbol{y}}_{nl},\widetilde{\boldsymbol{H}}_n) \\ &= 1 - \mathrm{E}_{c^{\lambda}|\tilde{\boldsymbol{y}}_{nl},\widetilde{\boldsymbol{H}}_n}\left(\log_2 \frac{\sum_{\hat{c}^{\lambda}\in 0,1} p(\tilde{\boldsymbol{y}}_{nl}|\hat{c}^{\lambda},\widetilde{\boldsymbol{H}}_n)}{p(\tilde{\boldsymbol{y}}_{nl}|c^{\lambda},\widetilde{\boldsymbol{H}}_n)}\right), \end{aligned} \tag{3.15}$$

where $\mathrm{H}(\cdot)$ is the entropy, and

$$p(\tilde{\boldsymbol{y}}_{nl}|c^{\lambda},\widetilde{\boldsymbol{H}}_n) = \frac{1}{\#\mathcal{X}_c^{\lambda}} \sum_{\tilde{\mathbf{x}}\in\mathcal{X}_c^{\lambda}} p(\tilde{\boldsymbol{y}}_{nl}|\tilde{\mathbf{x}},\widetilde{\boldsymbol{H}}_n), \tag{3.16}$$

and $\#\mathcal{X}_c^{\lambda}$ denotes the cardinality of $\mathcal{X}_c^{\lambda}$. $p(\tilde{\boldsymbol{y}}_{nl}|\tilde{\mathbf{x}},\widetilde{\boldsymbol{H}}_n)$ is the conditional PDF, defined in (3.6). Here we implement the scaled channel to present the cooperation system, with $\tilde{\boldsymbol{y}}_{nl}$ and $\widetilde{\boldsymbol{H}}_n$ defined in (3.3) and (3.4) respectively. Thus the conditional AMI in (3.15) can be calculated as,

$$\begin{aligned} I(c^{\lambda};\tilde{\boldsymbol{y}}_{nl}|\widetilde{\boldsymbol{H}}_n) &= 1 - \underset{c^{\lambda}|\tilde{\boldsymbol{y}}_{nl},\widetilde{\boldsymbol{H}}_n}{\mathrm{E}}\left(\log_2 \frac{\sum_{\tilde{\mathbf{x}}\in\mathcal{X}} p\{\tilde{\boldsymbol{y}}_{nl}|\tilde{\mathbf{x}},\widetilde{\boldsymbol{H}}_n\}}{\sum_{\tilde{\mathbf{x}}\in\mathcal{X}_c^{\lambda}} p\{\tilde{\boldsymbol{y}}_{nl}|\tilde{\mathbf{x}},\widetilde{\boldsymbol{H}}_n\}}\right) \\ &= 1 - \underset{c^{\lambda}|\tilde{\boldsymbol{y}}_{nl},\widetilde{\boldsymbol{H}}_n}{\mathrm{E}}\left(\log_2 \frac{\sum_{\tilde{\mathbf{x}}\in\mathcal{X}} \exp\left(-\|\tilde{\boldsymbol{y}}_{nl} - \widetilde{\boldsymbol{H}}_n\tilde{\mathbf{x}}\|^2/N_0\right)}{\sum_{\tilde{\mathbf{x}}\in\mathcal{X}_c^{\lambda}} \exp\left(-\|\tilde{\boldsymbol{y}}_{nl} - \widetilde{\boldsymbol{H}}_n\tilde{\mathbf{x}}\|^2/N_0\right)}\right). \end{aligned} \tag{3.17}$$

Since block fading channels are considered between the transmitter and the receiver group throughout this chapter, we assume a fading envelope $\mathcal{H} = (\boldsymbol{H}_1, ..., \boldsymbol{H}_N)$. Assuming ideal interleaving, the channel can be considered to be ergodic [55]. The system throughput is obtained by averaging the AMI for each bit level over the fading channels, and summing the results as follows,

$$\begin{aligned} C_{\mathrm{CF}} &= \sum_{\lambda=1}^{mN_t} \underset{\boldsymbol{H}_n\in\mathcal{H}}{\mathrm{E}}\left[I(c^{\lambda};\tilde{\boldsymbol{y}}_{nl}|\widetilde{\boldsymbol{H}}_n)\right] \\ &= mN_t - \underset{\boldsymbol{H}_n\in\mathcal{H}}{\mathrm{E}}\left[\sum_{\lambda=1}^{mN_t} \underset{c^{\lambda}|\tilde{\boldsymbol{y}}_{nl},\widetilde{\boldsymbol{H}}_n}{\mathrm{E}}\left(\log_2 \frac{\sum_{\tilde{\mathbf{x}}\in\mathcal{X}} \exp\left(-\|\tilde{\boldsymbol{y}}_{nl} - \widetilde{\boldsymbol{H}}_n\tilde{\mathbf{x}}\|^2/N_0\right)}{\sum_{\tilde{\mathbf{x}}\in\mathcal{X}_c^{\lambda}} \exp\left(-\|\tilde{\boldsymbol{y}}_{nl} - \widetilde{\boldsymbol{H}}_n\tilde{\mathbf{x}}\|^2/N_0\right)}\right)\right]. \end{aligned} \tag{3.18}$$

In general, the expectation in (3.18) cannot be calculated in closed form. Thus we resort to numerical integration via the Monte Carlo method: We generate the channel coefficient $h_{in}(i \in [1, ..., 4])$ randomly according to the normalized Rayleigh distribution, and calculate the conditional AMI for each $\boldsymbol{H}_n$. The process is repeated a sufficient number of times, so that C_{CF} is obtained by averaging those AMIs.

Moreover, the system throughput C_{CF} is compared against the lower bound of corresponding MIMO system. With connected receivers, the system becomes an ideal MIMO system with a two-antenna receiver. For such a MIMO system, we have,

$$C_{\text{MIMO}} = mN_t - \mathop{\text{E}}_{\boldsymbol{H}_n \in \mathcal{H}} \left[\sum_{\lambda=1}^{mN_t} \mathop{\text{E}}_{c^\lambda | \boldsymbol{y}_{\text{mimo}}, \boldsymbol{H}_n} \left(\log_2 \frac{\sum_{\tilde{\boldsymbol{x}} \in \mathcal{X}} \exp(-\|\boldsymbol{y}_{\text{mimo}} - \boldsymbol{H}_n \tilde{\boldsymbol{x}}\|^2 / N_0)}{\sum_{\tilde{\boldsymbol{x}} \in \mathcal{X}_c^\lambda} \exp(-\|\boldsymbol{y}_{\text{mimo}} - \boldsymbol{H}_n \tilde{\boldsymbol{x}}\|^2 / N_0)} \right) \right], \quad (3.19)$$

where $\boldsymbol{y}_{\text{mimo}}$ presents the received signals at the two-antenna receiver for the MIMO system $\boldsymbol{y}_{\text{mimo}} = [y_{rnl} \quad y_{dnl}]^T$. The difference between C_{CF} and C_{MIMO} lies in the mutual information $I(c^\lambda; \tilde{\boldsymbol{y}}_{nl} | \widetilde{\boldsymbol{H}}_n)$ and $I(c^\lambda; \boldsymbol{y}_{\text{mimo}} | \boldsymbol{H}_n)$, and therefore the difference between $\widetilde{\boldsymbol{H}}_n$ and $\boldsymbol{H}_n$. For a fixed SNR, as R_c increases ($C = R_c$ due to the error-free conference link), $\bar{\sigma}_{cn}^2$ decreases to 0 from (3.7). Since the Voronoi VQ employed to perform CF cooperation has the feature that the codebook is optimal and the performance is quite close to the Shannon coding bound, we have σ_{cn}^2 decreasing to 0 as well. Then $\widetilde{\boldsymbol{H}}_n$ tends toward $\boldsymbol{H}_n$ in value from (3.4), and $\tilde{\boldsymbol{y}}_{nl} \to [y_{rnl} \; y_{dnl}]^T$ thanks to the conference link. Thus, with R_c increasing, C_{CF} is increasing and approaches almost ideal MIMO performance. In practice, when R_c is large enough, i.e. the codebook could express the constellation of $(h_{1n}x_{1nl} + h_{2n}x_{2nl})$ efficiently, the cooperative virtual-MIMO system will achieve almost ideal MIMO performance, as will be shown in Section 3.6.

3.4.2 Upper Bounds on System Error Probabilities

In this subsection, we derive an upper bound on the bit error ratio (BER) and block error ratio (BLER) of the cooperative virtual MIMO system with ML decoding. We assume ideal interleaving, and that perfect CSI is available at the receiver. Given a specific $\boldsymbol{H}_n$, we denote $P_d(d|\boldsymbol{H}_n)$ as the conditional pairwise error probability (PEP) for two codewords differing in d bits. For memoryless binary-input output-symmetric (BIOS) channels, the union upper bound on the conditional BER for linear binary convolutional codes can be expressed as [71],

$$P_b(\boldsymbol{H}_n) \leq \sum_{d=d_{\text{free}}}^{\infty} A_d \, P_d(d|\boldsymbol{H}_n), \quad (3.20)$$

where A_d denotes the sum of bit errors (the information error weight) for error events of distance d [72], which is related to the signal constellation $\mathcal{X}$ and the mapping labelling rule μ. The scalar d_{free} is the minimum free Hamming distance. The average error probability after

decoding is obtained by averaging $P_b(\boldsymbol{H}_n)$ over the fading channel matrices,

$$P_b = \underset{\boldsymbol{H}_n \in \mathcal{H}}{\mathrm{E}} \left[P_b(\boldsymbol{H}_n) \right] \leq \underset{\boldsymbol{H}_n \in \mathcal{H}}{\mathrm{E}} \left[\sum_{d=d_{\text{free}}}^{\infty} A_d P_d(d|\boldsymbol{H}_n) \right]. \tag{3.21}$$

Since the BER of a Viterbi decoder is limited to $1/2$ in practical cases [73], a much tighter upper bound could be obtained by limiting $P_b(\boldsymbol{H}_n)$ before averaging,

$$P_b \leq \underset{\boldsymbol{H}_n \in \mathcal{H}}{\mathrm{E}} \left[\min \left\{ \frac{1}{2}, \sum_{d=d_{\text{free}}}^{\infty} A_d P_d(d|\boldsymbol{H}_n) \right\} \right]. \tag{3.22}$$

Estimating the error probability therefore reduces to computing the conditional PEP.

One thing to note here is the bound (3.20) holds under the assumption that the channel is BIOS. For our case, the block fading channel and the signal constellation $\mathcal{X}$ may lead to a BICM channel which is not symmetric [74]. For instance, if 16 QAM is used for modulation, it is not necessarily true that any symbol pair with the same Hamming distance will have the same Euclidean distance. Therefore, we adopt the approach of [55] and force the BICM channel to behave as a BIOS system by using a random modulation concept. Let t denote a random variable, which independently selects, for every symbol, either Gray-labelling mapping or its complement with probability 1/2. Then, any symbol has probability 1/2 of being complemented before transmission (which occurs when $t = 1$), so that the BICM block fading channels are made symmetric. Furthermore, due to the symmetry of the channel output, the error performance does not depend on the values of the codewords, and we can safely assume that the all-zero codewords are transmitted.

When we are considering the CF cooperation and the random modulation concept, the form of the LLR defined practically in (3.5) will be changed slightly,

$$\begin{aligned} \mathcal{L}(c^\lambda | \tilde{\boldsymbol{y}}_{nl}, \widetilde{\boldsymbol{H}}_n) &= \ln \frac{\Pr\{c^\lambda = \bar{t} | \tilde{\boldsymbol{y}}_{nl}, \widetilde{\boldsymbol{H}}_n\}}{\Pr\{c^\lambda = t | \tilde{\boldsymbol{y}}_{nl}, \widetilde{\boldsymbol{H}}_n\}} = \ln \frac{\sum_{\tilde{\boldsymbol{x}} \in \mathcal{X}_{\bar{t}}^\lambda} p\{\tilde{\boldsymbol{y}}_{nl} | \tilde{\boldsymbol{x}}, \widetilde{\boldsymbol{H}}_n\}}{\sum_{\tilde{\boldsymbol{x}} \in \mathcal{X}_t^\lambda} p\{\tilde{\boldsymbol{y}}_{nl} | \tilde{\boldsymbol{x}}, \widetilde{\boldsymbol{H}}_n\}} \\ &= \ln \frac{\sum_{\tilde{\boldsymbol{x}} \in \mathcal{X}_{\bar{t}}^\lambda} \exp\left(-\|\tilde{\boldsymbol{y}}_{nl} - \widetilde{\boldsymbol{H}}_n \tilde{\boldsymbol{x}}\|^2 / N_0 \right)}{\sum_{\tilde{\boldsymbol{x}} \in \mathcal{X}_t^\lambda} \exp\left(-\|\tilde{\boldsymbol{y}}_{nl} - \widetilde{\boldsymbol{H}}_n \tilde{\boldsymbol{x}}\|^2 / N_0 \right)}, \end{aligned} \tag{3.23}$$

where $\tilde{\boldsymbol{y}}_{nl}$ and $\widetilde{\boldsymbol{H}}_n$ are defined in (3.3) and (3.4). The conditional PEP for the symmetric virtual-

MIMO BICM channels is then given by [71],

$$\begin{aligned} P_d(d|\boldsymbol{H}_n) &= \Pr\left(\sum_{j=1}^{d} \mathcal{L}_j(c^{\lambda_j}|\tilde{\boldsymbol{y}}_{nl}, \widetilde{\boldsymbol{H}}_n) > 0\right) \\ &= \Pr\left(d\ \mathcal{L}(c^{\lambda}|\tilde{\boldsymbol{y}}_{nl}, \widetilde{\boldsymbol{H}}_n) > 0\right), \end{aligned} \tag{3.24}$$

where λ_j is the bit position in the transmitted symbol's binary label which corresponds to the j^{th} equivalent binary-input transmission. Thanks to the presence of the ideal interleaver, the variables $\mathcal{L}_j(c^{\lambda_j}|\tilde{\boldsymbol{y}}_{nl}, \widetilde{\boldsymbol{H}}_n)$ can be considered i.i.d.. Hence, when we are considering the log likelihood ratio statistics at a single instant in time, we drop the subscript on $\mathcal{L}(c^{\lambda}|\tilde{\boldsymbol{y}}_{nl}, \widetilde{\boldsymbol{H}}_n)$. Since $\mathcal{L}(c^{\lambda}|\tilde{\boldsymbol{y}}_{nl}, \widetilde{\boldsymbol{H}}_n)$ has a complicated distribution, $P_d(d|\boldsymbol{H}_n)$ in (3.24) is difficult to calculate. As shown in [71] and [75] , the tail of the PDF of $\mathcal{L}(c^{\lambda}|\tilde{\boldsymbol{y}}_{nl}, \widetilde{\boldsymbol{H}}_n)$ at the output of the BICM channel is very close to the corresponding output of a binary-input AWGN channel. Therefore, the method of analysing the BER performance of the AWGN channel, called the Gaussian approximation (GA), is a simple and accurate way to approximate $P_d(d|\boldsymbol{H}_n)$. Using the GA, we obtain:

$$P_d(d|\boldsymbol{H}_n) \approx Q\left(\sqrt{-2dK_{\mathcal{L}}(\hat{s})}\right), \tag{3.25}$$

where $Q(\cdot)$ is the Q-function, and $K_{\mathcal{L}}(s)$ is the cumulant generating function of $\mathcal{L}(c^{\lambda}|\tilde{\boldsymbol{y}}_{nl}, \widetilde{\boldsymbol{H}}_n)$,

$$\begin{aligned} &K_{\mathcal{L}}(s) = \log \underset{\boldsymbol{x},\lambda,t,N_0|\boldsymbol{H}_n}{\mathrm{E}}\left[\exp\left(s\ \mathcal{L}(c^{\lambda}|\tilde{\boldsymbol{y}}_{nl}, \widetilde{\boldsymbol{H}}_n)\right)\right] \\ &= \log \underset{\boldsymbol{x},\lambda,t,N_0|\boldsymbol{H}_n}{\mathrm{E}}\left[\left(\frac{\sum_{\tilde{\boldsymbol{x}}\in\mathcal{X}_{\hat{t}}^{\lambda}} \exp\left(-\|\tilde{\boldsymbol{y}}_{nl} - \widetilde{\boldsymbol{H}}_n\tilde{\boldsymbol{x}}\|^2/N_0\right)}{\sum_{\tilde{\boldsymbol{x}}\in\mathcal{X}_{t}^{\lambda}} \exp\left(-\|\tilde{\boldsymbol{y}}_{nl} - \widetilde{\boldsymbol{H}}_n\tilde{\boldsymbol{x}}\|^2/N_0\right)}\right)^{s}\right] \\ &\approx \log \underset{\boldsymbol{x},\lambda,t,N_0|\boldsymbol{H}_n}{\mathrm{E}}\left(\exp\left[\left(\min_{\tilde{\boldsymbol{x}}\in\mathcal{X}_{t}^{\lambda}} \|\tilde{\boldsymbol{y}}_{nl} - \widetilde{\boldsymbol{H}}_n\tilde{\boldsymbol{x}}\|^2 - \min_{\tilde{\boldsymbol{x}}\in\mathcal{X}_{\hat{t}}^{\lambda}} \|\tilde{\boldsymbol{y}}_{nl} - \widetilde{\boldsymbol{H}}_n\tilde{\boldsymbol{x}}\|^2\right)\frac{s}{N_0}\right]\right). \end{aligned} \tag{3.26}$$

In the third step, we employ the approximate LLR to avoid LLR computations yielding infinity, especially when SNR is high. For BIOS channels, symmetry dictates that the saddlepoint $\hat{s}$ in (3.25) is placed at $\hat{s} = 1/2$ [71]. Substituting (3.26) into (3.25), and then into (3.22) gives us an upper bound on the system BER.

Furthermore, we denote the system BLER as P_{block}. For a given channel $\boldsymbol{H}_n$, the conditional P_{block} for a block of L decoded bits can be expressed as:

$$P_{\text{block}}(\boldsymbol{H}_n) = 1 - (1 - P_b(\boldsymbol{H}_n))^L, \tag{3.27}$$

where $P_b(\boldsymbol{H}_n)$ is given by (3.20). We limit the union bound of $P_b(\boldsymbol{H}_n)$ before averaging over the fading channels, so that a tighter upper bound for the block error probability is obtained,

$$\begin{aligned} P_{\text{block}} &= \mathrm{E}_{\boldsymbol{H}_n \in \mathcal{H}} \left[P_{\text{block}}(\boldsymbol{H}_n) \right] \\ &\leq 1 - \mathrm{E}_{\boldsymbol{H}_n \in \mathcal{H}} \left[\left(1 - \min \left\{ \frac{1}{2}, \sum_{d=d_{\text{free}}}^{\infty} A_d P_d(d|\boldsymbol{H}_n) \right\} \right)^L \right]. \end{aligned} \tag{3.28}$$

With using the GA to approximate $P_d(d|\boldsymbol{H}_n)$, i.e. inserting (3.25) in (3.28), we will obtain an upper bound on the system BLER.

In order to compute the expectations in (3.22) and (3.28), because of the function $\min\{1/2, \cdot\}$, we have to resort to the Monte Carlo method in practice. But the analytical expressions are very useful since they provide insights into the asymptotic behavior of the system error probabilities in block fading channels. And the upper bounds computed using the GA are very tight to the simulation results of the BER and BLER performance, as will be seen in Section 3.6.

3.5 Impact of a Non-ideal Cooperation Link

Since the relay and destination are closely spaced, an ideal, error-free, one-shot conference or cooperation link is assumed between them to enable CF, as described in Section 3.2. The ideal conference link may be realized via an orthogonal channel to the transmitter array with sufficiently long coding blocks. However, in practice, if the link is not ideal, or the coding blocks are not long enough, cooperation may suffer from fading channel and noise effects. Now for practical considerations, we illustrate the impact of a non-ideal cooperation link on the system performance.

3.5.1 Outage Probability of the Non-ideal Link

As we assume the relay is close to the destination, it is reasonable to expect a line-of-sight link existing between them. It is realistic to model this non-ideal link as a block fading channel with a Rician distribution. Then the destination receives the symbol from the relay,

$$y'_{rnl} + \frac{h^*_{rdn}}{|h_{rdn}|^2} w_{3nl} = y_{rnl} + w_{cnl} + \frac{h^*_{rdn}}{|h_{rdn}|^2} w_{3nl}, \tag{3.29}$$

where $w_{3nl} \sim \mathcal{CN}(0, N_0)$ and h_{rdn} denotes the channel coefficient from the relay to the destination. For Rician fading channels, h_{rdn} can be decomposed into the sum of a deterministic (line-of-sight) component and a variable component [76], i.e.,

$$h_{rdn} = \sqrt{\mathrm{E}[|h_{rdn}|^2]\frac{K_{rd}}{1+K_{rd}}} + \sqrt{\mathrm{E}[|h_{rdn}|^2]\frac{1}{1+K_{rd}}}\,\tilde{h}_{rdn}, \tag{3.30}$$

where $\tilde{h}_{rdn}$ is i.i.d. complex Gaussian random variable with zero mean and unit variance. The notation K_{rd} represents the Rician factor. The cumulative distribution function (CDF) of the instantaneous $|h_{rdn}|^2$ [77] is given by:

$$F(x) \triangleq \Pr\{|h_{rdn}|^2 < x\} = 1 - Q_1\left(\sqrt{2K_{rd}}, \sqrt{\frac{2(1+K_{rd})x}{\mathrm{E}[|h_{rdn}|^2]}}\right), \tag{3.31}$$

where $Q_1(\cdot\,,\cdot\,)$ is the first-order Marcum Q function. Suppose that the channel powers $\mathrm{E}[|h_{in}|^2]$ and $\mathrm{E}[|h_{rdn}|^2]$ are proportional to $1/d_{in}^{3.32}$ and $1/d_{rdn}^{3.32}$ respectively, where d_{in} is the distance from the transmitter to the receiver cluster and d_{rdn} is the distance of the relay-destination link. Since the two receivers are close together, the case of interest is when $d_{in} > d_{rdn}$. Therefore we have $\mathrm{E}[|h_{rdn}|^2] = 10\mathrm{E}[|h_{in}|^2] = 10$ dB for $d_{rdn} = d_{in}/2$, and $\mathrm{E}[|h_{rdn}|^2] = 20$ dB for $d_{rdn} = d_{in}/4$.

In the above sections, we assumed a fixed source coding rate R_c at the relay. The ideal conference link could support this rate, so that the link capacity C is equal to R_c. But for the non-ideal conference link, reliable communication can be achieved when the channel gain is strong enough to support R_c, and outage occurs otherwise. We define the data rate of the non-ideal link as C'. Suppose we still use rate R_c to quantize and transmit the data at the relay. If $C' < R_c$, i.e. the channel realization h_{rd} is such that $\log(1 + |h_{rdn}|^2\mathrm{E}[|y'_{rnl}|^2]/N_0) < R_c$, the link is in outage. The outage probability ϵ of the non-ideal cooperation link can be calculated as,

$$\epsilon = \Pr\left\{C' < R_c\right\} = \Pr\left\{\log\left(1 + |h_{rdn}|^2\frac{\mathrm{E}[|y_{rnl}|^2] + \sigma_{cn}^2}{N_0}\right) < R_c\right\}, \tag{3.32}$$

where $\mathrm{E}[|y_{rnl}|^2] = N_0 + \frac{1}{2}|h_{1n}|^2 + \frac{1}{2}|h_{2n}|^2$. Since the relay transmits the data at the desired rate R_c but with outage probability ϵ, the compression noise variance σ_{cn}^2 is lower bounded by

$\mathrm{E}[|y_{rnl}|^2]/(2^{R_c}-1)$ according to (3.7). Then we obtain,

$$\begin{aligned}\epsilon &\leq \Pr\left\{\log\left(1+|h_{rdn}|^2\frac{\mathrm{E}[|y_{rnl}|^2]}{N_0}\frac{2^{R_c}}{2^{R_c}-1}\right)<R_c\right\}\\ &= \Pr\left\{|h_{rdn}|^2<\frac{N_0}{\mathrm{E}[|y_{rnl}|^2]}\frac{(2^{R_c}-1)^2}{2^{R_c}}\right\}\\ &= F\left(\frac{N_0}{\mathrm{E}[|y_{rnl}|^2]}\frac{(2^{R_c}-1)^2}{2^{R_c}}\right).\end{aligned} \tag{3.33}$$

Inserting (3.31) in (3.33), we will get an upper bound of ϵ. For $R_c = 4$ bits/sample and 7

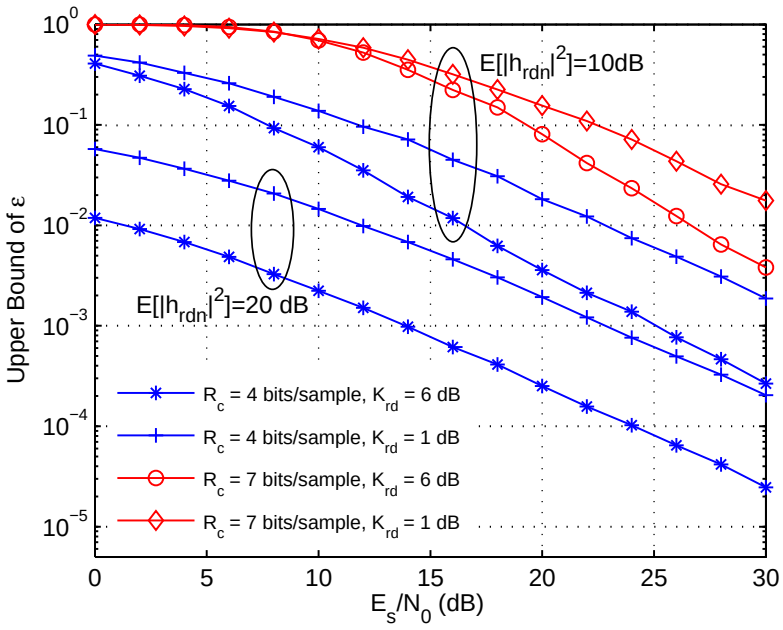

Figure 3.5: *Upper bounds of the outage probability ϵ for non-ideal cooperation links.*

bits/sample, the upper bounds of ϵ which are averaged over $|h_{1n}|^2$ and $|h_{2n}|^2$ are shown in Figure 3.5. When we consider $R_c = 4$ bits/sample, it can be seen that, with either the SNR or the Rician factor increasing, the upper bound of ϵ is decreasing. A higher $\mathrm{E}[|h_{rdn}|^2]$, i.e. a shorter d_{rdn} will result in a lower outage probability as well. The corresponding impact of the non-ideal cooperation link on the system performance will then decrease. When $R_c = 7$ bits/sample, the upper bounds of ϵ are larger than that for $R_c = 4$ bits/sample, as outages occur more frequently when the cooperation link tries to support a higher R_c.

The upper bound of ϵ is calculated based on the lower bound of the compression noise variance $\bar{\sigma}^2_{cn}$. We employ Voronoi VQ which has the feature that the codebook is optimal in the sense of

minimising average distortion. This efficient VQ enables the theoretical upper bound of ϵ to be approached in practice. Since the relay and the destination are assumed to be closely spaced, it is reasonable to expect a high Rician factor or a higher $\mathrm{E}[|h_{rdn}|^2]$ than 20 dB. Thus, the outage probability ϵ will be quite small in practice.

3.5.2 A channel-aware adaptive CF scheme

The basic motivation of the channel-aware adaptive CF scheme is the fact that fixed-rate cooperation cannot adapt well to the non-ideal conference link. When ϵ is high, the non-ideal link will affect the overall system performance significantly. The channel-aware adaptive CF scheme, which requires the relay to be aware of the quality of the cooperation link, may help the relay to choose different source coding rates according to different realisations of h_{rdn}, so that the compression could always adapt the quantization level to meet the data rate C'.

The channel-aware requirement can be realized via sharing CSI between the relay and destination, once the conference link is formed between them. Take $R_c = 7$, 5, 3 and 0 bits/sample as an example. We present the switching criterion for the adaptive CF scheme,

$$R_c = \begin{cases} 7 \text{ bits/sample}, & \text{if } C' \geq 7 \text{ bits/sample}; \\ 5 \text{ bits/sample}, & \text{if } 5 \leq C' \leq 7 \text{ bits/sample}; \\ 3 \text{ bits/sample}, & \text{if } 3 \leq C' \leq 5 \text{ bits/sample}; \\ 0 \text{ bits/sample } (\text{MISO decoding at the destination}), & \text{if } C' < 3 \text{ bits/sample}. \end{cases} \tag{3.34}$$

For a given channel condition h_{rdn}, if C' is expected to be equal to or larger than 7 bits/sample, the outage probability will be zero and the conference link becomes ideal. If $C' < 7$ bits/sample, i.e. $|h_{rdn}|^2 < N_0(2^7-1)^2/2^7/\mathrm{E}[|y_{rnl}|^2]$ according to (3.33), in order to avoid outage, the relay will switch back to a lower source coding rate, e.g. 5 or 3 bits/sample. If 3 bits/sample is still too large for the cooperation link to support, the relay will then keep silent. The channel-aware adaptive CF scheme is not limited to switching among the four rates we mentioned. It can be extended to multiple source coding rates, and applied to various modulation types.

For ill-conditioned conference links, the relay switches to use lower R_c, in order to guarantee reliable communications on these links. Even though the signals experience a higher compression noise power, this channel-aware adaptive CF scheme helps the destination to receive the

signals y'_{rnl} with higher probability than for a fixed R_c. The impact of the non-ideal conference links is therefore due to the effect from lower source coding rates and higher compression noise. Thus the channel-aware adaptive CF scheme diminishes the negative and unexpected effects of the non-ideal conference link, when the relay can access the conference link CSI.

Since the relay and the destination are assumed to be closely spaced, it is reasonable to expect a large Rician factor or a high $\mathrm{E}[|h_{rdn}|^2]$. The outage probability ϵ is likely to be very small in practice. Additionally, the corresponding impact of the non-ideal link on the overall system performance is diminished by the proposed channel-aware adaptive CF scheme. Therefore, we can expect that the impact of the non-ideal cooperation link is quite slight, as will be shown in Section 3.6.

3.6 Numerical Results

In this section, we present the error performance of the cooperative virtual-MIMO-BICM ($N_t = N_r = 2$) system. At the transmitter, a binary convolutional code is assumed with constraint length 7 and generator polynomials $[133, 171]_{\text{octal}}$. The corresponding code rate $R_b = 1/2$ and the minimum Hamming distance $d_{\text{free}} = 10$. Gray-labeled QPSK and 16QAM modulations are considered. The channels between the transmitter and receivers are assumed to be i.i.d normalized block Rayleigh fading, with 10^5 fading blocks and each block has 200 consecutive symbol periods. In addition, an error-free conference link is assumed between the relay and the destination. The destination performs joint ML demodulation and employs soft-input Viterbi decoding. The simulation results are obtained using the Monte Carlo method, and we plot error ratios against the information bit SNR, i.e E_b/N_0, with the total transmitted power E_s normalized to unity.

The BLER performance of the cooperative virtual-MIMO system with QPSK mapping, under various fixed source coding rates, is shown in Figure 3.6. Because of the error-free conference link, the link capacity $C = R_c$. The BLERs are compared against the lower bound of the corresponding MIMO system, and the non-cooperative MISO system. The BLER upper bounds (UBs) computed using the GA are also shown in this figure. To perform CF cooperation, the Voronoi VQ whose codebook is optimal in the sense of minimising average distortion is implemented. Figure 3.6 shows that, with help from the relay, the system always performs better than the MISO system, as the CF protocol always provides a gain over direct transmission. As R_c

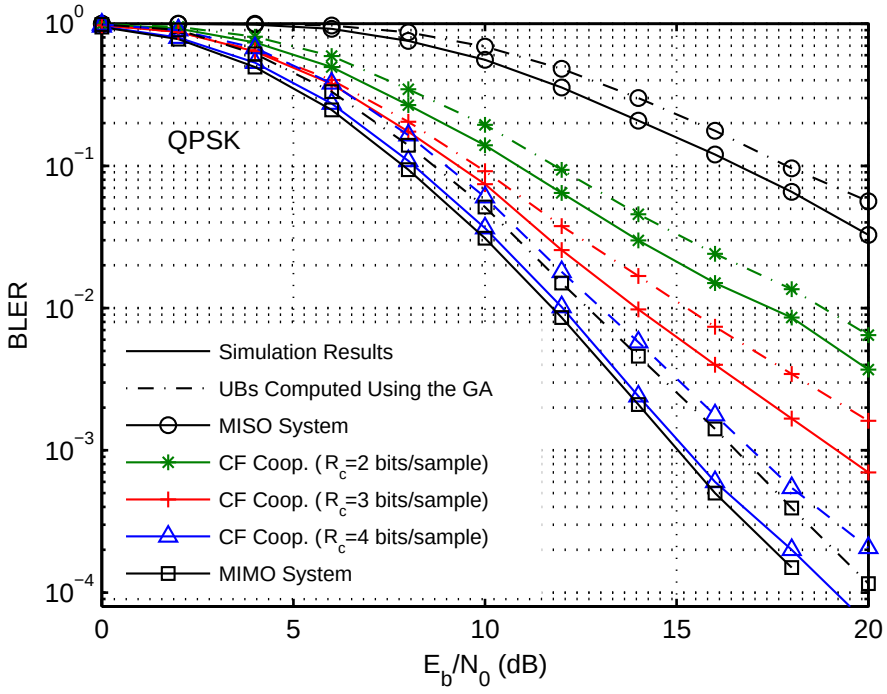

Figure 3.6: *Simulation results and UBs on the BLER of the cooperative virtual-MIMO system with QPSK mapping and ML receiver over block Rayleigh fading channels.*

increases beyond 3 bits/sample, both UBs and the simulation results decrease and approach the ideal MIMO system performance. The UBs match well to the simulation results and provide good insights into the BLER behaviour. When $R_c = 4$ bits/sample, the BLER of CF cooperation performs very close to the ideal MIMO system. This means that the helping relay enables the proposed single-antenna system to achieve MIMO performance.

Moreover, similar to Figure 3.6, Figure 3.7 also presents the system BLER performance, but for 16QAM modulation. As its constellation size is larger than that of QPSK, higher source coding rates are considered. The simulation results of BLER is also very well approximated by the upper bound, for all considered quantization rates. It is obvious that the BLER of the CF cooperation performs closer to the MIMO system with larger value of R_c, since the corresponding compression noise variance reduces. Compared with $R_c = 4$ bits/sample for QPSK, the system with 16QAM mapping requires $R_c = 7$ bits/sample to approach the ideal MIMO performance.

In Figure 3.8, we demonstrate the system throughput of the CF cooperation and the corresponding MIMO system using numerical integration to evaluate (3.18) and (3.19), respectively.

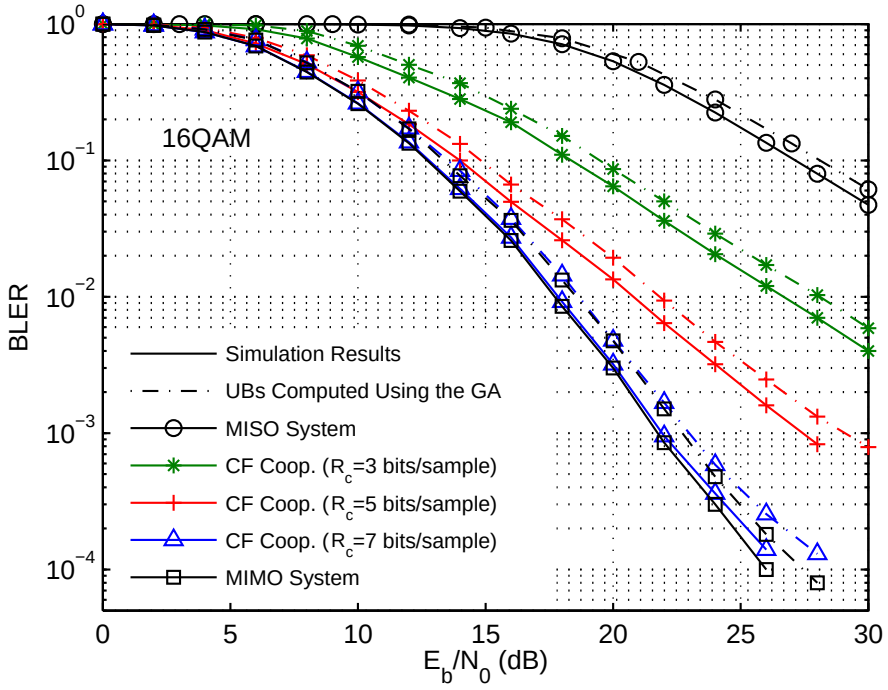

Figure 3.7: *Simulation results and UBs on the BLER of the cooperative virtual-MIMO system with 16QAM mapping and ML receiver over block Rayleigh fading channels.*

Figure 3.8 shows the results for both QPSK and 16QAM mappings. In accordance with Figure 3.6 and Figure 3.7, quantization rates 2, 3, 4 bits/sample are considered for QPSK mapping, and 3, 5, 7 bits/sample for 16QAM mapping. We can see that as the E_b/N_0 increases, the system throughputs of the CF cooperation for both QPSK and 16QAM mappings reach a limit of mN_t bits/s. As indicated in Section 3.4.1, the gap between the CF and MIMO curves becomes smaller as R_c increases. Choosing $R_c = 4$ bits/sample for QPSK mapping, and $R_c = 7$ bits/sample for 16QAM mapping, will result in the cooperative system achieving close to the ideal MIMO throughput.

Furthermore, in Figure 3.9, we compare the BER results of the CF cooperation against the performance of the system with Shannon coding bound. According to equation (3.2), the compression noise w_{cnl} is considered for this kind of system, with the Shannon coding bound of the variance calculated via equation (3.7). Since a large value of R_c will result in $\bar{\sigma}^2_{cn}$ approaching 0 so that the Shannon coding bound gives ideal MIMO performance, smaller source coding rates are considered, i.e. 3 bits/sample for QPSK mapping and 6 bits/sample for 16QAM mapping. We can see that the Shannon coding bound provides a lower bound and good insight into the

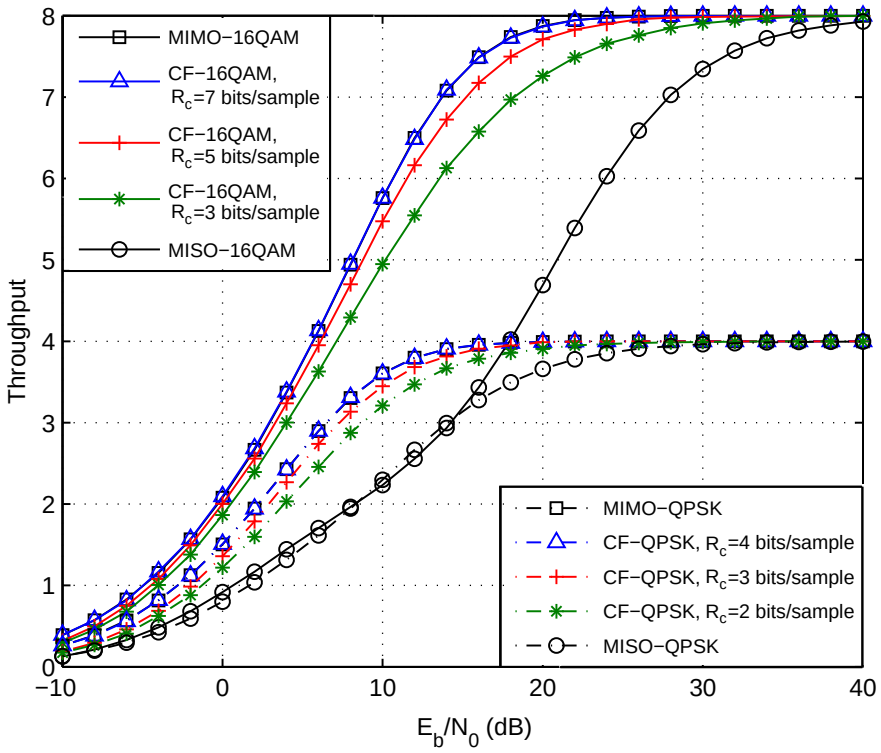

Figure 3.8: *Throughput of the cooperative virtual-MIMO system with ML receiver over block Rayleigh fading channels. (Solid curves correspond to 16QAM mapping, while dash-dotted curves correspond to QPSK mapping.)*

BER behaviour of the CF cooperation system. The system with Voronoi VQ at the relay obtains performance which is close to the Shannon coding bound.

To illustrate the benefit of CF cooperation in this virtual-MIMO system, we compare it with the Alamouti STBC based DF scheme in Figure 3.10. As discussed in Section 3.3, the spectral efficiency of the Alamouti DF scheme is only one-half of that in our CF cooperative system. To make a fair comparison, we consider 16QAM modulation for the Alamouti DF scheme, compared to QPSK modulation for CF, since both of them allow a spectral efficiency of 2 bits/s/Hz. Also, the CF scheme with 16QAM and the Alamouti DF with 256QAM are compared. As shown in Figure 3.10, only at high E_b/N_0, the Alamouti DF can achieve similar error ratios comparable to the CF scheme which uses $R_c = 2$ bits/sample for QPSK and $R_c = 4$ bits/sample for 16QAM. Specifically, for a target BLER of 10^{-2}, the CF scheme using a reasonable R_c, i.e. $R_c \geq 2$ bits/sample for QPSK and $R_c \geq 4$ bits/sample for 16QAM, is expected to perform much better than the Alamouti DF scheme.

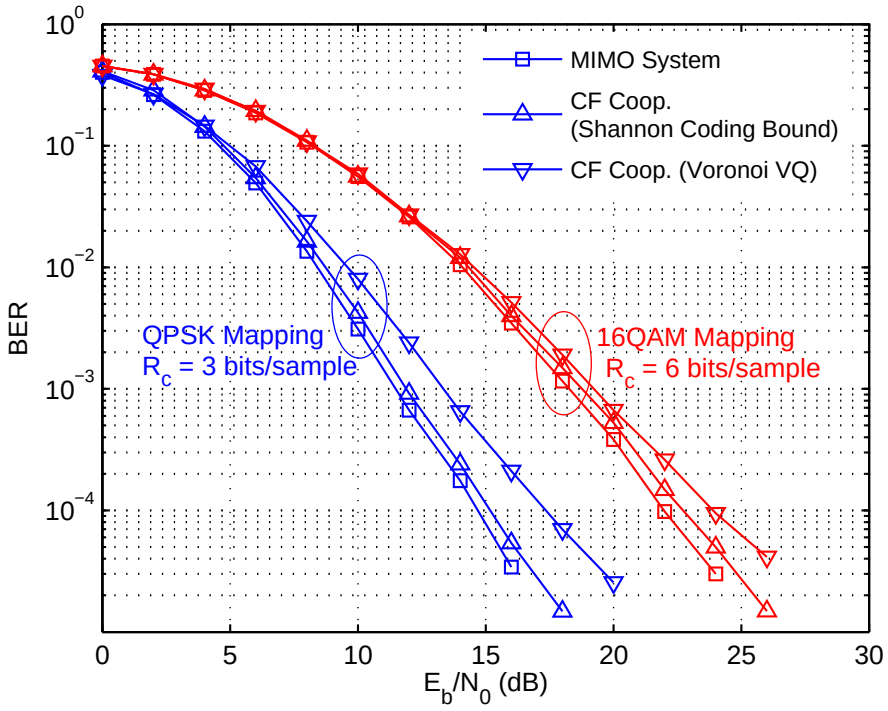

Figure 3.9: *BER comparison between the cooperative virtual-MIMO system and the system with Shannon coding bound. (QPSK and 16QAM mappings are considered.)*

All the above analytical and simulation results are based on an assumption that an error-free conference link exists between the relay and the destination. In accordance with Section 3.5, the impacts of non-ideal cooperation link are shown in Figure 3.11 and Figure 3.12, where a Rician fading channel model with $\mathrm{E}[|h_{rd}|^2] = 10$ dB is assumed on this link. Note that, when we consider the non-ideal cooperation link, the received symbol at the destination from the relay is given by (3.29). Then the degradation factor η_n previously defined in (3.4) will be changed to $N_0/(N_0 + \sigma_{cn}^2 + \frac{N_0}{|h_{rdn}|^2})$. We implement the channel-aware adaptive CF cooperation at the relay. For 16QAM mapping, $R_c = 7, 5, 3, 0$ bits/sample are chosen as switching candidates, as illustrated in (3.34). For QPSK mapping, $R_c = 4, 3, 2, 0$ bits/sample are selected. A fixed-rate CF case with 7 bits/sample for 16QAM and $R_c = 4$ bits/sample for QPSK, is given for comparison in Figure 3.11. If the fixed rates cannot be supported on some cooperation channels, the destination could only use MISO decoding. Figure 3.11 shows that, when the Rician factor K_{rd} = 1 dB, for both 16QAM and QPSK, the BLER performance of the channel-aware adaptive CF system will be impaired slightly compared to the ideal case. That is because the relay sometimes switches back to lower source coding rates or keeps silent to match the

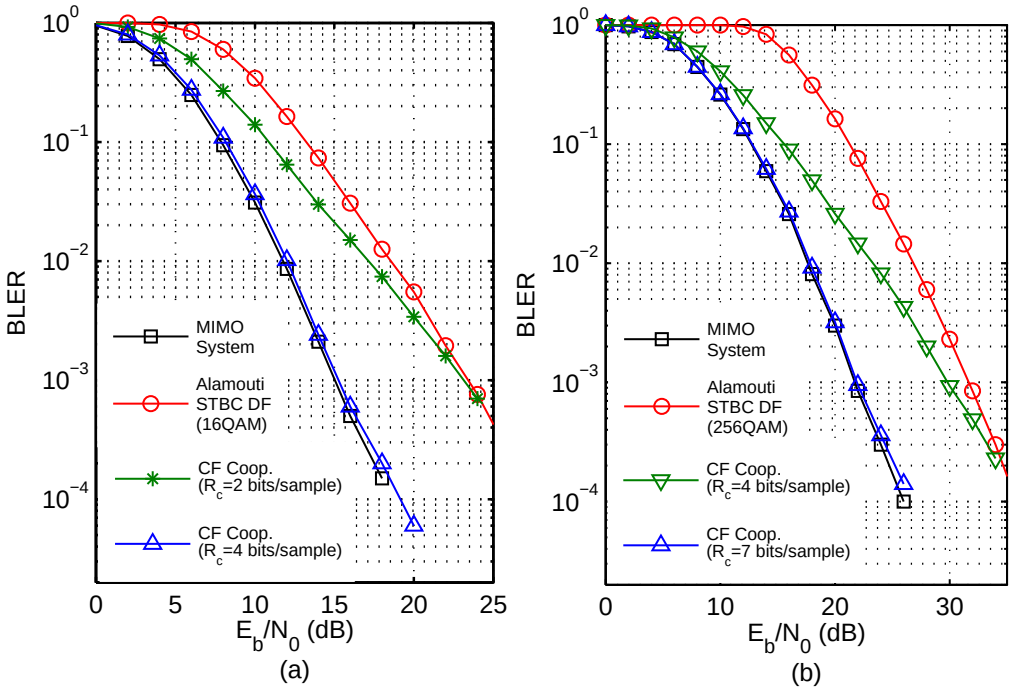

Figure 3.10: *BLER comparison for same spectral efficiency between the CF cooperation scheme and the Alamouti STBC-based DF scheme. (CF with QPSK and Alamouti DF with 16QAM are compared in (a), while CF with 16QAM and Alamouti DF with 256QAM are considered in (b).)*

cooperation channel conditions, as shown in Figure 3.12. The overall system performance will then be affected by the increased compression noise power. But the adaptive CF scheme offers a great improvement compared to the fixed-rate case, e.g. a performance gap of 1.8 dB for QPSK and 3 dB for 16QAM at BLER of 10^{-2}. Furthermore, for K_{rd} = 6 dB, i.e. the cooperation channels are stronger, the system BLER with non-ideal conference link performs almost the same as the case with an ideal link. It is obvious that the probability of staying at the high source coding rates is increasing as K_{rd} increases. Since the receivers are assumed to be close together in the virtual-MIMO system, it is appropriate to expect a high Rician factor or a higher $\mathrm{E}[|h_{rdn}|^2]$ than 10 dB. With using the channel-aware adaptive CF scheme at the relay, the impact of the non-ideal cooperation link is likely to be very small in practice.

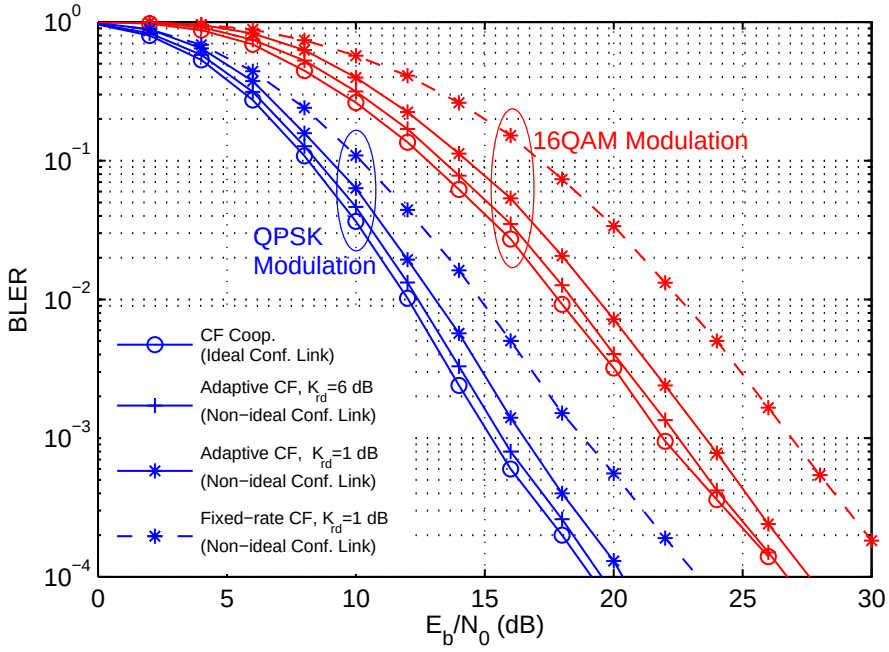

Figure 3.11: *BLER comparison of the ideal and non-ideal fading conference links. (Rician fading channel with $E[|h_{rdn}|^2] = 10$ dB is considered for the non-ideal case; A fixed-rate CF case with R_c= 7 bits/sample for 16QAM and R_c= 4 bits/sample for QPSK, is given for comparison.)*

3.7 Conclusions

This chapter presented a practical virtual-MIMO system that implemented BICM transmission and CF cooperation. To demonstrate the achievable cooperation gain, we started with a simple configuration that a single two-antenna transmitter sending information to two closely spaced single-antenna receivers. Evaluating performance bounds for virtual-MIMO systems, it was found that there was not a huge advantage from the WZ coding compared to standard source coding techniques. In addition, the low correlation between the signals received at the relay and the destination would diminish the benefit of the WZ coding. So standard source coding techniques are studied here for application to virtual MIMO systems.

The system throughput and upper bounds on the system error probabilities were derived in this chapter. It was shown that upper bounds computed using the GA matched well to the simulation results and provided good insights into the error behaviour of CF cooperation. With Voronoi VQ at the relay, $R_c = 4$ bits/sample for QPSK mapping, and 7 bits/sample for 16QAM, would result in a cooperative system achieving almost ideal MIMO performance. To illustrate the benefit of

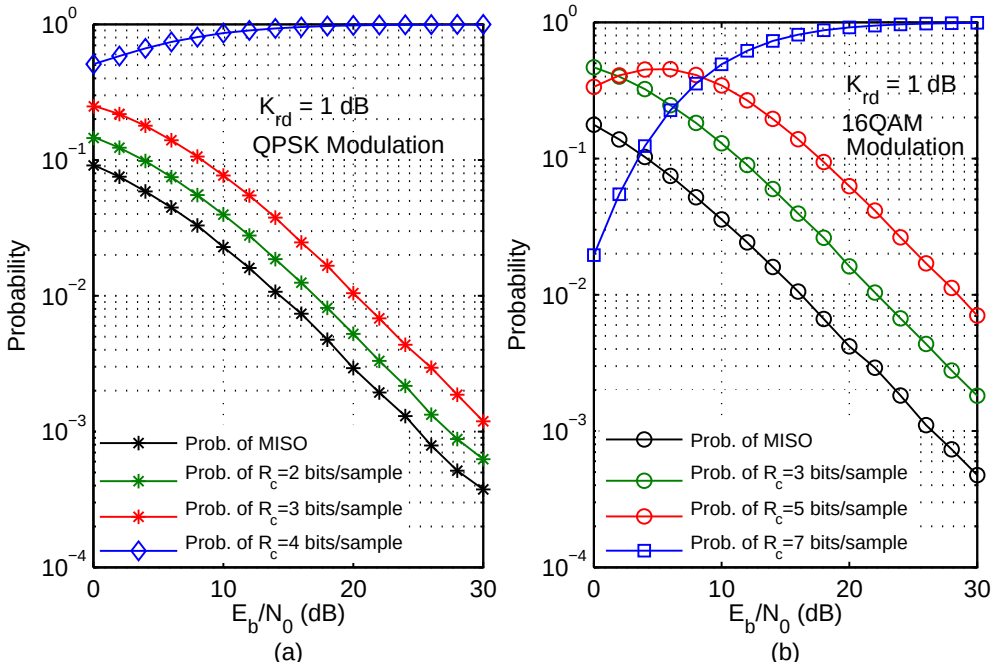

Figure 3.12: *Probabilities of choosing different source coding rates for the channel-aware adaptive CF scheme, under non-ideal fading conference links with $K_{rd} = 1$ dB and $E[|h_{rdn}|^2] = 10$ dB. (QPSK mapping is considered in (a), while 16QAM is considered in (b).)*

CF cooperation in virtual-MIMO systems, we also compared it with a pure distributed diversity technique, i.e. the well-known Alamouti STBC based DF scheme. For a target BLER of 10^{-2}, the CF scheme using a reasonable source coding rate, i.e. $R_c \geq 2$ bits/sample for QPSK and $R_c \geq 4$ bits/sample for 16QAM, provided a significant improvements over the Alamouti DF scheme.

Furthermore, from practical considerations, we also investigated the outage probability of the non-ideal cooperation link, modelled as Rician fading. To weaken its impact on the overall system performance, we proposed the channel-aware adaptive CF scheme. Then the relay could always adapt its quantization level to match the data rate on the non-ideal link. It was shown that, considering the short-range communication and using the proposed scheme, the impact of the non-ideal cooperation link was too slight to impair the system performance significantly.

The system we presented in this chapter showed that the CF cooperation using standard source coding could enable the virtual-MIMO system to achieve almost ideal 2×2 MIMO performance. The principles are not limited to this specific system: It can be applied to any virtual-

MIMO configuration with more antennas or more receiver nodes. By extending to a wide range of applications, the virtual-MIMO system with CF cooperation is therefore particularly valuable and attractive to enable single-antenna user devices to obtain the benefits of MIMO decoding.

To enhance the practicality of the virtual-MIMO system, an efficient source coding technique at the relay will be designed in next chapter. The effects of carrier frequency offsets and how to overcome them will also be illustrated.

Chapter 4
Practical Design and Sensitivity Analysis of CF Cooperation

The virtual MIMO wireless system is an alternative to a point-to-point MIMO system, when a receiver is not equipped with multiple antennas due to size and cost limitations. Receiver-side cooperation using the CF protocol is used to realize effective MIMO detection capability. In Chapter 3, we were concentrating on the system performance assessment, including a comparison between the standard source coding and Wyner-Ziv coding technique at the relay, and an impact analysis of a non-ideal cooperation link. But only an optimal vector quantization (VQ), i.e. the Voronoi VQ, was considered.

It is evident that the practicality of CF cooperation will be greatly enhanced if an efficient source coding technique can be used at the relay. It is even more desirable that CF cooperation should not be unduly sensitive to carrier frequency offsets (CFOs). This chapter presents a practical study of these two issues. Firstly, codebook designs of the Voronoi VQ and the tree-structure vector quantization (TSVQ) to enable CF cooperation at the relay are described. A comparison in terms of the codebook design complexity and encoding complexity is analyzed. It is shown that the TSVQ is much simpler to design and operate, and can achieve a favourable performance-complexity tradeoff. Furthermore, this chapter demonstrates that CFO can lead to significant performance degradation for the virtual MIMO system. To overcome it, it is proposed to maintain clock synchronization and jointly estimate the CFO between the relay and the destination. This approach is shown to provide a significant performance improvement.

The chapter is organized as follows: Section 4.2 specifies the system model of the cooperative virtual-MIMO system. Codebook design methods and the corresponding complexity analyses are investigated in Section 4.3. The effects of CFO and how to overcome them are illustrated in Section 4.4. Section 4.5 shows the simulation results, and Section 4.6 concludes the chapter.

4.1 Introduction

As mentioned in Chapter 3, the benefits of the MIMO system have encouraged extensive research on a virtual MIMO system where one remote multi-antenna transmitter sends information to several closely spaced single-antenna receivers. When the transmitter does not have perfect CSI for the wireless link to each receiver, which is a common scenario in practical situations, single-antenna receivers can work together to form a virtual antenna array and reap some of the performance benefits of MIMO systems [8] [14]. The idea of receiver-side local cooperation is attractive for wireless networks since a wireless receiver may not have multiple antennas due to size and cost limitations.

Many of the techniques developed for MIMO systems can be extended to be used in this virtual-MIMO system. For example, we also implement the BICM technique [55], which introduces a spatial and temporal bit interleaver into the transmitter, to provide FEC and improve system performance. But unlike point-to-point MIMO systems, we need to perform cooperation among the receivers. As for the cooperation protocol, since the relays get closer to the destination in our scenario, it has been shown in Chapter 3 that, compared to AF and DF, the CF protocol provides superior performance and therefore serves as the best candidate for this system. A virtual-MIMO system with CF cooperation is introduced in [5], but only the theoretical achievable cooperative capacity is analysed. Paper [11] and Chapter 3 of this thesis concentrated on the performance assessment of the virtual-MIMO system, including the comparison between the standard source coding and Wyner-Ziv coding technique at the relay, and an impact analysis for a non-ideal cooperation link. But only the optimal VQ, i.e. the Voronoi VQ, was considered.

Many algorithms have been developed to perform vector quantization, which can be divided into two kinds, unstructured VQ and structured VQ [67]. The codebook generated by the Voronoi VQ is unstructured, and is optimal in the sense of minimising average distortion. But the Voronoi VQ requires an exhaustive search algorithm and implies a high computational complexity. The structured VQs with structured partitions or reproduction codebooks are proposed to reduce the complexities. Many of these techniques are discussed in [66] and [78], such as the lattice VQ [79], shape-gain VQ [80], block-constrained VQ [81], and tree-structure VQ [82]. It is reported in [67] that, when taking both performance and complexity into account, tree-structure VQ (TSVQ) is a very competitive VQ method. TSVQ can also be realized in two main forms: binary TSVQ and multistage TSVQ [66]. Even though TSVQ a well-known compression technique, we apply it to a new problem: Design the codebook at the relay to reduce

the complexity and enhance the practicality of CF cooperation. To the best of our knowledge, it is the first time that TSVQ is applied to digital modulation signals.

Another major distinction in the virtual-MIMO system compared to the traditional MIMO case is that cooperating antennas are running with different oscillator frequencies. For MIMO systems, all the antennas at the transmitter are fed with the same clock, and the same holds for the receiver side. Carrier frequency offset (CFO), which is caused by oscillator mismatch between the transmitter and the receiver, can be estimated and compensated at the receiver in MIMO systems. The MIMO system performance will therefore not be severely degraded by CFO. However, for the virtual-MIMO system, receiver-side cooperating antennas need to estimate and compensate their CFOs independently. Their different residual CFOs will result in interblock interference and distort the correlation properties of the signals received at the destination, so that the system performance maybe impaired significantly.

Estimation of CFO in a MIMO system has been investigated in the literature [83–89]. The methods in [83–85] are pilot aided, and they require an additional overhead of symbols. Chogho and Swami [83] and McKeown et al. [84] directly measure the phase shift of pilot sequences to estimate the CFO, whereas Sun et al. [85] designed pilot symbols for CFO estimation and incorporated this CFO estimation into the expectation-maximization (EM) iterative receiver. Yao and Giannakis [87] developed a blind CFO estimator by using a kurtosis-type optimization criterion. But these methods are only for MIMO systems. In [89], a joint CFO estimator and signal detector algorithm was proposed, but for particular MIMO Bell Laboratories Layered Space-Time (BLAST) systems. In cooperative systems, the use of equalization has been proposed to mitigate effects from CFOs, such as in [90–92], but only for a single-antenna transmitter: The signals received from the transmitter and the relay contain the same data but have different delays. This chapter focuses on the effects of CFO in the virtual-MIMO system with multi-antennas transmitting different data. To the best of our knowledge, it is the first study of the CFO effects in the cooperative system with a multi-antenna transmitter.

The main contributions of this chapter are twofold. Firstly, we present a practical virtual-MIMO system that implements CF cooperation with a standard source coding technique at the relay. To perform source coding, we consider two codebook design algorithms, Voronoi VQ and TSVQ. To the best of our knowledge, it is the first time that TSVQ is applied to digital modulation signals. Their codebook design complexities and encoding complexities are investigated. Simulation results show that the TSVQ approach we designed is much simpler

for encoding and more computationally efficient than the base-line Voronoi VQ. Moreover, for practical considerations, this chapter studies the effects of CFO, and demonstrates that CFO can lead to severe performance degradation for the virtual MIMO system. To overcome these effects, a clock synchronization and joint CFO estimation scheme is proposed, to exploit the benefits of MIMO CFO estimation. Simulation results show that the proposed scheme provides a significant performance advantage.

4.2 Virtual-MIMO System with CF Cooperation

4.2.1 Channel Model

We consider the same cooperative virtual-MIMO network as in Chapter 3: One remote two-antenna transmitter sends information to two colocated single-antenna receivers. We implement the BICM technique at the transmitter to provide FEC. The structure of the system is shown in Figure 4.1 (also shown in Figure 3.2). Note that the system studied here is not limited to BICM, other FEC coding schemes, such as Turbo coding or LDPC coding, could also be employed according to different application requirements.

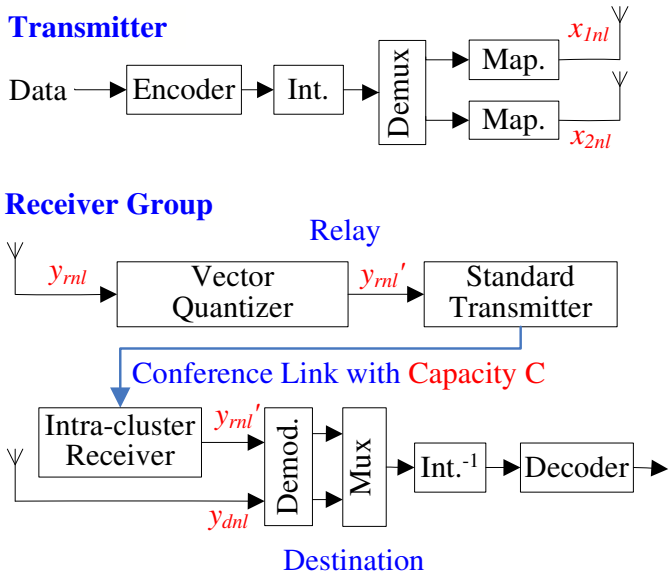

Figure 4.1: *Model for the receiver group of the cooperative virtual-MIMO system.*

As shown in Chapter 3, a block fading channel model with N Rayleigh fading blocks is assumed between the transmitter and the receiver group: each block having length L symbol

periods. When we consider a single time instance l for the nth channel, the channel model $\boldsymbol{H}_n$ is given by the equation (3.1). We assume normalized Rayleigh fading, i.e. $\mathrm{E}[|h_{in}|^2]=1$. The average transmitted power per symbol is $\mathrm{E}[|x_{i'nl}|^2]=E_s/N_t$. We normalize the total power E_s to unity, and the corresponding power per bit is $E_b=E_s/(mR_b)$. We assume that perfect CSI is available at the receivers only.

The model for the receiver group is shown in Figure 4.1. As the destination and the assisting relay are closely spaced, it is reasonable to expect that a high capacity communication link can be formed between them. In Section 3.5, the degradation from a fading channel and noise effects on this link are analysed. As the link is short range, it is shown that the degradation is too slight to impair the system performance significantly. That is, we may achieve high channel capacity with high reliability on this short range link. Hence as also considered in [7] [63] and [58], we assume the two receivers cooperate by way of an error-free conference link, as shown in Figure 4.1. One-shot conference operation [58] [64] used in Chapter 3 is also considered here. In practice, the short-range conference link is realized via an orthogonal channel (i.e. a different frequency band) to the transmitter array. Compared with the long data channel $\boldsymbol{H}_n$, the orthogonal conference link is short-range allowing much higher rate transmission, and could be reused many times over the coverage area of the long range link.

4.2.2 Compress-and-Forward Cooperation

The conference link enables cooperation, and CF serves as a protocol since it provides a higher rate when the relay is closer to the destination [10]. To perform CF cooperation, a standard source coding technique is employed for practical considerations. The reason why we do not employ the WZ coding technique is presented in Section 3.3.2: The virtual-MIMO system with multiple antennas at the transmitter has the feature that y_{rnl} and y_{dnl} are not highly correlated. The WZ Coding technique therefore does not improve the performance significantly [68] [12], but introduces extra complexity. Since standard source coding is simpler and also performs well in practical scenarios, we choose to implement it at the relay. That is, the relay is equipped with a vector quantizer. The quantization rate (i.e. source coding rate), which is denoted by R_c in Chapter 3, is measured in bits per compressed sample.

Note that, in the rest of this thesis, an error-free conference link is always assumed between the relay and destination, and therefore the link capacity C is always equal to the quantization rate R_c. For convenience, we will use the symbol C to denote both the link capacity and the

quantization rate in the rest of this thesis.

The model of the compressed signal y'_{rnl} is given by the equation (3.2) on page 45, where the compression noise w_{cnl} is i.i.d. complex Gaussian: $w_{cnl} \sim \mathcal{CN}(0, \sigma^2_{cn})$. From Shannon's rate-distortion theory, we can lower bound the variance of the compression noise, as shown in (3.7). The lower bound presents an indication for the codebook design at the relay.

The general structure of the destination is shown in Figure 4.1. It receives signals $\boldsymbol{y}_{nl} = [y'_{rnl}\ y_{dnl}]^{\mathrm{T}}$. The destination requires knowledge of h_{1n}, h_{2n}, and σ^2_{cn} sent from the relay. With knowledge of σ^2_{cn}, and assuming w_{cnl} is i.i.d. complex Gaussian, we get the scaled signal $\tilde{\boldsymbol{y}}_{nl}$ and the scaled channel matrix $\widetilde{\boldsymbol{H}}_n$ shown in equations (3.3) and (3.4), which will help the destination to mitigate the effects of the compression noise. Next the destination performs joint ML demodulation of $\tilde{\boldsymbol{y}}_{nl}$ and employs a soft-input Viterbi algorithm to decode the signals. Thus with help from the relay, the single-antenna destination receives two path signals. As shown in equations (3.4) and (3.7), with fixed SNR, a high source coding rate C will result in σ^2_{cn} decreasing to 0, and then $\widetilde{\boldsymbol{H}}_n$ tends towards $\boldsymbol{H}_n$ in value. Thus a good quality compression scheme with a high value of C will allow the destination to use y'_{rnl} for MIMO decoding, and enable the virtual-MIMO system to achieve almost ideal MIMO performance.

4.3 Vector Quantization Design at the Relay

To perform CF cooperation, codebook design is very important. The key tasks of the relay include constructing a good codebook, quantizing the received signals, and forwarding the compressed signals y'_{rnl} to the destination. The codebook design techniques and the corresponding complexities will be analysed in this section.

4.3.1 Codebook Design

The codebook design at the relay is based on the number of codebook vectors which equals 2^C and requires knowledge of the noise-free constellation. Note that, besides signal symbols, some control information such as the modulation type is also transmitted on control channels in practice. It is reasonable to expect the relay could construct the noise-free constellation of the received signals, i.e. the constellation of $h_{1n}x_{1nl}+h_{2n}x_{2nl}$, denoted by y^c_{rnl}. The codebook design which use the noise-free constellation as the training set, will be simple and efficient. In

this chapter, Voronoi VQ, and TSVQ are employed at the relay.

4.3.1.1 Voronoi VQ

Voronoi VQ is considered first, as it has the advantage that the codebook is optimal in the sense of minimising average distortion. To design this VQ, the LBG algorithm which is based on the iterative use of codebook modification, is used [44]. Specifically, assuming a mean squared error (MSE) distortion measure, the condition to identify the codebook entry could be described as:

$$S_q = \{y^c_{rnl} : \|y^c_{rnl} - v_q\|^2 \leq \|y^c_{rnl} - v_{q'}\|^2,\ \forall q' = 1, 2, ..., 2^C\}, \tag{4.1}$$

where S_q denotes the encoding region associated with the codevector v_q, and the desired number of codevectors in the codebook equals to 2^C. This condition says that the encoding region S_q should consist of all vectors that are closer to v_q than any other codevector. Furthermore, for the MSE criterion, the codevector v_q should be average of all those signal vectors that are in the encoding region:

$$v_q = \frac{\sum_{y^c_{rnl} \in S_q} y^c_{rnl}}{\sum_{y^c_{rnl} \in S_q} 1},\ q = 1, 2, ..., 2^C. \tag{4.2}$$

The equations (4.1) and (4.2) are the two key steps of the LBG algorithm, with equation (4.1) to design the partition, and then equation (4.2) to update the codebook. Finally the relay node obtains the complete codebook for quantization.

However, Voronoi VQ implies a high computational complexity and requires an exhaustive search to find the correct codeword, especially for high-order modulations and large C, as will be shown in Section 4.3.2. To reduce the complexity, we also consider TSVQ for high-order modulations.

4.3.1.2 Tree-structured VQ

TSVQ can be realized in two main forms: One is binary TSVQ where the codebook is grown on a binary tree; The other one is multistage TSVQ where the encoding task is divided into several stages [66]. A standard method for designing the binary TSVQ is based on application of the LBG algorithm to successive levels, which may not be enough to reduce the encoding complexity. The multistage TSVQ allows different design methods at different stages, and is more efficient for designing the codebook.

Another reason for adoption of the multistage TSVQ is due to the specific implementation scenario. Simulation results suggest that, as a combination of two path high-order rotationally symmetric constellations (e.g. 16QAM), y^c_{rnl} is four-fold rotationally symmetric, as shown in Fig. 4.2 (a): The origin is the centre of rotation, and $\pi/2$ is the angle of rotation. The first stage quantization of the multistage TSVQ could therefore come from the classification, i.e. classifying y^c_{rnl} into four subsets. The sub-codebook designed for one subset would be easily extended to the whole codebook, with the phase angles of the sub-codevectors changing by $\pi/2$ every time. The final stage of the TSVQ could be determined by applying the LBG algorithm on the subsets to obtain optimal final-stage codebooks. That is, equation (4.1) is used to design the partition and (4.2) to update the codebook, but the codebook size equals to $2^C/4$ this time.

If there exist more than two stages, the middle stage could be resolved by using the LBG algorithm or by classifying the training vectors based on their magnitudes and phases. The disadvantage of the LBG algorithm for the middle stage is that it requires to store the entire training subsets corresponding to the sub-codebooks for further stage TSVQ design. That is, it not only implies a higher design complexity, but also needs more storage than using the classification approach. For practical considerations, the classification method is a better choice to design the middle stage of TSVQ. Here we denote the quantization rates for the three stages of TSVQ as C_1, C_2 and C_3, and we have $C = C_1 + C_2 + C_3$.

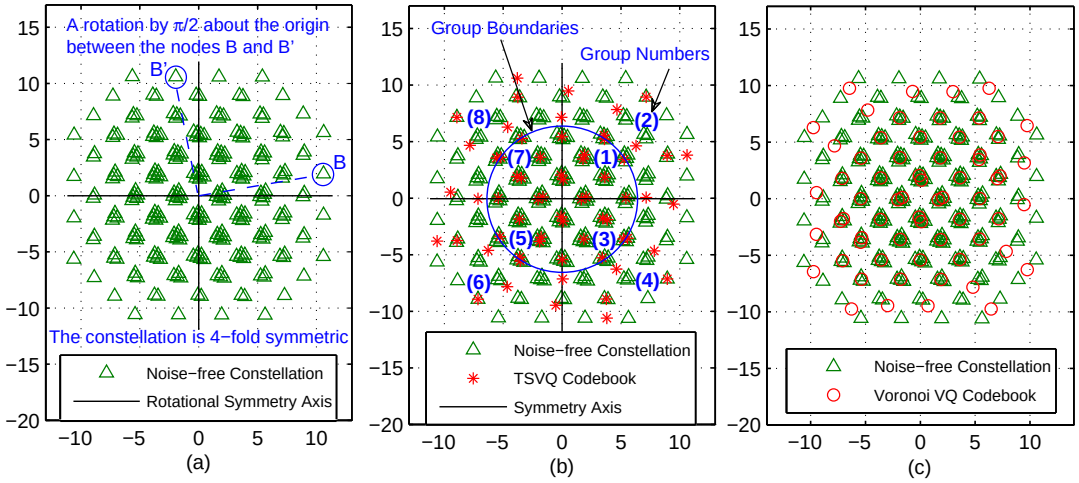

Figure 4.2: *Noise-free constellation of the received signals and the codebook designed at the relay with C= 6 bits/sample. (The rotational symmetry of the noise-free constellation is shown in (a); The TSVQ codebook with C_1= 2 bits/sample and C_2= 1 bits/sample is shown in (b); The Voronoi VQ codebook is shown in (c).)*

For example, we suppose the two signals from the transmitters are 16QAM constellations. An instantaneous version of y_{rnl}^{c} is shown in Figure 4.2. The points could be firstly divided into four subsets according to their rotational symmetry (see Fig. 4.2 (a)). That is, one subset includes the training vectors in one quadrant and $C_1 = 2$ bits/sample. Then we only need to design one sub-codebook in one subset, as the whole codebook could be obtained by phase rotations. Moreover, for one subset, we sort the constellation points in ascending order by their magnitudes and phases. To further decrease the computational complexity, we divide the subset into two groups in ascending order, i.e. $C_2 = 1$ bits/sample. Thus after two stages of TSVQ, we have 8 groups, labeled (1) - (8), as shown in Figure 4.2 (b). Then the LBG algorithm is employed twice for group No. (1) and (2) to obtain the sub-codebook for one quadrant. The final stage quantization for TSVQ is then completed by phase rotations. Finally the relay node obtains the complete codebook. The codebook designed by the Voronoi VQ is also shown in Figure 4.2 (c) for comparison. Even though the TSVQ we implemented here is suboptimal, it is much simpler to design and can achieve similar performance to the optimal but more complicated Voronoi VQ, as will be shown in Section 4.5.

The illustrative example we present above uses $C_2 = 1$ bits/sample. Since $C_3 = C - C_1 - C_2$, a higher value of C_2 could be considered to further decrease the computational complexity, or $C_2 = 0$ bits/sample for a high-accuracy quantization. Moreover, for those mappings which require higher quantization rates at the relay, e.g. 64QAM, a higher C_2 will be helpful. But for lower-order mappings, e.g. QPSK, two-stage TSVQ ($C_2 = 0$ bits/sample) may be a better choice to achieve a favourable performance-complexity tradeoff.

4.3.2 Complexity Analysis

A comparison of the Voronoi VQ and TSVQ in terms of the codebook design complexity and encoding complexity will be investigated in this subsection.

4.3.2.1 Codebook Design Complexity

As described in Section 4.3.1, both the Voronoi VQ and TSVQ use the LBG algorithm, but with a different size of training sequence. The codebook design complexity therefore comes from the computational complexity of the LBG algorithm. The computational time for the LBG

algorithm is given by [93]:

$$T_{\text{LBG}} = I_s 2^C Q_t T_d + I_s(2^C - 1) Q_t T_c, \tag{4.3}$$

where 2^C is the codebook size, I_s is the number of iterations needed to meet the stopping criterion, and Q_t is the number of training vectors. The scalars T_d and T_c denote the computational time for one distortion value and comparing two distortion values respectively. Since $I_s \leq Q_t/2^C$ [93], we obtain:

$$T_{\text{LBG}} \leq Q_t^2 T_d + Q_t^2 \frac{(2^C - 1)}{2^C} T_c. \tag{4.4}$$

For the Voronoi VQ which implements the LBG algorithm on the whole noise-free constellation y_{rnl}^c, we have $Q_t = M^2 = 2^{2m}$. Then we have,

$$T_{\text{d,Voronoi}} = T_{\text{LBG}} \leq 2^{4m} T_d + 2^{4m} \frac{(2^C - 1)}{2^C} T_c. \tag{4.5}$$

For the TSVQ we implemented, the computational time is a summation of three stages,

$$T_{\text{d,TSVQ}} \leq \begin{cases} \left[\frac{2^{2m}}{4} T_d + \frac{2^{2m}}{8}\left(\frac{2^{2m}}{4} - 1\right) T_c\right] \\ \quad + 2^{C_2}\left[\frac{2^{4m}}{2^{2(C_1+C_2)}} T_d + \frac{2^{4m}}{2^{2(C_1+C_2)}} \frac{2^{C_3} - 1}{2^{C_3}} T_c\right] & \text{if } C_2 \neq 0 \\ \frac{2^{4m}}{2^{2C_1}} T_d + \frac{2^{4m}}{2^{2C_1}} \frac{2^{C_3} - 1}{2^{C_3}} T_c & \text{if } C_2 = 0 \end{cases}. \tag{4.6}$$

A justification for (4.6) is as follows: In accordance with the multistage TSVQ we designed in Section 4.3.1, we get $C_1 = 2$ bits/sample for the first stage quantization of TSVQ. Then we firstly consider the case $C_2 \neq 0$. In one quadrant, there are $2^{2m}/4$ vectors, the distortion values of which are to be computed and sorted to obtain several separate groups for the second stage quantization. Here the selection sort algorithm is considered, requiring $\frac{2^{2m}}{4}(\frac{2^{2m}}{4} - 1)/2$ comparison operations. For the final stage, the LBG algorithm is implemented 2^{C_2} times for the 2^{C_2} groups in one quadrant. In one group, there are $Q_t = 2^{2m}/2^{(C_1+C_2)}$ training vectors and the codebook size is 2^{C_3}. So we obtain an upper bound of $T_{\text{d,TSVQ}}$ as shown in the equation (4.6). As to the case $C_2 = 0$, it is obvious that the computational complexity comes from the LBG algorithm used in the final stage quantization where $2^{2m}/2^{C_1}$ training vectors are considered.

Use the illustrative example presented in Section 4.3.1. When we consider $C_1 = 2$ bits/sample and $C_2 = 1$ bit/sample, we have $T_{\text{d,Voronoi}} = \mathcal{O}(2^{4m}(T_d + T_c))$ and $T_{\text{d,TSVQ}} = \mathcal{O}(2^{4m-5}T_d + 2^{4m-4}T_c)$, for a high-order modulation (e.g 16QAM) and a large value of C.

$$\frac{T_{\text{d,TSVQ}}}{T_{\text{d,Voronoi}}} = \frac{\mathcal{O}(2^{4m-5}T_d + 2^{4m-4}T_c)}{\mathcal{O}(2^{4m}(T_d + T_c))} < \frac{1}{16}. \tag{4.7}$$

That is, compared with the Voronoi VQ, TSVQ decreases the computational complexity for the codebook design to less than one sixteenth.

4.3.2.2 Encoding Complexity

As to the symbol encoding, TSVQ will also allow a faster codebook search. Specifically, the encoding algorithm for a Voronoi VQ can be viewed as an exhaustive search algorithm. For a codebook of size 2^C, the codevector selection for one symbol requires 2^C distortion evaluations and $2^C - 1$ comparisons. The required time to search the codebook for one symbol is shown as:

$$T_{\text{s,Voronoi}} = 2^C T_d + (2^C - 1)T_c. \tag{4.8}$$

For the TSVQ we designed, the search procedure includes two steps: finding out an appropriate group, and performing a full search on the group. Thus the search time of TSVQ is,

$$T_{\text{s,TSVQ}} = (C_2 + 2^{C_3})T_d + (C_2 + 2^{C_3} - 1)T_c. \tag{4.9}$$

When $C_1 = 2$ bits/sample and $C_2 = 1$ bit/sample, the multistage TSVQ will allow almost 8 times faster encoding than the Voronoi VQ. Thus TSVQ also has a much lower encoding complexity.

Therefore, compared with the Voronoi VQ, the multistage TSVQ not only decreases the computational complexity for the codebook design, but also allows a faster codebook search for the encoding. Since the multistage TSVQ can also achieve a good performance, it is a better choice to enable CF cooperation in practice.

4.4 Effects of Carrier Frequency Offset

With CF cooperation, the destination may expect traditional MIMO benefits in the virtual-MIMO system. However, due to the different oscillator frequencies at the source, relay and destination, carrier frequency offsets (CFOs) occur [90] [88]. It will cause severe performance degradation, since CFOs between the transmitter-to-relay and the transmitter-to-destination can result in interblock interference and distort the correlation properties of the signals at the destination. This section thus focuses on the effects of CFO in the virtual-MIMO system. A clock synchronization and joint CFO estimation scheme is then proposed.

4.4.1 CFO Estimation

CFOs cause continuous phase rotations of the corresponding signals, and thus impair the detection performance. To alleviate this effect, the CFOs have to be estimated and then compensated at the receivers. The estimation of CFO in a MIMO system has been investigated in the literature [84, 86, 87]. But these methods are only for MIMO systems. The methods in [84] and [86] are pilot aided requiring training sequences to estimate CFO, whereas [87] develops a blind CFO estimation technique based on a kurtosis-type optimisation criterion. The CFO estimator in [84] is based on the measurement of the phase shift between consecutive channel estimation sequences. As it is simple and effective in practice, we firstly implement it at the relay and the destination as a baseline case.

Since N_t antennas at the transmitter are fed with the same clock, frequency offsets at the relay and destination are defined as f_{rn} and f_{dn} respectively. We let $[\boldsymbol{u}_{nl}, \boldsymbol{u}_{n(l+1)}]$ denote the channel estimation sequence, which occupies two symbol periods as $N_t = 2$, and $\boldsymbol{u}_{nl}$ is an $N_t \times 1$ vector transmitted through the channel matrix $\boldsymbol{H}_n$. Channel estimation sequences are transmitted continuously on a dedicated pilot channel. The received signals at the relay and the destination corresponding to $\boldsymbol{u}_{nl}$ at time t_{nl} is then given by,

$$\begin{bmatrix} y^u_{rnl} \\ y^u_{dnl} \end{bmatrix} = \begin{bmatrix} e^{j(2\pi f_{rn} t_{nl})} & 0 \\ 0 & e^{j(2\pi f_{dn} t_{nl})} \end{bmatrix} \boldsymbol{H}_n \boldsymbol{u}_{nl} + \boldsymbol{w}^u_{nl}, \tag{4.10}$$

where $\boldsymbol{w}^u_{nl}$ is the $N_t \times 1$ complex Gaussian noise vector, with the noise samples $\sim \mathcal{CN}(0, N_0)$. According to [84], we let the matrix $\boldsymbol{P}_{rn1}$ be formed by collecting the received signals at the relay corresponding to $[\boldsymbol{u}_{nl}, \boldsymbol{u}_{n(l+1)}]$, i.e. $\boldsymbol{P}_{rn1} = [y^u_{rnl}, y^u_{rn(l+1)}]$, and let $\boldsymbol{P}_{rn2}$ be defined as

containing that pertaining to the next transmission of the channel estimation sequence. Likewise, $\boldsymbol{P}_{dn1}$ and $\boldsymbol{P}_{dn2}$ are defined for the destination. Then CFOs f_{rn} and f_{dn} can be estimated as,

$$\tilde{f}_{rn} = \arg[\boldsymbol{P}_{rn2} \cdot \boldsymbol{P}_{rn1}^{\dagger}]/(2\pi \cdot 2t_s), \tag{4.11}$$

$$\tilde{f}_{dn} = \arg[\boldsymbol{P}_{dn2} \cdot \boldsymbol{P}_{dn1}^{\dagger}]/(2\pi \cdot 2t_s), \tag{4.12}$$

where $\arg[\cdot]$ denotes the angle operation, t_s denotes the symbol interval, and $\{\cdot\}^{\dagger}$ represents the Hermitian transpose.

4.4.2 Clock Synchronization and Joint CFO Estimation Scheme

The basic motivation for this proposed scheme is the fact that CFO causes severe performance degradation for the 2×2 virtual MIMO system. It is shown in [84, 86, 88] that increasing the number of transmit and receive antennas, e.g. 4×4 and 8×8 MIMO systems, leads to significant improvement in the accuracy of the CFO estimate. However, for the simpler 2×2 MIMO or 2×1 MISO systems, residual CFO will still impair the detection performance. Meanwhile, cooperative virtual-MIMO systems also suffer from the distinction as compared to conventional MIMO where all the antennas at the receiver are fed with the same clock. In virtual-MIMO systems, cooperating antennas which are running with different clocks need to estimate and compensate their CFOs independently, as shown in equations (4.11) and (4.12). Their residual CFOs, i.e. $(\tilde{f}_{rn} - f_{rn})$ and $(\tilde{f}_{dn} - f_{dn})$, are different and independent. Since the operation at the relay does not cause extra phase rotations, the different residual CFOs will then distort the correlation properties of the received signals at the destination, so that the system performance is impaired. To mitigate this effect, the use of frequency-domain equalization has been proposed in cooperative systems [90] [92]. However, such previous work has only focused on a single-antenna transmitter: The signals received from the transmitter and the relay contain the same data but have different delays. For our virtual-MIMO system which has multiple-antennas transmitting different data, we propose to maintain clock synchronization across the receivers, and then jointly estimate CFO between both terminals.

The proposed scheme involves two steps. Clock synchronization is the first step for providing a common notion of time across the relay and the destination, so that traditional MIMO decoding is applicable in the virtual-MIMO system. State of the art synchronization algorithms are

described in [94], assuming that the transmissions for delivering time information are line of sight. To estimate the frequency difference between the receivers, a two-way message exchange (which is a classical timing message signalling approach) could be implemented. Consider the destination as the reference node, so that the relay needs to synchronize with the destination. It requires timing messages to be exchanged several times to achieve a certain synchronization accuracy. As shown in Figure 4.3, in the jth round of message exchange for a specific $\boldsymbol{H}_n$, the relay sends a synchronization message to the destination at t_{1nj}. The destination records its time t_{2nj} and replies the message to the relay at t_{3nj}, which arrives at t_{4nj}. So we have,

$$t_{2nj} = f_{rdn}(t_{1nj} + \tau_n + p_{nj}) + \theta_n, \tag{4.13}$$

$$t_{3nj} = f_{rdn}(t_{4nj} - \tau_n - q_{nj}) + \theta_n, \tag{4.14}$$

where f_{rdn} and θ_n denote the relative frequency difference and phase difference of the relay

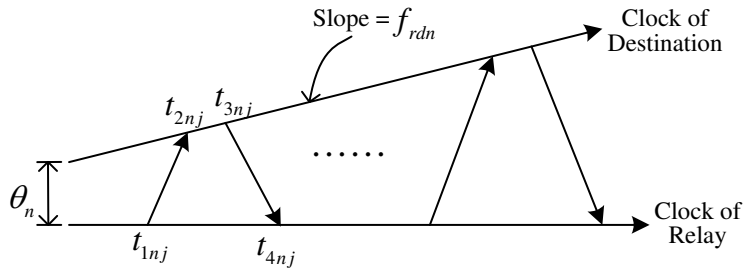

Figure 4.3: *Two-way timing message exchange between the relay and destination.*

with respect to the destination, τ_n is the fixed delay, p_{nj} and q_{nj} are the variable delays in the transmissions. Assuming p_{nj} and q_{nj} are i.i.d. zero mean Gaussian or exponential random variables, after several times message exchanges, the estimations of f_{rdn} and θ_n can be obtained [94] [95]. The stable nature of the error-free conference link between the relay and the destination is helpful for this synchronization process. In practice, the conference link is short range and realized via an orthogonal channel to the transmitter array. It is reasonable to expect that in many cases the conference link is a reliable line-of-sight link with high bandwidth, which may support frequent timing message exchanges. Hence, on the stable short-range conference link, the relay and the destination could maintain clock synchronization.

The clock synchronization approach studied here focuses specifically on frequency locking, as the effect of frequency offset is the main reason why clock offsets drift over time [96].

Compensating the frequency offset guarantees long-term reliability of synchronization, so that re-synchronization only need to be preformed for each channel condition $\boldsymbol{H}_n$. Maintaining frequency synchronization could provide a big performance advantage, as will be shown in Section 4.5. Without loss of generality, after the clock synchronization, frequency offsets at the relay and the destination are modelled by (as shown in Figure 4.4),

$$f_{rn} = f_{dn} + \Delta_n, \tag{4.15}$$

where Δ_n denotes the frequency synchronization error, which is determined by the synchronization algorithm, the delays in timing message delivery, and the number of observations of timing messages. Efficient algorithms relying on two-way message exchanges have been reported in [94]. For algorithms that do not compensate the frequency offsets, such as the timing-sync protocol for sensor networks (TPSN), synchronization has to be performed more frequently to maintain the required accuracy. The algorithm in [96] computes and corrects the frequency offsets, and thus serves as a good candidate for our system. It is reported that the frequency synchronization error decreases as the number of timing messages exchanged increases.

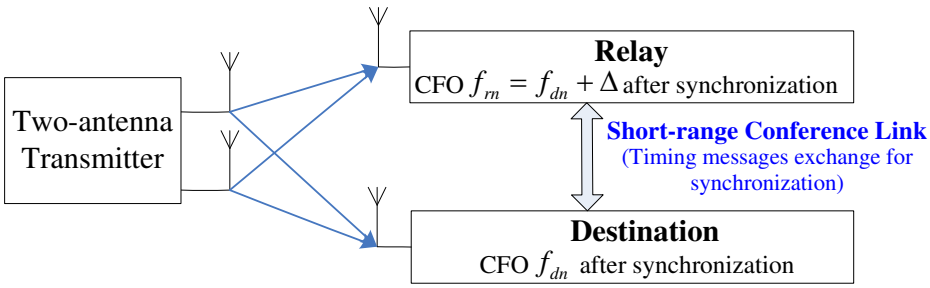

Figure 4.4: *Carrier frequency offsets at the relay and the destination.*

The second step of the proposed scheme is to perform joint CFO estimation between the relay and the destination, to obtain the benefit of MIMO CFO estimation. Specifically, the relay computes $J_{rn} = \boldsymbol{P}_{rn2} \cdot \boldsymbol{P}_{rn1}^{\dagger}$ and transmits it to the destination via the conference link. The destination receives $J_{dn} = \boldsymbol{P}_{dn2} \cdot \boldsymbol{P}_{dn1}^{\dagger}$ and estimates f_{dn} based on J_{rn} and J_{dn},

$$\tilde{f}_{dn} = \arg[J_{rn} + J_{dn}]/(2\pi \cdot 2t_s). \tag{4.16}$$

The estimated CFO is then shared with the relay, i.e. $\tilde{f}_{rn} = \tilde{f}_{dn}$, to help the relay compensate

its CFO f_{rn} before the vector quantization. Here we compare $\tilde{f}_{dn}$ against the estimated CFO of the corresponding MIMO system which is denoted by $\tilde{f}_n$.

Proposition 4.1: Given a specific channel realisation $\boldsymbol{H}_n$, when the synchronization error $\Delta_n = 0$, we have $\tilde{f}_{dn}$ computed using the joint CFO estimation scheme equals $\tilde{f}_n$ in value, and therefore the benefits of MIMO CFO estimation are exploited.

A brief proof of the proposition is as follows: For the MIMO system, the received signals corresponding to $\boldsymbol{u}_{nl}$ is given by,

$$\boldsymbol{y}^u_{nl} = \boldsymbol{H}_n \boldsymbol{u}_{nl} e^{j(2\pi f_n t_{nl})} + \boldsymbol{w}^u_{nl}, \tag{4.17}$$

According to [84], $\boldsymbol{P}_{n1}$ is defined as $[\boldsymbol{y}^u_{nl}, \boldsymbol{y}^u_{n(l+1)}]$, and $\boldsymbol{P}_{n2}$ is for next transmission of the channel estimation sequence. Then we get a square matrix $\boldsymbol{J}_n = \boldsymbol{P}_{n2} \cdot \boldsymbol{P}^{\dagger}_{n1}$, so that f_n can be estimated by,

$$\tilde{f}_n = \arg[\ \mathrm{tr}(\boldsymbol{J}_n)\ ]/(2\pi \cdot 2t_s), \tag{4.18}$$

where $\mathrm{tr}(\cdot)$ denotes the trace operation. If $\Delta_n = 0$, we have $\boldsymbol{y}^u_{nl} = [y^u_{rnl} \ \ y^u_{dnl}]^{\mathrm{T}}$, so that,

$$\begin{aligned} \mathrm{tr}(\boldsymbol{P}_{n2} \cdot \boldsymbol{P}^{\dagger}_{n1}) &= \mathrm{tr}\left(\begin{bmatrix} \boldsymbol{P}_{rn2} \\ \boldsymbol{P}_{dn2} \end{bmatrix} \cdot [\boldsymbol{P}^{\dagger}_{rn1} \ \ \boldsymbol{P}^{\dagger}_{dn1}] \right) \\ &= \boldsymbol{P}_{rn2} \cdot \boldsymbol{P}^{\dagger}_{rn1} + \boldsymbol{P}_{dn2} \cdot \boldsymbol{P}^{\dagger}_{dn1} \end{aligned} \tag{4.19}$$

Substituting (4.19) into (4.18), and comparing it with (4.16), we finally get $\tilde{f}_{dn} = \tilde{f}_{rn} = \tilde{f}_n$. The joint CFO estimation scheme therefore exploits spatial diversity of the MIMO receiver (when $\Delta_n = 0$), and offers significant improvement compared to (4.12). The performance of the joint CFO estimation scheme is thus lower bounded by the perfect frequency-synchronized case.

For the case $\Delta_n \neq 0$, at high SNR, $\tilde{f}_{dn}$ will tend toward $f_{dn} + \Delta_n/2$,

$$\tilde{f}_{rn} = \tilde{f}_{dn} = f_{dn} + \Delta_n/2 = f_{rn} - \Delta_n/2. \tag{4.20}$$

That is because the estimated $\tilde{f}_{dn}$ from the equation (4.16) is based on two CFO observations. When $\Delta_n \neq 0$, with SNR increasing, $\tilde{f}_{dn}$ will equal the average of f_{dn} and f_{rn}. Thus for

both the relay and the destination, the magnitude of CFO mismatch is $\Delta_n/2$. In this case, the joint CFO estimation scheme may still take advantage of the cooperative estimation, but the benefit will be reduced as Δ_n increases. Different values of Δ_n represents different degrees of synchronization across the relay and the destination. The distribution of Δ_n is complicated, and is related to the synchronization algorithms, various delays in timing message delivery and the number of timing messages exchanged, as mentioned before. In this chapter we consider a fixed value of Δ_n for all channel conditions and will drop its subscript n in simulations (in Section 4.5), in order to demonstrate the effects of the value of Δ on performance.

Using the two steps, we get the clock synchronization and joint CFO estimation scheme to counteract the performance degradations caused by CFOs. Note that, the joint CFO estimation studied here is based on McKeown's algorithm in [84], but it is not limited to that algorithm. Other estimation algorithms could also be employed, with suitable changes to the shared information to complete the joint CFO estimation operation.

4.5 Numerical Results

In this section, we present the error performance of our cooperative virtual-MIMO system ($N_t = N_r = 2$). At the transmitter, a binary convolutional code is assumed with the generator polynomials $[133, 171]_{\text{octal}}$ ($R_b = 1/2$). Gray-labeled QPSK or 16QAM modulation are considered. The channels between the transmitter and receivers are assumed to be i.i.d normalized block Rayleigh fading, with 10^6 fading blocks and each block has 196 consecutive symbol periods. The simulation results are obtained using the Monte Carlo method. We plot the BER or BLER against the information bit SNR, i.e E_b/N_0.

4.5.1 BER Evaluation of VQ Design

The BLER performance of the cooperative virtual-MIMO system with the Voronoi VQ under various quantization rates, has already been shown in Chapter 3 in Figure 3.6 (for QPSK modulation) and Figure 3.7 (for 16QAM modulation). The BLERs are compared against the corresponding ideal MIMO system, and the non-cooperative MISO system. We can see that, with Voronoi VQ at the relay, $C = 7$ bits/sample for 16QAM and $C = 4$ bits/sample for QPSK modulation, will enable the system with CF cooperation to approach ideal MIMO performance.

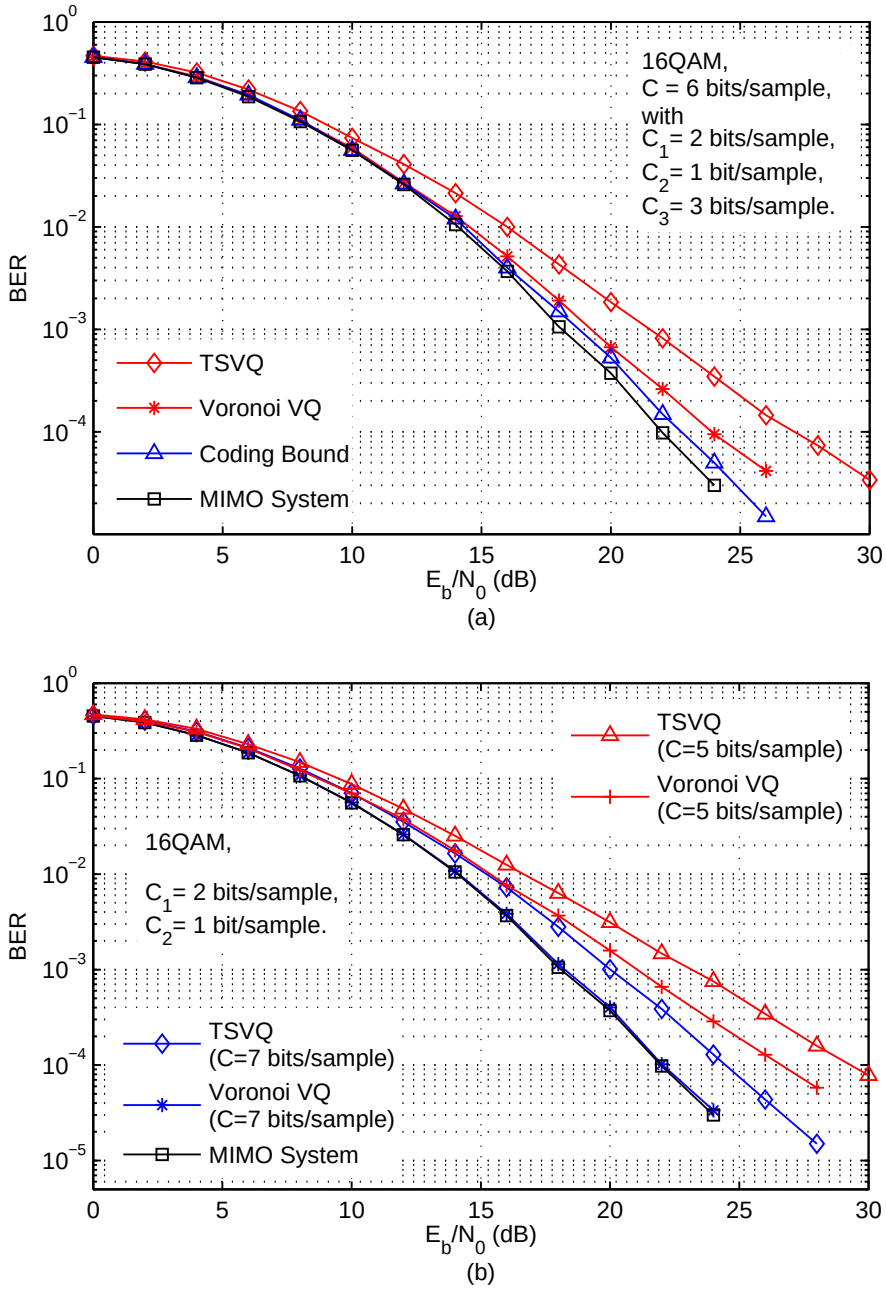

Figure 4.5: *BER performance of the cooperative virtual-MIMO system with TSVQ or Voronoi VQ at the relay. (Quantization rate 6 bits/sample is considered in (a), while 5 and 7 bits/sample are considered in (b).)*

As mentioned above, the codebook design complexity and encoding complexity of the Voronoi VQ is quite high. To reduce the complexity and enhance the practicality of CF cooperation, we propose to employ TSVQ to design the codebook at the relay. When $C = 6$ bits/sample, Figure 4.5 (a) shows the BER results of the TSVQ cooperative system which is set up in accordance with the example for 16QAM mapping in Section 4.3.1. Its BER is compared against the performance of the system with the Shannon coding bound. According to equation (3.2), the compression noise w_{cnl} is considered for this kind of system, with the Shannon coding bound of the variance calculated via (3.7). As shown in this figure, the Voronoi VQ obtains performance which is close to the Shannon coding bound. Even though the TSVQ we designed here is suboptimal, it is much simpler to design and operate and can achieve error ratios comparable to the optimal but more complicated Voronoi VQ. As an example, at A BER of 10^{-3}, a performance gap of 2.5 dB exists between the two VQs. But for a given quantization rate 6 bits/sample, the Voronoi VQ requires a $\mathcal{O}(65536(T_d + T_c))$ computations which is much larger than that of TSVQ requiring $\mathcal{O}(2048T_d + 4096T_c)$ computations. The TSVQ we employed allows a lower encoding complexity as well.

Additionally, considering the quantization rates 5 bits/sample and 7 bits/sample, we compare the performance of the Voronoi VQ and TSVQ in Figure 4.5 (b). It can be seen that the performance gaps are 2.5 dB for $C = 5$ bits/s, and 2 dB for $C = 7$ bits/s, at BER of 10^{-3}. And more importantly, the BER of TSVQ for $C = 6$ bits/sample in Figure 4.5 (a) performs almost the same as the Voronoi VQ for $C = 5$ bits/sample in Figure 4.5 (b). According to equations (4.8) and (4.9), that means the TSVQ with encoding complexity $(9T_d + 8T_c)$ is able to achieve the performance of the Voronoi VQ with $(32T_d + 31T_c)$ complexity. Also, the TSVQ for $C = 7$ bits/sample performs similarly to the Voronoi VQ for $C = 6$ bits/sample. That is, TSVQ could approach the performance of Voronoi VQ with roughly 4 times lower encoding complexity. TSVQ always requires a much lower computational complexity for the codebook design as well. Thus the TSVQ we implemented here is more efficient than the Voronoi VQ, and is a better choice for the CF cooperation to enable the virtual-MIMO system to achieve MIMO performance in practice.

The above TSVQ results use $C_2 = 1$ bit/sample accorded to the illustrative example in Section 4.3.1. But C_2 is not limited to that value: a higher C_2 could be considered to further decrease the computational complexity, or $C_2 = 0$ bits/sample for a high-accuracy quantization, since

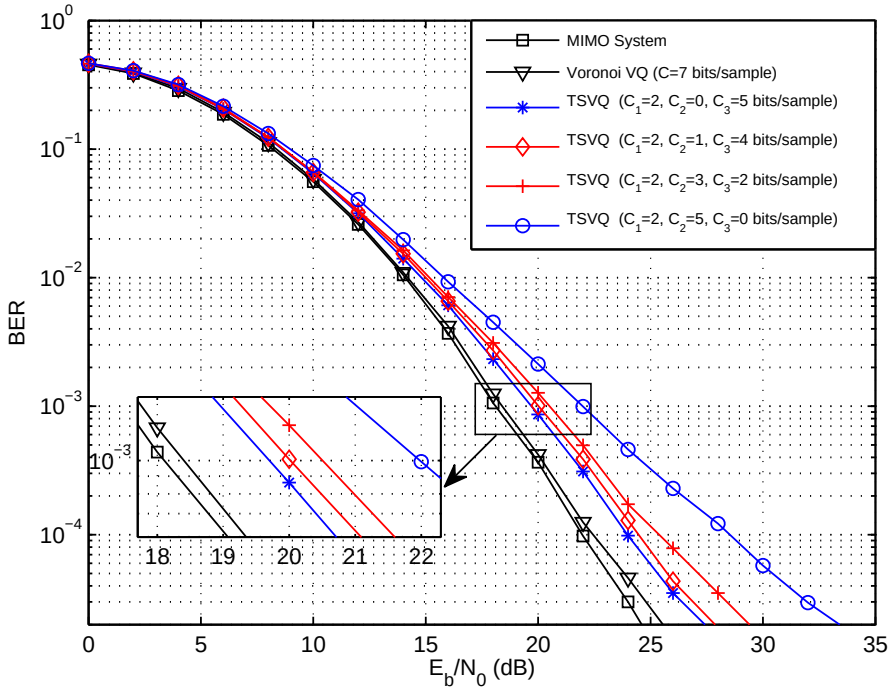

Figure 4.6: *BER comparison between the Voronoi VQ and TSVQ in the virtual-MIMO system. ($C = 7$ bits/sample for the Voronoi VQ, and various C_2 for TSVQ are considered.)*

Design Algorithm (C uses bits/sample unit)	Design Complexity	Encoding Complexity	E_b/N_0 Loss (BER=10^{-3})
Voronoi VQ (C= 7)	$\mathcal{O}(65536(T_d + T_c))$	$128T_d + 127T_c$	0 dB
TSVQ (C_1= 2, C_2= 0, C_3= 5)	$\mathcal{O}(4096(T_d + T_c))$	$32T_d + 31T_c$	1.3 dB
TSVQ (C_1= 2, C_2= 1, C_3= 4)	$\mathcal{O}(2048T_d + 4096T_c)$	$17T_d + 16T_c$	1.6 dB
TSVQ (C_1= 2, C_2= 3, C_3= 2)	$\mathcal{O}(512T_d + 2048T_c)$	$5T_d + 10T_c$	2.2 dB
TSVQ (C_1= 2, C_2= 5, C_3= 0)	$\mathcal{O}(192T_d + 2048T_c)$	$T_d + 31T_c$	3.6 dB

Table 4.1: *Complexity and performance comparison between the Voronoi VQ and TSVQ when C= 7 bit/sample.*

$C_3 = C - C_1 - C_2$. The comparison of values of C_2 for the TSVQ cooperative system is shown in Figure 4.6. We assume a total quantization rate $C = 7$ bits/sample for 16QAM mapping in this figure. The corresponding design and encoding complexities at BER of 10^{-3}, are shown in Table 4.1. Compared to the Voronoi VQ, the TSVQ with $C_2 = 0$ bits/sample can reduce the codebook design complexity to one sixteenth, and decrease the encoding complexity to one quarter, for a E_b/N_0 performance penalty of only 1.3 dB. Then as C_2 increases, both the design and encoding complexities reduce, but the BER performance becomes worse. Since both the second and third stage of TSVQ contribute to the complexities according to (4.6) and (4.9), the complexity reduction is not proportional to the increase of C_2. Neither does the performance loss (i.e. the E_b/N_0 Loss). To achieve a favourable performance-complexity tradeoff, $C_2 = 1$ bit/sample is a good choice for this case.

Design Algorithm (C uses bits/sample unit)	Design Complexity	Encoding Complexity	E_b/N_0 Loss (BER=10^{-3})
Voronoi VQ (C= 5)	$\mathcal{O}(65536(T_d + T_c))$	$32T_d + 31T_c$	0 dB
TSVQ (C_1= 2, C_2= 0, C_3= 3)	$\mathcal{O}(4096(T_d + T_c))$	$8T_d + 7T_c$	1 dB
TSVQ (C_1= 2, C_2= 1, C_3= 2)	$\mathcal{O}(2048T_d + 3584T_c)$	$5T_d + 4T_c$	1.4 dB
TSVQ (C_1= 2, C_2= 2, C_3= 1)	$\mathcal{O}(1024T_d + 2560T_c)$	$3T_d + 4T_c$	2.2 dB
TSVQ (C_1= 2, C_2= 3, C_3= 0)	$\mathcal{O}(512T_d + 2048T_c)$	$T_d + 7T_c$	4.2 dB

Table 4.2: *Complexity and performance comparison between the Voronoi VQ and TSVQ when C= 5 bit/sample.*

Moreover, similar to Figure 4.6, Figure 4.7 also presents the comparison of various C_2 in the TSVQ cooperative system, but for a total quantization rate $C = 5$ bits/sample. According to Table 4.2, compared to the Voronoi VQ, the TSVQ with $C_2 = 0$ and $C_2 = 1$ bits/sample decrease the complexities significantly, at the cost of 1 dB and 1.4 dB E_b/N_0 loss respectively.

4.5.2 Effects of Carrier Frequency Offsets

According to the 3GPP standards, the tolerance required for frequency accuracy is from $\pm$0.1 ppm (parts per million) to $\pm$0.25 ppm (allowed in a wider temperature range) [97]. It translates to a CFO in the range up to $\pm$500 Hz at a carrier frequency of 2 GHz. For practical considera-

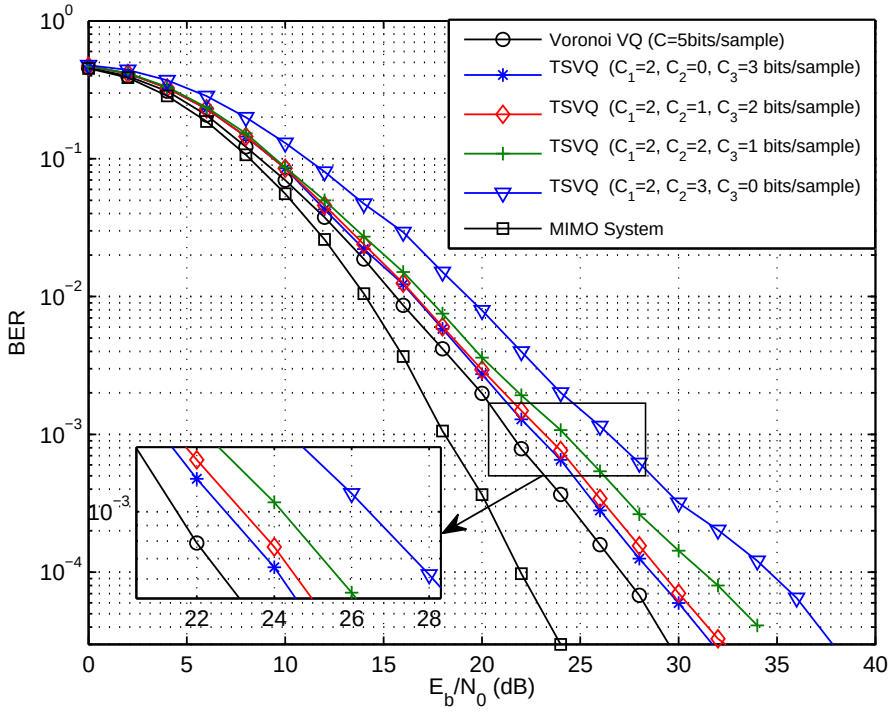

Figure 4.7: *BER comparison between the Voronoi VQ and TSVQ in the virtual-MIMO system. ($C = 5$ bits/sample for the Voronoi VQ, and various C_2 for TSVQ are considered.)*

tions, we assume the CFO at the destination follows a uniform distribution, i.e. $f_{dn} \sim$ U[-500, 500] Hz, and again $f_{rn} = f_{dn} + \Delta$. Channel estimation sequences (pilot symbols) are transmitted continuously on a dedicated pilot channel. Moreover, a generic sub-frame structure defined in 3GPP LTE is adopted [98]: one sub-frame is made up of two 0.5 ms slots, each made of seven symbols, and thus the symbol interval $t_s = 71.4$ μs. Based on the channel estimation sequences, the frequency range that can be estimated is therefore $\pm$3500 Hz [84], which can cover the maximum CFO assumed here. Since 196 symbol periods are assumed in each block for block fading channels, there exist 14 sub-frames on one specific channel. Given a specific $\boldsymbol{H}_n$, the relay and the destination perform clock synchronization, and then jointly estimate and compensate their CFOs for each sub-frame.

The BLER performance of the 2×2 virtual-MIMO system with or without clock synchronization for QPSK modulation is shown in Figure 4.8. To focus on the effects of residual CFO, we firstly apply the Voronoi VQ with C= 4 bits/sample for cooperation. For the cooperative system without clock locking, the relay and the destination need to estimate and compensate their CFOs

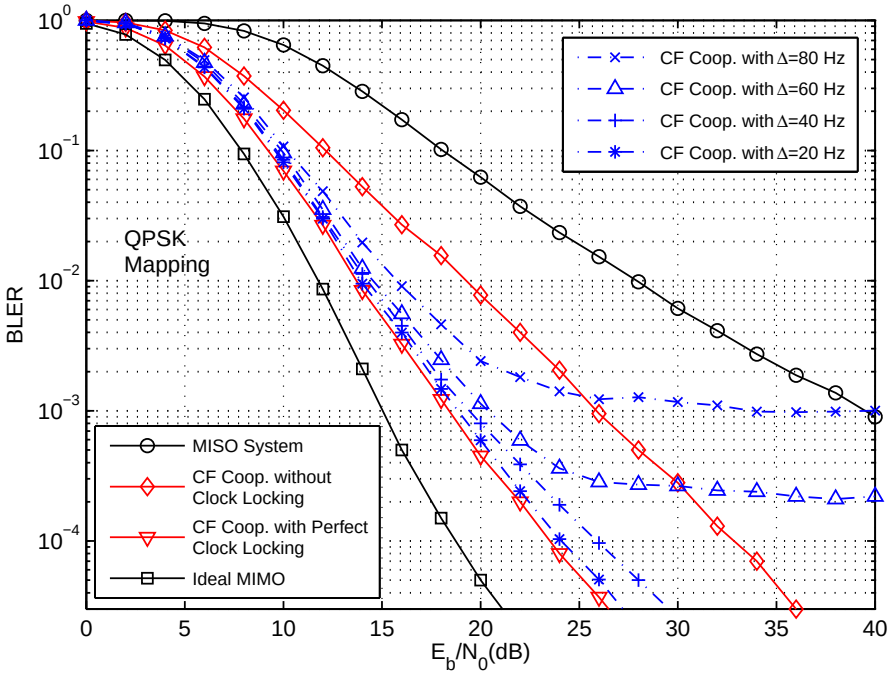

Figure 4.8: *BLER performance of the virtual-MIMO system with or without frequency synchronization for QPSK mapping. (Various degrees of synchronization and Voronoi VQ are considered.)*

independently, causing a drastic performance degradation compared to the ideal MIMO case. In contrast, the proposed clock synchronization and joint CFO estimation scheme provides a significant performance advantage, which is lower bounded by the perfect clock locking case (i.e. $\Delta = 0$ Hz). Then a family of dash-dot curves shows the performance of various degrees of synchronization.

For the case $\Delta \neq 0$, there exists an error floor at high E_b/N_0, which is caused by the residual CFO which equals $\Delta/2$ according to the equation (4.20). But a small value of Δ guarantees a very low error floor. For a target BLER of 10^{-2}, a synchronization error smaller than 60Hz provides a good performance close to the lower bound.

A similar trend can be seen in Figure 4.9 for 16QAM mapping: Maintaining clock synchronization and jointly estimating CFO at the relay and the destination could provide a big BER improvement which is quite close to the ideal MIMO case. Comparing the results for 16QAM and QPSK, it is obvious that 16QAM needs a higher level of synchronization because of its higher-order constellation, but QPSK could tolerate a larger synchronization error. For 16QAM,

$\Delta \leq 20$ Hz could offer a reasonable and acceptable performance for the virtual-MIMO system.

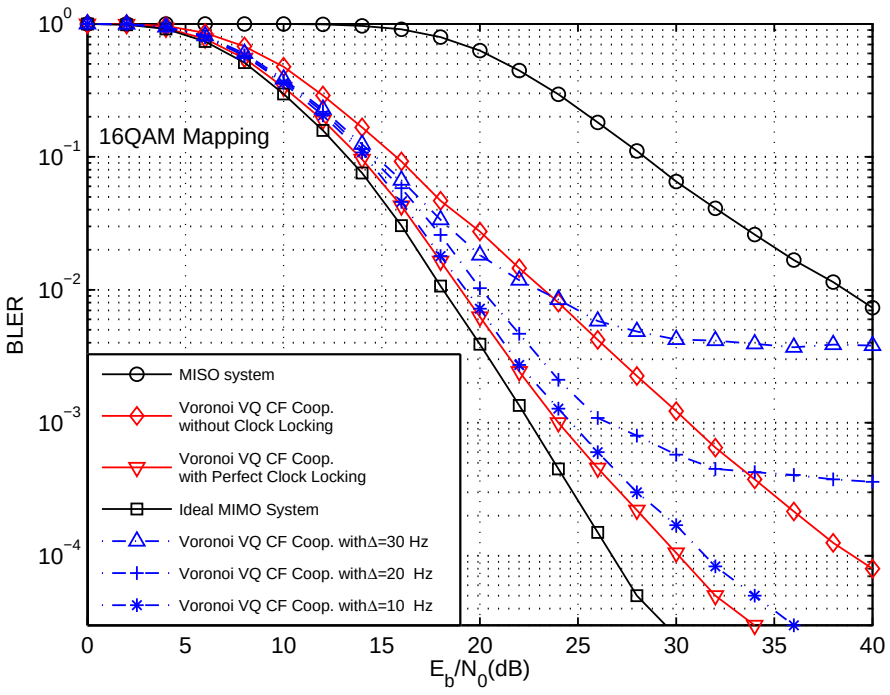

Figure 4.9: *BLER performance of the virtual-MIMO system with various degrees of frequency synchronization for 16QAM mapping. (Various degrees of synchronization and Voronoi VQ are considered.)*

Moreover, besides the Voronoi VQ with C= 7 bits/sample, Figure 4.10 also applies the TSVQ we designed (C_1= 2, C_2= 1, C_3= 4 bits/sample) to enable CF cooperation for specific cases of the proposed scheme where $\Delta = 10$ Hz and $\Delta = 20$ Hz are considered. The system performance with TSVQ follows the same trend as the system with the Voronoi VQ, without causing any extra performance degradation. Thus TSVQ could be used here to obtain a favourable performance-complexity tradeoff in the virtual-MIMO system.

4.6 Conclusions

In this chapter, a cooperative virtual-MIMO system using two transmit antennas that implements BICM transmission and CF cooperation among two receiving nodes was presented. This chapter concentrated on the practical analysis of codebook design and frequency offset estimation in this system. Firstly, two codebook design algorithms were presented, Voronoi VQ

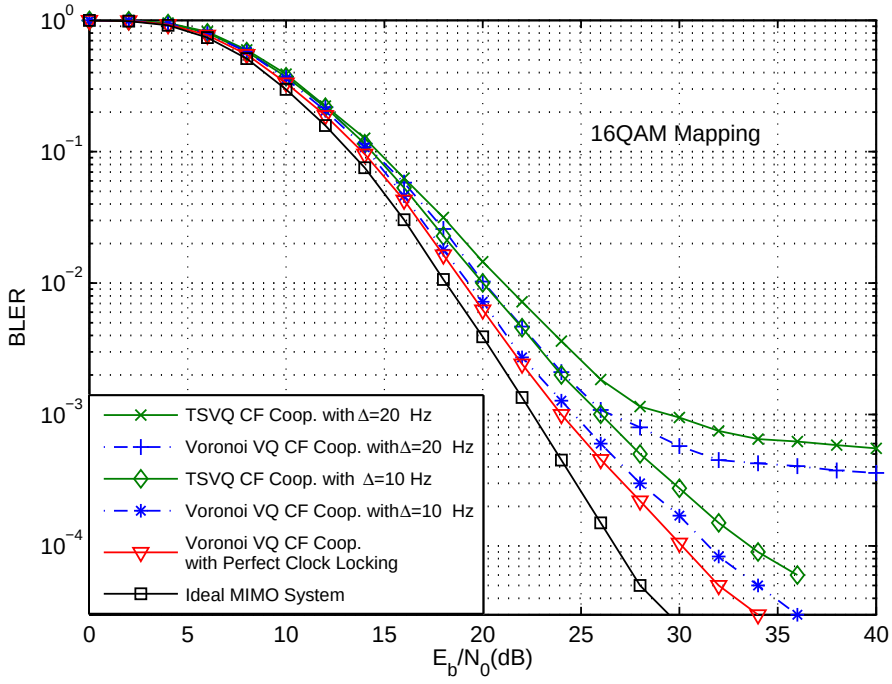

Figure 4.10: *BLER performance of the virtual-MIMO system with frequency synchronization for 16QAM mapping. (Both Voronoi VQ and TSVQ are considered.)*

and TSVQ, based on knowledge of the noise-free constellation. A comparison in terms of the codebook design complexity and encoding complexity was also presented. We have shown that, compared to the Voronoi VQ, the TSVQ can reduce the codebook design complexity to less than one sixteenth, and decrease the encoding complexity to less than one quarter, for a performance penalty of only 1.3 - 1.6 dB. A higher middle-stage quantization rate C_2 could be considered to further decrease the complexities, or $C_2 = 0$ bits/sample used for high-accuracy quantization. In practice, the TSVQ is a better choice for CF cooperation to achieve a favourable performance-complexity tradeoff in the virtual-MIMO system.

Additionally, for practical considerations, we also investigated the effects of CFO, and demonstrated that CFO could lead to drastic performance degradation for the 2×2 virtual MIMO system. A scheme which maintains clock synchronization and jointly estimates CFO between the relay and the destination, is proposed to overcome the limitations of separate CFO estimation at the relay and destination. Simulation results showed that the proposed scheme provided a significant performance improvement. For a target BLER of 10^{-2}, a synchronization error smaller than 60 Hz for QPSK and 20 Hz for 16QAM mapping, could offer good performance

close to the case with perfect clock locking.

This chapter dealt with two practical issues for the virtual-MIMO system with CF cooperation. We designed the efficient TSVQ as source coding technique at the relay, and proposed the clock synchronization and joint CFO estimation scheme so that the cooperation is not unduly sensitive to CFOs. The TSVQ is not limited to 16QAM mapping, the principles of which could easily be applied to multiple modulation types and quantization rates. Also, the clock synchronization and joint CFO estimation scheme could employ other estimation algorithms, besides McKeown's method. By extending to a wide range of applications, the virtual-MIMO system is therefore particularly valuable and attractive to some realistic wireless communication systems. The extension to more practical receivers will be described in next chapter.

Chapter 5
A Singular Value-based Adaptive Modulation and Cooperation Scheme

In last two chapters, we concentrated on the virtual-MIMO-BICM system with ML detection. The disadvantage of ML receiver is the high computational complexity, which increases exponentially with the number of bits per symbol. In this chapter, we extend the study to the minimum mean square error (MMSE) detection, as it has low complexity and allows good performance when combined with BICM techniques.

In this chapter, a closed-form upper bound for the system error probability is derived, based on which we prove that the smallest singular value of the cooperative channel matrix determines the system error performance. Accordingly, an adaptive modulation and cooperation scheme is proposed, which uses the smallest singular value as the threshold strategy. Depending on the instantaneous channel conditions, the system could therefore adapt to choose a suitable modulation type for transmission and an appropriate quantization rate to perform CF cooperation. It is shown that the adaptive modulation and cooperation scheme not only enables the system to achieve comparable performance to the case with fixed quantization rates, but also eliminates unnecessary complexity for quantization operations and conference link communication.

The chapter is organized as follows. Section 5.1 introduce the background and motivation of this chapter. Section 5.2 specifies the model of the virtual-MIMO system with MMSE receiver. The closed-form upper bound for the system BER is derived in Section 5.3. Details of the proposed adaptive modulation and cooperation scheme are presented in Section 5.4. Section 5.5 shows the simulation results, and Section 5.6 concludes the chapter.

5.1 Introduction

As mentioned in Chapters 3 and 4, the virtual-MIMO system has been proposed as an alternative to a point-to-point MIMO system, to improve channel capacity and link reliability of wireless communications [53] [7]. Our research focuses on such a virtual-MIMO network with one

remote multi-antenna transmitter sending information to several closely spaced single-antenna receivers. Virtual-MIMO operation is realized via receiver-side local cooperation. Through cooperation, it is possible to exploit the performance of traditional MIMO techniques without each node needing multiple antennas. The CF protocol, which is shown to provide better performance when the relays are closer to the destination, is selected to realize receiver-side local cooperation.

Similar to Chapters 3 and 4, we implement the BICM technique [55], which separates the aspects of coding and modulation by using a bit-interleaver, as a FEC coding scheme to mitigate the effects of multipath fading and improve performance. Recently, BICM has been studied in MIMO systems with ML detection or linear detection. The disadvantage of the ML receiver is the high computational complexity, which increases exponentially with the product of the number of transmit antennas and the number of bits per symbol, making it prohibitive in practice. A significant complexity reduction can be obtained by employing linear receivers, i.e. linear zero-forcing (ZF) and minimum mean square error (MMSE) receivers. For uncoded systems, linear receivers do not perform well in comparison with ML [99]. Coded MIMO-BICM systems with ZF and MMSE receivers were proposed and analyzed in [70, 100, 101]. In contrast to the uncoded case, [70] and [101] show that both linear receivers perform remarkably well compared with ML, especially for high-order modulation and when $N_r \geq N_t$. An important conclusion in [100] explained this phenomenon: the log-likelihood criterion combined with BICM transmission acts to counteract any noise enhancement from the linear receiver. This is because the deinterleaver evenly distributes the low reliability bit metrics from noise-enhanced subchannels, and then the soft-input decoder is able to correct the errors. Furthermore, the corresponding VBLAST (Vertical-Bell Laboratories Layered Space-Time) (ZF and MMSE) receivers were examined, and it is shown that they suffer severely from error propagation [100]. Thus, as the linear MMSE receiver implies the same complexity order with the ZF receiver, but outperforms ZF and VBLAST receivers when combined with BICM techniques, we implement the MMSE receiver at the destination in the virtual-MIMO system. The challenge now is to investigate the performance of the MMSE receiver when considering the impact of cooperation.

The above recent works focus on the non-adaptive MIMO scenarios. It is well known that, adapting the transmission parameters such as the modulation and coding rate to the changing channel conditions, have recently emerged as a powerful technique for improving the system in terms of the data rate and spectral efficiency [102, 103]. Adaptive modulation designs based on

perfect or imperfect CSI at both the transmitter and receiver have been proposed in [104–106], rely on approximations for their BER calculations. More recently, the MIMO transmission method (i.e. diversity, multiplexing or hybrid) adaptation is combined with the conventional adaptive modulation and coding, e.g. [103] and [107]. In the latter, an adaptive transmission scheme considered MIMO BICM is proposed to maximize the system throughput. In practice, the current wireless standards employing MIMO technology (i.e., IEEE 802.11n, IEEE 802.16e, and 3GPP LTE) define different sets of modulation orders and coding rates. Standard wireless communication systems therefore use the lookup tables with predefined sets to enable adaptation. As the adaptive modulation technique has the potential of increasing the system throughput and spectral efficiency, we use it for our virtual-MIMO system in this chapter. Different from previous works which are typically based on BER calculations, in this work we adopt the smallest singular value as the switching criterion. Additionally, an adaptive-rate CF scheme will be proposed at the relay, so that minimum possible quantization rate could be selected to eliminate unnecessary complexity.

In this chapter, we consider a virtual-MIMO-BICM system that implements CF cooperation and MMSE detection. Chapter 3 and Chapter 4 use a similar system model, but with ML detection. Chapter 3 concentrates on the system performance assessment, including a comparison between the standard source coding and Wyner-Ziv coding technique at the relay, and an impact analysis of a non-ideal cooperation link. Chapter 4 focuses on the codebook design algorithms at the relay to enable CF cooperation, and proposes a clock synchronization and joint CFO estimation scheme to overcome the effects of CFO. The expression for the upper bound on error ratio in Chapter 3 cannot be expressed in a simple closed form, due to the use of ML detection, and needs to be evaluated using the Monte Carlo method. Compared to ML detection, the MMSE receiver used in this chapter is a better choice to achieve low complexity receiver implementations. Moreover, compared to Chapter 3 and Chapter 4 where no adaptation is considered, this chapter will propose an adaptive modulation and cooperation scheme.

We now summarize the main contributions of this chapter. First, for the practical virtual-MIMO-BICM system (with MMSE detection), we derive an expression to upper bound the system BER. The expression is obtained in closed form and shows that the smallest singular value of the cooperative channel matrix dominates the system BER. Moreover, an adaptive modulation and cooperation scheme is proposed, adopting the smallest singular value as the threshold strategy. The closed-form cumulative distribution function for the smallest singular

value is derived as well. The system could therefore adapt its modulation type to the prevailing channel conditions and choose the minimum possible quantization rate. It is shown that the proposed scheme eliminates unnecessary complexity, and enables the system to achieve comparable performance to the case with fixed quantization rates.

5.2 The Virtual-MIMO System with MMSE Detection

5.2.1 Channel Model

Similar to Chapters 3 and 4, we consider a virtual-MIMO wireless network with one remote N_t-antenna transmitter that implements BICM transmission, and N_r closely spaced single-antenna receivers, where $N_t = N_r = 2$. Further improvements are expected for the case of more cooperating terminals with larger numbers of antennas. The structure of the transmitter is the same as shown in Figure 3.2 (also given in Figure 5.1 for convenience). At the transmitter, the information bits are encoded through a rate-R_b linear binary convolutional encoder, and then interleaved through a random bit interleaver (int.). Gray-labeled $2^m = M$-ary QAM or PSK is considered for each stream after the demultiplexer (or demux).

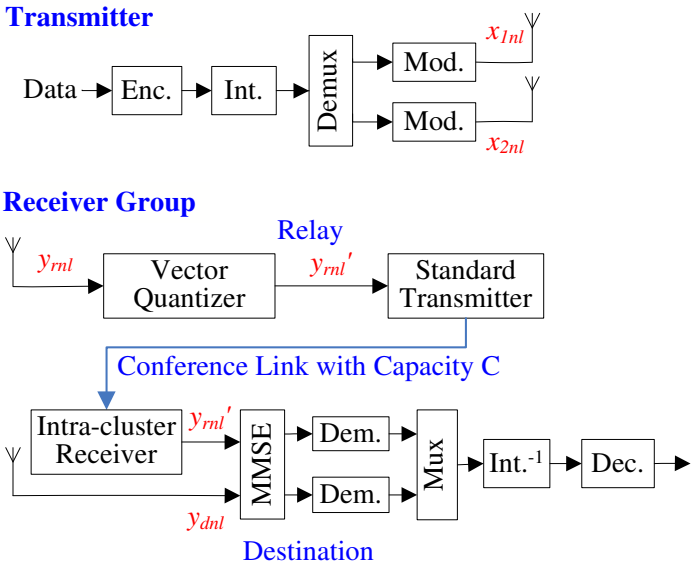

Figure 5.1: *System model of the cooperative virtual-MIMO system with MMSE detection. ($N_t = 2$, $N_r = 2$.)*

As the transmitter is far away from the receiver group, we also assume the channels between

them are block fading, with N Rayleigh fading blocks and each block has L consecutive time instants. When we consider a single time instance l for the nth channel, the channel model is shown in equation (3.1). We assume normalized Rayleigh fading, i.e. $\mathrm{E}[|h_{in}|^2] = 1$. We also normalize the total power E_s to unity. Then the average signal-to-noise ratio (SNR) will be $\mathrm{SNR} = E_s/N_0 = 1/N_0$. The corresponding power per bit is $E_b = E_s/(mR_b)$.

As the destination and the helping relay are closely spaced, it is highly likely that a high capacity communication link with high reliability can be formed between them [11]. As also considered in [7] [63] [58] and Chapter 4, we assume the two receivers cooperate by way of an one-shot error-free conference link, with capacity C, as shown in Figure 5.1. In practice, compared with the long range data channel $\boldsymbol{H}_n$, the orthogonal conference link is short-range with low transmission power, and could be reused many times over the coverage area of the long range link.

The conference link enables cooperation, and CF is the preferred protocol when the relay is closer to the destination [10]. Vector quantization is chosen here to implement CF at the relay. In order to demonstrate the achievable performance improvements and sensitivities with MMSE detection, we apply the Voronoi VQ only, to design the codebook needed for the quantization. Voronoi VQ has the feature that the codebook is optimal in the sense of minimising average distortion. Some other quantization methods, such as tree-structure VQ (shown in Chapter 4), could also be implemented, but at the cost of a small performance loss. Here the quantization rate is equal to the capacity C of the error-free conference link. Then a compressed version of the signal y'_{rnl} will be transmitted over the conference link, where $y'_{rnl} = y_{rnl} + w_{cnl}$. The destination receives signals $\boldsymbol{y}_{nl}$, where $\boldsymbol{y}_{nl} = [y'_{rnl} \;\; y_{dnl}]^{\mathrm{T}}$, as shown in Figure 5.1. With knowledge of σ^2_{cn}, and assuming w_{cnl} is i.i.d. complex Gaussian noise, we scale y'_{rnl} so that y'_{rnl} and y_{dnl} have the same power of additive Gaussian noise. Then we obtain the scaled channel matrix $\widetilde{\boldsymbol{H}}_n$ as shown in (3.4). For a wired conference link with high capacity C, σ^2_{cn} decreases to 0, and the system will behave as in the ideal MIMO case.

Note that, in the rest of this chapter, when we are considering a single time instance l on the nth channel, we will drop the subscript nl for the symbols and n for the channel matrix, since the received symbols are treated independently.

5.2.2 MMSE-based BICM Demodulation

The general structure of the destination with a linear MMSE receiver is shown in Figure 5.1. The first MMSE filtering step is,

$$\boldsymbol{z} = \boldsymbol{W}\tilde{\boldsymbol{y}} = \boldsymbol{x} + \boldsymbol{e} + \boldsymbol{v}, \text{ with } \boldsymbol{W} = \boldsymbol{B}\left(\widetilde{\boldsymbol{H}}^{\dagger}\widetilde{\boldsymbol{H}} + \frac{N_t}{\text{SNR}}\boldsymbol{I}\right)^{-1}\widetilde{\boldsymbol{H}}^{\dagger}, \tag{5.1}$$

where $\boldsymbol{e} = (\boldsymbol{W}\widetilde{\boldsymbol{H}} - \boldsymbol{I})\boldsymbol{x}$ is the residual inter-symbol interference (ISI), and $\boldsymbol{v} = \boldsymbol{W}[\tilde{w}_1 \;\; w_2]^{\text{T}}$ denotes the colored Gaussian noise vector. Here $\boldsymbol{H}^{\dagger}$ denotes the conjugate transpose of $\boldsymbol{H}$. Also, $\boldsymbol{B}$ is a diagonal matrix which removes the bias from the MMSE estimates, with kth diagonal component given by,

$$\boldsymbol{B}_{k,k} = \frac{\rho_k + 1}{\rho_k} = \left[\boldsymbol{I} + \frac{N_t}{\text{SNR}}(\widetilde{\boldsymbol{H}}^{\dagger}\widetilde{\boldsymbol{H}})^{-1}\right]_{k,k}. \tag{5.2}$$

The scalar ρ_k is the instantaneous received signal to interference and noise ratio (SINR) for the kth stream [108], given by,

$$\rho_k = \frac{1}{\left[(\boldsymbol{I}_{N_t} + \frac{\text{SNR}}{N_t}\widetilde{\boldsymbol{H}}^{\dagger}\widetilde{\boldsymbol{H}})^{-1}\right]_{k,k}} - 1. \tag{5.3}$$

We denote $\mathcal{X}_b^{\lambda,k}$ as the subset within the kth transmit constellation where the λth bit is equal to b. For MMSE detection, the BICM LLR for each coded bit corresponding to x_k is calculated from z_k and denoted by $\mathcal{L}(c^{\lambda}|z_k, \boldsymbol{W})$, as [100],

$$\begin{aligned}\mathcal{L}(c^{\lambda}|z_k, \boldsymbol{W}) &= \ln\frac{\Pr\{c^{\lambda}=1|z_k,\boldsymbol{W}\}}{\Pr\{c^{\lambda}=0|z_k,\boldsymbol{W}\}} = \ln\frac{\sum_{\tilde{x}_k\in\mathcal{X}_1^{\lambda,k}} p\{z_k|\tilde{x}_k,\boldsymbol{W}\}}{\sum_{\tilde{x}_k\in\mathcal{X}_0^{\lambda,k}} p\{z_k|\tilde{x}_k,\boldsymbol{W}\}} \\ &= \ln\frac{\sum_{\tilde{x}_k\in\mathcal{X}_1^{\lambda,k}} \exp\left(-\rho_k|z_k-\tilde{x}_k|^2\right)}{\sum_{\tilde{x}_k\in\mathcal{X}_0^{\lambda,k}} \exp\left(-\rho_k|z_k-\tilde{x}_k|^2\right)},\end{aligned} \tag{5.4}$$

where $\lambda = 1, ..., m$. The two path LLRs are combined into one output stream by the multiplexer, and reordered by the deinterleaver. Finally, the decoder accepts the LLRs of all coded bits and employs a soft-input Viterbi algorithm to decode the signals.

The benefit of the MMSE receiver is the lower computational complexity. However, it suffers from residual ISI caused by the compression noise w_c, as will be illustrated in Section 5.3. A good quantization scheme with low compression noise at the relay, will enable the virtual-

MIMO system to achieve almost ideal MIMO performance.

5.3 Upper Bound on Bit Error Ratio

Throughout the chapter, we consider block fading channels, for which a fading envelope is given by $\mathcal{H} = (\boldsymbol{H}_1, ..., \boldsymbol{H}_N)$. For a specific channel condition $\boldsymbol{H}$, the union bound on the conditional BER for linear binary convolutional codes over a memoryless binary-input output-symmetric (BIOS) channel can be expressed as [71],

$$P_b(\boldsymbol{H}) \leq \sum_{d=d_{\text{free}}}^{\infty} A_d P_d(d|\boldsymbol{H}) \approx \sum_{d=d_{\text{free}}}^{d_{\text{free}}+10} A_d P_d(d|\boldsymbol{H}), \tag{5.5}$$

where $P_d(d|\boldsymbol{H})$ is the conditional PEP for two codewords differing in d bits, and A_d is the sum of bit errors for error events of distance d, as defined in Chapter 3 for (3.20). With d increasing, the influence of A_d and $P_d(d|\boldsymbol{H})$ on the conditional BER will decrease dramatically. Truncation to 10 terms in (5.5), yields a very good upper bound (UB) of the true $P_b(\boldsymbol{H})$ [72] [109]. The average BER after decoding is obtained by averaging $P_b(\boldsymbol{H})$ over the fading channel matrices,

$$P_b \leq \mathop{\mathrm{E}}_{\boldsymbol{H}\in\mathcal{H}} \left[\min \left\{ \frac{1}{2}, \sum_{d=d_{\text{free}}}^{d_{\text{free}}+10} A_d P_d(d|\boldsymbol{H}) \right\} \right], \tag{5.6}$$

where a BER limit of $1/2$ for the Viterbi decoder is included [73], as also shown in (3.22). The expectation in (5.6) can be evaluated using the Monte Carlo method in practice.

Similar to Chapter 3, for our block fading channel which is not BIOS [74], we adopt the approach of [55] and force the BICM channel to behave as BIOS by using a random modulation concept. Furthermore, due to the symmetry of the channel output, we can safely assume that the all-zero codewords are transmitted. Thus when we are considering the random modulation concept and all-zero codewords, the form of LLR for the MMSE receiver (which is given in (5.4)) will be changed slightly,

$$\mathcal{L}(c^{\lambda}|z_k, \boldsymbol{W}) = \ln \frac{\sum_{\tilde{x}_k \in \mathcal{X}_{\tilde{t}}^{\lambda,k}} \exp\left(-\rho_k |z_k - \tilde{x}_k|^2\right)}{\sum_{\tilde{x}_k \in \mathcal{X}_{t}^{\lambda,k}} \exp\left(-\rho_k |z_k - \tilde{x}_k|^2\right)}. \tag{5.7}$$

We employ the Gaussian approximation (GA) [71] [75], which is a simple and accurate way to

approximate $P_d(d|\boldsymbol{H}_n)$, and obtain,

$$P_d(d|\boldsymbol{H}) \approx Q\left(\sqrt{-2dK_{\mathcal{L}}(\hat{s})}\right), \tag{5.8}$$

where $K_{\mathcal{L}}(s)$ is the cumulant generating function of the variable $\mathcal{L}(c^{\lambda}|z_k, \boldsymbol{W})$ defined in (5.7). By contrast to (3.26) for ML detection, $K_{\mathcal{L}}(s)$ for MMSE detection is given by,

$$\begin{aligned} K_{\mathcal{L}}(s) &= \log \mathop{\mathrm{E}}_{\mathbf{z},\lambda,t,k,\boldsymbol{W}} \left[\exp\left(s\ \mathcal{L}(c^{\lambda}|z_k, \boldsymbol{W})\right)\right] \\ &= \log \mathop{\mathrm{E}}_{\mathbf{z},\lambda,t,k,\rho_k|\boldsymbol{H}} \left[\exp\left(s \ln \frac{\sum_{\tilde{x}_k \in \mathcal{X}_{\bar{t}}^{\lambda,k}} \exp\left(-\rho_k |z_k - \tilde{x}_k|^2\right)}{\sum_{\tilde{x}_k \in \mathcal{X}_{t}^{\lambda,k}} \exp\left(-\rho_k |z_k - \tilde{x}_k|^2\right)}\right)\right] \\ &= \log \mathop{\mathrm{E}}_{\mathbf{z},\lambda,t,k,\rho_k} \left[\left(\frac{\sum\limits_{\tilde{x}_k \in \mathcal{X}_{\bar{t}}^{\lambda,k}} \exp\left(-\rho_k |(x_k - \tilde{x}_k) + e_k + \upsilon_k|^2\right)}{\sum\limits_{\tilde{x}_k \in \mathcal{X}_{t}^{\lambda,k}} \exp(-\rho_k |(x_k - \tilde{x}_k) + e_k + \upsilon_k|^2)}\right)^s\right]. \end{aligned} \tag{5.9}$$

The SINR ρ_k defined in (5.3) is related with the channel condition $\boldsymbol{H}$. For BIOS channels, symmetry dictates that the saddlepoint $\hat{s}$ in (5.8) is placed at $\hat{s} = 1/2$ [71]. A closed form of $K_{\mathcal{L}}(s)$ for high SNR can be stated as follows:

Theorem 1: For a receiver using MMSE detection, when SNR is high, the cumulant generating function of $\mathcal{L}(c^{\lambda}|z_k, \boldsymbol{W})$ can be obtained in closed form,

$$K_{\mathcal{L}}(s) = \log\left[\frac{1}{m2^m N_t} \sum_{\lambda=1}^{m} \sum_{t=0}^{1} \sum_{k=1}^{N_t} \sum_{x_k \in \mathcal{X}_t^{\lambda,k}} \left[\exp(-\rho_k (s - s^2) |x_k - \tilde{x}_k|^2)\right]\right]. \tag{5.10}$$

The proof is presented as follows: As defined in (5.9), averaging over λ, t, k, $x_k \in \mathcal{X}_t^{\lambda,k}$, $K_{\mathcal{L}}(s)$ is given by,

$$K_{\mathcal{L}}(s) = \log\left[\frac{1}{m2^m N_t} \sum_{\lambda=1}^{m} \sum_{t=0}^{1} \sum_{k=1}^{N_t} \sum_{x_k \in \mathcal{X}_t^{\lambda,k}} \Lambda(s, \lambda, t, k, x_k, \rho_k)\right], \tag{5.11}$$

$$\text{with } \Lambda(s, \lambda, t, k, x_k, \rho_k) = \mathop{\mathrm{E}}_{e_k, \upsilon_k} \left[\left(\frac{\sum\limits_{\tilde{x}_k \in \mathcal{X}_{\bar{t}}^{\lambda,k}} \exp\left(-\rho_k |(x_k - \tilde{x}_k) + e_k + \upsilon_k|^2\right)}{\sum\limits_{\tilde{x}_k \in \mathcal{X}_{t}^{\lambda,k}} \exp(-\rho_k |(x_k - \tilde{x}_k) + e_k + \upsilon_k|^2)}\right)^s\right]. \tag{5.12}$$

At high SNR, the ratio in (5.12) is dominated by a single minimum distance term in the numerator and denominator. Thus we can apply the Dominated Convergence Theorem [71] and

obtain,

$$\Lambda(s,\lambda,t,k,x_k,\rho_k) = \underset{e_k,\upsilon_k}{\mathrm{E}}\left[\left(\frac{\exp\left(-\rho_k|(x_k-\tilde{x}_k)+e_k+\upsilon_k|^2\right)}{\exp(-\rho_k|e_k+\upsilon_k|^2)}\right)^s\right],$$

where $\tilde{x}_k \in \mathcal{X}_t^{\lambda,k}$ is the nearest neighbour to $x_k \in \mathcal{X}_t^{\lambda,k}$. Then we simplify $\Lambda(s,\lambda,t,k,x_k,\rho_k)$ as follows

$$\begin{aligned}
&\Lambda(s,\lambda,t,k,x_k,\rho_k)\\
&= \underset{e_k,\upsilon_k}{\mathrm{E}}\left[\exp\left(-\rho_k\left(s|(x_k-\tilde{x}_k)+e_k+\upsilon_k|^2-s|e_k+\upsilon_k|^2\right)\right)\right]\\
&= \underset{e_k,\upsilon_k}{\mathrm{E}}\left[\exp\left(-\rho_k\left(s|x_k-\tilde{x}_k|^2-2s\mathrm{Re}\{(x_k-\tilde{x}_k)(e_k+\upsilon_k)^*\}\right)\right)\right] \qquad (5.13)\\
&= \underset{e_k,\upsilon_k}{\mathrm{E}}[\exp(-\rho_k s|x_k-\tilde{x}_k|^2)\cdot\exp(-2\rho_k s\mathrm{Re}\{(x_k-\tilde{x}_k)e_k^*\})\\
&\qquad \cdot\exp(\rho_k(-|\upsilon_k+s(x_k-\tilde{x}_k)|^2+s^2|x_k-\tilde{x}_k|^2+|\upsilon_k|^2))].
\end{aligned}$$

It is well known that for Gray-labeled signal constellation,

$$\sum_{\lambda=1}^{m}\sum_{t=0}^{1}\sum_{k=1}^{N_t}\sum_{x_k\in\mathcal{X}_t^{\lambda,k}}(x_k-\tilde{x}_k)=0. \qquad (5.14)$$

Thus we proceed to average $\Lambda(s,\lambda,t,k,x_k,\rho_k)$ over the random noise υ_k and then over the residual ISI e_k. We now have,

$$\begin{aligned}
&\Lambda(s,\lambda,t,k,x_k,\rho_k)\\
&= \underset{e_k}{\mathrm{E}}\left[\exp(-\rho_k(s-s^2)|x_k-\tilde{x}_k|^2)\cdot\exp(-2\rho_k s\mathrm{Re}\{(x_k-\tilde{x}_k)e_k^*\})\right] \qquad (5.15)\\
&= \left[\exp(-\rho_k(s-s^2)|x_k-\tilde{x}_k|^2)\right].
\end{aligned}$$

Substituting (5.15) into (5.11), we obtain (5.10). □

We can see that now $K_{\mathcal{L}}(s)$ depends on ρ_k and the squared Euclidean distance from x_k to its nearest neighbour $\tilde{x}_k$ in the complement subset. According to the Gray-labeled PSK/QAM constellations used in this system, we can further simplify $K_{\mathcal{L}}(s)$ by exploiting multiplicities of the Euclidean distance. Table 5.1 presents (for various constellations) the set of all distinct squared Euclidean distances ($|x_k-\tilde{x}_k|^2$), and the corresponding frequency of occurrence of each distance (normalized by the total number of distances $m2^m$) [1]. The corresponding values of $(s-s^2)|x_k-\tilde{x}_k|^2$ in Table 5.1 could be used directly in our case to further simplify $K_{\mathcal{L}}(s)$ in (5.10).

For example, when we consider the saddlepoint $\hat{s}=1/2$, we obtain $K_{\mathcal{L}}(\hat{s})$ for Gray-labelled

	Squared Euclidean distances ($\|x_k - \tilde{x}_k\|^2$)	Occurrence frequencies (normalized by $m2^m$)	$(s - s^2)\|x_k - \tilde{x}_k\|^2$ in (5.10) when $\hat{s} = 1/2$
BPSK	{4.0}	{1}	{1.0}
QPSK	{2.0}	{1}	{0.5}
16QAM	{0.4, 1.6}	{3/4, 1/4}	{0.1, 0.4}
64QAM	{0.0952, 0.3810, 0.8571, 1.5238}	{7/12, 1/4, 1/12, 1/12}	{0.0238, 0.0953, 0.2143, 0.3810}

Table 5.1: *Breakdown of distance multiplicities for various Gray-labeled constellations [1].*

16QAM and 64QAM,

$$K_{\mathcal{L}}(\hat{s})_{16\text{QAM}} = \log\left[\frac{1}{N_t}\sum_{k=1}^{N_t}\left(\frac{3}{4}\exp(-0.1\rho_k)+\frac{1}{4}\exp(-0.4\rho_k)\right)\right], \tag{5.16}$$

$$K_{\mathcal{L}}(\hat{s})_{64\text{QAM}} = \log\left[\frac{1}{N_t}\sum_{k=1}^{N_t}\left(\frac{7}{12}\exp(-0.0238\rho_k)+\frac{1}{4}\exp(-0.0953\rho_k)\right.\right.$$
$$\left.\left.+\frac{1}{12}\exp(-0.2143\rho_k)+\frac{1}{12}\exp(-0.3810\rho_k)\right)\right]. \tag{5.17}$$

After the simplification, compared to BPSK and QPSK which have N_t terms in equation (5.10), 16QAM has $2N_t$ terms (as shown in (5.16)), and 64QAM has $4N_t$ terms (as shown in (5.17)). The simplification is helpful to reduce computational complexities of $K_{\mathcal{L}}(\hat{s})$ with higher-order modulations.

Now, substituting (5.10) into (5.8) gives a closed-form expression for approximating $P_d(d|\boldsymbol{H})$, leading to a closed-form solution for the UB of $P_b(\boldsymbol{H})$ from (5.5). The conditional BER UB is very useful since it provides insight into the asymptotic behaviour of the system error probability and can be used to judge the condition of the specific channel $\boldsymbol{H}$. The bound computed using GA is very close to the simulation results, as will be seen in Section 5.5.

Additionally, for a receiver using MMSE detection, ρ_k suffers from the residual ISI caused by the compression noise w_c. From (5.10), it is obvious that a lower value of ρ_k results in a larger value of $K_{\mathcal{L}}(s)$ and finally a higher $P_b(\boldsymbol{H})$. Compared to the corresponding MIMO system, the virtual-MIMO system will have an impaired BER performance since it uses CF cooperation and MMSE detection. A higher quantization rate C is one solution with decreasing w_c, but will introduce additional operational complexity for quantizations at the relay. Another solution

is to employ a lower-order modulation at the transmitter, but this will decrease the system throughput as a result. Thus an adaptive modulation and cooperation scheme will be a suitable solution here, as will be described in Section 5.4.

5.4 Adaptive Modulation and Cooperation Scheme

The basic motivation for this proposed scheme is the fact that fixed modulation or fixed-rate cooperation can not adapt well to varying channel conditions, especially for a system with MMSE detection. If we could apply a suitable threshold strategy to judge the conditions of the instantaneous channels, the system could choose different modulation types and quantization rates, according to different realisations of $\widetilde{\boldsymbol{H}}$. Furthermore, when the channel is quite well conditioned, a smaller C may be sufficient for the system to achieve a good performance. It would eliminate unnecessary complexity for quantization when performing CF cooperation. Thus, the key issues of the adaptive modulation and cooperation scheme are exploiting the relationship between the system performance and the channel properties, and finding an appropriate switching criterion.

5.4.1 Threshold Strategy

For the threshold design, we propose to adopt the smallest singular value of the cooperative channel matrix as the threshold strategy, and the following theorem shows the reason.

Theorem 2: For the virtual-MIMO system using MMSE detection, the smallest singular value of the cooperative channel matrix has a direct impact on the system performance. We have,

$$K_{\mathcal{L}}(\hat{s}) \leq \log\left[\frac{1}{m2^m}\sum_{\lambda=1}^{m}\sum_{t=0}^{1}\sum_{x_k\in\mathcal{X}_t^{\lambda,k}}\left(\exp(-\frac{\mathrm{SNR}}{4N_t}\lambda_{\min}^2(\widetilde{\boldsymbol{H}})\cdot|x_k-\tilde{x}_k|^2)\right)\right]. \tag{5.18}$$

A proof of the theorem is as follows: From (5.10), it is obvious that, for a given channel condition and a specific constellation, $K_{\mathcal{L}}(s)$ only depends on the SINR ρ_k. Further the value $\rho_{\min}$ which equals to $\min\{\rho_k\}(k\in[1,N_t])$ dominates $K_{\mathcal{L}}(s)$. When $\hat{s}=1/2$, we have,

$$K_{\mathcal{L}}(\hat{s}) \leq \log\left[\frac{1}{m2^m}\sum_{\lambda=1}^{m}\sum_{t=0}^{1}\sum_{x_k\in\mathcal{X}_t^{\lambda,k}}\left(\exp(-\rho_{\min}|x_k-\tilde{x}_k|^2/4)\right)\right]. \tag{5.19}$$

Using the fact that the largest eigenvalue majorizes the largest diagonal term of a square matrix [110], from (5.3) we have

$$\begin{aligned}\rho_{\min} &\geq \frac{1}{\lambda_{\max}\left((\boldsymbol{I}_{N_t}+\frac{\text{SNR}}{N_t}\widetilde{\boldsymbol{H}}^{\dagger}\widetilde{\boldsymbol{H}})^{-1}\right)}-1 \\ &= \lambda_{\min}\left(\boldsymbol{I}_{N_t}+\frac{\text{SNR}}{N_t}\widetilde{\boldsymbol{H}}^{\dagger}\widetilde{\boldsymbol{H}}\right)-1 \;=\; \frac{\text{SNR}}{N_t}\lambda^2_{\min}\left(\widetilde{\boldsymbol{H}}\right). \end{aligned} \tag{5.20}$$

For a given channel $\widetilde{\boldsymbol{H}}$, it is obvious that a large value of $\lambda_{\min}\left(\widetilde{\boldsymbol{H}}\right)$ guarantees a large value of $\rho_{\min}$, and then guarantees a small value of $K_{\mathcal{L}}(s)$, and thus results in a low BER. In other words, for a symbol error to occur, a necessary condition is that $\lambda_{\min}$ for the scaled channel matrix falls below a certain threshold. Inserting (5.20) into (5.19), we obtain (5.18). For example, when we consider Gray-labelled 16QAM and 64QAM, we obtain,

$$K_{\mathcal{L}}(\hat{s})_{16\text{QAM}} \leq \log\left[\frac{3}{4}\exp\left(-0.1\frac{\text{SNR}}{N_t}\lambda^2_{\min}(\widetilde{\boldsymbol{H}})\right)+\frac{1}{4}\exp\left(-0.4\frac{\text{SNR}}{N_t}\lambda^2_{\min}(\widetilde{\boldsymbol{H}})\right)\right], \tag{5.21}$$

$$\begin{aligned}K_{\mathcal{L}}(\hat{s})_{64\text{QAM}} \leq \log\Bigg[&\frac{7}{12}\exp\left(-0.0238\frac{\text{SNR}}{N_t}\lambda^2_{\min}(\widetilde{\boldsymbol{H}})\right)+\frac{1}{4}\exp\left(-0.0953\frac{\text{SNR}}{N_t}\lambda^2_{\min}(\widetilde{\boldsymbol{H}})\right) \\ &+\frac{1}{12}\exp\left(-0.2143\frac{\text{SNR}}{N_t}\lambda^2_{\min}(\widetilde{\boldsymbol{H}})\right)+\frac{1}{12}\exp\left(-0.3810\frac{\text{SNR}}{N_t}\lambda^2_{\min}(\widetilde{\boldsymbol{H}})\right)\Bigg]. \end{aligned} \tag{5.22}$$

Hence $\lambda_{\min}\left(\widetilde{\boldsymbol{H}}\right)$ has a direct impact on the system performance.

As will shown in Section 5.5, the BER performance is very well approximated by the UB based on $\rho_{\min}$ for various quantization rates. Thus it is reasonable and efficient to characterise the quality of the cooperative virtual-MIMO channel based on its smallest singular value squared. In practice, the nature of the short-range conference link is helpful for information exchanges. Once the conference link formed, the channel CSI and the estimated value of σ_c^2 will be shared between the relay and the destination, so that the channel singular values $\lambda_{\min}\left(\widetilde{\boldsymbol{H}}\right)$ can be computed.

5.4.2 Adaptive Modulation Scheme

As shown in Chapter 4, with the Voronoi VQ, when the quantization codebook could represent the constellation accurately at the relay, e.g. $C = 4$ bits/sample for QPSK modulation and $C = 8$ bits/sample for 16QAM, the cooperative virtual-MIMO system will perform very close to the ideal MIMO system, and therefore $\widetilde{\boldsymbol{H}}$ will tend towards $\boldsymbol{H}$ in value. Combining Table

5.1 and (5.18) (also from (5.21) and (5.22)), it is obvious that for a given channel $\boldsymbol{H}$, $K_{\mathcal{L}}(\hat{s})$ for lower-order modulation is always smaller than that for higher-order modulation, which means that its conditional BER is always lower (at the cost of reduced bit rate). Thus when the channels are poorly conditioned, the system could adapt to provide reliable communications using a lower-order modulation, e.g. QPSK, and C=4 bits/sample at the relay.

As shown in Chapter 3, the throughput of the cooperative virtual MIMO-BICM system is calculated by considering the AMI for each bit level. When we consider the MMSE detection, different from (3.17), the conditional AMI for the λth bit level is given by [70] ,

$$\begin{aligned} I(c^{\lambda}; z_k|\boldsymbol{W}) &= 1 - \underset{c^{\lambda}|z_k,\boldsymbol{W}}{\mathrm{E}} \left(\log_2 \frac{\sum_{\tilde{x}_k \in \mathcal{X}^k} p\{z_k|\tilde{x}_k, \boldsymbol{W}\}}{\sum_{\tilde{x}_k \in \mathcal{X}_0^{\lambda,k}} p\{z_k|\tilde{x}_k, \boldsymbol{W}\}} \right). \\ &= 1 - \underset{c^{\lambda}|z_k,\boldsymbol{W}}{\mathrm{E}} \left(\log_2 \frac{\sum_{\tilde{x}_k \in \mathcal{X}^k} \exp\left(-\rho_k |z_k - \tilde{x}_k|^2\right)}{\sum_{\tilde{x}_k \in \mathcal{X}_0^{\lambda,k}} \exp\left(-\rho_k |z_k - \tilde{x}_k|^2\right)} \right) \end{aligned} \tag{5.23}$$

Assuming ideal interleaving, the channel can be considered to be ergodic [55]. Then the system throughput C_{CF} is obtained by averaging the AMI over the fading channels,

$$\begin{aligned} C_{\mathrm{CF}} &= \underset{\boldsymbol{H}\in\mathcal{H}}{\mathrm{E}} \left[\sum_{\lambda=1}^{mN_t} I(c^{\lambda}; z_k|\boldsymbol{W}) \right] \\ &= mN_t - \underset{\boldsymbol{H}\in\mathcal{H}}{\mathrm{E}} \left[\sum_{\lambda=1}^{mN_t} \underset{c^{\lambda}|z_k,\boldsymbol{W}}{\mathrm{E}} \left(\log_2 \frac{\sum_{\tilde{x}_k \in \mathcal{X}^k} \exp\left(-\rho_k |z_k - \tilde{x}_k|^2\right)}{\sum_{\tilde{x}_k \in \mathcal{X}_0^{\lambda,k}} \exp\left(-\rho_k |z_k - \tilde{x}_k|^2\right)} \right) \right]. \end{aligned} \tag{5.24}$$

It is obvious that a higher-order modulation (with a large m) at the transmitter guarantees a higher system throughput. Thus when the channels are well-conditioned or the SNR is high, the system should adapt to achieve large bit rates using a higher-order modulation, e.g. 64QAM, and a sufficient quantization rate at the relay. The adaptive-rate CF scheme will be illustrated in Section 5.4.3.

Now, we present a check criterion for the adaptive modulation scheme. Specifically, we set a threshold ξ for the UB of $P_b(\boldsymbol{H})$. For different modulations (e.g. 64QAM and 16QAM), according to (5.5), (5.8), (5.21) and (5.22), we could obtain corresponding thresholds of the smallest singular value, which are denoted by λ_{64QAM} and λ_{16QAM} as examples. The system would implement 64QAM for well-conditioned channels ($\lambda_{\min}(\boldsymbol{H}) \geq \lambda_{\text{64QAM}}$), and 16QAM for "in-between" channels ($\lambda_{\text{16QAM}} \leq \lambda_{\min}(\boldsymbol{H}) < \lambda_{\text{64QAM}}$). Otherwise, for poorly conditioned channels ($\lambda_{\min}(\boldsymbol{H}) < \lambda_{\text{16QAM}}$), 16QAM signals may not be decoded successfully, and the sys-

tem would switch back to QPSK modulation.

Note that the adaptive modulation scheme studied here switches between QPSK, 16QAM and 64QAM modulations, but the approach could easily be extended to multiple modulation and coding rate choices, for example, applied to High Speed Packet Access (HSPA) and Long Term Evolution (LTE) systems [111].

5.4.3 Adaptive-rate CF Scheme

When channel conditions are good and a high-order modulation is selected, vector quantization with a large C may cause a high processing burden for the relay to perform CF cooperation. If the channel is quite well conditioned, a smaller quantization rate may be enough for the system to achieve a good performance. Thus an adaptive-rate CF scheme is also proposed at the relay, with choosing different quantization rates according to different channel conditions.

To facilitate the threshold design, we investigate the closed-form cumulative distribution function (CDF) and the probability density function (PDF) of the smallest singular value. Recall the scaled channel matrix $\widetilde{\boldsymbol{H}}$ in (3.4), where we know that the scaled factor η is due to the compression noise σ_c^2. The lower bound on the compression noise variance is given in (3.7), i.e.

$$\bar{\sigma}_c^2 = \frac{N_0 + \frac{1}{2}|h_1|^2 + \frac{1}{2}|h_2|^2}{2^C - 1}. \tag{5.25}$$

If $|h_1|^2+|h_2|^2$ could be replaced by its expected value, $\bar{\eta}$ would become constant for a certain SNR and C according to (3.4). The scaled channel $\widetilde{\boldsymbol{H}}$ will be a complex Gaussian matrix, whose smallest singular value has been discussed in [112]. Hence it is reasonably appropriate to implement the expected value $\mathrm{E}[|h_1|^2+|h_2|^2]$ for the analysis of the smallest singular value and the corresponding threshold design. Then we have,

$$\widetilde{\boldsymbol{H}} = \begin{bmatrix} \sqrt{\bar{\eta}}h_1 & \sqrt{\bar{\eta}}h_2 \\ h_3 & h_4 \end{bmatrix} = \begin{bmatrix} \sqrt{\frac{2^C-1}{2^C+\mathrm{SNR}}}h_1 & \sqrt{\frac{2^C-1}{2^C+\mathrm{SNR}}}h_2 \\ h_3 & h_4 \end{bmatrix}, \tag{5.26}$$

which is distributed as $\mathcal{CN}(0, \boldsymbol{I} \otimes \boldsymbol{\Psi})$. $\boldsymbol{\Psi}$ is the covariance matrix, shown as,

$$\boldsymbol{\Psi} = \mathrm{E}\left[\begin{pmatrix} \sqrt{\bar{\eta}}h_1 \\ h_3 \end{pmatrix}\begin{pmatrix} \sqrt{\bar{\eta}}h_1 & h_3 \end{pmatrix}\right] = \begin{bmatrix} \bar{\eta} & 0 \\ 0 & 1 \end{bmatrix} = \begin{bmatrix} \frac{2^C-1}{2^C+\mathrm{SNR}} & 0 \\ 0 & 1 \end{bmatrix}. \tag{5.27}$$

Thus employing the results from [112], the CDF and PDF of $\lambda_{\min}(\widetilde{\boldsymbol{H}})$ is given by,

$$\begin{aligned} F_{\lambda_{\min}}(\lambda) &= 1 - \exp\left(-(1+\bar{\eta}^{-1})\lambda^2\right); \\ f_{\lambda_{\min}}(\lambda) &= 2(1+\bar{\eta}^{-1})\lambda \cdot \exp\left(-(1+\bar{\eta}^{-1})\lambda^2\right). \end{aligned} \tag{5.28}$$

Knowledge of the closed-form CDF and PDF provides direct insight into the distribution of $\lambda_{\min}(\widetilde{\boldsymbol{H}})$. Setting a CDF threshold helps us obtain the corresponding threshold for the smallest singular values. One attractive feature of the proposed threshold approach is that, with the CDF threshold, it is readily apparent what percent of the channels are well-conditioned. Our simulation results suggest that well-conditioned channels could support a lower quantization rate, and poorly-conditioned channels will need a higher quantization rate. The final average quantization rate is therefore predictable, which is another advantage of the threshold approach.

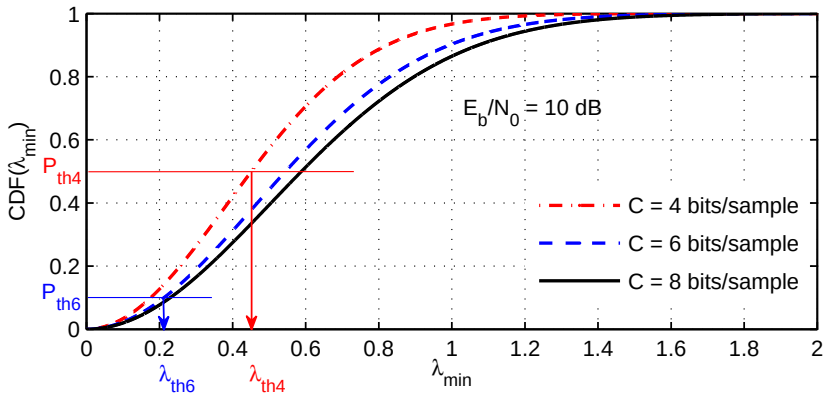

Figure 5.2: *CDF curves of the smallest singular value $\lambda_{\min}$ for various quantization rates, when $E_b/N_0 = 10$ dB.*

Take the quantization rates $C = 4$, 6 bits/sample and 8 bits/sample as an example. The CDF curves of $\lambda_{\min}(\widetilde{\boldsymbol{H}})$ for various values of C are shown in Figure 5.2. Based on the settings of the CDF thresholds, i.e. P_{th4} and P_{th6} shown in Figure 5.2, we will get λ_{th4} and λ_{th6} as the thresholds. For a given channel condition, the relay could design a codebook needed for each quantization rate. An estimate of the average distortion of the compression noise will be obtained, e.g. $\sigma^2_{c,4}$ for $C=4$ bits/sample, and $\sigma^2_{c,6}$ for $C=6$ bits/sample. Substituting them into (3.4), we get estimates of $\widetilde{\boldsymbol{H}}_4$ and $\widetilde{\boldsymbol{H}}_6$ respectively. Then $\lambda_{\min}(\widetilde{\boldsymbol{H}}_4)$ and $\lambda_{\min}(\widetilde{\boldsymbol{H}}_6)$ are obtained. Switching criterion for the adaptive-rate CF scheme is shown as (5.30) in Table 5.2. When 16QAM is selected, the channel conditions could be classified into three levels, and the relay

(0) Give the desired modulation types and quantization rates; (Here QPSK, 16QAM, and 64QAM, and $C = 4$, 6, 8, 10, 12 bits/sample are chosen as candidates as an example.)

(1) Confirm the thresholds λ_{16QAM}, λ_{64QAM}, λ_{th4}, λ_{th6}, λ_{th8}, and λ_{th10}; Compute the smallest singular values $\lambda_{\min}(\boldsymbol{H})$, $\lambda_{\min}(\widetilde{\boldsymbol{H}}_4)$, $\lambda_{\min}(\widetilde{\boldsymbol{H}}_6)$, $\lambda_{\min}(\widetilde{\boldsymbol{H}}_8)$, and $\lambda_{\min}(\widetilde{\boldsymbol{H}}_{10})$;

(2) Implement the adaptive modulation and cooperation scheme:

If $\lambda_{\min}(\boldsymbol{H}) \geq \lambda_{\text{64QAM}}$, then 64QAM is selected;

$$\begin{cases} \text{If } \lambda_{\min}(\widetilde{\boldsymbol{H}}_8) \geq \lambda_{\text{th8}} \text{ and } \lambda_{\min}(\widetilde{\boldsymbol{H}}_{10}) \geq \lambda_{\text{th10}}, \text{ then C=8 bits/sample;} \\ \text{If } \lambda_{\min}(\widetilde{\boldsymbol{H}}_8) < \lambda_{\text{th8}} \text{ and } \lambda_{\min}(\widetilde{\boldsymbol{H}}_{10}) \geq \lambda_{\text{th10}}, \text{ then C=10 bits/sample;} \\ \text{If } \lambda_{\min}(\widetilde{\boldsymbol{H}}_8) < \lambda_{\text{th8}} \text{ and } \lambda_{\min}(\widetilde{\boldsymbol{H}}_{10}) < \lambda_{\text{th10}}, \text{ then C=12 bits/sample;} \end{cases} \tag{5.29}$$

Else if $\lambda_{\text{16QAM}} \leq \lambda_{\min}(\boldsymbol{H}) \leq \lambda_{\text{64QAM}}$, then 16QAM is selected;

$$\begin{cases} \text{If } \lambda_{\min}(\widetilde{\boldsymbol{H}}_4) \geq \lambda_{\text{th4}} \text{ and } \lambda_{\min}(\widetilde{\boldsymbol{H}}_6) \geq \lambda_{\text{th6}}, \text{ then C=4 bits/sample;} \\ \text{If } \lambda_{\min}(\widetilde{\boldsymbol{H}}_4) < \lambda_{\text{th4}} \text{ and } \lambda_{\min}(\widetilde{\boldsymbol{H}}_6) \geq \lambda_{\text{th6}}, \text{ then C=6 bits/sample;} \\ \text{If } \lambda_{\min}(\widetilde{\boldsymbol{H}}_4) < \lambda_{\text{th4}} \text{ and } \lambda_{\min}(\widetilde{\boldsymbol{H}}_6) < \lambda_{\text{th6}}, \text{ then C=8 bits/sample;} \end{cases} \tag{5.30}$$

Else $(\lambda_{\min}(\boldsymbol{H}) < \lambda_{\text{16QAM}})$, QPSK and C=4 bits/sample is selected.

Table 5.2: *Switching criterion of the adaptive modulation and cooperation scheme.*

chooses the minimum possible quantization rate. That is, 4 bits/sample VQ will be sufficient for the channels with $\lambda_{\min}(\widetilde{\boldsymbol{H}}_4) \geq \lambda_{\text{th4}}$ and $\lambda_{\min}(\widetilde{\boldsymbol{H}}_6) \geq \lambda_{\text{th6}}$; and 6 bits/sample VQ will be selected for those with $\lambda_{\min}(\widetilde{\boldsymbol{H}}_4) < \lambda_{\text{th4}}$ and $\lambda_{\min}(\widetilde{\boldsymbol{H}}_6) \geq \lambda_{\text{th6}}$. Otherwise, we employ a 8 bits/sample VQ.

The estimated average quantization rate C_{ave} is then shown as follows,

$$C_{ave} = 4(1 - P_{\text{th4}}) + 6(P_{\text{th4}} - P_{\text{th6}}) + 8P_{\text{th6}}. \tag{5.31}$$

With the proposed adaptive-rate CF scheme, C_{ave} is always smaller than the fixed quantization rate which is needed to obtain the ideal MIMO performance. As the encoding complexity of Voronoi VQ grows exponentially with the quantization rate [12], the proposed scheme with a small C_{ave} will reduce the complexity for quantization significantly.

The scheme can also be extended to multiple modulation and code rates, including high-order modulation types which require higher C values, e.g. 64QAM. We presented an illustrative

switching criterion in Table 5.2, where the adaptive modulation and the adaptive-rate CF are combined. QPSK, 16QAM and 64QAM are chosen as the desired modulation types, and $C = 4, 6, 8, 10, 12$ bits/sample are selected as the quantization rate candidates. The impact of varying the CDF thresholds will be investigated in Section 5.5.

Therefore, for a specific channel condition, given the thresholds, the system could adapt to choose a suitable modulation type for transmission and an appropriate C to perform CF cooperation. The scheme not only enables the system to achieve a high throughput with reliable communication, but also eliminates unnecessary complexity for quantization operations and conference link communication.

5.4.4 Practical Setup and Maintenance

In general, to support this cooperative virtual-MIMO system with an adaptive modulation and cooperation scheme, some setup and maintenance issues should be specified for practical considerations. As depicted in Figure 5.3, there are several key steps:

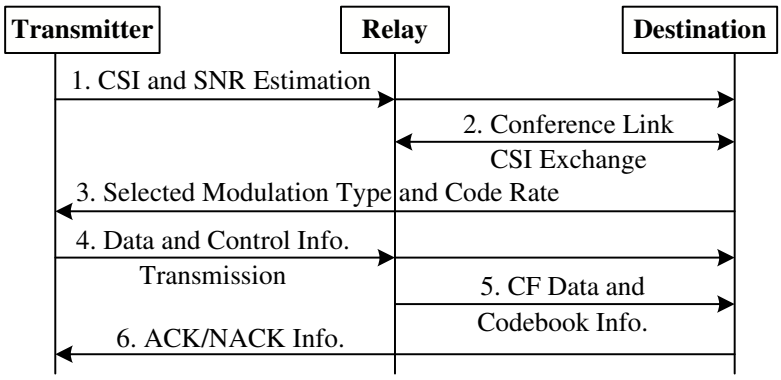

Figure 5.3: *Practical setup and maintenance issues for the virtual-MIMO system with the adaptive modulation and cooperation scheme. (ACK and NACK stand for acknowledgement and negative acknowledgement, respectively.)*

1. CSI and SNR are estimated at the relay and destination.
2. An orthogonal conference link is formed between the relay and the destination. The conference link is short-range and could be reused many times over the coverage area of the long range link (between the transmitter and the receivers). The channel CSI is then shared between them, i.e. $\boldsymbol{H}_n$ is known at both the relay and the destination.

3. An adaptive modulation scheme related computation is executed at the destination, to choose a suitable modulation type according to the quality of $\boldsymbol{H}_n$ and predefined threshold ξ, and feed back the information to the transmitter.

4. The transmitter broadcasts the data symbols through two antennas simultaneously. Some control information, e.g. the modulation type and coding rate, is also included.

5. The relay implements the adaptive-rate CF scheme to decide an appropriate quantization rate for the CF cooperation. Then the relay quantizes the received signals based on the selected rate C, and transmits the compressed signals y'_{rnl} to the destination. Codebook information, and some control information, such as the selected value of C and the estimated value of σ^2_{cn}, is included.

6. The destination performs MMSE detection on the received signal $\boldsymbol{y}_{nl}$, with the knowledge of $\widetilde{\boldsymbol{H}}_n$. Finally an acknowledgement/negative acknowledgement (ACK/NACK) information is fed back to let the transmitter know the outcome of the decoding process. If errors still occur, the destination may request a retransmission.

5.5 Numerical Results

In this section, we present the error performance of our cooperative virtual-MIMO-BICM system ($N_t = N_r = 2$). At the transmitter, a 1/2-rate convolutional code with the generator polynomials $[133, 171]_{\text{octal}}$ ($d_{\text{free}} = 10$) is used for QPSK and 16QAM modulations. Further, a 2/3-rate code punctured from $[133, 171]_{\text{octal}}$ is considered for 64QAM. We assume 10^6 block Rayleigh fading channels between the transmitter and receivers, with each block having 200 consecutive symbol periods. An error-free conference link is assumed between the relay and the destination. In addition, a Voronoi VQ is implemented at the relay to enable CF cooperation. The destination performs joint MMSE demodulation and employs soft-input Viterbi decoding. The simulation results are computed via the Monte Carlo method.

5.5.1 BER Evaluation

The BER performance of the cooperative virtual-MIMO-BICM system with various modulations, under fixed quantization rates, is shown in Figure 5.4. The conference link rates $C = 4$ bits/sample for QPSK, $C = 8$ bits/sample for 16QAM, and $C = 12$ bits/sample for 64QAM

modulation will enable the system with CF cooperation to approach the ideal MIMO performance, since the quantization codebook could represent the constellation points accurately at the relay. The BER UBs and their simplified versions based on $\rho_{\min}$ are presented as well. According to (5.10) and (5.19), the BER UB based on $\rho_{\min}$ is a little larger but follows the same trend with BER UB, as also shown in this figure. The BER UBs match well to the simulation results and thus could be used to predict the practical BER performance.

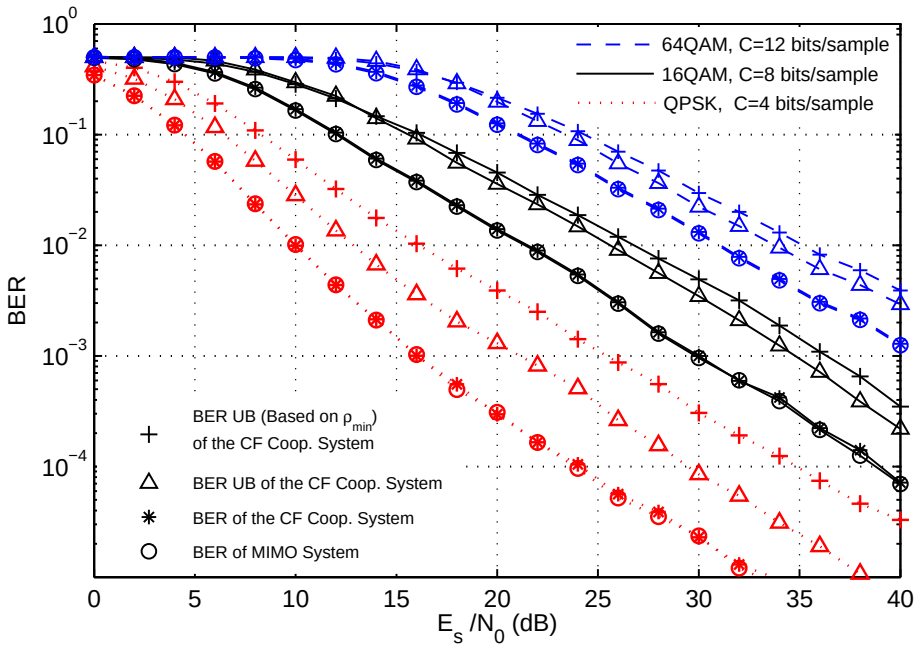

Figure 5.4: *Simulation results and UBs on the BER performance of the 2×2 virtual-MIMO-BICM system with CF cooperation and MMSE receiver. (1/2-rate coded QPSK, 1/2-rate coded 16QAM, and 2/3-rate coded 64QAM are considered.)*

The UBs and simulation results of the system BER performance for 16QAM modulation, under various quantization rates, are presented in Figure 5.5. We plot the BER against the information bit SNR, i.e E_b/N_0. For all considered quantization rates, the BER performance is very well approximated by the UB based on $\rho_{\min}$. A smaller quantization rate results in stronger compression noise. As shown in this figure, for smaller C, such as 4 bits/sample and 6 bits/sample, there exists an error floor, which means the MMSE receiver cannot remove the residual ISI because of the compression noise. For larger C, such as 8 bits/sample, an error floor is also expected. But it is too low to impair the system performance. Hence in order to achieve almost ideal MIMO performance and simultaneously eliminate unnecessary complexity for the quantization, it is appropriate to implement the singular value-based adaptive-rate CF scheme, which

exploits different C according to different channel conditions. Since the BER performance is very well approximated by the UB based on $\rho_{\min}$ for all considered quantization rates, it is reasonable to characterise the quality of the scaled channel by using its smallest singular value.

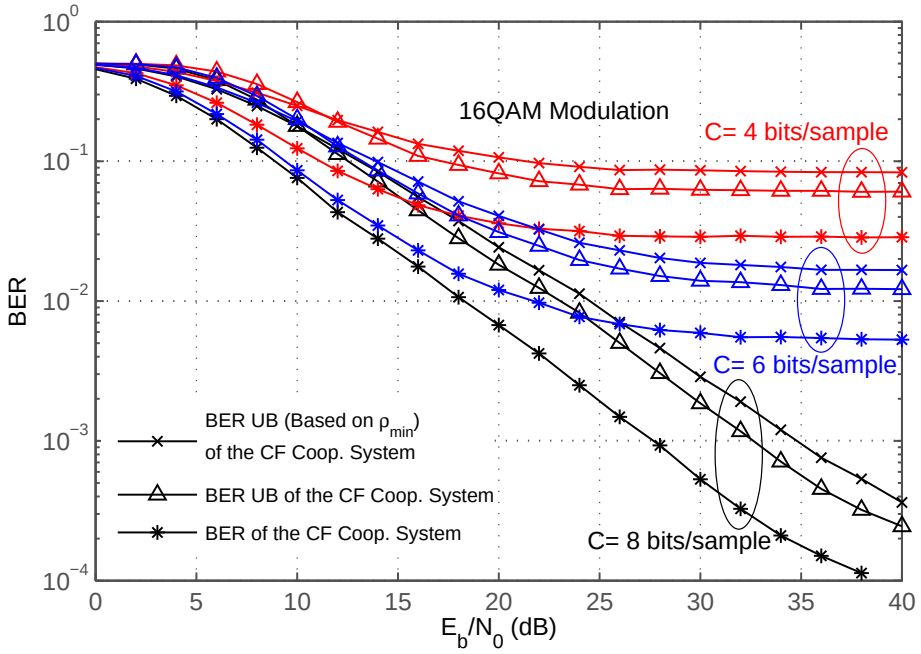

Figure 5.5: *Simulation results and UBs on the system BER performance for 1/2-rate coded 16QAM with various quantization rates.*

5.5.2 Application of the Adaptive Modulation and Cooperation Scheme

Here we present an illustrative simulation example, which is set up in accordance with the example in Table 5.2. The switching criterion of the adaptive modulation and cooperation scheme is two levelled. Firstly, the destination should choose a suitable modulation type via comparing $\lambda_{\min}(\boldsymbol{H})$ to $\lambda_{16\text{QAM}}$ and $\lambda_{64\text{QAM}}$. Here we assume the threshold $\xi = 10^{-5}$ so that the realistic BER will be smaller than 10^{-5}. We use the value of A_d in [72] for 16QAM modulation and [109] for 64QAM modulation, then a threshold for $K_{\mathcal{L}}(\hat{s})$ which equals -1.1284 for 16QAM and -2.0103 for 64QAM are obtained from (5.5) and (5.8). According to (5.21) and (5.22), we finally obtain the corresponding thresholds $\lambda_{16\text{QAM}} = \sqrt{10.3465N_t/\text{SNR}}$ and $\lambda_{64\text{QAM}} = \sqrt{62.0480N_t/\text{SNR}}$. Secondly, if 16QAM is chosen, an adaptive-rate CF cooperation scheme ($C = 4$, 6, 8 bits/sample are chosen as candidates in accordance with Table 5.2) will be employed. If 64QAM is selected, $C = 8$, 10, 12 bits/sample will be considered. The thresholds

λ_{th4} and λ_{th6} for 16QAM, and λ_{th8} and λ_{th10} for 64QAM are computed based on the settings of P_{th4}, P_{th6}, P_{th8} and P_{th10}.

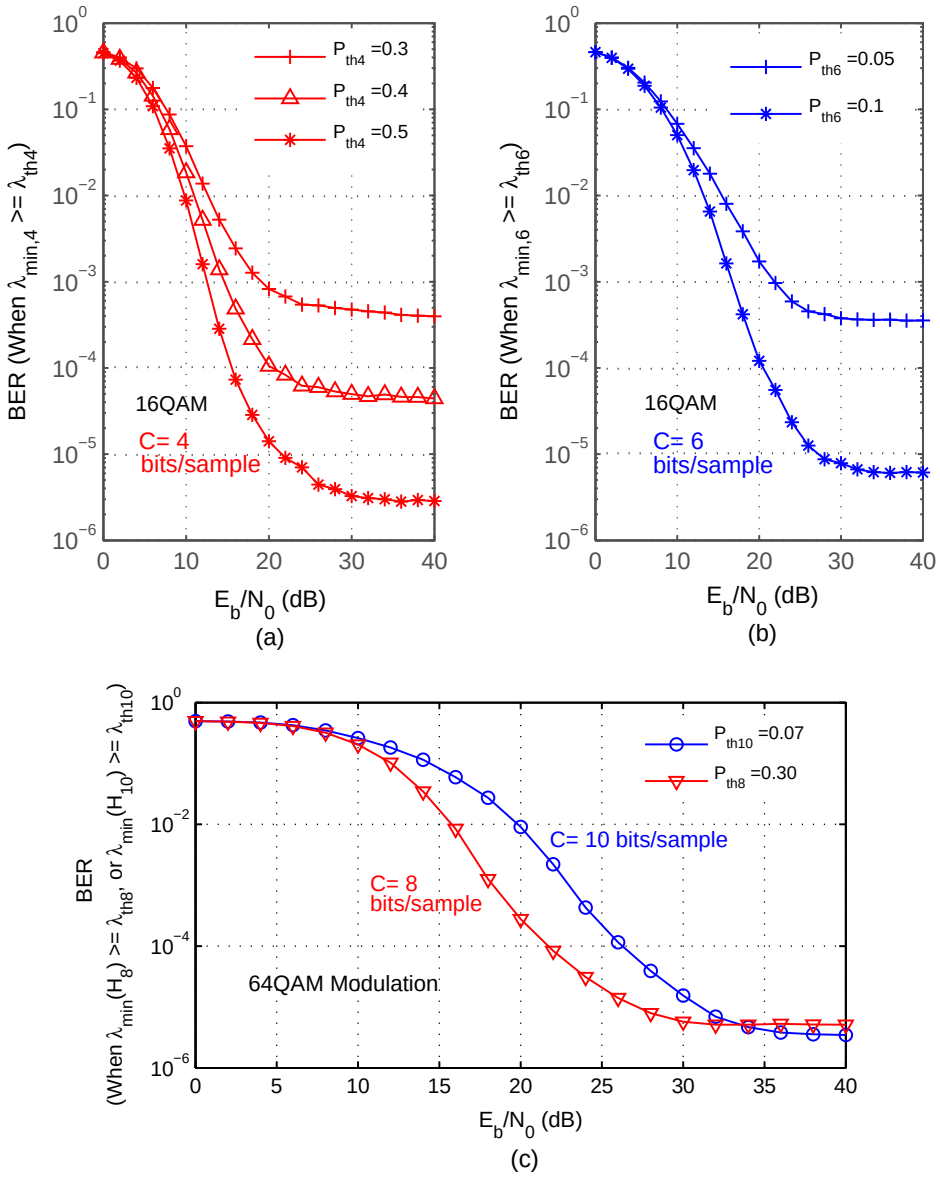

Figure 5.6: *The effects of varying the thresholds on the conditional BER performance. (1/2-rate coded 16QAM with C=4 bits/sample is considered in (a) and 6 bits/sample in (b), while 2/3-rate coded 64QAM with C=8, 10 bits/sample is considered in (c).)*

In Figure 5.6 (a) and (b), we investigate the impact of varying the thresholds on the conditional BER for 16QAM modulation, by changing the operating thresholds P_{th4} and P_{th6} for $C = 4$ bits/sample and 6 bits/sample. The conditional BERs are calculated on the channels satisfying

$\lambda_{\min}(\widetilde{\boldsymbol{H}}_4) \geq \lambda_{\text{th4}}$ and $\lambda_{\min}(\widetilde{\boldsymbol{H}}_6) \geq \lambda_{\text{th6}}$ respectively, where λ_{th4} and λ_{th6} are computed based on the settings of P_{th4} and P_{th6}. It is obvious that as the threshold P_{th} increases, for both the $C = 4$ bits/sample and 6 bits/sample cases, the conditional BER decreases. As long as $P_{\text{th4}} = 0.5$ and $P_{\text{th6}} = 0.1$, the error floor is too small to impact the system performance.

For 64QAM modulation, we also investigate the impact of varying the thresholds and simulate the conditional BERs to an error floor of roughly 10^{-5}, using $C = 8$ and 10 bits/sample in Figure 5.6 (c). Hence $P_{\text{th4}} = 0.5$, $P_{\text{th6}} = 0.1$, $P_{\text{th8}} = 0.3$, and $P_{\text{th10}} = 0.06$ are good choices for the adaptive-rate CF scheme to achieve a favourable performance-complexity tradeoff. Then based on (5.28), we calculate λ_{th4} and λ_{th6} (for 16QAM), and λ_{th8} and λ_{th10} (for 64QAM) as the singular value thresholds to select various values of C for the scheme.

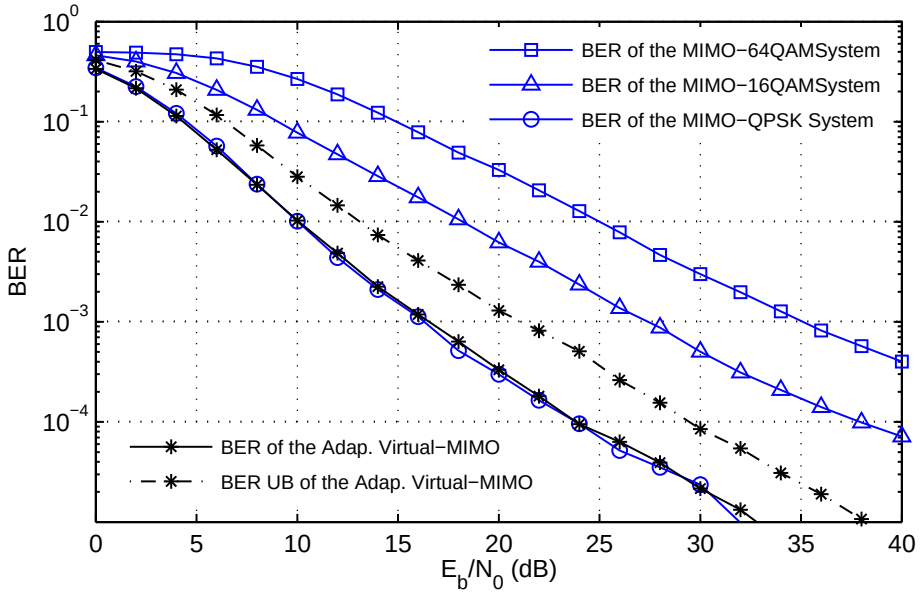

Figure 5.7: *BER performance of the* 2×2 *virtual-MIMO system with the adaptive modulation and cooperation scheme.*

Corresponding to the criterion in Table 5.2, the simulation results of the adaptive virtual-MIMO system are presented in Figure 5.7 and Figure 5.8. With the adaptive modulation and cooperation scheme we proposed, the system obtains a BER performance almost the same as the MIMO system with QPSK modulation, and provides a significant improvement compared to the 64QAM case, as shown in Figure 5.7. Also, at high E_b/N_0, the adaptive system throughput can approach almost MIMO-64QAM performance, i.e. reach the upper limit of 12 bits/s, as shown Figure 5.8. Compared with the cases of fixed modulation and fixed-rate CF, the adaptive

scheme allows the virtual-MIMO system to achieve a high throughput with reliable communication.

The switching thresholds for the adaptive virtual-MIMO system have been chosen conservatively to achieve the same BER performance as for QPSK modulation, as shown in Figure 5.7. A higher BER threshold for changing modulation scheme could be used to improve throughput, at the cost of higher BER and higher quantisation rates at the relay.

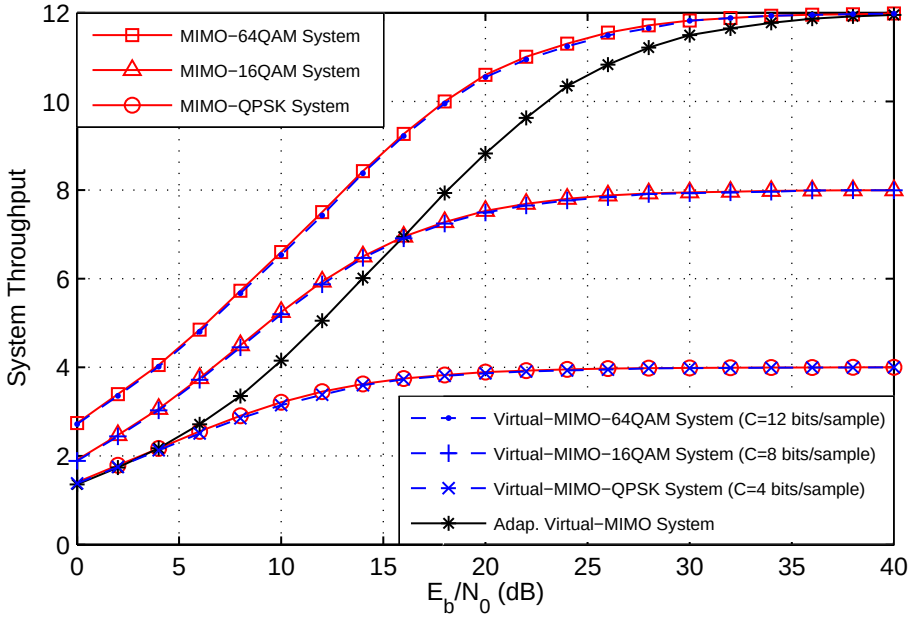

Figure 5.8: *Throughput of the* 2×2 *virtual-MIMO system with the adaptive modulation and cooperation scheme.*

The probabilities of choosing different modulation types and quantization rates are shown in Figure 5.9. At low E_b/N_0, QPSK is always selected to try to provide reliable communication. As the E_b/N_0 increases, 16QAM and 64QAM are chosen more frequently to obtain high throughputs, and adaptive-rate CF cooperation is implemented. When the E_b/N_0 is high, the relay uses 12 bits/sample VQ for less than 6% of channel realisations (with lower $\lambda_{\min}$), and for more than 70% of the channels (with higher $\lambda_{\min}$), 8 bits/sample VQ will be sufficient for acceptable performance. As shown in Figure 5.10, the final average quantization rate is between 4 bits/sample and around 8.6 bits/sample, which could also be predicted from (5.31). Thus at low E_b/N_0, the adaptive scheme helps the system to reduce complexity for quantization operations significantly, without large performance loss compared to the 64QAM case

with $C = 12$ bits/sample (see Figure 5.8). When the E_b/N_0 is high, the adaptive scheme is capable of eliminating more than 3 bits complexity for quantization at the relay and more than 3 bits/sample on the conference link communications relative to the $C = 12$ bits/s/sample case, while still achieving almost ideal MIMO-64QAM performance.

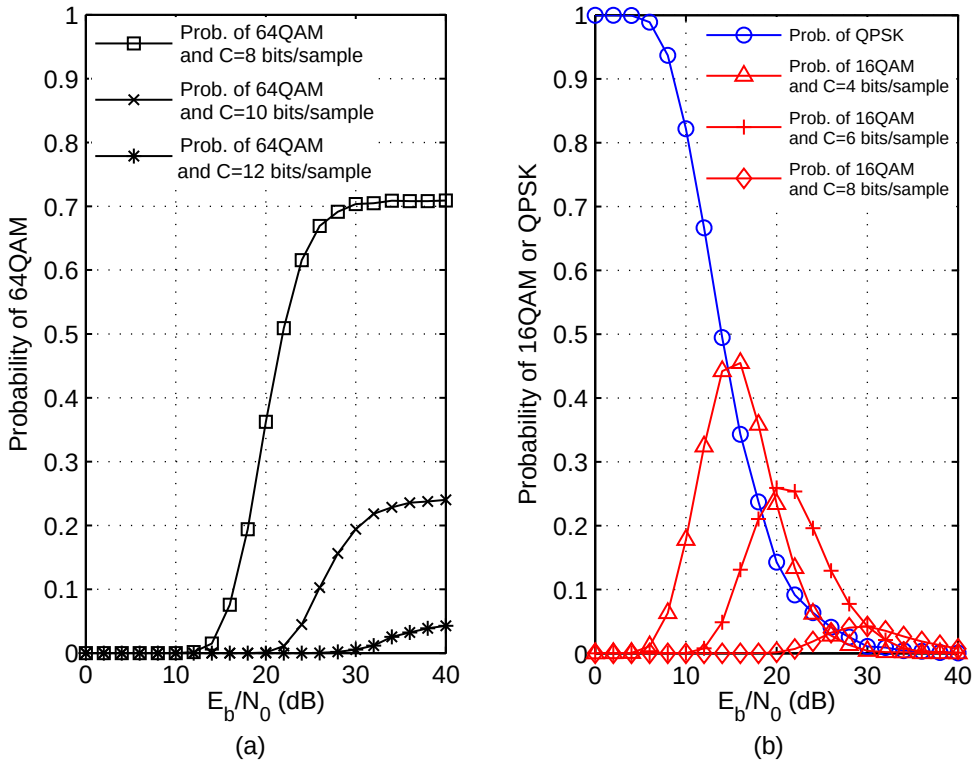

Figure 5.9: *Probability of choosing different modulation types and quantization rates for the adaptive virtual-MIMO system.*

5.6 Conclusions

This chapter presented a practical virtual-MIMO-BICM system with a single two-antenna wireless transmitter sending information to two closely spaced single-antenna receivers. Virtual-MIMO operation was realized via receiver-side local communication using the CF cooperation, and MMSE detection was employed at the destination. In this chapter, we derived an expression to upper bound the system BER. The expression was obtained in closed form, based on which we showed that the smallest singular value of the cooperative channel matrix dominates the system error performance. Moreover, an adaptive modulation and cooperation scheme was

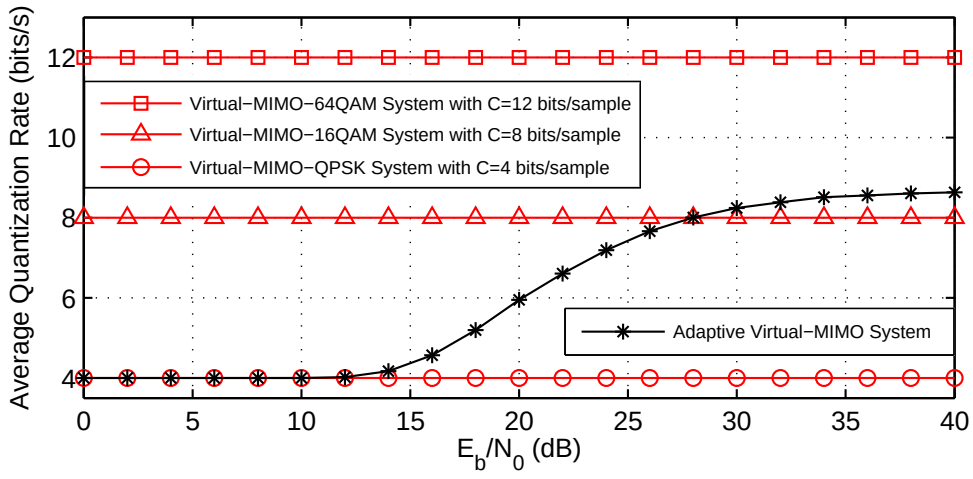

Figure 5.10: *Average quantization rate at the relay for the adaptive virtual-MIMO system, compared to the* $C = 4, 8, 12$ *bits/sample cases.*

proposed, adopting the smallest singular value as the threshold strategy. The closed-form CDF expression of the smallest singular value was also derived.

With the adaptive modulation and cooperation scheme, the system could adapt its modulation type to the prevailing channel conditions. The relay could also choose the minimum possible quantization rate to eliminate unnecessary complexity. We presented an illustrative example for simulation, where QPSK, 16QAM and 64QAM were chosen as the desired modulation types, and $C = 4, 6, 8, 10, 12$ bits/sample were selected as the quantization rate candidates. The simulation results confirmed that the 2×2 virtual-MIMO system was able to achieve a high throughput with reliable communication. For our illustrative example, at low E_b/N_0, the adaptive scheme helps the system to reduce complexity for quantization operations significantly, without large performance loss. When the E_b/N_0 is high, the adaptive scheme is capable of eliminating more than 3 bits complexity, while still achieving almost ideal MIMO-64QAM performance.

The illustrative example showed how to find the appropriate switching criterion and the system performance. The adaptive modulation and cooperation scheme is not limited to this example, the principles of which could easily be applied to multiple modulation types and quantization rates. The virtual-MIMO system studied here is not limited to BICM transmission. Other FEC coding schemes, such as Turbo coding or LDPC coding, could also be employed, subject

to different switching criterion analyses. By extending to a wide range of applications, the virtual-MIMO system implementing the adaptive modulation and cooperation scheme is therefore particularly valuable and attractive to some realistic wireless communication systems, such as High Speed Packet Access (HSPA) and Long Term Evolution (LTE) systems.

Chapter 6
Conclusions and Future Work

This thesis has contributed to the performance evaluation and practical design of CF cooperation in virtual-MIMO systems. In this concluding chapter, Section 6.1 will look for three key points from the thesis. Some limitations of the work and several suggestions for possible future research areas will be discussed in Section 6.2.

6.1 Conclusions

This thesis presented a practical virtual-MIMO system that implemented BICM transmission and CF cooperation. To demonstrate the achievable performance improvements and sensitivities, we focused on a simple configuration that a single two-antenna transmitter sending information to two closely spaced single-antenna receivers. The key contributions of this thesis are summarized as follows.

6.1.1 Performance Evaluation of Virtual-MIMO Systems

Evaluating performance bounds for virtual-MIMO systems, it was found that the CF cooperation using standard source coding at the relay could enable the virtual-MIMO system to achieve almost ideal MIMO performance. Simulation results showed that, with Voronoi VQ at the relay, a quantization rate of 4 bits/sample for QPSK mapping, and 7 bits/sample for 16QAM, would result in the virtual-MIMO system achieving almost ideal MIMO performance. In addition, TSVQ was shown to be a good choice for CF cooperation to achieve a favourable performance-complexity tradeoff: It could reduce the codebook design complexity and encoding complexity significantly, for a very small performance penalty. Considering the practicality, the proposed virtual-MIMO system with CF cooperation is particularly valuable and attractive to some realistic wireless communication systems, and enables single-antenna user devices to obtain the benefits of MIMO decoding.

6.1.2 New Theoretical Results

The system throughput and upper bounds on the error probabilities of the virtual-MIMO-BICM system with CF cooperation were derived. It was shown that upper bounds computed using the Gaussian approximation matched well to the simulation results and provided good insights into the error behaviour of CF cooperation.

The system theoretical analysis was also extended to the low-complexity MMSE detection. The expression to upper bound the system BER was then obtained in closed form, based on which we proved that the smallest singular value of the cooperative channel matrix dominated the system error performance. The closed-form cumulative distribution function of the smallest singular value of the cooperative channel matrix was also derived.

6.1.3 Sensitivity Analysis

It was demonstrated that the 2×2 virtual MIMO system with CF cooperation was sensitive to carrier frequency offsets. Separate CFO estimation at the relay and destination could lead to drastic performance degradation for the 2×2 virtual MIMO system, even though increasing the number of transmit and receive antennas might improve the accuracy of the CFO estimation. To overcome this problem, a clock synchronization and joint CFO estimation scheme was proposed, which was shown to provide a significant performance improvement.

Comparing ideal and non-ideal conference links within the receiver group, it was found that the virtual MIMO system was not necessarily so sensitive to fading cooperation links. Considering the short-range communication between the relay and destination and using a channel-aware adaptive CF scheme, the impact of a non-ideal cooperation link is too slight to impair the system performance significantly. So an error-free conference link is always assumed between the relay and destination through the remainder of the thesis.

The theoretical expression for the upper bound on system BER showed that the virtual-MIMO system with MMSE detection was sensitive to the compression noise caused by the CF cooperation. A low quantization rate which results in strong compression noise, would impair the system BER performance and lead to an error floor. To solve this problem, an adaptive modulation and cooperation scheme was proposed, adopting the smallest singular value as the threshold strategy. Depending on the instantaneous channel conditions, the system could therefore adapt to choose a suitable modulation type for transmission and an appropriate quantization rate to

perform CF cooperation. It was shown that the proposed scheme not only enabled the system to achieve comparable performance to the case with fixed quantization rates, but also eliminated unnecessary complexity for quantization operations and conference link communication.

6.2 Future Work

Following the investigations described in this thesis, there are several research directions that can be extended. Some suggestions are listed below:

- This thesis focused on a 2×2 virtual-MIMO system, i.e. two-antenna transmitter sending information to two closely spaced single-antenna receivers. Further improvements are expected for the case of more antennas and more cooperating terminals: Suitable cooperation schemes at the relays will enable the virtual-MIMO system to achieve almost ideal $N_t \times N_r$ MIMO performance. However, the power allocation among those relays should be considered to guarantee fairness and efficiency of the cooperative communications. If larger numbers of antennas are equipped at the cooperating terminals, the situation will become more complicated. Thus, extending the analysis to more transmit antennas and more cooperating terminals equipped with more antennas will be one promising future research area.

- In the system model of this thesis, an error-free conference link is assumed between the relay and the destination. If the link is not ideal, cooperation and control information transmission may suffer from fading channel and noise effects. That is, the clock synchronization and joint CFO estimation proposed in Chapter 4, and the computation of the smallest singular value of the cooperative channel matrix used in Chapter 5 may be affected. Chapter 3 considers the impact of data transmission errors on the system performance, but other transmission errors (such as CSI errors) are not specifically considered, which is left as another future research subject.

- In Chapter 4, the proposed joint CFO estimation scheme was based on McKeown's algorithm in [84], where the phase shift of pilot sequences is measured to estimate the CFO. McKeown's algorithm is simple and effective in practice. But other estimation algorithms could also be employed and may give better performance at the cost of increased complexity. Hence, an interesting topic for future research is to extend the analysis to other CFO estimation algorithms and examine their potential.

- The virtual-MIMO system studied in this thesis implements BICM as a forward error correction coding scheme to improve performance. The system is not limited to BICM, other FEC coding schemes, such as Turbo coding or LDPC coding, could also be employed. For Chapter 5, when other FEC coding schemes are used, the switching criterion analyses (for the adaptive modulation and cooperation scheme) will be different. How to implement other FEC coding schemes in virtual-MIMO systems to optimize performance will be another interesting area for future research.

Appendix A
Proof of Proposition 3.1

In [67], it is demonstrated that under the assumption of high resolution and smooth densities, the quantization error behaves like an additive white noise: it has small correlation with the signal y_{rnl} and an approximately white spectrum. Thus we could model the quantization error as $ay_{rnl} + u_{nl}$, where a is a real constant, u_{nl} is $\mathcal{CN}(0, \sigma_u^2)$ and independent of y_{rnl}. Then,

$$y'_{rnl} = \frac{1}{1+a}(y_{rnl} + ay_{rnl} + u_{nl}). \tag{A.1}$$

Comparing (3.2) and (A.1), it is obvious that the compression noise $w_{cnl} = u_{nl}/(1+a)$, and $\sigma_{cn}^2 = \sigma_u^2/(1+a)^2$. We choose a and σ_u^2 according to Shannon's rate-distortion theory. That is, the variance of the quantization error satisfies,

$$\mathrm{E}[|ay_{rnl} + u_{nl}|^2] = a^2\mathrm{E}[|y_{rnl}|^2] + \sigma_u^2 \geq 2^{-C}\mathrm{E}[|y_{rnl}|^2], \tag{A.2}$$

Also, the correlation between the quantization error and y_{rnl} is the negative of the mean-squared error $\mathrm{E}[|ay_{rnl} + u_{nl}|^2]$ [66], i.e.

$$\mathrm{E}[y_{rnl}^*(ay_{rnl} + u_{nl})] = a\mathrm{E}[|y_{rnl}|^2] = -\mathrm{E}[|ay_{rnl} + u_{nl}|^2], \tag{A.3}$$

where y^* denotes the complex conjugate of y. Solving (A.3) and (A.2), we get

$$\sigma_u^2 = \mathrm{E}[|y_{rnl}|^2]a(1+a), \tag{A.4}$$

and $a \geq -2^{-C}$. Then we have

$$\sigma_{cn}^2 = \frac{\sigma_u^2}{(1+a)^2} \geq \frac{\mathrm{E}[|y_{rnl}|^2]}{2^C - 1}. \tag{A.5}$$

Thus the lower bound of σ_{cn}^2 is obtained.

Appendix B
Original publications

The author of this thesis has the following accepted or submitted publications during her Ph.D. research:

B.1 Journal papers

- J. Jiang, J. S. Thompson, and H. Sun, "A Singular Value-based Adaptive Modulation and Cooperation Scheme for Virtual-MIMO Systems," *IEEE Trans. Vehicular Technology*, to appear.

- J. Jiang, J. S. Thompson, H. Sun, and P. M. Grant, "Performance assessment of virtual-MIMO systems with compress-and-forward cooperation," *IET Communications*, submitted in Feb. 2011.

- J. Jiang, J. S. Thompson, H. Sun, and P. M. Grant, "Practical Analysis of Codebook Design and Frequency Offsets Estimation for Virtual-MIMO Systems," *IEEE Trans. Vehicular Technology*, submitted in April 2011.

B.2 Conference papers

- J. Jiang, J. S. Thompson, and P. M. Grant, "Design and analysis of compress-and-forward cooperation in a virtual-MIMO detection system," *in 2010 IEEE GLOBECOM Workshop on Heterogeneous, Multi-hop, Wireless and Mobile Networks (HeterWMN)*, Miami, USA, pp. 126-130, Dec. 2010.

- J. Jiang, J. S. Thompson, X.Wu, and P. M. Grant, "An adaptive rate compress-and-forward cooperation for virtual-MIMO systems," *in The 2nd UK-India-IDRC International Workshop on Cognitive Wireless Systems (UKIWCWS)*, New Delhi, India, pp. 1-5, Dec. 2010.

- J. Jiang, J. S. Thompson, P. M. Grant, and N. Goertz, "Practical compress-and-forward cooperation for the classical relay network," *in European Signal Processing Conference (EUSIPCO)*, Glasgow, Scotland, pp. 2421-2425, Aug. 2009.

The accepted and published original publications are included in the following pages.

IEEE Globecom 2010 Workshop on Heterogeneous, Multi-hop Wireless and Mobile Networks

Design and Analysis of Compress-and-Forward Cooperation in a Virtual-MIMO Detection System

Jing Jiang, John S. Thompson, Peter M. Grant
Institute for Digital Communications, Joint Research Institute for Signal & Image Processing
School of Engineering, University of Edinburgh, Edinburgh, EH9 3JL, UK.
Email: J.Jiang@ed.ac.uk, John.Thompson@ed.ac.uk, Peter.Grant@ed.ac.uk

***Abstract*—A cooperative virtual-MIMO system that implements bit-interleaved coded modulation (BICM) transmission and compress-and-forward (CF) cooperation is presented in this paper. The key tasks of the relay include constructing a good codebook, and forwarding a compressed version of the received signals to the destination. Codebook designs of the Voronoi vector quantization (VQ) and the tree-structure vector quantization (TSVQ) to enable CF cooperation are described in this paper. A comparison in terms of the codebook design complexity and encoding complexity is presented. It is shown that the TSVQ is much simpler to design and operate and can achieve performance comparable to the optimal but more complicated Voronoi VQ. Error performance results show that the helping relay enables the proposed cooperative virtual-MIMO system to achieve close to MIMO performance.**

I. Introduction

Recently the use of multiple antennas at the transmitter and a single antenna at each of the receivers, known as virtual multiple-input multiple-output (MIMO) wireless system, has received significant interest [1]. In a typical virtual-MIMO system, coordination is allowed among the transmit antennas, but not among the receive nodes (see, e.g. [2]). However, it requires the transmitter to have perfect or partial channel side information (CSI) for the wireless link to each receiver, which is not realistic in many cases. When the transmitter does not have CSI in the virtual-MIMO system, receiver-side local cooperation is a good way for achieving MIMO capacity gains. The helping receiver (i.e. the relay) could choose to amplify-and-forward (AF), decode-and-forward (DF), or compress-and-forward (CF) its observation to the destination [3]. Since the relay is generally close to the destination in our virtual-MIMO system, the CF protocol which provides higher rates [4], is a better choice at the relay.

In virtual-MIMO communications, we need a robust coding technique to improve system performance. Bit-interleaved coded modulation (BICM) [5], which introduces a spatial and temporal bit interleaver into the transmitter, is employed here to mitigate the effects of multipath fading. The virtual-MIMO system studied in this paper employs the BICM technique, but the virtual-MIMO system studied here is not limited to BICM in general. Any forward error correction coding schemes, such as Turbo coding or LDPC coding, could be used, according to different application requirements.

We now summarize the main contributions of this paper. Firstly, we present a practical virtual-MIMO-BICM system that implements CF cooperation with a standard source coding technique at the relay. We prove that the cooperation of the receivers enables our virtual-MIMO system to achieve almost ideal MIMO performance. Furthermore, to perform source coding for CF cooperation, we consider two codebook design algorithms, Voronoi vector quantization (VQ) and tree-structure vector quantization (TSVQ). To the best of our knowledge, it is the first time that VQ and TSVQ are applied to digital modulation signals. Their codebook design complexities and encoding complexities are investigated. The simulation results show that the TSVQ approach we implemented is much simpler for encoding and more computationally efficient than the complicated Voronoi VQ.

The paper is organized as follows: Section II specifies the system model. In section III, we analyze the CF protocol. Codebook design methods and the corresponding complexity analyses are investigated in section IV. Section V shows the simulation results, and section VI concludes the paper.

II. System Model

Consider a cooperative virtual-MIMO network with one remote N_t-antenna transmitter sending information to N_r colocated single-antenna receivers, as shown in Fig. 1. To focus on the performance and practical implementation of the CF cooperation, we simplify the system with $N_t = 2$ and $N_r = 2$ antennas. BICM is employed here to improve performance. At the transmitter, a rate-R_c linear binary convolutional encoder is considered, and hence the information bits are encoded to yield codewords. The codewords are then interleaved through an ideal random bit interleaver, which rearranges the codewords using a random permutation. In each steam after the demultiplexer (or demux), groups of m bits are mapped onto complex data symbols via Gray-coded $2^m = M$-ary modulation whose signal constellations are denoted as $\mathcal{X}$.

Since the transmitter is far away from the receiver group, a block fading channel model with N Rayleigh fading blocks

We would like to thank Prof. Norbert Goertz of the Vienna University of Technology for providing the idea of implementing the tree-structure vector quantization in the system. We acknowledge the support of the Scottish Funding Council for the Joint Research Institute with Edinburgh and the Heriot-Watt Universities, which is a part of the Edinburgh Research Partnership. Jing Jiang gratefully acknowledges the support from the UK/China Scholarships for Excellence programme in funding her PhD studies.

978-1-4244-8865-0/10/$26.00 ©2010 IEEE

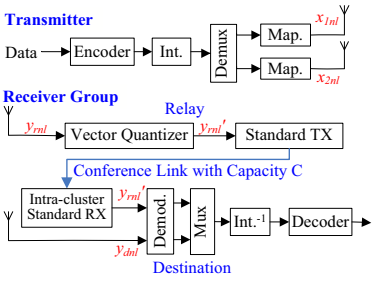

Fig. 1. System model of the cooperative virtual-MIMO system. (TX and RX stand for the transmitter and receiver.)

is assumed here, with each block having length L symbol periods. When we consider a single time instance l for the nth channel, the channel model is given by:

$$\begin{bmatrix} y_{rnl} \\ y_{dnl} \end{bmatrix} = \boldsymbol{H}_n \boldsymbol{x}_{nl} + \boldsymbol{w}_{nl}, \text{ with } \boldsymbol{H}_n = \begin{bmatrix} h_{1n} & h_{2n} \\ h_{3n} & h_{4n} \end{bmatrix}, \quad (1)$$

where $\boldsymbol{H}_n$ denotes the nth block fading channel matrix, with each $h_{in} (i \in [1, ..., 4])$ is independent and identically distributed (i.i.d.). We also define the vector $\boldsymbol{x}_{nl} = [x_{1n1}, x_{2nl}]^{\mathrm{T}}$, where $x_{i'nl} (i' \in [1, 2])$ presents the lth M-ary symbol transmitted on the nth channel from the i'th antenna. The noise vector $\boldsymbol{w}_{nl} = [w_{1n1}, w_{2nl}]^{\mathrm{T}}$, with components $w_{i'nl} \sim \mathcal{CN}(0, N_0)$. Moreover, we assume normalized Rayleigh fading, i.e. $\mathrm{E}[|h_{in}|^2] = 1$. The average transmitted power per symbol is $\mathrm{E}[|x_{i'nl}|^2] = E_s/2$. We normalize the total transmitted power E_s to unity, and the corresponding power per bit is $E_b = E_s/(mR_c)$. We assume that perfect channel state information (CSI) is available at the receivers only.

There exist two clustered receivers, the destination and the helping relay. As the receivers are closely spaced, it is highly likely that the communication between the two receivers is much better and more stable than that between the transmitter and receivers. It is reasonable to expect that we could achieve high channel capacity with high reliability on this short range link. Hence we assume the two receivers cooperate by way of an error-free conferencing link [6], as shown in blue in Fig. 1, which may be realized via an orthogonal channel to the transmitter array with sufficiently long coding blocks. We consider one-shot conferencing cooperation, which requires the destination to decode the signal sent over the conferencing link from the relay. The CF protocol is chosen here, so that a compressed version of the signal y_{rnl}' will be passed into a standard transmitter and transmitted over the conferencing link. The capacity of this link is denoted by C, which is measured in bits per compressed sample.

The destination is assumed to be equipped with a receiver which observes signals y_{dnl} from the transmitter, and an intra-cluster receiver observes signals from the relay, written as y_{rnl}', as shown in Fig. 1. We denote the received signals at the destination as $\boldsymbol{y}_{nl} = [y_{rnl}' \; y_{dnl}]^{\mathrm{T}}$. Next the destination performs joint maximum-likelihood (ML) demodulation of $\boldsymbol{y}_{nl}$, with computing the log-likelihood ratio (LLR) for each coded bit. The two path LLRs are combined into one output stream by the multiplexer, and then reordered by the deinterleaver. Finally the decoder accepts the LLRs of all coded bits and employs a soft-input Viterbi algorithm to decode the signals. Thus with help from the relay, the single-antenna destination receives two path signals. Good compression will allow the destination to use y_{rnl}' for MIMO decoding.

III. Compress-and-Forward Cooperation

In our virtual-MIMO system, we implement the CF protocol with a standard source coding technique to realize the receiver-side cooperation. Note that, we do not employ Wyner-Ziv (WZ) Coding technique for the CF protocol. The reason is, our virtual-MIMO system with two antennas at the transmitter has the feature that y_{rnl} and y_{dnl} are not highly correlated. The WZ Coding technique therefore does not improve the performance signicantly [7], but introduces extra complexity.

Since standard source coding is much simpler to enable CF cooperation and also performs well in practical scenarios, we choose to implement it at the relay. That is, the relay is equipped with a vector quantizer (VQ). The quantization rate is equal to the link capacity C, as the two receivers cooperate by way of an error-free conference link. In [8], it is demonstrated that the quantization error behaves like an additive Gaussian noise. Thus we may write:

$$y_{rnl}' = y_{rnl} + w_{cnl}, \quad (2)$$

where w_{cnl} is the compression noise, independent of y_{rnl}, with variance σ_{cn}^2, i.e. $w_{cnl} \sim \mathcal{CN}(0, \sigma_{cn}^2)$. The lower bound of the compression noise variance in [9] could be extended to our virtual-MIMO system, i.e.,

$$\bar{\sigma}_{cn}^2 = \frac{\mathrm{E}[|y_{rnl}|^2]}{2^C - 1} = \frac{N_0 + \frac{1}{2}|h_{1n}|^2 + \frac{1}{2}|h_{2n}|^2}{2^C - 1}. \quad (3)$$

Then after each block of the compressed signal y_{rnl}', the relay also sends the value of σ_{cn}^2 over the conferencing link. With knowledge of σ_{cn}^2, and assuming w_{cnl} is i.i.d. complex Gaussian noise, the destination could scale y_{rnl}' so that y_{rnl}' and y_{dnl} have the same power of additive Gaussian noise [10]:

$$\tilde{\boldsymbol{y}}_{nl} = [\tilde{y}_{rnl}' \;\; y_{dnl}]^{\mathrm{T}} = \widetilde{\boldsymbol{H}}_n \boldsymbol{x}_{nl} + [\tilde{w}_{1nl} \;\; w_{2nl}]^{\mathrm{T}}, \quad (4)$$

$$\text{with} \quad \widetilde{\boldsymbol{H}}_n \triangleq \begin{bmatrix} \sqrt{\eta_n} h_{1n} & \sqrt{\eta_n} h_{2n} \\ h_{3n} & h_{4n} \end{bmatrix}, \; \eta_n \triangleq \frac{N_0}{N_0 + \sigma_{cn}^2}. \quad (5)$$

$\tilde{w}_{1nl} \sim$ i.i.d. $\mathcal{CN}(0, N_0)$, η_n is the degradation factor due to the compression noise, and $\tilde{y}_{rnl}' = \sqrt{\eta_n} y_{rnl}'$. Thus the LLR for each coded bit c^λ at the destination will be calculated as,

$$\begin{aligned} \mathcal{L}(c^\lambda | \tilde{\boldsymbol{y}}_{nl}, \widetilde{\boldsymbol{H}}_n) &= \ln \frac{\sum_{\tilde{\boldsymbol{x}} \in \mathcal{X}_1^\lambda} p\{\tilde{\boldsymbol{y}}_{nl} | \tilde{\boldsymbol{x}}, \widetilde{\boldsymbol{H}}_n\}}{\sum_{\tilde{\boldsymbol{x}} \in \mathcal{X}_0^\lambda} p\{\tilde{\boldsymbol{y}}_{nl} | \tilde{\boldsymbol{x}}, \widetilde{\boldsymbol{H}}_n\}}, \\ &= \ln \frac{\sum_{\tilde{\boldsymbol{x}} \in \mathcal{X}_1^\lambda} \exp\left(-\|\tilde{\boldsymbol{y}}_{nl} - \widetilde{\boldsymbol{H}}_n \tilde{\boldsymbol{x}}\|^2 / N_0\right)}{\sum_{\tilde{\boldsymbol{x}} \in \mathcal{X}_0^\lambda} \exp\left(-\|\tilde{\boldsymbol{y}}_{nl} - \widetilde{\boldsymbol{H}}_n \tilde{\boldsymbol{x}}\|^2 / N_0\right)}. \end{aligned} \quad (6)$$

where $\forall \lambda = 1, ..., mN_t$. The notation $\mathcal{X}_b^\lambda$ is the subset of the hypersymbol constellation where the λth bit is equal to b. The scaled channel matrix $\widetilde{\boldsymbol{H}}_n$ will help the destination to mitigate the effects of the compression noise.

127

The achievable sum rate of this cooperative system with this channel model is given by:

$$R_{\mathrm{CF}} = \log\ \det\left[\boldsymbol{I} + \widetilde{\boldsymbol{H}}_n \left(\frac{\mathrm{SNR}}{2}\boldsymbol{I}\right)\widetilde{\boldsymbol{H}}_n^{\dagger}\right]. \tag{7}$$

Here, $\boldsymbol{H}^{\dagger}$ denotes the conjugate transpose of $\boldsymbol{H}$. Inserting (3) to (5) and (7), we will get an upper bound for the achievable sum rate, denoted as $\bar{R}_{\mathrm{CF}}$. For a wired conferencing link between the relay and destination, where $C \to \infty$, the system will approach the ideal MIMO case. The achievable sum rate of the MIMO system is then given by:

$$R_{\mathrm{MIMO}} = \log\det\left[\boldsymbol{I} + \boldsymbol{H}_n \left(\frac{\mathrm{SNR}}{2}\boldsymbol{I}\right)\boldsymbol{H}_n^{\dagger}\right]. \tag{8}$$

Comparing (7) and (8), we find out that their difference lies in the channel matrices $\widetilde{\boldsymbol{H}}_n$ and $\boldsymbol{H}_n$. With fixed SNR, a high quantization rate C will result in σ_{cn}^2 decreasing to 0, and then $\widetilde{\boldsymbol{H}}_n$ tends towards $\boldsymbol{H}_n$ in value. As shown in Fig. 2, with C increasing, the bound $\bar{R}_{\mathrm{CF}}$ is increasing and approaches R_{MIMO}. Thus a good VQ with high C will enable the virtual-MIMO system to achieve almost ideal MIMO performance.

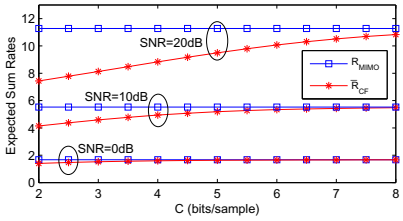

Fig. 2. Sum rate comparison between MIMO and virtual-MIMO systems.

IV. Vector Quantization Design at the Relay

To perform CF cooperation, a standard source coding technique is employed. The key tasks of the relay thus include constructing a good codebook and compressing the received signals. The codebook design techniques and the corresponding complexities will be analysed in this section.

A. Codebook Design

The codebook design at the relay is based on the desired codebook size which equals 2^C and the knowledge of the noise-free constellation. Note that, besides signal symbols, some control information such as the modulation type is also transmitted on control channels in practice. It is reasonable to expect the relay could construct the noise-free constellation of the received signals, i.e. the constellation of $h_{1n}x_{1nl}+h_{2n}x_{2nl}$, denoted by y_{rnl}^c. The codebook design based on the noise-free constellation will be simple and efficient.

In this paper, Voronoi vector quantization (VQ), and tree-structured vector quantization (TSVQ) [11] are employed at the relay. Voronoi VQ is considered first, as it has the advantage that the codebook is optimal in the sense of minimising average distortion. To design this VQ, the LBG algorithm which is based on the iterative use of codebook modification, is used [12]. However, Voronoi VQ implies a high computational complexity and requires an exhaustive search to find the correct codeword, especially when C is high, as will be shown in Section IV-B. To reduce the complexity, we also consider TSVQ. TSVQ can be realized in two main forms, binary TSVQ and multistage TSVQ. It is known that the multistage technique is more efficient when used for only two or three stages [11]. Thus for QPSK or 16QAM mappings which do not require quite high quantization rates in the CF system, multistage TSVQ is a better algorithm to design the codebook. Another reason for adoption of the multistage TSVQ is due to the specific implementation scenario. Note that, as a combination of two path symmetric constellations, y_{rnl}^c is therefore symmetric. The first stage quantization of the multistage TSVQ comes from the classification, i.e. classifying y_{rnl}^c into several subsets, based on the constellation symmetry or other relationships. The second stage is determined by applying the LBG algorithm on the subsets.

For example, we suppose the two signals from the transmitters are 16QAM constellations. An instantaneous version of y_{rnl}^c is shown in Fig. 3. The points could be firstly divided into four subsets according to their quadrants. The sub-codebook designed for one subset would be extended to the whole codebook easily, with the phase angles of the sub-codevectors changing by $\pi/2$ every time. Moreover, for one subset, we sort the constellation points in ascending order by their magnitude. To further decrease the computational complexity, we divide the subset into two groups in ascending order. We denote the quantization rate for the first stage quantization of TSVQ as C_1. Thus we have 8 groups, labelled (1) - (8), i.e. $C_1 = 3$ bits/sample, as shown in Fig. 3 (a). Then the LBG algorithm is employed twice for group No. (1) and (2) to obtain the sub-codebook for one quadrant. Based on a simple extension, the second stage quantization for TSVQ is completed. Finally the relay node obtains the complete codebook. The codebook designed by the Voronoi VQ is also shown in Fig. 3 (b) for comparison. Even though the TSVQ we implemented here is suboptimal, it is much simpler to design and can achieve similar performance to the optimal but more complicated Voronoi VQ, as will be shown in Section V.

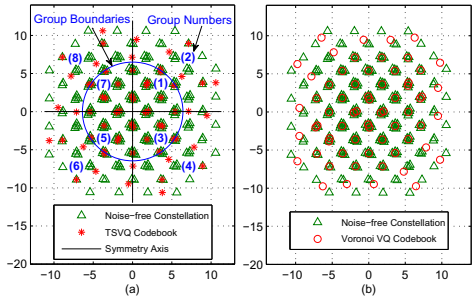

Fig. 3. Noise-free constellation of the received signals and the codebook designed at the relay with C= 6 bits/sample. (The TSVQ codebook with C_1= 3 bits/sample is shown in (a); the Voronoi VQ codebook is shown in (b).)

Additionally, when we are considering the mappings which require higher quantization rates at the relay, e.g. 64QAM,

128

two-stage TSVQ with the full-search VQ applied in the second stage may not be enough to reduce the encoding complexity. One useful technique is to replacing the full search VQ in the second stage with a binary VQ. This in effect is a hybrid of multistage and binary TSVQ [11], and will help to reduce the complexity of the codebook design and quantization process for higher order mappings.

B. Complexity Analysis

As described in Section IV-A, both the Voronoi VQ and TSVQ use the LBG algorithm, but with a different size of training sequence. The codebook design complexity therefore comes from the computational complexity of the LBG algorithm. The computational time for the LBG algorithm is given by [13]:

$$T_{\text{LBG}} = I_s 2^C Q T_d + I_s(2^C - 1)QT_c, \tag{9}$$

where 2^C is the codebook size, I_s is the number of iterations, and Q is the number of training vectors. T_d and T_c denote the computational time for one distortion value and comparing two distortion values respectively. For the Voronoi VQ which implements the LBG algorithm on the whole noise-free constellation y^c_{rnl}, we have $Q = M^2 = 2^{2m}$. Since $I_s \leq Q/2^C$ [13], we obtain:

$$T_{\text{d,Voronoi}} = T_{\text{LBG}} \leq 2^{4m} T_d + 2^{4m} \frac{(2^C - 1)}{2^C} T_c. \tag{10}$$

But for the TSVQ we implemented, the computational time is a summation of two stages,

$$\begin{aligned} T_{\text{d,TSVQ}} \leq & \left[\frac{2^{2m}}{4} T_d + \frac{2^{2m}}{8} \left(\frac{2^{2m}}{4} - 1 \right) T_c \right] \\ & + 2 \left[\frac{2^{4m}}{2^{2C_1}} T_d + \frac{2^{4m}}{2^{2C_1}} \frac{2^{C-C_1} - 1}{2^{C-C_1}} T_c \right]. \end{aligned} \tag{11}$$

A justification for (11) is as follows: In accordance with the 16QAM design example in Section IV-A, we assume $C_1 = 3$ bits/sample for the first stage quantization of TSVQ. In one quadrant, there are $2^{2m}/4$ vectors, the distortion values of which are to be computed and sorted to obtain two separate groups. Here the selection sort algorithm is considered, requiring $\frac{2^{2m}}{4}(\frac{2^{2m}}{4} - 1)/2$ times comparison. For the second stage, the LBG algorithm is implemented twice for the two groups. In one group, there are $Q = 2^{2m}/2^{C_1}$ training vectors and codebook size is 2^{C-C_1}. Therefore when we consider a large m and a high C, we have $T_{\text{d,Voronoi}} = \mathcal{O}(2^{4m}(T_d + T_c))$ and $T_{\text{d,TSVQ}} = \mathcal{O}(2^{4m-5}T_d + 2^{4m-4}T_c)$ as $C_1 = 3$ bits/sample. That is, compared with the Voronoi VQ, TSVQ decreases the computational complexity for the codebook design significantly.

As to the symbol encoding, TSVQ will also allow a faster codebook search. Specifically, the encoding algorithm for a Voronoi VQ can be viewed as an exhaustive search algorithm. For a codebook of size 2^C, the codevector selection for one symbol requires 2^C distortion evaluations and $2^C - 1$ comparisons. Its operation time of the codebook search for one symbol is shown as:

$$T_{\text{s,Voronoi}} = 2^C T_d + (2^C - 1)T_c. \tag{12}$$

For the TSVQ we implemented, the search procedure includes two stages: finding out an appropriate group, and performing a full search on the group. Thus the search time of TSVQ is,

$$T_{\text{s,TSVQ}} = (2^{C-C_1} + 1)T_d + 2^{C-C_1} T_c. \tag{13}$$

When $C_1 = 3$ bits/sample, the two-stage TSVQ will allow almost 8 times faster encoding than the Voronoi VQ. Thus TSVQ also has a much lower encoding complexity.

Therefore, compared with the Voronoi VQ, the TSVQ not only decreases the computational complexity for the codebook design, but also allows a faster codebook search for the encoding. Since TSVQ can also achieve a good performance, it is a better choice to enable CF cooperation in practice.

V. Numerical Results

In this section, we present the error performance of our cooperative virtual-MIMO system. At the transmitter, a binary convolutional code is assumed with the generator polynomials $[133, 171]_{\text{octal}}$ ($R_c = 1/2$, $d_{\text{free}} = 10$). A random interleaver and Gray-labeled QPSK or 16QAM modulation are considered as well. We assume 10^5 block fading channels and each block has 200 consecutive symbol periods. The CF protocol is implemented, with Voronoi VQ or TSVQ at the relay. The simulation results are obtained using the Monte Carlo method. We plot the BER or BLER against the information bit SNR, i.e E_b/N_0.

The block error rate (BLER) performance of the cooperative virtual-MIMO system with 16QAM modulation under various quantization rates, is shown in Fig. 4 (a). The BLERs are compared against the lower bound of the corresponding MIMO system, and the non-cooperative MISO system. To perform CF cooperation, Voronoi VQ is implemented. Fig. 4 (a) shows that, with help from the relay, the system always performs better than the non-cooperative MISO system, as the CF protocol always provides a gain over direct transmission. As C increases, the simulation result decreases and approaches the ideal MIMO system performance, since the corresponding compression noise variance reduces. When $C = 7$ bits/sample, the BLER of CF cooperation performs very close to the ideal MIMO system. Moreover, similar to Fig. 4 (a), Fig. 4 (b) also presents the system BLER results, but for QPSK modulation. As its constellation size is smaller than that for 16QAM, lower quantization rates are considered. Compared with $C = 7$ bits/sample for 16QAM, the system with QPSK mapping requires $C = 4$ bits/sample to approach the ideal MIMO performance.

As mentioned above, to decrease the complexity, we proposed to employ TSVQ to design the codebook at the relay. When C equals 6 bits/sample, Fig. 5 (a) shows the bit error rate (BER) results of the TSVQ cooperative system which is set up in accordance with the example for 16QAM mapping in Section IV-A. Its BER is compared against the performance of the system with Shannon coding bound. According to equation (2), the compression noise w_{cnl} is considered for this kind of system, with the Shannon coding bound of the variance calculated via equation (3). As shown in this figure, the

129

Voronoi VQ obtains performance which is quite close to the Shannon coding bound. Even though the TSVQ we designed here is suboptimal, it is much simpler to design and operate and can achieve error rates comparable to the optimal but more complicated Voronoi VQ. As an example, at BER of 10^{-3}, a performance gap of 2.5 dB exists between the two VQs. But for a given quantization rate 6 bits/sample, the Voronoi VQ requires a $\mathcal{O}(65536(T_d + T_c))$ computations which is much larger than that of TSVQ requiring $\mathcal{O}(2048T_d + 4096T_c)$ computations. The TSVQ we employed allows a lower encoding complexity as well.

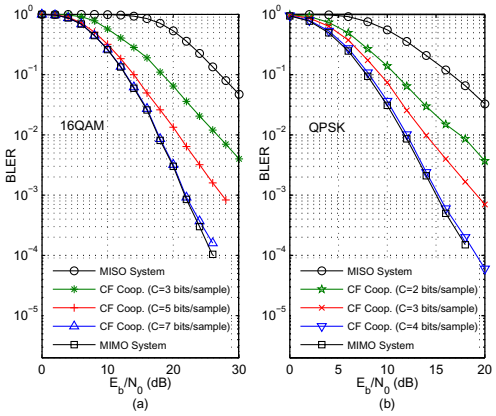

Fig. 4. BLER results of the cooperative virtual-MIMO system with Voronoi VQ at the relay and ML receiver at the destination. (16QAM mapping is considered in (a), while QPSK mapping is considered in (b).)

Additionally, considering the quantization rates 5 bits/sample and 7 bits/sample, we compare the performance of the Voronoi VQ and TSVQ in Fig. 5 (b). It can be seen that the BER of TSVQ for $C=6$ bits/sample in Fig. 5 (a) performs almost the same as the Voronoi VQ for $C=5$ bits/sample in Fig. 5 (b). According to (12) and (13), that means the TSVQ with encoding complexity $(9T_d + 8T_c)$ is able to achieve the performance of the Voronoi VQ with $(32T_d + 31T_c)$ complexity. Also, the TSVQ for $C = 7$ bits/sample performs similarly to the Voronoi VQ for $C=6$ bits/sample. That is, TSVQ could approach the performance of Voronoi VQ with roughly 4 times lower encoding complexity. TSVQ always requires a much lower computational complexity for the codebook design as well. Thus the TSVQ we implemented here is more efficient than the Voronoi VQ, and is a better choice for the CF cooperation to enable the virtual-MIMO system to achieve MIMO performance in practice.

VI. Conclusions

In this paper, a virtual-MIMO-BICM system that implements CF cooperation was presented. We proposed to employ standard source coding techniques at the relay node. Then two codebook design algorithms were presented, Voronoi VQ and TSVQ, based on the knowledge of the noise-free constellation. A comparison in terms of the codebook design complexity and encoding complexity was also presented.

It was shown that, with Voronoi VQ, $C = 7$ bits/sample for 16QAM mapping and $C = 4$ bits/sample for QPSK mapping will result in a cooperative system which achieves almost ideal MIMO performance. As to the codebook design algorithms, we found that the TSVQ not only decreases the computational complexity for the codebook design, but also allows a faster codebook search for the encoding, at the cost of a small performance loss. Thus in practice, the TSVQ is a better choice for CF cooperation to enable the virtual-MIMO system to achieve almost MIMO performance.

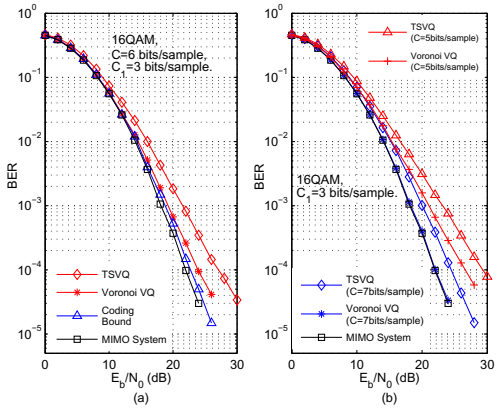

Fig. 5. BER performance of the cooperative virtual-MIMO system with TSVQ or Voronoi VQ at the relay. (Quantization rate 6 bits/sample is considered in (a), while 5 and 7 bits/sample are considered in (b).)

References

[1] S. Jayaweera, "Virtual MIMO-based cooperative communication for energy-constrained wireless sensor networks," *IEEE Trans. Wireless Commun.*, vol. 5, no. 5, pp. 984 – 989, May 2006.

[2] W. Yu and J. Cioffi, "Sum capacity of gaussian vector broadcast channels," *IEEE Trans. Inform. Theory*, vol. 50, no. 9, pp. 1875 – 1892, Sept. 2004.

[3] G. Kramer, M. Gastpar, and P. Gupta, "Cooperative strategies and capacity theorems for relay networks," *IEEE Trans. Inform. Theory*, vol. 51, no. 9, pp. 3037 – 3063, Sept. 2005.

[4] A. Host-Madsen and J. Zhang, "Capacity bounds and power allocation for wireless relay channels," *IEEE Trans. Inform. Theory*, vol. 51, no. 6, pp. 2020 –2040, June 2005.

[5] G. Caire, G. Taricco, and E. Biglieri, "Bit-interleaved coded modulation," *IEEE Trans. Inform. Theory*, vol. 44, no. 3, pp. 927 –946, 1998.

[6] C. Ng, I. Maric, A. Goldsmith, S. Shamai, and R. Yates, "Iterative and one-shot conferencing in relay channels," in *Information Theory Workshop. ITW '06 Punta del Este. IEEE*, 13-17 2006, pp. 193 –197.

[7] M. Kuhn, J. Wagner, and A. Wittneben, "Cooperative processing for the WLAN uplink," in *IEEE WCNC*, march 2008, pp. 1294 –1299.

[8] R. Gray and D. Neuhoff, "Quantization," *IEEE Trans. Inform. Theory*, vol. 44, no. 6, pp. 2325 –2383, Oct 1998.

[9] T. Kim, M. Skoglund, and G. Caire, "Quantifying the loss of compressforward relaying without Wyner-Ziv coding," *IEEE Trans. Inform. Theory*, vol. 55, no. 4, pp. 1529 –1533, April 2009.

[10] C. Ng, N. Jindal, A. Goldsmith, and U. Mitra, "Capacity gain from two-transmitter and two-receiver cooperation," *IEEE Trans. Inform. Theory*, vol. 53, no. 10, pp. 3822 –3827, Oct. 2007.

[11] A. Gersho and R. M. Gray, *Vector quantization and. signal compression*. Kluwer Academic Publisher, 1992.

[12] J. Jiang, J. Thompson, P. Grant, and N. Goertz, "Practical compress-and-forward cooperation for the classical relay network," in *European Signal Processing Conference, Glasgow, Scotland*, Aug. 2009, pp. 2421–2425.

[13] J. Shanbehzadeh and P. Ogunbona, "On the computational complexity of the LBG and PNN algorithms," *IEEE Transactions on Image Processing*, vol. 6, no. 4, pp. 614 –616, April 1997.

An Adaptive Rate Compress-and-Forward Cooperation for Virtual-MIMO Systems

Jing Jiang, John S. Thompson, Xiang Wu, Peter M. Grant
Institute for Digital Communications, Joint Research Institute for Signal & Image Processing
School of Engineering, University of Edinburgh, Edinburgh, EH9 3JL, UK.
Email: J.Jiang@ed.ac.uk, John.Thompson@ed.ac.uk, X.Wu@ed.ac.uk, Peter.Grant@ed.ac.uk

***Abstract*—A practical virtual multiple-input multiple-output (MIMO) system that implements compress-and-forward (CF) cooperation is proposed in this paper. Bit-interleaved coded modulation (BICM) technique is implemented here to provide forward error correction and improve the system performance. A closed-form union bound for the system error probability is derived, based on which we prove that the smallest singular value of the cooperative channel matrix dominates the system error performance. Accordingly, an adaptive rate CF scheme is proposed, which uses the smallest singular value as the switching criterion. Depending on the instantaneous channel conditions, the relay could therefore choose various quantization rates. It is shown that the adaptive rate CF scheme eliminates unnecessary complexity for the quantization at the relay, and enables the virtual-MIMO system to achieve almost MIMO performance.**

I. Introduction

In recent years the virtual MIMO wireless communication system has been proposed as an alternative to a point-to-point MIMO system, with the transmitter having multiple antennas and each of the receivers having a single antenna [1]. In practical situations, when the transmitter does not have channel side information (CSI) for the wireless link to each receiver, receiver-side local cooperation in the virtual-MIMO system is a good way for achieving higher throughput. To perform cooperation, the protocols can be grouped into three major categories: amplify-and-forward (AF), decode-and-forward (DF), and compress-and-forward (CF). Since the relay is close to the destination in our scenario, it is shown in [2] that the CF protocol, which provides better performance, is the best candidate for this virtual-MIMO system.

In virtual-MIMO communications, we implement bit-interleaved coded modulation (BICM) [3] as a forward error correction (FEC) coding scheme to mitigate the effects of multipath fading. But the system is not limited to BICM, other FEC coding schemes could also be employed. Recently, BICM has been studied in MIMO systems with maximum likelihood (ML) detection or linear detection. The disadvantage of the ML receiver is the high computational complexity, making it impractical in many cases. It is shown that the linear minimum mean square error (MMSE) receiver outperforms zero-forcing (ZF) and VBLAST receivers when combined with BICM technique [4]. Thus we implement a MMSE receiver at the destination in this virtual-MIMO system. One relevant work is [5], in which a virtual-MIMO channel with partial cooperation among users is presented. But only a simple AF protocol is considered. Our recent work [6] proposes a new virtual-MIMO-BICM system with CF cooperation, but focuses on the codebook design at the relay to enable CF cooperation.

We acknowledge the support of the Scottish Funding Council for the Joint Research Institute with Edinburgh and the Heriot-Watt Universities, which is a part of the Edinburgh Research Partnership. Jing Jiang gratefully acknowledges the support from the UK/China Scholarships for Excellence programme in funding her PhD studies.

We now summarize the main contributions of this paper. First, we present a practical virtual-MIMO-BICM system that implements CF cooperation. With help from the relay, MIMO performance could be achieved in this virtual-MIMO system. Next, we derive a tight analytical expression for the system bit error rate (BER). The expression is in closed form and shows that the smallest singular value of the cooperative channel matrix dominates the system BER. Moreover, an adaptive rate CF scheme is proposed, with adopting the smallest singular value as the switching criterion. The closed-form cumulative distribution function (CDF) for the smallest singular value is derived as well. It is shown that the adaptive rate CF scheme eliminates unnecessary complexity, and enables the virtual-MIMO system to achieve almost ideal MIMO performance.

The paper is organized as follows. Section II specifies the model of the cooperative virtual-MIMO system. The analytical BER expression and details of the proposed adaptive rate CF scheme are presented in Section III. Section IV shows the simulation results, and Section V concludes the paper.

II. Virtual-MIMO System with CF Cooperation

A. Channel Model

Consider a cooperative virtual-MIMO network with one remote N_t-antenna transmitter sending information to N_r colocated single-antenna receivers, as shown in Fig. 1. BICM is employed here to improve system performance. At the transmitter, a linear binary rate-R_c convolutional encoder and an ideal random bit interleaver which rearranges the coded bits via a random permutation are considered. In each steam after the demultiplexer (or demux), groups of m bits are mapped onto complex data symbols via Gray-labelled 2^m-ary modulation whose signal constellations are denoted as $\mathcal{X}$.

Since the transmitter is far away from the receiver group, we assume the channels between them are block fading, with N Rayleigh fading blocks, and each block has L consecutive

978-1-4244-9147-6/10/$26.00 ©2010 IEEE

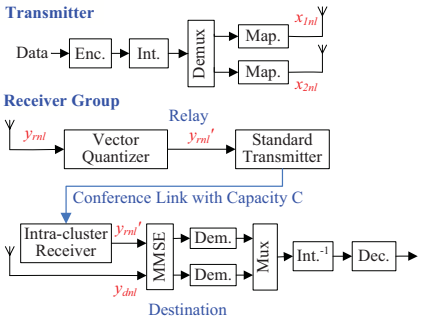

Fig. 1. System Model of the Cooperative Virtual-MIMO System. (TX and RX stand for the transmitter and receiver. $N_t = 2$, $N_r = 2$.)

time instants. When we consider a single time instance l for the nth channel, the channel model is given by:

$$\begin{bmatrix} y_{rnl} \\ y_{dnl} \end{bmatrix} = \boldsymbol{H}_n \boldsymbol{x}_{nl} + \boldsymbol{w}_{nl}, \text{ with } \boldsymbol{H}_n = \begin{bmatrix} h_{1n} & h_{2n} \\ h_{3n} & h_{4n} \end{bmatrix}, \quad (1)$$

where we assume $N_t = 2$, $N_r = 2$. $\boldsymbol{H}_n$ denotes the nth block fading channel matrix, where each $h_{in} (i \in [1, ..., 4])$ is independent and identically distributed (i.i.d.). We also define the vector $\boldsymbol{x}_{nl} = [x_{1n1}, x_{2nl}]^{\mathrm{T}}$ and $\boldsymbol{w}_{nl} = [w_{1n1}, w_{2nl}]^{\mathrm{T}}$, where the noises $w_{i'nl} \sim \mathcal{CN}(0, N_0)$. Moreover, we assume normalized Rayleigh fading, that is $\mathrm{E}[|h_{in}|^2] = 1$. The average transmitted power per symbol is $\mathrm{E}[|x_{i'nl}|^2] = E_s/2$. We normalize the total transmitted power E_s to unity, and the corresponding power per bit is $E_b = E_s/(mR_c)$. We assume the perfect channel side information (CSI) is available at the receivers.

B. CF Cooperation

There exist two clustered receivers, the destination and the helping relay. As the receivers are close together, it is highly likely that we could achieve high channel capacity with high reliability on this short range link. Hence we assume the two receivers cooperate by way of an error-free one-shot conference link [7], with capacity C, shown in blue in Fig. 1. The conference link enables cooperation, and CF could reasonably serve as a cooperation protocol since it provides higher rate when the relay is closer to the destination.

To perform CF cooperation, a standard source coding technique is employed for practical considerations. That is, the relay is equipped with a vector quantizer (VQ). The nearest neighbour algorithm [8], whose codebook is optimal in the sense of minimising average distortion, is implemented to design the codebook needed for the quantization. Here the quantization rate is equal to the capacity C of the error-free conference link. Then a compressed version of the signal y'_{rnl} will be passed into a standard transmitter and transmitted over the conference link. Thus we have,

$$y'_{rnl} = y_{rnl} + w_{cnl}, \quad (2)$$

where w_{cnl} is the compression noise, independent of y_{rnl}, with variance σ^2_{cn}, i.e. $w_{cnl} \sim \mathcal{CN}(0, \sigma^2_{cn})$. Note that, for a wired conferencing link with high capacity C, σ^2_{cn} decreases to 0, and the system will become the ideal MIMO case.

The destination is assumed to be equipped with a receiver which observes signals y_{dnl} from the transmitter, and a intra-cluster receiver which observes signals y'_{rnl} from the relay, as shown in Fig. 1. We denote the received signals at the destination as $\boldsymbol{y}_{nl} = [y'_{rnl} \;\; y_{dnl}]^{\mathrm{T}}$. Since w_{cnl} is i.i.d. complex Gaussian noise as well, y'_{rnl} could be scaled so that y'_{rnl} and y_{dnl} have the same power of Gaussian noise. That is,

$$\tilde{\boldsymbol{y}}_{nl} = [\tilde{y}'_{rnl} \;\; y_{dnl}]^{\mathrm{T}} = \widetilde{\boldsymbol{H}}_n \boldsymbol{x}_{nl} + [\tilde{w}_{1nl} \;\; w_{2nl}]^{\mathrm{T}}, \quad (3)$$

$$\text{with } \widetilde{\boldsymbol{H}}_n \triangleq \begin{bmatrix} \sqrt{\eta_n} h_{1n} & \sqrt{\eta_n} h_{2n} \\ h_{3n} & h_{4n} \end{bmatrix}, \; \eta_n \triangleq \frac{N_0}{N_0 + \sigma^2_{cn}}. \quad (4)$$

$\tilde{w}_{1nl} \sim$ i.i.d. $\mathcal{CN}(0, N_0)$, and η_n is the degradation factor due to the compression noise. Finally $\tilde{y}'_{rnl} = \sqrt{\eta_n} y'_{rnl}$.

Note that, in the rest of this paper, when we are considering a single time instance l on the nth channel, we will drop the subscript nl for the symbols and n for the channel matrix, since the received symbols are treated independently.

C. MMSE-based BICM Demodulation

The general structure of the destination with a linear MMSE receiver is shown in Fig. 1. The first MMSE filtering step is

$$\boldsymbol{z} = \boldsymbol{W}\tilde{\boldsymbol{y}} = \boldsymbol{x} + \boldsymbol{e} + \boldsymbol{v}, \text{ with } \boldsymbol{W} = \boldsymbol{B}\left(\widetilde{\boldsymbol{H}}^{\dagger}\widetilde{\boldsymbol{H}} + \frac{N_t}{\mathrm{SNR}}\boldsymbol{I}\right)^{-1}\widetilde{\boldsymbol{H}}^{\dagger}, \quad (5)$$

where $\boldsymbol{e} = (\boldsymbol{W}\widetilde{\boldsymbol{H}} - \boldsymbol{I})\boldsymbol{x}$ is the residual inter-symbol interference (ISI) and $\boldsymbol{v} = \boldsymbol{W}[\tilde{w}_1 \;\; w_2]^{\mathrm{T}}$. Also, $\boldsymbol{B}$ is a diagonal matrix which removes the bias from the MMSE estimates, with kth diagonal component given by $\boldsymbol{B}_{k,k} = (\rho_k + 1)/(\rho_k)$, where

$$\rho_k = \frac{1}{\left[(\boldsymbol{I}_{N_t} + \frac{\mathrm{SNR}}{N_t}\widetilde{\boldsymbol{H}}^{\dagger}\widetilde{\boldsymbol{H}})^{-1}\right]_{k,k}} - 1. \quad (6)$$

The scalar ρ_k is the instantaneous received signal to interference and noise ratio (SINR) for the kth stream [9].

The BICM log-likelihood ratio (LLR) for each coded bit corresponding to $\boldsymbol{x}_k$ is calculated from $\boldsymbol{z}_k$ as,

$$\begin{aligned} \mathcal{L}(c^{\lambda}|z_k, \boldsymbol{W}) &= \ln \frac{\sum_{\tilde{x}_k \in \mathcal{X}_1^{\lambda,k}} p\{z_k|\tilde{x}_k, \boldsymbol{W}\}}{\sum_{\tilde{x}_k \in \mathcal{X}_0^{\lambda,k}} p\{z_k|\tilde{x}_k, \boldsymbol{W}\}} \\ &= \ln \frac{\sum_{\tilde{x}_k \in \mathcal{X}_1^{\lambda,k}} \exp\left(-\rho_k |z_k - \tilde{x}_k|^2\right)}{\sum_{\tilde{x}_k \in \mathcal{X}_0^{\lambda,k}} \exp\left(-\rho_k |z_k - \tilde{x}_k|^2\right)}. \end{aligned} \quad (7)$$

where $\forall \lambda = 1, ..., m$. Note that $\mathcal{X}_b^{\lambda,k}$ is the signal subsets within the kth transmit constellation where the λth bit is equal to b. The two path LLRs are combined into one output stream by the multiplexer, and then reordered by the deinterleaver. Finally, the decoder accepts the LLRs of all coded bits and employs a soft Viterbi algorithm to decode the signals.

The benefit of the MMSE receiver is the lower computational complexity. However, it suffers from the residual ISI caused by the compression noise w_c. A higher quantization rate C is one solution with decreasing w_c, but will introduce additional operational complexity for the quantization at the

relay. Another solution is to employ an adaptive rate CF scheme, as will be described in Section III. A good quantization with lower w_c at the relay, will enable the virtual-MIMO system to achieve almost ideal MIMO performance.

III. Adaptive Rate CF Scheme

The basic motivation for the proposed adaptive rate CF cooperation is the fact that the quantization rate at the relay is unnecessarily high, when channel is well-conditioned. If we could apply a suitable threshold check strategy to judge the conditions of the instantaneous channels, the relay could choose different quantization rates according to different channel conditions. It would eliminate unnecessary complexity for the quantization when performing CF cooperation. Thus, the key issues of the adaptive rate CF cooperation are exploiting the relationship between the system performance and the channel properties, and finding an appropriate threshold strategy.

A. Error Performance Analysis

Throughout the paper, we consider block fading channels, for which a fading envelope is given by $\mathcal{H} = (\boldsymbol{H}_1, ..., \boldsymbol{H}_N)$. For a specific channel condition $\boldsymbol{H}$, the conditional union bound (UB) on BER for linear binary convolutional codes over memoryless binary-input output-symmetric (BIOS) channels can be expressed as [10], $P_b(\boldsymbol{H}) \leq \sum_{d=d_{\text{free}}}^{\infty} A_d\, P_d(d|\boldsymbol{H})$, where A_d denotes the sum of bit errors for error events of distance d [11]. The scalar $P_d(d|\boldsymbol{H})$ is the conditional pairwise error probability (PEP) for two codewords differing in d bits. The scalar d_{free} is the minimum free Hamming distance. The average BER after decoding is obtained by averaging $P_b(\boldsymbol{H})$ over the fading channel matrices,

$$P_b = \mathop{\mathrm{E}}_{\boldsymbol{H}\in\mathcal{H}}\left[P_b(\boldsymbol{H})\right] \leq \mathop{\mathrm{E}}_{\boldsymbol{H}\in\mathcal{H}}\left[\sum_{d=d_{\text{free}}}^{\infty} A_d P_d(d|\boldsymbol{H})\right]. \tag{8}$$

One thing to note here is the bound $P_b(\boldsymbol{H})$ holds under the assumption that the channels are BIOS. For our block fading channel, which is not symmetric, we adopt the approach of [3] and force the BICM channel to behave as BIOS by using a random modulation concept. Let t denote a random variable, which independently selects, for every symbol, either Gray-labelling mapping or its complement with probability 1/2. Furthermore, due to the symmetry of the channel output, we can safely assume that the all-zero codewords are transmitted.

We employ Gaussian approximation (GA) [10] to approximate $P_d(d|\boldsymbol{H})$, and we obtain,

$$P_d(d|\boldsymbol{H}) \approx Q\left(\sqrt{-2dK_{\mathcal{L}}(\hat{s})}\right), \tag{9}$$

where $K_{\mathcal{L}}(s)$ is the cumulant generating function (c.g.f.) of the variable $\mathcal{L}(c^{\lambda}|z_k, \boldsymbol{W})$ defined in (7),

$$\begin{aligned} K_{\mathcal{L}}(s) &= \log \mathop{\mathrm{E}}_{z,\lambda,t,k,\boldsymbol{W}}\left[\exp\left(s\ \mathcal{L}(c^{\lambda}|z_k, \boldsymbol{W})\right)\right] \\ &= \log \mathop{\mathrm{E}}_{z,\lambda,t,k,\rho_k}\left[\left(\frac{\sum_{\tilde{x}_k\in\mathcal{X}_{\bar{t}}^{\lambda,k}} \exp\left(-\rho_k|(z_k-\tilde{x}_k)|^2\right)}{\sum_{\tilde{x}_k\in\mathcal{X}_t^{\lambda,k}} \exp(-\rho_k|(x_k-\tilde{z}_k)|^2)}\right)^s\right]. \end{aligned} \tag{10}$$

For BIOS channels, symmetry dictates that the saddlepoint $\hat{s}$ in (9) is placed at $\hat{s} = 1/2$ [10]. Inserting (10) into (9) gives us an upper bound on the system BER. The bound can be evaluated via numerical integration using the Monte Carlo method in practice.

We can show that at high SNR, the result of $K_{\mathcal{L}}(s)$ can be written in closed form. Specifically, averaging over λ, t, k, and $x_k \in \mathcal{X}_t^{\lambda,k}$, $K_{\mathcal{L}}(s)$ is given by

$$K_{\mathcal{L}}(s) = \log\left[\frac{1}{m2^m N_t}\sum_{\lambda=1}^{m}\sum_{t=0}^{1}\sum_{k=1}^{N_t}\sum_{x_k\in\mathcal{X}_t^{\lambda,k}} \underset{\lambda,t,k,x_k,\rho_k}{\Lambda}(s)\right], \tag{11}$$

$$\text{with } \underset{\lambda,t,k,x_k,\rho_k}{\Lambda}(s) = \mathop{\mathrm{E}}_{\tilde{x}_k,e_k,v_k}\left[\left(\frac{\exp\left(-\rho_k|(x_k-\tilde{x}_k)+e_k+v_k|^2\right)}{\exp(-\rho_k|e_k+v_k|^2)}\right)^s\right],$$

where we apply the Dominated Convergence Theorem [12]. That is, at high SNR the ratio in (10) is dominated by a single minimum distance term in the numerator and denominator, and $\tilde{x}_k \in \mathcal{X}_{\bar{t}}^{\lambda,k}$ is the nearest neighbour to $x_k \in \mathcal{X}_t^{\lambda,k}$. Then we proceed to average $\Lambda_{\lambda,t,k,x_k,\rho_k}(s)$ over the random noise v_k and the residual ISI e_k as follows,

$$\begin{aligned} &\underset{\lambda,t,k,x_k,\rho_k}{\Lambda}(s) \\ &= \mathop{\mathrm{E}}_{\tilde{x}_k,e_k,v_k}\left[\exp\left(-\rho_k\left(s|(x_k-\tilde{x}_k)+e_k+v_k|^2 - s|e_k+v_k|^2\right)\right)\right] \\ &= \mathop{\mathrm{E}}_{\tilde{x}_k,e_k,v_k}\left[\exp\left(-\rho_k\left(s|x_k-\tilde{x}_k|^2 - 2s\mathrm{Re}\{(x_k-\tilde{x}_k)(e_k+v_k)^*\}\right)\right)\right] \\ &= \mathop{\mathrm{E}}_{\tilde{x}_k,e_k,v_k}\left[\exp(-\rho_k s|x_k-\tilde{x}_k|^2)\cdot\exp(-2\rho_k s\mathrm{Re}\{(x_k-\tilde{x}_k)e_k^*\})\right. \\ &\qquad \left.\cdot\exp\left(\rho_k(-|v_k+s(x_k-\tilde{x}_k)|^2+s^2|x_k-\tilde{x}_k|^2+|v_k|^2)\right)\right] \\ &= \mathrm{E}_{\tilde{x}_k}\left[\exp(-\rho_k(s-s^2)|x_k-\tilde{x}_k|^2)\right]. \end{aligned} \tag{12}$$

Now, substituting (12) into (11) gives a closed-form expression for c.g.f. $K_{\mathcal{L}}(s)$, so that we can get a closed-form solution for the BER UB of our virtual-MIMO system. The BER UB is very useful since it provides insight into the asymptotic behaviour of the error probability of the system, and it is very close to the simulation result, as will be seen in Section IV.

B. Threshold Strategy

For the threshold design, we propose to adopt the smallest singular value of the cooperative (scaled) channel matrix as the switching criterion, and the following discussion shows the reasons and the corresponding threshold strategy.

From (12), we can see that $\Lambda_{\lambda,t,k,x_k,\rho_k}(s)$ depends on ρ_k and the squared Euclidean distance from x_k to its nearest neighbour $\tilde{x}_k$ in the complement subset. According to the signal constellation used in this system, we can further simplify $K_{\mathcal{L}}(s)$ by exploiting multiplicities of the Euclidean distance (see Table I in [12]). Moreover, it is obvious that, for a given channel condition and a specific constellation, $K_{\mathcal{L}}(s)$ only depends on the SINR ρ_k. The value $\rho_{\min}$ which equals to $\min\{\rho_k\}(k \in [1, N_t])$ dominates $K_{\mathcal{L}}(s)$. For example, when we are considering the Gray-labelled 16QAM constellation and the saddlepoint $\hat{s} = 1/2$, we obtain,

$$K_{\mathcal{L}}(\hat{s}) \leq \log\left[\left(\frac{3}{4}\exp(-0.1\rho_{\min}) + \frac{1}{4}\exp(-0.4\rho_{\min})\right)\right]. \tag{13}$$

Using the fact that the largest eigenvalue majorizes the largest diagonal term of a square matrix, from (6) we have,

$$\rho_{\min} \geq \frac{1}{\lambda_{\max}\left((\boldsymbol{I}_{N_t}+\frac{\mathrm{SNR}}{N_t}\widetilde{\boldsymbol{H}}^{\dagger}\widetilde{\boldsymbol{H}})^{-1}\right)_{k,k}} - 1 = \frac{\mathrm{SNR}}{N_t}\lambda^2_{\min}\left(\widetilde{\boldsymbol{H}}\right). \tag{14}$$

Thus, for a given channel $\widetilde{\boldsymbol{H}}$, it is obvious that a large value of $\lambda_{\min}\left(\widetilde{\boldsymbol{H}}\right)$ guarantees a large value of $\rho_{\min}$, and then guarantees a small value of $K_{\mathcal{L}}(s)$, and thus results in a low BER. In other words, for a symbol error to occur, a necessary condition is that $\lambda_{\min}$ for the scaled channel matrix falls below a certain threshold. Thus it is reasonable and efficient to characterise the quality of the cooperative virtual-MIMO channel based on the impact of its smallest singular value.

Additionally, to facilitate our threshold design and reduce the calculation complexity, we investigate the closed-form CDF of the smallest singular value. Recall the scaled channel matrix $\widetilde{\boldsymbol{H}}$ in (4), where we know that the scaled factor η is due to the compression noise σ_c^2. When we employ the standard source coding technique to perform CF cooperation, the lower bound of the compression noise variance is given by [6],

$$\bar{\sigma}_c^2 = \frac{\mathrm{E}[|y_r|^2]}{2^C-1} = \frac{N_0+\frac{1}{2}|h_1|^2+\frac{1}{2}|h_2|^2}{2^C-1}. \tag{15}$$

If $|h_1|^2+|h_2|^2$ could be replaced by its expected value, $\bar{\eta}$ would become constant for a certain SNR and C. The scaled channel $\widetilde{\boldsymbol{H}}$ will be a complex Gaussian matrix, whose smallest singular value has been discussed in [13]. Hence it is reasonably appropriate to implement the expected value $\mathrm{E}[|h_1|^2+|h_2|^2]$ for the analysis of the smallest singular value and the corresponding threshold design. Then we have

$$\widetilde{\boldsymbol{H}} = \begin{bmatrix} \sqrt{\bar{\eta}}h_1 & \sqrt{\bar{\eta}}h_2 \\ h_3 & h_4 \end{bmatrix} = \begin{bmatrix} \sqrt{\frac{2^C-1}{2^C+\mathrm{SNR}}}h_1 & \sqrt{\frac{2^C-1}{2^C+\mathrm{SNR}}}h_2 \\ h_3 & h_4 \end{bmatrix}, \tag{16}$$

which is distributed as $\mathcal{CN}(0, \boldsymbol{I}\otimes\boldsymbol{\Psi})$. $\boldsymbol{\Psi}$ is the covariance matrix, shown as

$$\boldsymbol{\Psi} = \mathrm{E}\left[\begin{pmatrix}\sqrt{\bar{\eta}}h_1 \\ h_3\end{pmatrix}\begin{pmatrix}\sqrt{\bar{\eta}}h_1 & h_3\end{pmatrix}\right] = \begin{bmatrix}\bar{\eta} & 0 \\ 0 & 1\end{bmatrix} = \begin{bmatrix}\frac{2^C-1}{2^C+\mathrm{SNR}} & 0 \\ 0 & 1\end{bmatrix}. \tag{17}$$

Thus employing the results from [13], the CDF of the smallest singular value $\lambda_{\min}(\widetilde{\boldsymbol{H}})$ are given by,

$$F_{\lambda_{\min}}(\lambda) = 1-\exp\left(-(1+\bar{\eta}^{-1})\lambda^2\right); \tag{18}$$

In Fig. 2, we plotted the CDF curves of the $\lambda_{\min}(\widetilde{\boldsymbol{H}})$ for quantization rates $C=4$, 6 bits/s and 8 bits/s. Note that in practical implementation, for a given channel condition, it is assumed that the corresponding SNR and the modulation type of the received signals are known at the receivers. Then we could design the codebook needed for the quantization at the relay, via the nearest neighbour algorithm, based on knowledge of the noise-free constellation. Next an estimation of the average distortion of the compression noise will be obtained, e.g. $\sigma^2_{c,4}$ for $C=4$ bits/s, and $\sigma^2_{c,6}$ for $C=6$ bits/s. Substituting $\sigma^2_{c,4}$ and $\sigma^2_{c,6}$ into (4), we will get estimates of the scaled channel $\widetilde{\boldsymbol{H}}_4$ and $\widetilde{\boldsymbol{H}}_6$ respectively. Now, we present the threshold check criterion for our adaptive rate CF scheme (rate 4, 6, 8 bits/s are chosen as candidates as an example),

$$C = \begin{cases} 4 \text{ bits/s}, & \text{if } \lambda_{\min}(\widetilde{\boldsymbol{H}}_4) \geq \lambda_{\text{th4}} \text{ and } \lambda_{\min}(\widetilde{\boldsymbol{H}}_6) \geq \lambda_{\text{th6}} \\ 6 \text{ bits/s}, & \text{if } \lambda_{\min}(\widetilde{\boldsymbol{H}}_4) < \lambda_{\text{th4}} \text{ and } \lambda_{\min}(\widetilde{\boldsymbol{H}}_6) \geq \lambda_{\text{th6}} \\ 8 \text{ bits/s}, & \text{if } \lambda_{\min}(\widetilde{\boldsymbol{H}}_4) < \lambda_{\text{th4}} \text{ and } \lambda_{\min}(\widetilde{\boldsymbol{H}}_6) < \lambda_{\text{th6}} \end{cases}, \tag{19}$$

where λ_{th4} and λ_{th6} are the thresholds that select various quantization rates, based on the settings of the corresponding CDF thresholds, P_{th4} and P_{th6}, as shown in Fig. 2. The impact of varying the CDF thresholds will be investigated in Section IV. Thus for ill-conditioned channels, the relay will implement a 8 bits/s VQ; and for well-conditioned channels, a 4 bits/s VQ will be enough for a good performance; otherwise, we employ 6 bits/s VQ. The adaptive rate CF scheme is able to eliminate unnecessary complexity for the quantization and conference link communication.

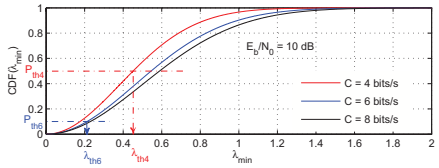

Fig. 2. CDF Curves of the Smallest Singular Value $\lambda_{\min}$.

IV. Numerical Results

In this section, we present the error rate performance of our cooperative virtual-MIMO system. At the transmitter, a binary convolutional code is assumed with the generator polynomials $[133, 171]_{\text{octal}}$ ($R_c = 1/2$, $d_{\text{free}} = 10$). A random interleaver and Gray-labelled 16QAM modulation is considered as well. We assume 10^5 block fading channels and each block having 200 consecutive symbol periods. The nearest neighbour VQ is implemented at the relay to perform CF cooperation. The simulation results are computed via the Monte Carlo method.

The BER performance of the cooperative virtual-MIMO-BICM system with 16QAM modulation, under various fixed quantization rates, is shown in Fig. 3. We can see that the BER UB from (8) and that based on $\rho_{\min}$ from (13) match well to the simulation results and provide good insights into the BER behaviour. When $C=8$ bits/s, the BER of the CF cooperation performs quite close to the corresponding MIMO system, which means that the relay enables the proposed single-antenna receiver to achieve almost MIMO performance. But for smaller C, such as 4 bits/s and 6 bits/s, there exists an error floor, which means the MMSE receiver cannot remove the residual ISI because of the compression noise. Hence it is appropriate to implement an adaptive-rate CF cooperation to exploit different C according to the channel conditions.

In Fig. 4, we investigate the impact of varying the threshold on the conditional BER, by changing the operating thresholds P_{th4} and P_{th6} for $C=4$ bits/s and 6 bits/s. The conditional BERs are calculated on the channels satisfying $\lambda_{\min,4} \geq \lambda_{th4}$

and $\lambda_{\min,6} \geq \lambda_{th6}$ respectively, where λ_{th4} and λ_{th6} are computed based on the settings of P_{th4} and P_{th6}. In Fig. 4, it is obvious that as the threshold P_{th} increases, for both $C=4$ bits/s and 6 bits/s cases, the conditional BER decreases. As long as $P_{\text{th4}}=0.5$ and $P_{\text{th6}}=0.1$, the error floor is too small to impact the system performance. Thus $P_{\text{th4}}=0.5$ and $P_{\text{th6}}=0.1$ are good choices for our adaptive-rate CF scheme to achieve a favourable performance-complexity tradeoff.

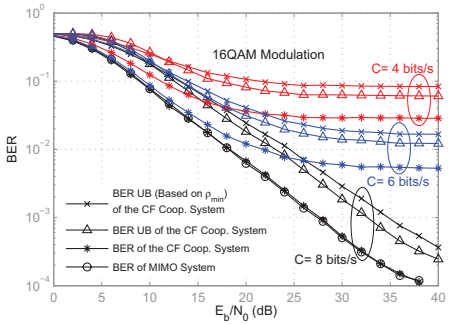

Fig. 3. BER Performance of the Virtual-MIMO-BICM System with CF Cooperation and MMSE Receiver.

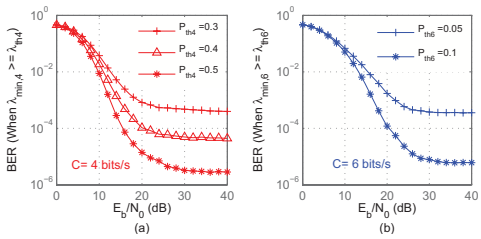

Fig. 4. The Effects of Varying the Thresholds on BER Performance for C = 4 bits/s and 6 bits/s.

Corresponding to $P_{\text{th4}}=0.5$ and $P_{\text{th6}}=0.1$, we calculate the thresholds λ_{th4} and λ_{th6} based on (18), in order to select various quantization rates for our adaptive rate CF scheme. According to the criterion (19), the simulation results are shown in Fig. 5. Since the CDF of the smallest singular value is based on an approximated $\bar{\eta}$, the practical probability is around 0.5 for $C=4$ bits/s, and around 0.1 for $C=8$ bits/s. That is, only for 10% channels which are ill-conditioned, the relay needs a 8 bits/s VQ, and for 50% of the channels which are well-conditioned, 4 bits/s VQ will be sufficient for acceptable performance. The final averaged quantization rate is around 5.2 bits/s. It means with saving almost 3 bits complexity for the quantization at the relay and 3 bits/sample on the conference link, the Virtual-MIMO system can achieve almost ideal MIMO performance.

V. Conclusion

In this paper, a practical virtual-MIMO-BICM system that implements CF cooperation and MMSE demodulation was presented. Based on the closed-form UB expression of the system BER, the adaptive rate CF scheme was proposed, with the relay able to choose various quantization rates according to the prevailing channel conditions. As to the threshold strategy, we proposed to adopt the smallest singular value of the cooperative (scaled) channel matrix as the switching criterion. The closed-form CDF expression of the smallest singular value was derived as well. The simulation results confirmed that the adaptive rate CF scheme was capable of eliminating unnecessary complexity for the quantization at the relay, and enabled the virtual-MIMO system to achieve almost ideal MIMO performance.

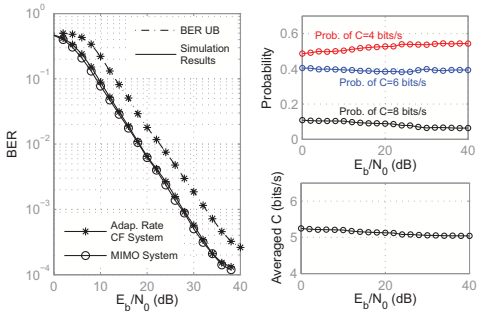

Fig. 5. BER Performance of the Virtual-MIMO System with the Adaptive Rate CF Cooperation.

References

[1] S. Jayaweera, "Virtual MIMO-based cooperative communication for energy-constrained wireless sensor networks," *IEEE Trans. Wireless Commun.*, vol. 5, no. 5, pp. 984–989, May 2006.

[2] A. Host-Madsen and J. Zhang, "Capacity bounds and power allocation for wireless relay channels," *IEEE Trans. Inform. Theory*, vol. 51, no. 6, pp. 2020–2040, June 2005.

[3] G. Caire, G. Taricco, and E. Biglieri, "Bit-interleaved coded modulation," *IEEE Trans. Inform. Theory*, vol. 44, no. 3, pp. 927–946, 1998.

[4] I. Collings, M. Butler, and M. McKay, "Low complexity receiver design for MIMO bit-interleaved coded modulation," in *IEEE ISSSTA*, 30 Aug. 2004, pp. 12–16.

[5] H. Kwon and J. Cioffi, "Multi-user MISO broadcast channel with user-cooperating decoder," in *IEEE 68th VTC*, Sept. 2008, pp. 1–5.

[6] J. Jiang, J. Thompson, and P. Grant, "Design and analysis of compress-and-forward cooperation in a virtual-MIMO detection system," accepted in IEEE GLOBECOM 2010 Workshops, Dec. 2010.

[7] C. Ng, I. Maric, A. Goldsmith, S. Shamai, and R. Yates, "Iterative and one-shot conferencing in relay channels," in *Information Theory Workshop. ITW '06 Punta del Este. IEEE*, March 2006, pp. 193–197.

[8] A. Gersho and R. M. Gray, *Vector quantization and. signal compression*. Kluwer Academic Publisher, 1992.

[9] D. Seethaler, G. Matz, and F. Hlawatsch, "An efficient MMSE-based demodulator for MIMO bit-interleaved coded modulation," in *IEEE GLOBECOM '04.*, vol. 4, 29 Nov. 2004, pp. 2455–2459.

[10] A. Martinez, A. Guillen i Fabregas, and G. Caire, "Error probability analysis of bit-interleaved coded modulation," *IEEE Trans. Inform. Theory*, vol. 52, no. 1, pp. 262–271, Jan. 2006.

[11] P. Frenger, P. Orten, and T. Ottosson, "Convolutional codes with optimum distance spectrum," *IEEE Commun. Lett.*, vol. 3, no. 11, pp. 317–319, Nov 1999.

[12] M. McKay and I. Collings, "Error performance of MIMO-BICM with zero-forcing receivers in spatially-correlated Rayleigh channels," *IEEE Trans. Wireless Commun.*, vol. 6, no. 3, pp. 787–792, March 2007.

[13] P. Dharmawansa and M. McKay, "Exact minimum eigenvalue distribution of a correlated complex non-central wishart matrix," in *IEEE GLOBECOM 2008*, Nov. 2008, pp. 1–5.

17th European Signal Processing Conference (EUSIPCO 2009) Glasgow, Scotland, August 24-28, 2009

PRACTICAL COMPRESS-AND-FORWARD COOPERATION FOR THE CLASSICAL RELAY NETWORK

Jing Jiang, John S. Thompson, Peter M. Grant, and Norbert Goertz

Institute for Digital Communication,
Joint Reasearch Institute for Signal & Image Processing,
School of Engineering, University of Edinburgh,
Edinburgh, UK
(J.Jiang, John.Thompson, Peter.Grant)@ed.ac.uk

Institute of Communications and Radio-Frequency Engineering,
Vienna University of Technology
Vienna, Austria
norbert.goertz@nt.tuwien.ac.at

ABSTRACT

This paper proposes a practical compress-and-forward cooperation scheme with vector coding at the relay node for a three-terminal classical relay network. We discuss the framework of the relay receiver and analyse two practical vector coding algorithms for the cooperation, nearest neighbour quantization and lattice vector quantization. The error rate performance of the compress-and-forward cooperation and some other protocols under different SNRs is investigated. The impact of the quantization rate at the relay node is also characterised. It is shown that for a quantization rate larger than 2 bits/sample, the vector coding whether employing nearest neighbour quantization or lattice vector quantization, outerforms both the decode-and-forward protocol and scalar coding.

1. INTRODUCTION

It is well known that cooperative communication is a new and good way of improving the performance of wireless networks [1]. Multiple nodes in a network can cooperate by jointly encoding or decoding the transmission signals, to realise spatial diversity and increase channel rates [2, 3]. Cooperation protocols for wireless relay networks is currently a hot research topic [4]. These protocols determine what the individual relay should do, decode-and-forward (DF), amplify-and-forward (AF), or compress-and-forward (CF), after receiving the signal [5]. It was shown that CF protocol can be applied to a variety of wireless channels and always gives a rate gain over direct transmission [6]. In [7], the authors also showed that CF outperforms DF when the link between the relay and destination is better than that between the source and relay. In this paper, we consider a scenario where there are one transmitter and two clustered receivers, i.e. the relay is close to the destination. When the clustered nodes do cooperate, the CF protocol is a better choice providing higher communication rates than DF protocol. Hence here the focus in this paper is on the CF protocol.

The compress-and-forward protocol has the relay forwarding a quantized and compressed version of the received signal. The relay node can employ standard source coding, or the Wyner-Ziv coding (WZC) technique, when compressing the signal. The CF protocol with WZC at the relay following the rate distortion theory with side information [8], could support a slightly higher achievable rate in theory, compared with standard source coding [7]. However, for the WZC technique in practice, how to efficiently take advantage of the statistical dependence between the relay and the destination, and how to realise the theoretical performance limit of the CF protocol, are still open problems [9, 10]. If there exist multiple independent transmitters, the performance of CF protocol with WZC will be impaired by a larger compression noise when employing side information [11]. Since standard source coding is much simpler for the CF protocol and also performs well in practical scenarios, we choose to implement it at the relay.

In this work, we examine the improvement in bit error rate (BER) from a practical CF cooperation scheme with standard source coding at the relay node. For standard source coding, there are a number of algorithms to perform quantization, which can be divided into two kinds, scalar coding and vector coding. The scalar coding technique for compressing the signal has been studied in [12]. A more sophisticated coding technique, vector coding, for the CF protocol is desirable and still an open area of research. Our work differs from previous research in this area in that: i) we propose vector coding at the relay node, which is tailored for multi-dimensional signals; ii) we recommend two practical vector coding algorithms for the cooperation and examine their BER improvements from cooperation; and iii) we characterise the impact of quantization rate at the relay node.

The remainder of the paper is organized as follows. Section 2 presents the channel model. In section 3, we analyse the framework of the relay receiver, and propose that vector coding for CF protocol at the relay is a better choice. Two practical design algorithms for vector coding, nearest neighbour coding and lattice vector coding, are recommended in section 4. Section 5 shows some simulation results about BER improvements from CF cooperation, and section 6 concludes the paper.

2. CHANNEL MODEL

Consider a classical relay network with one transmitter (source) and two clustered receivers (relay and destination), as shown in Figure 1. We assume the nodes within a cluster are close together, but the distance between the transmitter and receiver cluster is large.

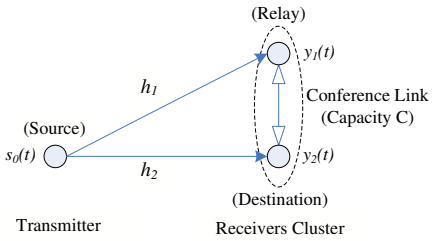

Figure 1: *System model of a classical relay network with one transmitter (source) and two clustered receivers (relay and destination).*

To focus on the performance of source coding techniques at the relay, we consider a simplified channel environment. We assume the channels from the transmitter to the two clustered receivers are quasi-static phase fading [13]: the channels have unit magnitude with independent and identically distributed (i.i.d.) random phase. Thus the channel gains are denoted by $h_i = e^{j\theta_i}, i = 1,2$, where $\theta_i \sim U[0,2\pi]$. The channel side information (CSI) is known to the receivers.

Let $s_0(t)$ denotes the source signal. We assume it is encoded and QPSK modulated before transmission. The signal energy per bit equals to $A^2/2r_b$, where A denotes the amplitude of the source signal, r_b denotes the bit rate which is twice the symbol rate r_s for QPSK signal. Let $\boldsymbol{y(t)} \triangleq [y_1(t), y_2(t)]^T$ denotes the corresponding received signals. In vector form, the data channel can be written as

$$\boldsymbol{y(t)} = \begin{bmatrix} h_1 \\ h_2 \end{bmatrix} s_0(t) + \begin{bmatrix} n_1(t) \\ n_2(t) \end{bmatrix}, \qquad (1)$$

where $n_1(t)$ and $n_2(t)$ are i.i.d zero-mean circularly symmetric complex Gaussian (ZMCSCG) white noise samples, with one-sided power spectral density (PSD) N_0.

As the clustered receivers are close together, it is reasonable to expect that the communication between the two receivers is much better and more stable than that between the transmitter and receivers. It is highly possible that we could achieve the channel capacity with high reliability on this short range link. Hence we assume the two receivers cooperate by way of an error-free conference link, with capacity C, as shown in Figure 1. We consider one-shot conferencing cooperation [14], which requires the destination to decode the signal from the relay which is sent over the conference link. In the CF cooperation protocol, the relay sends a compressed version of its observed signal to the destination. The destination then performs maximal-ratio combining (MRC) of the compressed signal and its own observation. As the relay chooses standard source coding to perform the CF protocol, the quantization rate at the relay will be equal to the capacity C of the error-free conferencing link.

3. COMPRESS-AND-FORWARD COOPERATION AT THE RELAY

The CF protocol has the relay forwarding a quantized version of the received signal. The relay node can employ different source coding techniques for compressing the signal. Vector quantization (VQ) is desirable for 2D QPSK source signals.

3.1 Vector Quantisation at the Relay

When implementing the CF protocol, the relay and the destination receives the i.i.d. $y_1(t)$ and $y_2(t)$, and $y_1(t)$ is compressed with a quantization rate and forwarded to destination. Here the quantization rate is equal to the capacity C of the error-free conferencing link. Then this system is equivalent to a system where destination has two antennas that receive the signals

$$\begin{bmatrix} y_1(t) + n_c(t) \\ y_2(t) \end{bmatrix}, \qquad (2)$$

where $n_c(t)$ is compression noise [6], which is independent of $y_1(t)$ and $y_2(t)$.

If the relay node chooses vector quantization to compress the signal with a quantization rate C, we could compute the power of $n_c(t)$ according to Shannon rate-distortion theory

$$\sigma^2_{c,standard} = \frac{E[|y_1(t)|^2]}{2^{2C}} = \frac{N_0 r_s + \frac{A^2}{2}|h_1|^2}{2^{2C}}. \qquad (3)$$

If the relay node employs the Wyner-Ziv Coding technique, the compression noise n_c has variance [13]

$$\sigma^2_{c,WZC} = \frac{N_0 r_s (\frac{A^2}{2}|h_1|^2 + \frac{A^2}{2}|h_2|^2 + N_0 r_s)}{(2^{2C}-1)(\frac{A^2}{2}|h_2|^2 + N_0 r_s)}. \qquad (4)$$

Considering 2D QPSK source signals, the quantization rate C should be at least 2 bits/sample. A more detailed discussion of the impact of C at the relay node will be presented in Section 4. For C smaller than 2 bits, the CF protocol will not give us any benefits over other protocols. For C equal to or larger than 2 bits, a comparison of the compression noises is shown in Figure 2.

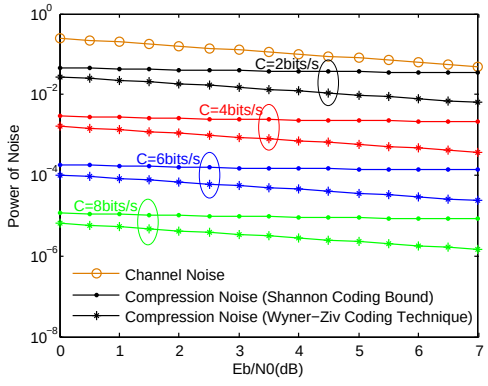

Figure 2: *Power comparison between channel noise and compression noise at the relay node.*

It can be seen that compared with the power of channel noise, the powers of the two compression noises are too

small to impair significantly the achievable channel rates or BER performance, especially for higher quantization rates C. Since vector coding is much simpler than WZC technique in practice, we choose it for compressing the signals at the relay.

3.2 Relay Framework

The relay receiver is shown in Figure 3. For purpose of analysis, we consider the operation of the receiver during the signal interval $(0, T_s)$, with $T_s = 1/r_s$. In QPSK, one of four possible waveforms are transmitted during each signalling interval. These waveforms are:

$$s_0(t) = A\cos(\omega_c t + \varphi), \text{ with } \varphi = [\frac{\pi}{4}, \frac{3\pi}{4}, \frac{5\pi}{4}, \frac{7\pi}{4}]. \quad (5)$$

We denote the signal components at the output of the correlators by $s_{01}(T_s)$ for I-channel and $s_{02}(T_s)$ for Q-channel respectively, with the values calculated as

$$s_{01}(T_s) = \frac{1}{T_s}\int_0^{T_s} h_1 s_0(t)\cos\omega_c t dt = \pm\frac{A}{2}e^{j\theta_1}\cos\frac{\pi}{4}; \quad (6)$$

$$s_{02}(T_s) = \frac{1}{T_s}\int_0^{T_s} h_1 s_0(t)\sin\omega_c t dt = \pm\frac{A}{2}e^{j\theta_1}\sin\frac{\pi}{4}. \quad (7)$$

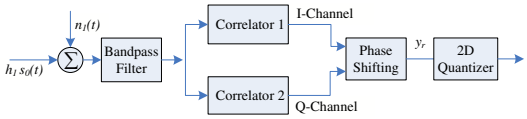

Figure 3: *Relay Receiver Block Diagram.*

We denote the noise components at the output of the correlators by $n_{11}(T_s)$ for I-channel and $n_{12}(T_s)$ for Q-channel respectively. We could calculate their values similarly with equation (6) and (7), just replacing $h_1 s_0(t)$ with $n_1(t)$. Since $n_1(t)$ is i.i.d ZMCSCG white noise with one-sided PSD N_0, we can show that $n_{11}(T_s)$ and $n_{12}(T_s)$ are also independent Gaussian random variables, with zero mean and equal variance given by

$$E\{[n_{11}(T_s)]^2\} = E\{[n_{12}(T_s)]^2\} = \frac{N_0}{4T_s}A^2 \quad (8)$$

As the channel side information is known to the receivers, a phase shifting device at the relay could be used to eliminate the effect of the channel phase. The signal after the phase shifting is 2-dimensional(2D), denoted by y_r. For each dimension, its probability distribution is a Gaussian distribution with mean $\pm\frac{\sqrt{2}A}{4}$, and variance $\frac{N_0}{4T_s}A^2$. The probability density function (PDF) of y_r could be shown as

$$p(y_r) = \frac{1}{\sqrt{\pi A^2\frac{N_0}{2T_s}}}\exp\{\frac{-(y_r - (\pm\frac{\sqrt{2}A}{4} \pm \frac{\sqrt{2}A}{4}i))^2}{\frac{N_0}{2T_s}A^2}\} \quad (9)$$

With knowledge of the PDF of y_r, we could design a desired codebook for the quantizer at the relay. Then the relay will compress the signals y_r through this quantizer, and send the compressed signals to the destination.

4. VECTOR CODING DESIGN FOR THE CF PROTOCOL

When implementing the CF protocol, the relay chooses to employ vector quantization (VQ). VQ which is based on the principle of block coding, is desirable for 2D QPSK source signals. Here we recommend two algorithms to perform the vector coding.

4.1 Nearest Neighbour Quantization

An important special class of VQ, called Voronoi or nearest neighbour VQ, has the feature that the codebook is optimal in the sense of minimising average distortion [15]. Its advantage is that the encoding process does not require any explicit storage of the geometrical description of the cells. Assuming a mean squared error (MSE) distortion measure, the condition to identify the nearest neighbour VQ codebook entry could be described as:

$$S_m = \{y_r : \|y_r - c_m\|^2 \le \|y_r - c_{m'}\|^2, \forall m' = 1,2,...,M\}, \quad (10)$$

where S_m denotes the encoding region associated with codevector c_m, and M denotes the desired number of codevectors in the codebook which equals to 2^C. This condition says that the encoding region S_m should consists of all vectors that are closer to c_m than any other codevector. Furthermore, for the MSE criterion, the codevector c_m should be average of all those signal vectors that are in the encoding region:

$$c_m = \frac{\sum_{y_r\in S_m} y_r}{\sum_{y_r\in S_m} 1}, m = 1,2,...,M. \quad (11)$$

The objective of the relay is to design this kind of codebook, with the knowledge of signal vectors y_r and the desired number of codevectors. Here we propose the LBG algorithm [15] which is based on the iterative use of codebook modification, to design the nearest neighbour VQ. The equations (10) and (11) are the two key steps of the LBG algorithm. In this paper we use the splitting technique where an initial codevector is set as the average of the received signal vectors. This codevector is then split into two. The iterative algorithm is then run with the two codevectors as the initial codebook. We could use the equation (10) to design the partition, and then use equation (11) to update the codebook. The final two codevectors are split into four and the process is repeated until the desired number of codevectors is obtained. Finally the relay node obtains the complete codebook for quantization.

4.2 Hexagonal Lattice Quantization

In contrast to nearest neighbour VQ, which requires exhaustive search algorithm and implies a high computational complexity, lattice VQ has been developed to reduce the complexity of codebook design [16]. The codebook for lattice VQ has a special structure that allows faster encoding, while paying the price that the quantizer is suboptimal for a given set of signal vectors. For lattice VQ, the encoding regions S_m are regular lattices, either rectangular or hexagon. In fact the rectangular lattice VQ has the same performance

as employing optimal scalar quantization on each dimension. So considering that a hexagonal covering of the 2D space is more efficient than a rectangular partitioning, the hexagonal lattice quantizer could be an alternative to the vector quantizer.

With knowledge of signal vectors y_r and the number of codevectors, designing a hexagonal lattice VQ is much simpler. We just need to consider the entire covering region for the signal vectors. Design one hexagonal encoding region and then use it to fill the 2D space until the desired number is obtained. We should make sure the hexagonal lattices cover most of the expected signal vectors. The codevector c_m is also obtained according to (11), which is the average of all those signal vectors in the S_m. A more detailed comparison of the codevectors of nearest neighbour VQ and hexagonal lattice VQ can be seen in Figure 5 of Section 5.

The relay employs nearest neighbour VQ or hexagonal lattice VQ to design a codebook, and then forwards the encoded signals and the whole codebook to the destination. We assume the destination could decode the source coded signals correctly, and then it implements a maximum ratio combiner to combine the two received signals from source and relay, and finally makes a decision on the transmitted signal s_0.

5. NUMERICAL RESULTS

In this section, we present the the bit error rate performance of practical CF cooperation protocol for a three terminal classical relay network with QPSK source signals. The simulations are set up in accordance with the assumptions of the channel model in Section II and the analysis about the probability distribution of the relay received signals in Section III. The simulation results are computed via the Monte Carlo method. We assume $r_s = 1$ baud, and the signal-to-noise ratio (SNR) is defined here as E_b/N_0. We use 10^4 training vectors for both nearest neighbour VQ and hexagonal lattice VQ.

The BER performance of decode-forward, optimal scalar quantization (SQ), 2D hexagonal lattice VQ, and 2D nearest neighbour VQ, under different SNR assumptions, are shown in Figure 4. The bit error rates are compared against the lower bound of corresponding SIMO system as if the cooperating nodes were colocated and connected via a wire. With such colocated receivers, the channel becomes an ideal SIMO system with a two-antenna receiver. The bit error rates are also compared to the performance of the system with Shannon coding bound. According to equation (2), the compression noise $n_c(t)$ is considered for this kind of system, with variance calculated via equation (3). The destination then performs MRC of the two received signals as shown in equation (2), and finally makes a decision on the transmitted signal.

Figure 4 shows that, the CF protocol, whether using scalar or vector quantization, is expected to perform better than the DF protocol, because the relay and the destination are close together [7]. The 2D hexagonal lattice VQ, can achieve similar error rates comparable to the optimal one, nearest neighbour VQ. When the SNR is increasing, 2D nearest neighbour VQ offers much more improvement than the 2D optimal SQ, but is bounded by SIMO system.

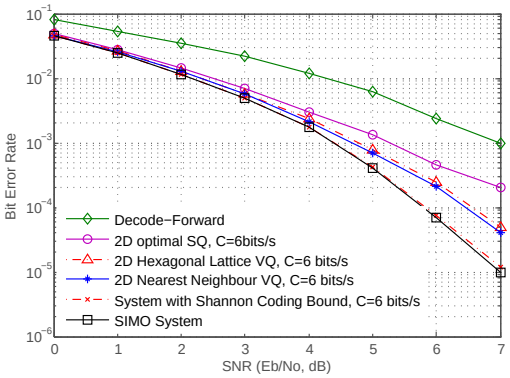

Figure 4: *Error performance of different protocols for the classical relay system with QPSK source signals ($r_s = 1$ baud).*

When the quantization rate C equals to 6 bits/s, we compare the distributions of the codevectors in the codebook for the hexagonal lattice VQ and the nearest neighbour VQ in Figure 5. The codebook for the nearest neighbour VQ is adapted to the received signal vectors, which is optimal in the sense of minimising average distortion. The codebook of hexagonal lattice VQ is designed when $SNR = 0$ dB, which is not changed for different SNRs. Even though the hexagonal lattice VQ is suboptimal for a given set of signal vectors, it is much simpler to design and can achieve similar error performance compared with the optimal VQ.

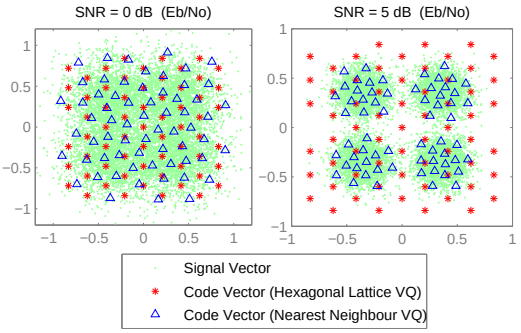

Figure 5: *The codevectors distributions for hexagonal lattice VQ and nearest neighbour VQ, under different SNRs. (QPSK source signals, $r_s = 1$ baud, $C = 6$ bits/s.)*

Considering the quantization rates 4 bits/s, 6 bits/s and 8 bits/s, we compare the performance of the 2D nearest neighbour VQ and 2D hexagonal lattice VQ in Figure 6. We also consider the performance of nearest neighbour VQ when the quantization rate $C = 2$ bits/s, and it is obvious that the CF

protocol degrades to the DF case. The relay node then performs as a simple data demodulator. As C increases, both the nearest neighbour VQ and hexagonal lattice VQ perform better and come closer to the lower bound. The 2D hexagonal lattice VQ can achieve error rates comparable to the optimal but more complicated nearest neighbour VQ.

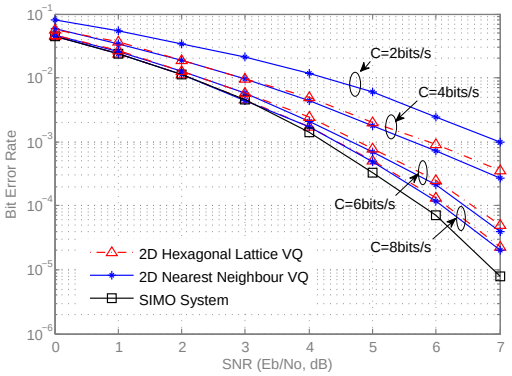

Figure 6: *Error performance of the CF protocol with vector coding at the relay, under different quantization rates. (Classical relay system with QPSK source signals, $r_s = 1$ baud.)*

6. CONCLUSIONS

Considering the classical relay network with one transmitter and two clustered receivers with phase fading channels, we proposed the vector coding technique for compress-and-forward cooperation at the relay node. We presented a framework for the relay receiver, and analysed the probability density function of the received signals. With this knowledge, two codebook design algorithms are recommended for VQ, nearest neighbour VQ and hexagonal lattice VQ.

Furthermore, we investigated the error rate performance of the CF cooperation under different SNRs. The impact of quantization rate at the relay node was also characterised. It was shown that for a quantization rate larger than 2 bits/sample, the vector coding outerformed the DF protocol and scalar coding in the sense of error performance. As for the two design algorithms, we found that the nearest neighbour VQ had the feature that the codebook is optimal, while the hexagonal lattice VQ was much simpler and could achieve similar error rates. Thus the two algorithms are both appropriate choices for designing the vector coding at the relay node in practice.

We note that our research work has focused on the case of a classical relay network; extension to more than three terminals will be included in our further work. Moreover, practical channel coding schemes will be implemented at the source node. A Wyner-Ziv coder, i.e. a source-channel coding scheme, will be considered as well for the relay node.

7. ACKNOWLEDGEMENT

Jing Jiang thanks the support from the UK/China Scholarships for Excellence programme. The authors acknowledge the support of the Scottish Funding Council for the Joint Research Institute with the Heriot-Watt University which is a part of the Edinburgh Research Partnership.

REFERENCES

[1] J. N. Laneman, D. N. C. Tse, and G. W. Wornell, "Cooperative diversity in wireless networks: Efficient protocols and outage behavior," *IEEE Trans. Info. Theory*, vol. 50, no. 10, pp. 3062–3080, Dec. 2004.

[2] A. Sendonaris, E. Erkip, and B. Aazhang, "User Cooperation Diversity Part I and Part II," *IEEE Trans. Commun.*, vol. 51, no. 11, pp. 1927-1948, Nov. 2003.

[3] Y. Fan, J.S. Thompson, "MIMO Configurations for Relay Channels: Theory and Practice," *IEEE Transactions on Wireless Communications*, vol. 6, no. 5, pp. 1774-1786, 2007.

[4] J. N. Laneman and G. W. Wornell, "Distributed Space-Time-Coded Protocols for Exploiting Cooperative Diversity In Wireless Networks," *IEEE Trans. Info. Theory*, vol. 49, no. 10, pp. 2415–2425, Oct. 2003.

[5] G. Kramer, M. Gastpar, and P. Gupta, "Cooperative strategies and capacity theorems for relay networks," *IEEE Trans. Inf. Theory*, vol. 51, no. 9, pp. 3037–3063, Sep. 2005.

[6] A. Host-Madsen, "Capacity bounds for cooperative diversity," *IEEE Trans. Inf. Theory*, vol. 52, pp. 1522–1544, Apr. 2006.

[7] A. Host-Madsen and J. Zhang, "Capacity bounds and power allocation for wireless relay channels," *IEEE Trans. Inf. Theory*, vol. 51, no. 6, pp. 2020–2040, Jun. 2005.

[8] A. Wyner and J. Ziv, "The rate-distortion function for source coding with side information at the decoder," *IEEE Trans. Inf. Theory*, vol. IT-22, no. 1, pp. 1–10, Jan. 1976.

[9] A. Nosratinia, T.E. Hunter, and A. Hedayat, "Cooperative communication in wireless networks," *IEEE Communications Magazine*, Vol. 42, no. 10, pp. 74–80, Oct. 2004.

[10] Z. Liu, V. Stankovic, and Z. Xiong, "Wyner-Ziv coding for the half-duplex relay channel," in *IEEE International Conference on Acoustics, Speech, and Signal Processing (ICASSP '05)*, March 2005, Vol. 5, pp. v/1113–v/1116.

[11] T. Cover and J. Thomas, *Elements of Information Theory*. Address: John Wiley and Sons, New York, 1991

[12] R. Hu, and J. Li, "Practical Compress-Forward in User Cooperation: Wyner-Ziv Cooperation," in *2006 IEEE International Symposium on Information Theory*, Seattle, WA, July 2006, pp. 489–493.

[13] C. T. Ng, N. Jindal, A. J. Goldsmith and U. Mitra, "Capacity gain from two-transmitter and two-receiver cooperation," *IEEE Trans. Inform. Theory*, vol. 53, no. 10, pp. 3822–3833, Oct. 2007.

[14] C. T. K. Ng, I. Maric, A. J. Goldsmith, S. Shamai, and R. D. Yates, "Iterative and one-shot conferencing in relay channels," in *Proc. IEEE Inform. Theory Workshop*, Uruguay, Mar. 2006, pp. 193–197.

[15] A. Gersho, R. M. Gray, *Vector quantization and. signal compression*. Address: Klower Academic Publisher, Boston, 1992.

[16] R. M. Gray and D. Neuhoff, "Quantization," *IEEE Transactions on Information Theory*, Vol. 44, No 6, pp. 2325–2383, Oct. 1998.

A Singular Value-based Adaptive Modulation and Cooperation Scheme for Virtual-MIMO Systems

Jing Jiang, *Student Member, IEEE,* John S. Thompson, *Member, IEEE,* and Hongjian Sun, *Member, IEEE,*

***Abstract*—This paper presents a practical virtual multiple-input multiple-output (MIMO) system that implements bit-interleaved coded modulation (BICM) and compress-and-forward (CF) cooperation. A minimum mean square error (MMSE) receiver is considered, since it has low complexity and allows good performance when combined with BICM techniques. A closed-form upper bound for the system error probability is derived, based on which we prove that the smallest singular value of the cooperative channel matrix determines the system error performance. Accordingly, an adaptive modulation and cooperation scheme is proposed, which uses the smallest singular value as the threshold strategy. Depending on the instantaneous channel conditions, the system could therefore adapt to choose a suitable modulation type for transmission and an appropriate quantization rate to perform CF cooperation. It is shown that the adaptive modulation and cooperation scheme not only enables the system to achieve comparable performance to the case with fixed quantization rates, but also eliminates unnecessary complexity for quantization operations and conference link communication.**

***Index Terms*—Virtual MIMO system, adaptive modulation, adaptive-rate CF cooperation, BICM technique, MMSE decoding.**

I. Introduction

THE use of multiple antennas at the transmitter and a single antenna at each of the receivers, also known as virtual multiple-input multiple-output (MIMO) system, has been proposed as an alternative to a point-to-point MIMO system, to improve channel capacity and link reliability of wireless communications [1] [2]. When the transmitter does not have perfect channel state information (CSI) for the wireless link to each receiver, which is a common scenario in practical situations, closely spaced single-antenna receivers can cooperate to form a virtual antenna array and reap some performance benefits of MIMO systems [3]. The idea of receiver-side local cooperation is attractive for wireless networks since a wireless receiver may not be able to have multiple antennas due to size and cost limitations [4]. To realize the cooperation, compared to amplify-and-forward(AF) and decode-and-forward (DF), the compress-and-forward (CF) protocol has been shown to provide better performance, when the helping receivers (i.e. the relays) are closer to the destination [5].

Motivated by the above practical scenario, we consider such a cooperative virtual-MIMO system, with one remote multi-antenna wireless transmitter sending information to several closely spaced single-antenna receivers. Bit-interleaved coded modulation (BICM) [6] is implemented to provide forward error correction (FEC) and improve system performance. One relevant paper [7] presents a virtual-MIMO channel with partial cooperation among users, but only considers a simple AF protocol. Our recent work [8] and [9] proposes a new virtual-MIMO system with CF cooperation. But reference [8] focuses on the codebook design and complexity analysis at the relay. Paper [9] concentrates on the system performance assessment, including a comparison of different coding techniques at the relay, and the impact of a non-ideal cooperation link. Paper [9] only considers a maximum likelihood (ML) receiver. The disadvantage of ML detection is the high computational complexity. The minimum mean square error (MMSE) receiver, which is shown to perform well when combined with BICM technique [10], is a better choice to achieve low complexity receiver implementations.

In this paper, we present a practical 2×2 virtual-MIMO-BICM system that implements CF cooperation and MMSE detection. With help from the relay, MIMO performance could be achieved in this virtual-MIMO system. We now summarize the main contributions of this paper. First, we derive a closed form expression to upper bound the system bit error ratio (BER), based on which the smallest singular value of the cooperative channel matrix is shown to dominate the system BER. Moreover, an adaptive modulation and cooperation scheme is proposed, adopting the smallest singular value as the threshold strategy. The closed-form cumulative distribution function for the smallest singular value is derived as well. The system could therefore adapt its modulation type to the prevailing channel conditions and choose the minimum possible quantization rate. It is shown that the proposed scheme eliminates unnecessary complexity, and enables the system to achieve comparable performance to the case with fixed quantization rates.

The paper is organized as follows. Section II specifies the model of the cooperative virtual-MIMO system. The closed-form upper bound for the system BER is derived in Section III. Details of the proposed adaptive modulation and cooperation scheme are presented in Section IV. Section V shows the simulation results, and Section VI concludes the paper.

J. Jiang, and J. S. Thompson are with the Institute for Digital Communications, Joint Research Institute for Signal & Image Processing, School of Engineering, University of Edinburgh, Edinburgh, EH9 3JL, UK. (E-mail: J.Jiang@ed.ac.uk, John.Thompson@ed.ac.uk.)

H. Sun is with the Division of Engineering, Kings College London, London, WC2R 2LS, UK. (Email: hongjian.sun@kcl.ac.uk)

Manuscript received September 25, 2010; revised March 03, 2011; accepted April 20, 2011. The work of Jing Jiang was supported in part by the UK/China Scholarships for Excellence programme. The authors acknowledge the support of the Scottish Funding Council for the Joint Research Institute with the Heriot-Watt University which is a part of the Edinburgh Research Partnership.

Color versions of one or more of the figures in this paper are available online at http://ieeexplore.ieee.org.

II. Virtual-MIMO System with CF Cooperation

A. Channel Model

We consider a virtual-MIMO wireless network with one remote N_t-antenna transmitter that implements BICM transmission, and N_r closely spaced single-antenna receivers. We start with a simple configuration with $N_t = N_r = 2$, as shown in Fig. 1, to demonstrate the achievable performance improvements and sensitivities. Further improvements are expected for the case of more cooperating terminals with larger numbers of antennas. At the transmitter, the information bits are encoded through a rate-R_b linear binary convolutional encoder, and then interleaved through a random bit interleaver (int.). In each stream after the demultiplexer (or demux), groups of m bits are mapped onto complex data symbols via Gray-labeled $2^m = M$-ary quadrature modulation (QAM) or phase-shift keying (PSK) whose constellation is denoted as $\mathcal{X}$.

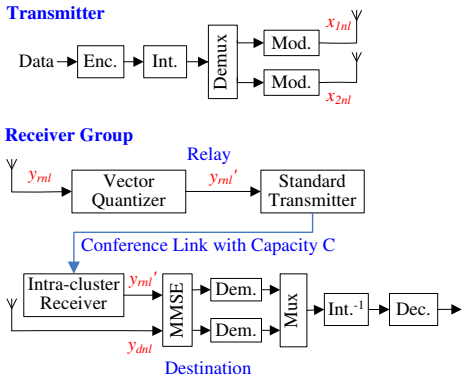

Fig. 1. System model of the cooperative virtual-MIMO system ($N_t = 2$, $N_r = 2$.)

As the transmitter is far away from the receiver group, we assume the channels between them are block fading, with N Rayleigh fading blocks and each block has L consecutive time instants, which is practical and particularly relevant in wireless communications situations [11]. When we consider a single time instance l for the nth channel, we have ($N_t = N_r = 2$),

$$[y_{rnl} \;\; y_{dnl}]^{\mathrm{T}} = \boldsymbol{H}_n \boldsymbol{x}_{nl} + \boldsymbol{w}_{nl}, \text{ with } \boldsymbol{H}_n = \begin{bmatrix} h_{1n} & h_{2n} \\ h_{3n} & h_{4n} \end{bmatrix}, \quad (1)$$

where y_{rnl} and y_{dnl} are the received signals at the relay and the destination. The vector $\boldsymbol{H}_n$ denotes the nth block fading channel matrix, where each $h_{in} (i \in [1, ..., 4])$ is independent and identically distributed (i.i.d.), and is assumed to be available at the receivers only. Without loss of generality, we assume normalized Rayleigh fading, i.e. $\mathrm{E}[|h_{in}|^2] = 1$, where $|\cdot|$ denotes the magnitude function and $\mathrm{E}[\cdot]$ denotes the expected value function. We also define the vector $\boldsymbol{x}_{nl} = [x_{1n1}, x_{2nl}]^{\mathrm{T}}$, where $x_{i'nl} (i' \in [1, 2])$ presents the lth M-ary symbol transmitted on the nth channel from the i'th antenna. The noise vector $\boldsymbol{w}_{nl} = [w_{1n1}, w_{2nl}]^{\mathrm{T}}$, with components $w_{i'nl} \sim \mathcal{CN}(0, N_0)$. The average transmitted power per symbol is $\mathrm{E}[|x_{i'nl}|^2] = E_s/N_t$, where we normalize the total power E_s to unity. The corresponding power per bit is $E_b = E_s/(mR_b)$.

B. CF Cooperation

As the destination and the helping relay are closely spaced, it is highly likely that a high capacity communication link with high reliability can be formed between them. Hence as also considered in [1] and [12], we assume the two receivers cooperate by way of an one-shot error-free conference link, with capacity C, as shown in Fig. 1. The one-shot operation requires the destination to directly decode the signal sent over the link without iterative conference communications. In practice, the conference link is realized via an orthogonal channel (i.e. a different frequency band) to the transmitter array. Compared with the long range data channel $\boldsymbol{H}_n$, the orthogonal conference link is short-range with low transmission power, and could be reused many times over the coverage area of the long range link.

The conference link enables cooperation, and CF is the preferred cooperation protocol when the relay is close to the destination [5]. A standard source coding technique is chosen here to implement CF at the relay [8]. That is, the relay is equipped with a vector quantizer (VQ). The Voronoi VQ [13], whose codebook is optimal in the sense of minimising average distortion, is used to design the codebook needed for the quantization. Here the quantization rate is equal to the capacity C of the error-free conference link. Note that the codebook design is based on the number of codebook vectors which equals 2^C and exploits knowledge of the noise-free constellation [8]. Then a compressed version of the signal could be modeled as $y'_{rnl} = y_{rnl} + w_{cnl}$, where w_{cnl} is the compression noise, independent of y_{rnl}, and $w_{cnl} \sim \mathcal{CN}(0, \sigma^2_{cn})$.

The destination receives signals y_{dnl} from the transmitter, and observes signals from the relay via an intra-cluster receiver, written as y'_{rnl} because of the error-free conference link, as shown in Fig. 1. We denote the received signals at the destination as $\boldsymbol{y}_{nl} = [y'_{rnl} \;\; y_{dnl}]^{\mathrm{T}}$. With knowledge of σ^2_{cn}, y'_{rnl} could be scaled so that y'_{rnl} and y_{dnl} have the same power of additive Gaussian noise. We denote η_n as the degradation factor due to the compression noise. Then we have,

$$\tilde{\boldsymbol{y}}_{nl} = [\tilde{y}'_{rnl} \;\; y_{dnl}]^{\mathrm{T}} = \widetilde{\boldsymbol{H}}_n \boldsymbol{x}_{nl} + [\tilde{w}_{1nl} \;\; w_{2nl}]^{\mathrm{T}}, \quad (2)$$

$$\text{with } \widetilde{\boldsymbol{H}}_n \triangleq \begin{bmatrix} \sqrt{\eta_n} h_{1n} & \sqrt{\eta_n} h_{2n} \\ h_{3n} & h_{4n} \end{bmatrix}, \; \eta_n \triangleq \frac{N_0}{N_0 + \sigma^2_{cn}}. \quad (3)$$

Here $\tilde{w}_{1nl} \sim$ i.i.d. $\mathcal{CN}(0, N_0)$, and $\tilde{y}'_{rnl} = \sqrt{\eta_n} y'_{rnl}$. For a wired conference link with high capacity C, σ^2_{cn} decreases to 0, and the system will behave as in the ideal MIMO case.

Note that, in the rest of this paper, when we are considering a single time instance l on the nth channel, we will drop the subscript nl for the symbols and n for the channel matrix, since the received symbols are treated independently.

C. MMSE-based BICM Demodulation

The general structure of the destination with a linear MMSE receiver is shown in Fig. 1. The first MMSE filtering step is,

$$\boldsymbol{z} = \boldsymbol{W}\tilde{\boldsymbol{y}} = \boldsymbol{x} + \boldsymbol{e} + \boldsymbol{v}, \text{ with } \boldsymbol{W} = \boldsymbol{B}\left(\widetilde{\boldsymbol{H}}^{\dagger}\widetilde{\boldsymbol{H}} + \frac{N_t}{\mathrm{SNR}}\boldsymbol{I}\right)^{-1}\widetilde{\boldsymbol{H}}^{\dagger}, \quad (4)$$

where $\boldsymbol{e}=(\boldsymbol{W}\widetilde{\boldsymbol{H}}-\boldsymbol{I})\boldsymbol{x}$ is the residual inter-symbol interference (ISI), and $\boldsymbol{v}=\boldsymbol{W}\left[\tilde{w}_1 \;\; w_2\right]^{\mathrm{T}}$ denotes the colored Gaussian noise vector. Here $\boldsymbol{H}^{\dagger}$ denotes the conjugate transpose of $\boldsymbol{H}$. Also, $\boldsymbol{B}$ is a diagonal matrix which removes the bias from the MMSE estimates, with kth diagonal component given by $\boldsymbol{B}_{k,k}=(\rho_k+1)/(\rho_k)$. The scalar ρ_k is the instantaneous received signal to interference and noise ratio (SINR) for the kth stream [14], given by,

$$\rho_k = \frac{1}{\left[(\boldsymbol{I}_{N_t}+\frac{\mathrm{SNR}}{N_t}\widetilde{\boldsymbol{H}}^{\dagger}\widetilde{\boldsymbol{H}})^{-1}\right]_{k,k}}-1. \tag{5}$$

We denote $\mathcal{X}_b^{\lambda,k}$ as the subset within the kth transmit constellation where the λth bit is equal to b. The BICM log-likelihood ratio (LLR) for each coded bit corresponding to x_k is calculated from z_k and denoted by $\mathcal{L}(c^{\lambda}|z_k,\boldsymbol{W})$, where $\lambda=1,...,m$. The two path LLRs are combined into one output stream by the multiplexer, and reordered by the deinterleaver. Finally, the decoder accepts the LLRs of all coded bits and employs a soft-input Viterbi algorithm to decode the signals.

The benefit of the MMSE receiver is the lower computational complexity. However, it suffers from residual ISI caused by the compression noise w_c, as will be illustrated in Section III. A good quantization scheme with low compression noise at the relay, will enable the virtual-MIMO system to achieve almost ideal MIMO performance.

III. Upper Bound on Bit Error Ratio

Throughout the paper, we consider block fading channels, for which a fading envelope is given by $\mathcal{H}=(\boldsymbol{H}_1,...,\boldsymbol{H}_N)$. For a specific channel condition $\boldsymbol{H}$, the union bound on the conditional BER for linear binary convolutional codes over a memoryless binary-input output-symmetric (BIOS) channel can be expressed as [15],

$$P_b(\boldsymbol{H}) \le \sum_{d=d_{\text{free}}}^{\infty} A_d\, P_d(d|\boldsymbol{H}) \approx \sum_{d=d_{\text{free}}}^{d_{\text{free}}+10} A_d\, P_d(d|\boldsymbol{H}), \tag{6}$$

where $P_d(d|\boldsymbol{H})$ is the conditional pairwise error probability (PEP) for two codewords differing in d bits. The scalar A_d denotes the sum of bit errors for error events of distance d and d_{free} is the minimum free Hamming distance. With d increasing, the influence of A_d and $P_d(d|\boldsymbol{H})$ on the conditional BER will decrease dramatically. Truncation to 10 terms in (6) yields a very good upper bound (UB) of the true $P_b(\boldsymbol{H})$ [16] [17]. The average BER after decoding is obtained by averaging $P_b(\boldsymbol{H})$ over the fading channel matrices,

$$P_b \le \mathop{\mathrm{E}}_{\boldsymbol{H}\in\mathcal{H}}\left[\min\left\{\frac{1}{2}, \sum_{d=d_{\text{free}}}^{d_{\text{free}}+10} A_d\, P_d(d|\boldsymbol{H})\right\}\right], \tag{7}$$

where a BER limit of $1/2$ for the Viterbi decoder is included [18]. The expectation in (7) can be evaluated using the Monte Carlo method in practice.

One thing to note here is the bound (6) holds under the assumption that the channels are BIOS. For our block fading channel, which is not symmetric [19], we adopt the approach of [6] and force the BICM channel to behave as BIOS by using a random modulation concept. Let t denote a random variable, which independently selects, for every symbol, either Gray-labelling mapping or its complement with probability 1/2. Furthermore, due to the symmetry of the channel output, we can safely assume that the all-zero codewords are transmitted. Then LLR for the MMSE receiver is given by [10],

$$\mathcal{L}(c^{\lambda}|z_k,\boldsymbol{W}) = \ln\frac{\sum_{\tilde{x}_k\in\mathcal{X}_{\tilde{t}}^{\lambda,k}}\exp\left(-\rho_k|z_k-\tilde{x}_k|^2\right)}{\sum_{\tilde{x}_k\in\mathcal{X}_t^{\lambda,k}}\exp\left(-\rho_k|z_k-\tilde{x}_k|^2\right)}. \tag{8}$$

We employ the Gaussian approximation (GA) [15] [20], which is a simple and accurate way to approximate $P_d(d|\boldsymbol{H}_n)$, and obtain,

$$P_d(d|\boldsymbol{H}) \approx Q\left(\sqrt{-2dK_{\mathcal{L}}(\hat{s})}\right), \tag{9}$$

where $K_{\mathcal{L}}(s)$ is the cumulant generating function of the variable $\mathcal{L}(c^{\lambda}|z_k,\boldsymbol{W})$ defined in (8).

$$\begin{aligned} K_{\mathcal{L}}(s) &= \log \mathop{\mathrm{E}}_{z,\lambda,t,k,\boldsymbol{W}}\left[\exp\left(s\mathcal{L}(c^{\lambda}|z_k,\boldsymbol{W})\right)\right] \\ &= \log \mathop{\mathrm{E}}_{z,\lambda,t,k,\rho_k}\left[\left(\frac{\sum_{\tilde{x}_k\in\mathcal{X}_{\tilde{t}}^{\lambda,k}}\exp\left(-\rho_k|(x_k-\tilde{x}_k)+e_k+v_k|^2\right)}{\sum_{\tilde{x}_k\in\mathcal{X}_t^{\lambda,k}}\exp(-\rho_k|(x_k-\tilde{x}_k)+e_k+v_k|^2)}\right)^s\right]. \end{aligned} \tag{10}$$

The SINR ρ_k defined in (5) is related with the channel condition $\boldsymbol{H}$. For BIOS channels, symmetry dictates that the saddlepoint $\hat{s}$ in (9) is placed at $\hat{s}=1/2$ [15]. A closed form of $K_{\mathcal{L}}(s)$ for high SNR can be stated as follows:

Theorem 1: For a receiver using MMSE detection, when SNR is high, the cumulant generating function of $\mathcal{L}(c^{\lambda}|z_k,\boldsymbol{W})$ can be obtained in closed form,

$$K_{\mathcal{L}}(s) = \log\left[\frac{1}{m2^m N_t}\sum_{\lambda=1}^{m}\sum_{t=0}^{1}\sum_{k=1}^{N_t}\sum_{x_k\in\mathcal{X}_t^{\lambda,k}}\left[\exp(-\rho_k(s-s^2)|x_k-\tilde{x}_k|^2)\right]\right]. \tag{11}$$

The proof is presented in Appendix A. We can see that now $K_{\mathcal{L}}(s)$ depends on ρ_k and the squared Euclidean distance from x_k to its nearest neighbour $\tilde{x}_k$ in the complement subset. According to the Gray-labeled PSK/QAM constellations used in this system, we can further simplify $K_{\mathcal{L}}(s)$ by exploiting multiplicities of the Euclidean distance. Table I in [21] presents (for various constellations) the set of all distinct squared Euclidean distances, and the corresponding frequency of occurrence of each distance (normalized by the total number of distances $m2^m$), which could be used in our case to further simplify $K_{\mathcal{L}}(s)$. For example, when we consider the Gray-labelled 16QAM and the saddlepoint $\hat{s}=1/2$, we obtain,

$$K_{\mathcal{L}}(\hat{s})_{16\text{QAM}} = \log\left[\frac{1}{N_t}\sum_{k=1}^{N_t}\left(\frac{3}{4}\exp(-0.1\rho_k)+\frac{1}{4}\exp(-0.4\rho_k)\right)\right]. \tag{12}$$

After simplification, compared to BPSK and QPSK which have N_t terms in equation (11), 16QAM has $2N_t$ terms (as shown in (12)), and 64QAM has $4N_t$ terms. The simplification is helpful for reducing computational complexities of $K_{\mathcal{L}}(\hat{s})$ with higher-order modulations.

Now, substituting (11) into (9) gives a closed-form expression for approximating $P_d(d|\boldsymbol{H})$, leading to a closed-form

solution for the UB of $P_b(\boldsymbol{H})$ from (6). The conditional BER UB is very useful since it provides insight into the asymptotic behaviour of the system error probability and can be used to judge the condition of the specific channel $\boldsymbol{H}$.

Additionally, for a receiver using MMSE detection, ρ_k suffers from the residual ISI caused by the compression noise w_c. From (11), it is obvious that a lower value of ρ_k results in a larger value of $K_{\mathcal{L}}(s)$ and finally a higher $P_b(\boldsymbol{H})$. Compared to the corresponding MIMO system, the virtual-MIMO system will have an impaired BER performance since it uses CF cooperation and MMSE detection. A higher quantization rate C is one solution, but will introduce additional operational complexity for quantizations at the relay. Another solution is to employ a lower-order modulation at the transmitter, but this will decrease the system throughput as a result. Thus an adaptive modulation and cooperation scheme will be a suitable solution here, as will be described in Section IV.

IV. Adaptive Modulation and Cooperation Scheme

The basic motivation for this proposed scheme is the fact that fixed modulation or fixed-rate cooperation can not adapt well to varying channel conditions, especially for a system with MMSE detection. If we could find a suitable threshold strategy to judge the conditions of the instantaneous channels, the system could choose different modulation types and quantization rates, according to different realisations of $\widetilde{\boldsymbol{H}}$.

A. Threshold Strategy

For the threshold design, we propose to adopt the smallest singular value of the cooperative channel matrix as the threshold strategy, and the following theorem shows the reason.

Theorem 2: For the virtual-MIMO system using MMSE detection, the smallest singular value of the cooperative channel matrix has a direct impact on the system performance:

$$K_{\mathcal{L}}(\hat{s}) \leq \log\left[\frac{1}{m2^m}\sum_{\lambda=1}^{m}\sum_{t=0}^{1}\sum_{x_k\in\mathcal{X}_t^{\lambda,k}}\left(\exp(-\frac{\mathrm{SNR}}{4N_t}\lambda_{\min}^2(\widetilde{\boldsymbol{H}})\cdot|x_k-\tilde{x}_k|^2)\right)\right]. \tag{13}$$

A proof of the theorem is as follows: From (11), it is obvious that, for a given channel condition and a specific constellation, $K_{\mathcal{L}}(s)$ only depends on the SINR ρ_k. Further the value $\rho_{\min}$ which equals to $\min\{\rho_k\}(k\in[1,N_t])$ dominates $K_{\mathcal{L}}(s)$. When $\hat{s}=1/2$, we have,

$$K_{\mathcal{L}}(\hat{s}) \leq \log\left[\frac{1}{m2^m}\sum_{\lambda=1}^{m}\sum_{t=0}^{1}\sum_{x_k\in\mathcal{X}_t^{\lambda,k}}\left(\exp(-\rho_{\min}|x_k-\tilde{x}_k|^2/4)\right)\right]. \tag{14}$$

Using the fact that the largest eigenvalue majorizes the largest diagonal term of a square matrix [22], from (5) we have,

$$\begin{aligned}\rho_{\min} &\geq \frac{1}{\lambda_{\max}\left((\boldsymbol{I}_{N_t}+\frac{\mathrm{SNR}}{N_t}\widetilde{\boldsymbol{H}}^{\dagger}\widetilde{\boldsymbol{H}})^{-1}\right)}-1 \\ &= \lambda_{\min}\left(\boldsymbol{I}_{N_t}+\frac{\mathrm{SNR}}{N_t}\widetilde{\boldsymbol{H}}^{\dagger}\widetilde{\boldsymbol{H}}\right)-1 \;=\; \frac{\mathrm{SNR}}{N_t}\lambda_{\min}^2\left(\widetilde{\boldsymbol{H}}\right).\end{aligned} \tag{15}$$

For a given channel $\widetilde{\boldsymbol{H}}$, it is obvious that a large value of $\lambda_{\min}\left(\widetilde{\boldsymbol{H}}\right)$ guarantees a small value of $K_{\mathcal{L}}(s)$, and thus results in a low BER. That is, for a symbol error to occur, a necessary condition is that $\lambda_{\min}$ for the scaled channel matrix falls below a certain threshold. Hence $\lambda_{\min}\left(\widetilde{\boldsymbol{H}}\right)$ has a direct impact on the system performance. Inserting (15) into (14), we obtain (13).

Thus it is reasonable and efficient to characterise the quality of the cooperative virtual-MIMO channel based on its smallest singular value squared. In practice, the nature of the short-range conference link is helpful for information exchange. Once the conference link formed, the channel CSI and the estimated value of σ_c^2 will be shared between the relay and the destination, so that $\lambda_{\min}\left(\widetilde{\boldsymbol{H}}\right)$ can be computed at the destination.

B. Adaptive Modulation Scheme

When the quantization codebook could represent the constellation accurately at the relay, $\widetilde{\boldsymbol{H}}$ will tend towards $\boldsymbol{H}$ in value [8]. Combining (13) and Table I in [21], it is obvious that for a given channel $\boldsymbol{H}$, $K_{\mathcal{L}}(\hat{s})$ for lower-order modulation is always smaller than that for higher-order modulation, which means that its conditional BER is always lower (at the cost of reduced bit rate). Thus when the channels are poorly conditioned, the system could adapt to provide reliable communications using a lower-order modulation, e.g. QPSK.

Moreover, as shown in [6], the throughput of the cooperative virtual MIMO-BICM system is calculated by considering the average mutual information (AMI) for each bit level, and then averaging the AMI over the fading channels,

$$C_{\mathrm{CF}} = mN_t - \mathop{\mathrm{E}}_{\boldsymbol{H}\in\mathcal{H}}\left[\sum_{\lambda=1}^{mN_t}\mathop{\mathrm{E}}_{c^{\lambda}|z_k,\boldsymbol{W}}\left(\log_2\frac{\sum_{\tilde{x}_k\in\mathcal{X}^k}\exp\left(-\rho_k|z_k-\tilde{x}_k|^2\right)}{\sum_{\tilde{x}_k\in\mathcal{X}_0^{\lambda,k}}\exp\left(-\rho_k|z_k-\tilde{x}_k|^2\right)}\right)\right]. \tag{16}$$

It is obvious that, when the channels are well-conditioned or the SNR is high, a higher-order modulation (with a large m) at the transmitter, e.g. 64QAM, will guarantee a higher system throughput.

Now, we present a check criterion for the adaptive modulation scheme. Specifically, we set a threshold ξ for the UB of $P_b(\boldsymbol{H})$. For different modulations (e.g. 64QAM and 16QAM), according to (6), (9) and (13), we could obtain corresponding thresholds of the smallest singular value, which are denoted by $\lambda_{64\mathrm{QAM}}$ and $\lambda_{16\mathrm{QAM}}$ as examples. The system would implement 64QAM for well-conditioned channels ($\lambda_{\min}(\boldsymbol{H})\geq\lambda_{64\mathrm{QAM}}$), and 16QAM for "in-between" channels ($\lambda_{16\mathrm{QAM}}\leq\lambda_{\min}(\boldsymbol{H})<\lambda_{64\mathrm{QAM}}$). Otherwise, for poorly conditioned channels ($\lambda_{\min}(\boldsymbol{H})<\lambda_{16\mathrm{QAM}}$), the system would switch back to QPSK modulation. Note that the adaptive modulation scheme studied here could easily be extended to multiple modulation and coding rate choices, for example, applied to High Speed Packet Access (HSPA) and Long Term Evolution (LTE) systems [23].

C. Adaptive-rate CF Scheme

When channel conditions are good and a high-order modulation is selected, vector quantization with a large C may cause a high processing burden for the relay to perform CF cooperation. Thus an adaptive-rate CF scheme is also proposed at the relay.

To facilitate the threshold design, we investigate the closed-form cumulative distribution function (CDF) of the smallest singular value. Recall the scaled channel matrix $\widetilde{\boldsymbol{H}}$ in (3), where we know that the scaled factor η is due to the compression noise σ_c^2. Since we employ the standard source coding technique to perform CF cooperation, a lower bound on the compression noise variance given in [24] could be extended to our virtual-MIMO system, i.e.,

$$\bar{\sigma}_c^2 = \frac{\mathrm{E}[|y_r|^2]}{2^C - 1} = \frac{N_0 + \frac{1}{2}|h_1|^2 + \frac{1}{2}|h_2|^2}{2^C - 1}. \tag{17}$$

If $|h_1|^2+|h_2|^2$ could be replaced by its expected value, $\bar{\eta}$ would become constant for a certain SNR and C. The scaled channel $\widetilde{\boldsymbol{H}}$ will be a complex Gaussian matrix, whose smallest singular value has been discussed in [25]. Hence it is reasonably appropriate to implement $\mathrm{E}[|h_1|^2+|h_2|^2]$ for the distribution analysis of $\lambda_{\min}$ and the corresponding threshold design. Then we have $\bar{\eta} = (2^C - 1)/(2^C + \mathrm{SNR})$, and $\widetilde{\boldsymbol{H}}$ is distributed as $\mathcal{CN}(0, \boldsymbol{I} \otimes \boldsymbol{\Psi})$. $\boldsymbol{\Psi}$ is the covariance matrix,

$$\boldsymbol{\Psi} = \mathrm{E}\left[\begin{pmatrix}\sqrt{\bar{\eta}}h_1\\ h_3\end{pmatrix}\left(\sqrt{\bar{\eta}}h_1 \quad h_3\right)\right] = \begin{bmatrix}\bar{\eta} & 0\\ 0 & 1\end{bmatrix} = \begin{bmatrix}\frac{2^C-1}{2^C+\mathrm{SNR}} & 0\\ 0 & 1\end{bmatrix}. \tag{18}$$

Thus employing the results from [25], the CDF of $\lambda_{\min}(\widetilde{\boldsymbol{H}})$ is given by,

$$F_{\lambda_{\min}}(\lambda) = 1 - \exp\left(-(1+\bar{\eta}^{-1})\lambda^2\right); \tag{19}$$

Knowledge of the closed-form CDF provides direct insight into the distribution of $\lambda_{\min}(\widetilde{\boldsymbol{H}})$. Setting a CDF threshold helps us obtain the corresponding threshold for the smallest singular values. One attractive feature of the proposed threshold approach is that, with the CDF threshold, it is readily apparent what percent of the channels are quite well-conditioned. The final average quantization rate is therefore predictable.

Take the quantization rates $C = 4$, 6 bits/s and 8 bits/s as an example. The CDF curves of $\lambda_{\min}(\widetilde{\boldsymbol{H}})$ for various values of C are shown in Fig. 2. Based on the settings of the CDF thresholds, i.e. P_{th4} and P_{th6} shown in Fig. 2, we will get λ_{th4} and λ_{th6} as the thresholds. For a given channel condition, an estimate of $\sigma_{c,4}^2$ for $C=4$ bits/s and $\sigma_{c,6}^2$ for $C=6$ bits/s could be obtained. Substituting them into (3), we get estimates of $\widetilde{\boldsymbol{H}}_4$ and $\widetilde{\boldsymbol{H}}_6$, and their smallest singular values. Switching criterion for the adaptive-rate CF scheme is shown as,

$$\begin{cases}\text{If } \lambda_{\min}(\widetilde{\boldsymbol{H}}_4) \geq \lambda_{\text{th4}} \text{ and } \lambda_{\min}(\widetilde{\boldsymbol{H}}_6) \geq \lambda_{\text{th6}}, \text{ then } C=4 \text{ bits/s};\\ \text{If } \lambda_{\min}(\widetilde{\boldsymbol{H}}_4) < \lambda_{\text{th4}} \text{ and } \lambda_{\min}(\widetilde{\boldsymbol{H}}_6) \geq \lambda_{\text{th6}}, \text{ then } C=6 \text{ bits/s};\\ \text{If } \lambda_{\min}(\widetilde{\boldsymbol{H}}_4) < \lambda_{\text{th4}} \text{ and } \lambda_{\min}(\widetilde{\boldsymbol{H}}_6) < \lambda_{\text{th6}}, \text{ then } C=8 \text{ bits/s};\end{cases} \tag{20}$$

The impact of varying the CDF thresholds will be investigated in Section V. The estimated average quantization rate is then shown as,

$$C_{ave} = 4(1 - P_{\text{th4}}) + 6(P_{\text{th4}} - P_{\text{th6}}) + 8P_{\text{th6}}. \tag{21}$$

The scheme can also be applied to multiple modulation and code rates, including high-order modulation types which require higher C values, e.g. 64QAM, as will shown in section V.

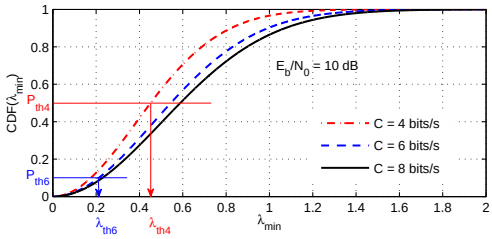

Fig. 2. CDF curves of the smallest singular value $\lambda_{\min}$ for various quantization rates, when $E_b/N_0 = 10$ dB.

With the proposed adaptive-rate CF scheme, C_{ave} is always smaller than the fixed quantization rate which is needed to obtain the ideal MIMO performance. As the encoding complexity of Voronoi VQ grows exponentially with the quantization rate [8], the proposed scheme with a small C_{ave} will reduce the complexity for quantization significantly.

Therefore, for a specific channel condition, given the thresholds, the system could adapt to choose a suitable modulation type for transmission and an appropriate C to perform CF cooperation. The scheme not only enables the system to achieve a high throughput with reliable communication, but also eliminates unnecessary complexity for quantization operations and conference link communication.

D. Practical Setup and Maintenance

In general, to support this cooperative virtual-MIMO system with an adaptive modulation and cooperation scheme, some setup and maintenance issues should be specified for practical considerations. As depicted in Fig. 3, there are several key steps:

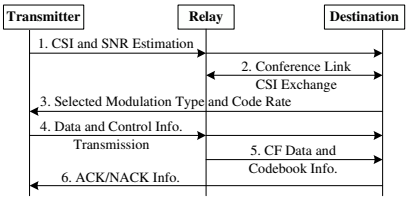

Fig. 3. Practical setup and maintenance issues for the virtual-MIMO system with the adaptive modulation and cooperation scheme. (ACK and NACK stand for acknowledgement and negative acknowledgement, respectively.)

1) CSI and SNR are estimated at the relay and destination.
2) A conference link is formed between the relay and the destination. CSI is then shared between them, i.e. $\boldsymbol{H}$ is known at both the relay and the destination.
3) An adaptive modulation scheme related computation is executed at the destination, to choose a suitable

modulation type according to the quality of $\boldsymbol{H}$ and predefined threshold ξ, and feed back the information to the transmitter.

4) The transmitter broadcasts the data symbols through two antennas simultaneously.
5) The relay implements the adaptive-rate CF scheme to decide an appropriate quantization rate C for the CF cooperation. Then the relay quantizes the received signals and transmits y'_{rnl} to the destination. Codebook information, and some control information, such as the selected value of C and the estimated value of σ^2_{cn}, is included.
6) The destination performs MMSE detection on the received signal $\boldsymbol{y}_{nl}$, with the knowledge of $\widetilde{\boldsymbol{H}}$. If errors still occur, the destination may request a retransmission from the transmitter.

V. Numerical Results

In this section, we present the error performance of our cooperative virtual-MIMO-BICM system ($N_t = N_r = 2$). At the transmitter, a 1/2-rate convolutional code with the generator polynomials $[133, 171]_{\text{octal}}$ ($d_{\text{free}} = 10$) is used for QPSK and 16QAM modulations. Further, a 2/3-rate code punctured from $[133, 171]_{\text{octal}}$ is considered for 64QAM. We assume 10^6 block Rayleigh fading channels between the transmitter and receivers, with each block having 200 consecutive symbol periods. An error-free conference link is assumed between the relay and the destination. The simulation results are computed via the Monte Carlo method.

A. BER Evaluation

The BER performance of the cooperative virtual-MIMO-BICM system with various modulations, under fixed quantization rates, is shown in Fig. 4. The conference link rates $C = 4$ bits/s for QPSK, $C = 8$ bits/s for 16QAM, and $C = 12$ bits/s for 64QAM modulation will enable the system with CF cooperation to approach the ideal MIMO performance, since the quantization codebook could represent the constellation points accurately at the relay. The BER UBs and their simplified versions based on $\rho_{\min}$ are presented as well. According to (11) and (14), the BER UB based on $\rho_{\min}$ is a little larger but follows the same trend with BER UB.

The UBs and simulation results of the system BER performance for 16QAM modulation, under various quantization rates, are presented in Fig. 5. We plot the BER against the information bit SNR, i.e E_b/N_0. A smaller quantization rate results in stronger compression noise. As shown in this figure, for smaller C, such as 4 bits/s and 6 bits/s, there exists an error floor, which means the MMSE receiver cannot remove the residual ISI because of the compression noise. Hence it is appropriate to implement the singular value-based adaptive-rate CF scheme. Since the BER performance is very well approximated by the UB based on $\rho_{\min}$ for all considered quantization rates, it is reasonable to characterise the quality of the scaled channel by using its smallest singular value.

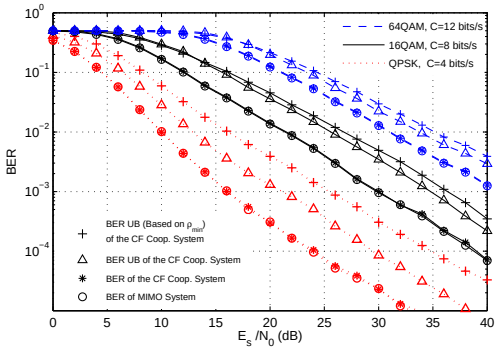

Fig. 4. Simulation results and upper bounds (UBs) on the BER performance of the 2×2 virtual-MIMO-BICM system with CF cooperation and MMSE receiver. (1/2-rate coded QPSK, 1/2-rate coded 16QAM, and 2/3-rate coded 64QAM are considered.)

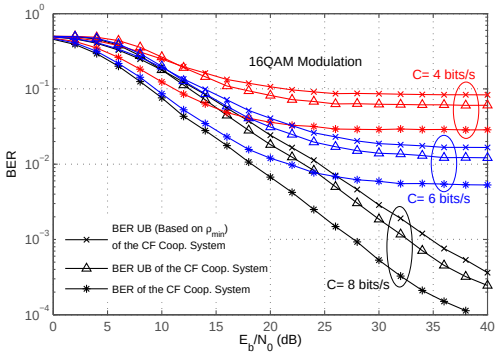

Fig. 5. Simulation results and UBs on the system BER performance for 1/2-rate coded 16QAM with various quantization rates.

B. Application of the Adaptive Modulation and Cooperation Scheme

As shown in Section IV, the switching criterion of the adaptive modulation and cooperation scheme is two levelled. Firstly, the destination should choose a suitable modulation type via comparing $\lambda_{\min}(\boldsymbol{H})$ to $\lambda_{16\text{QAM}}$ and $\lambda_{64\text{QAM}}$. Here we assume the threshold $\xi = 10^{-5}$ so that the realistic BER will be smaller than 10^{-5}. We use the value of A_d in [16] for 16QAM and [17] for 64QAM, then a threshold for $K_{\mathcal{L}}(\hat{s})$ which equals -1.1284 for 16QAM and -2.0103 for 64QAM are obtained from (6) and (9). According to (13), we finally obtain $\lambda_{16\text{QAM}} = \sqrt{10.3465 N_t/\text{SNR}}$ and $\lambda_{64\text{QAM}} = \sqrt{62.0480 N_t/\text{SNR}}$. Secondly, if 16QAM is chosen, an adaptive-rate CF cooperation scheme ($C = 4$, 6, 8 bits/s are chosen as candidates in accordance with the example in Section IV-C) will be employed. If 64QAM is selected, $C = 8$, 10, 12 bits/s will be considered.

In Fig. 6 (a), we investigate the impact of varying the thresholds on the conditional BER for 16QAM modulation, by changing the operating thresholds P_{th4} and P_{th6}. The

conditional BERs are calculated on the channels satisfying $\lambda_{\min}(\bar{\boldsymbol{H}}_4) \geq \lambda_{\text{th4}}$ and $\lambda_{\min}(\bar{\boldsymbol{H}}_6) \geq \lambda_{\text{th6}}$ respectively. As long as $P_{\text{th4}} = 0.5$ and $P_{\text{th6}} = 0.1$, the error floor is too small to impact the system performance. For 64QAM, we also simulate the conditional BERs to an error floor of roughly 10^{-5}, using $C=8$ and 10 bits/s in Fig. 6 (b). Hence $P_{\text{th4}}=0.5$, $P_{\text{th6}}=0.1$, $P_{\text{th8}}=0.3$, and $P_{\text{th10}}=0.06$ are good choices for the adaptive-rate CF scheme to achieve a favourable performance-complexity tradeoff. Then based on (19), we calculate singular value thresholds to select various values of C for the scheme.

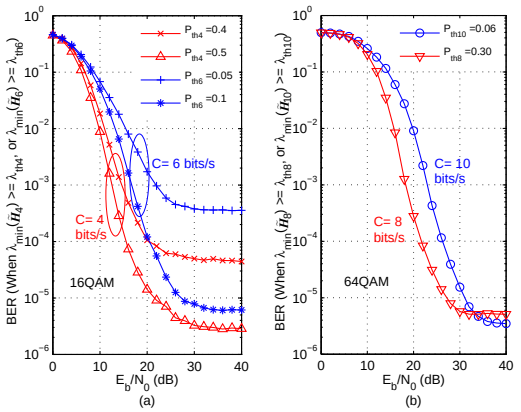

Fig. 6. The effects of varying the thresholds on the conditional BER performance. (1/2-rate coded 16QAM is considered in (a), while 2/3-rate coded 64QAM in (b).)

The simulation results of the adaptive virtual-MIMO system are presented in Fig. 7 and Fig. 8. With the adaptive modulation and cooperation scheme we proposed, the system obtains a BER performance almost the same as the MIMO system with QPSK modulation, and provides a significant improvement compared to the 64QAM case, as shown in Fig. 7. Also, at high E_b/N_0, the adaptive system throughput can approach almost MIMO-64QAM performance, i.e. reach the upper limit of 12 bits/s, as shown Fig. 8. Compared with the cases of fixed modulation and fixed-rate CF, the adaptive scheme allows the virtual-MIMO system to achieve a high throughput with reliable communication. The switching thresholds for the adaptive virtual-MIMO system have been chosen conservatively to achieve the same BER performance as for QPSK modulation, as shown in Fig. 7. A higher BER threshold for changing modulation scheme could be used to improve throughput, at the cost of higher BER and higher quantisation rates at the relay.

The probabilities of choosing different modulation types and quantization rates are shown in Fig. 9. At low E_b/N_0, QPSK is always selected to try to provide reliable communication. As the E_b/N_0 increases, 16QAM and 64QAM are chosen more frequently to obtain high throughputs, and adaptive-rate CF cooperation is implemented. When the E_b/N_0 is high, the relay uses 12 bits/s VQ for less than 6% of channel realisations (with lower $\lambda_{\min}$), and for more than 70% of the

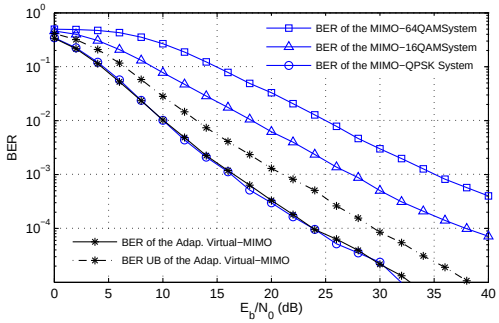

Fig. 7. BER performance of the 2×2 virtual-MIMO system with the adaptive modulation and cooperation scheme.

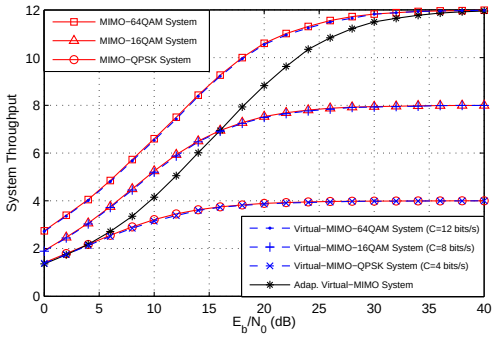

Fig. 8. Throughput of the 2×2 virtual-MIMO system with the adaptive modulation and cooperation scheme.

channels (with higher $\lambda_{\min}$), 8 bits/s VQ will be sufficient for acceptable performance. As shown in Fig. 10, the final average quantization rate is between 4 bits/s and around 8.6 bits/s, which could also be predicted from (21). Thus at low E_b/N_0, the adaptive scheme helps the system to reduce complexity for quantization operations significantly, without large performance loss compared to the 64QAM case with $C = 12$ bits/s (see Fig. 8). When the E_b/N_0 is high, the adaptive scheme is capable of eliminating more than 3 bits complexity for quantization at the relay and more than 3 bits/sample on the conference link communications relative to the $C=12$ bits/s/sample case, while still achieving almost ideal MIMO-64QAM performance.

VI. Conclusion

This paper presented a practical virtual-MIMO-BICM system with a single two-antenna wireless transmitter sending information to two closely spaced single-antenna receivers. Virtual-MIMO operation was realized via receiver-side local communication using the CF cooperation, and MMSE detection was employed at the destination. In this paper, we derived a closed form expression to upper bound the system BER. We proved that the smallest singular value of the channel matrix dominated the system error performance. Moreover, an

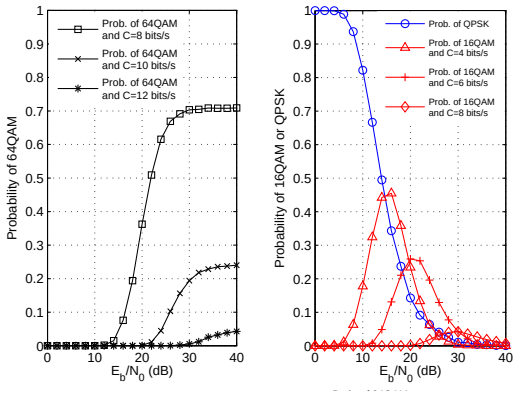

Fig. 9. Probability of choosing different modulation types and quantization rates for the adaptive virtual-MIMO system.

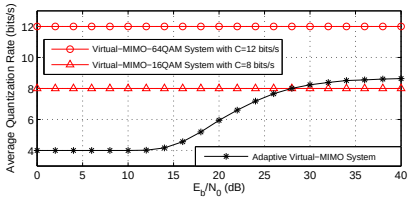

Fig. 10. Average quantization rate at the relay for the adaptive virtual-MIMO system, compared to the $C = 4, 8, 12$ bits/s cases.

adaptive modulation and cooperation scheme was proposed, adopting the smallest singular value as the threshold strategy. The closed-form CDF expression of the smallest singular value was also derived.

With the adaptive modulation and cooperation scheme, the system could adapt its modulation type to the prevailing channel conditions. The relay could also choose the minimum possible quantization rate to eliminate unnecessary complexity. We presented an illustrative example for simulation, where QPSK, 16QAM and 64QAM were chosen as the desired modulation types, and $C = 4, 6, 8, 10, 12$ bits/s were selected as the quantization rate candidates. The simulation results confirmed that, the 2×2 virtual-MIMO system was able to achieve a high throughput with reliable communication. For our illustrative example, at low E_b/N_0, the adaptive scheme helps the system to reduce complexity for quantization operations significantly, without large performance loss. When the E_b/N_0 is high, the adaptive scheme is capable of eliminating more than 3 bits complexity, while still achieving almost ideal MIMO-64QAM performance.

The illustrative example showed how to find the appropriate switching criterion and the system performance. The adaptive modulation and cooperation scheme is not limited to this example, the principles of which could easily be applied to multiple modulation types and quantization rates. The virtual-MIMO system studied here is not limited to BICM transmission neither. Other FEC coding schemes, such as Turbo coding or LDPC coding, could also be employed. By extending to a wide range of applications, the proposed system is therefore particularly valuable and attractive to some realistic wireless communication networks. The extension to more relays and more antennas is left as future work.

APPENDIX
PROOF OF EQUATION (11)

As defined in (10), averaging over λ, t, k, $x_k \in \mathcal{X}_t^{\lambda,k}$, $K_{\mathcal{L}}(s)$ is given by,

$$K_{\mathcal{L}}(s) = \log\left[\frac{1}{m2^m N_t}\sum_{\lambda=1}^{m}\sum_{t=0}^{1}\sum_{k=1}^{N_t}\sum_{x_k\in\mathcal{X}_t^{\lambda,k}}\Lambda(s,\lambda,t,k,x_k,\rho_k)\right], \tag{22}$$

with $\Lambda(s,\lambda,t,k,x_k,\rho_k) =$

$$\mathop{\mathrm{E}}_{e_k,v_k}\left[\left(\frac{\sum_{\tilde{x}_k\in\mathcal{X}_{\tilde{t}}^{\lambda,k}}\exp\left(-\rho_k|(x_k-\tilde{x}_k)+e_k+v_k|^2\right)}{\sum_{\tilde{x}_k\in\mathcal{X}_t^{\lambda,k}}\exp(-\rho_k|(x_k-\tilde{x}_k)+e_k+v_k|^2)}\right)^s\right]. \tag{23}$$

At high SNR, the ratio in (23) is dominated by a single minimum distance term in the numerator and denominator. Thus we can apply the Dominated Convergence Theorem [15] and obtain,

$$\Lambda(s,\lambda,t,k,x_k,\rho_k) = \mathop{\mathrm{E}}_{e_k,v_k}\left[\left(\frac{\exp\left(-\rho_k|(x_k-\tilde{x}_k)+e_k+v_k|^2\right)}{\exp(-\rho_k|e_k+v_k|^2)}\right)^s\right],$$

where $\tilde{x}_k \in \mathcal{X}_{\tilde{t}}^{\lambda,k}$ is the nearest neighbour to $x_k \in \mathcal{X}_t^{\lambda,k}$. Then we simplify $\Lambda(s,\lambda,t,k,x_k,\rho_k)$:

$$\begin{aligned}
&\Lambda(s,\lambda,t,k,x_k,\rho_k)\\
&= \mathop{\mathrm{E}}_{e_k,v_k}\left[\exp\left(-\rho_k\left(s|x_k-\tilde{x}_k|^2-2s\mathrm{Re}\{(x_k-\tilde{x}_k)(e_k+v_k)^*\}\right)\right)\right]\\
&= \mathop{\mathrm{E}}_{e_k,v_k}\left[\exp(-\rho_k s|x_k-\tilde{x}_k|^2)\cdot\exp(-2\rho_k s\mathrm{Re}\{(x_k-\tilde{x}_k)e_k^*\})\right.\\
&\qquad\left.\cdot\exp(\rho_k(-|v_k+s(x_k-\tilde{x}_k)|^2+s^2|x_k-\tilde{x}_k|^2+|v_k|^2))\right].
\end{aligned} \tag{24}$$

It is well known that for Gray-labeled signal constellation,

$$\sum_{\lambda=1}^{m}\sum_{t=0}^{1}\sum_{k=1}^{N_t}\sum_{x_k\in\mathcal{X}_t^{\lambda,k}}(x_k-\tilde{x}_k) = 0. \tag{25}$$

Thus we proceed to average $\Lambda(s,\lambda,t,k,x_k,\rho_k)$ over the random noise v_k and then over the residual ISI e_k. We now have,

$$\begin{aligned}
&\Lambda(s,\lambda,t,k,x_k,\rho_k)\\
&= \mathop{\mathrm{E}}_{e_k}\left[\exp(-\rho_k(s-s^2)|x_k-\tilde{x}_k|^2)\cdot\exp(-2\rho_k s\mathrm{Re}\{(x_k-\tilde{x}_k)e_k^*\})\right]\\
&= \left[\exp(-\rho_k(s-s^2)|x_k-\tilde{x}_k|^2)\right].
\end{aligned} \tag{26}$$

Substituting (26) into (22), we obtain (11).

ACKNOWLEDGMENT

We would like to thank Prof. Peter M. Grant and Dr. Xiang Wu of the University of Edinburgh for helpful comments and discussion. The authors acknowledge the support of the Scottish Funding Council for the Joint Research Institute with the Heriot-Watt University which is a part of the Edinburgh Research Partnership. Jing Jiang gratefully acknowledges the support from the UK/China Scholarships for Excellence programme in funding her PhD studies.

REFERENCES

[1] R. Dabora and S. D. Servetto, "Broadcast channels with cooperating decoders," *IEEE Trans. Inform. Theory*, vol. 52, no. 12, pp. 5438–5454, Dec. 2006.

[2] S. K. Jayaweera, "Virtual MIMO-based cooperative communication for energy-constrained wireless sensor networks," *IEEE Trans. Wireless Commun.*, vol. 5, no. 5, pp. 984–989, May 2006.

[3] Y. Liang and V. V. Veeravalli, "Cooperative relay broadcast channels," *IEEE Trans. Inform. Theory*, vol. 53, no. 3, pp. 900–928, March 2007.

[4] W. Chen, L. Dai, K. Ben Letaief, and Z. Cao, "A unified cross-layer framework for resource allocation in cooperative networks," *IEEE Trans. Wireless Commun.*, vol. 7, no. 8, pp. 3000–3012, Aug. 2008.

[5] A. Host-Madsen and J. Zhang, "Capacity bounds and power allocation for wireless relay channels," *IEEE Trans. Inform. Theory*, vol. 51, no. 6, pp. 2020–2040, June 2005.

[6] G. Caire, G. Taricco, and E. Biglieri, "Bit-interleaved coded modulation," *IEEE Trans. Inform. Theory*, vol. 44, no. 3, pp. 927–946, 1998.

[7] H. Kwon and J. M. Cioffi, "Multi-user MISO broadcast channel with user-cooperating decoder," in *IEEE VTC 2008-Fall.*, Calgary, Canada, Sept. 2008, pp. 1–5.

[8] J. Jiang, J. S. Thompson, and P. M. Grant, "Design and analysis of compress-and-forward cooperation in a virtual-MIMO detection system," in *IEEE GLOBECOM Workshop on Heterogeneous, Multi-hop, Wireless and Mobile Networks (HeterWMN)*, Miami, USA, Dec. 2010, pp. 126–130.

[9] J. Jiang, J. S. Thompson, H. Sun, and P. M. Grant, "Performance assessment of virtual-MIMO systems with compress-and-forward cooperation," Feb. 2011, submitted to IET Communications.

[10] I. B. Collings, M. R. G. Butler, and M. McKay, "Low complexity receiver design for MIMO bit-interleaved coded modulation," in *IEEE ISSSTA*, Sydney, Australia, Aug. 2004, pp. 12–16.

[11] A. Guillen I Fabregas and G. Caire, "Coded modulation in the block-fading channel: coding theorems and code construction," *IEEE Trans. Inform. Theory*, vol. 52, no. 1, pp. 91–114, Jan. 2006.

[12] C. T. K. Ng, I. Maric, A. J. Goldsmith, S. Shamai, and R. D. Yates, "Iterative and one-shot conferencing in relay channels," in *IEEE Information Theory Workshop*, Punta del Este, Uruguay, March 2006, pp. 193–197.

[13] A. Gersho and R. M. Gray, *Vector quantization and. signal compression*. Kluwer Academic Publisher, 1992.

[14] D. Seethaler, G. Matz, and F. Hlawatsch, "An efficient MMSE-based demodulator for MIMO bit-interleaved coded modulation," in *IEEE GLOBECOM '04.*, vol. 4, Dallas, Texas USA, 29 Nov. 2004, pp. 2455–2459.

[15] A. Martinez, A. Guillen I Fabregas, and G. Caire, "Error probability analysis of bit-interleaved coded modulation," *IEEE Trans. Inform. Theory*, vol. 52, no. 1, pp. 262–271, Jan. 2006.

[16] P. Frenger, P. Orten, and T. Ottosson, "Convolutional codes with optimum distance spectrum," *IEEE Commun. Lett.*, vol. 3, no. 11, pp. 317–319, Nov 1999.

[17] D. Haccoun and G. Begin, "High-rate punctured convolutional codes for Viterbi and sequential decoding," *IEEE Trans. Commun.*, vol. 37, no. 11, pp. 1113 –1125, Nov. 1989.

[18] E. Malkamaki and H. Leib, "Evaluating the performance of convolutional codes over block fading channels," *IEEE Trans. Inform. Theory*, vol. 45, no. 5, pp. 1643–1646, July 1999.

[19] P.-C. Yeh, S. A. Zummo, and W. E. Stark, "Error probability of bit-interleaved coded modulation in wireless environments," *IEEE Trans. Vehicular Technology*, vol. 55, no. 2, pp. 722–728, March 2006.

[20] A. Guillen I Fabregas, A. Martinez, and G. Caire, "Error probability of bit-interleaved coded modulation using the Gaussian approximation," in *2004 Conference on Information Sciences and Systems*, Princeton, USA, March 2004, pp. 1–4.

[21] M. R. McKay and I. B. Collings, "Error performance of MIMO-BICM with zero-forcing receivers in spatially-correlated Rayleigh channels," *IEEE Trans. Wireless Commun.*, vol. 6, no. 3, pp. 787–792, March 2007.

[22] R. Narasimhan, "Spatial multiplexing with transmit antenna and constellation selection for correlated MIMO fading channels," *IEEE Trans. on Signal Processing*, vol. 51, no. 11, pp. 2829–2838, Nov 2003.

[23] E. Dahlman, S. Parkvall, J. Skold, and P. Beming, *3G Evolution: HSPA and LTE for Mobile Broadband*, 2nd ed. Elsevier Academic Press, 2008.

[24] T. T. Kim, M. Skoglund, and G. Caire, "Quantifying the loss of compress-forward relaying without Wyner-Ziv coding," *IEEE Trans. Inform. Theory*, vol. 55, no. 4, pp. 1529–1533, April 2009.

[25] P. Dharmawansa and M. R. McKay, "Exact minimum eigenvalue distribution of a correlated complex non-central wishart matrix," in *IEEE GLOBECOM 2008*, New Orleans, USA, Nov. 2008, pp. 1–5.

Jing Jiang received the B.Eng. degree and M.Sc. degree from Harbin Institute of Technology (HIT), Heilongjiang, China, in 2005 and 2007, respectively. She is currently working toward the Ph.D. degree with the Institute for Digital Communications, School of Engineering, University of Edinburgh, Edinburgh, UK.

Her research interests include wireless and mobile communications, MIMO systems, relay and cooperation techniques, cognitive radio, and wireless sensor networks.

Dr John S. Thompson was appointed as a lecturer at what is now the School of Engineering at the University of Edinburgh in 1999. In October 2005, he was promoted to the position of reader. His research interests currently include energy efficient communications systems, antenna array techniques and multihop wireless communications. He has published over 200 papers to date including a number of invited papers, book chapters and tutorial talks, as well as co-authoring an undergraduate textbook on digital signal processing. He is overall project leader for the £1.2M EPSRC Islay project involving four Universities which investigates efficient hardware implementation of complex algorithms. He is also the external liasion for the £2M EPSRC/Mobile VCE Green Radio project, which involves a number of international communication companies. He is currently editor-in-chief of the IET Signal Processing journal and was a technical programme co-chair for the Globecom conference in Miami in December 2010.

Dr Hongjian Sun (S'07-M'11) received the B.Eng. and M.Sc. degree from Harbin Institute of Technology, China, in 2005 and 2007, respectively, and obtained the Ph.D. Degree in Electronic Engineering from the University of Edinburgh, UK, in 2010. From December 2010, he is a Postdoctoral researcher at King's College, London, UK. His research interests include cognitive radio, cooperative communication, power line communication, and smart grid.

References

[1] M. R. McKay and I. B. Collings, "Error performance of MIMO-BICM with zero-forcing receivers in spatially-correlated Rayleigh channels," *IEEE Trans. Wireless Commun.*, vol. 6, pp. 787–792, March 2007.

[2] A. Goldsmith, *Wireless Communications*. Cambridge University Press, 2005.

[3] A. J. Paulraj, D. A. Gore, R. U. Nabar, and H. Bolcskei, "An overview of MIMO communications-a key to gigabit wireless," *Proceedings of the IEEE*, vol. 92, pp. 198–218, Feb. 2004.

[4] V. Jungnickel, V. Pohl, and C. von Helmolt, "Capacity of MIMO systems with closely spaced antennas," *IEEE Commun. Lett.*, vol. 7, pp. 361–363, Aug. 2003.

[5] C. T. K. Ng, N. Jindal, A. J. Goldsmith, and U. Mitra, "Capacity gain from two-transmitter and two-receiver cooperation," *IEEE Trans. Inform. Theory*, vol. 53, pp. 3822–3827, Oct. 2007.

[6] W. Yu and J. M. Cioffi, "Sum capacity of Gaussian vector broadcast channels," *IEEE Trans. Inform. Theory*, vol. 50, pp. 1875–1892, Sept. 2004.

[7] R. Dabora and S. D. Servetto, "Broadcast channels with cooperating decoders," *IEEE Trans. Inform. Theory*, vol. 52, pp. 5438–5454, Dec. 2006.

[8] Y. Liang and V. V. Veeravalli, "Cooperative relay broadcast channels," *IEEE Trans. Inform. Theory*, vol. 53, pp. 900–928, March 2007.

[9] G. Kramer, M. Gastpar, and P. Gupta, "Cooperative strategies and capacity theorems for relay networks," *IEEE Trans. Inform. Theory*, vol. 51, pp. 3037–3063, Sept. 2005.

[10] A. Host-Madsen and J. Zhang, "Capacity bounds and power allocation for wireless relay channels," *IEEE Trans. Inform. Theory*, vol. 51, pp. 2020–2040, June 2005.

[11] J. Jiang, J. S. Thompson, H. Sun, and P. M. Grant, "Performance assessment of virtual-MIMO systems with compress-and-forward cooperation." IET Communications, submitted in Feb. 2011.

[12] J. Jiang, J. S. Thompson, and P. M. Grant, "Design and analysis of compress-and-forward cooperation in a virtual-MIMO detection system," in *IEEE GLOBECOM Workshop on Heterogeneous, Multi-hop, Wireless and Mobile Networks (HeterWMN)*, (Miami, USA), pp. 126–130, Dec. 2010.

[13] J. Jiang, J. S. Thompson, H. Sun, and P. M. Grant, "Practical analysis of codebook design and frequency offsets estimation for virtual-MIMO systems,." IEEE Trans. Vehicular Technology, submitted in April 2011.

[14] J. Jiang, J. S. Thompson, X. Wu, and P. M. Grant, "An adaptive rate compress-and-forward cooperation for virtual-MIMO systems," in *Proceedings The 2nd UK-India-IDRC International Workshop on Cognitive Wireless Systems (UKIWCWS)*, (New Delhi, India), pp. 1–5, Dec. 2010.

[15] J. Jiang, J. S. Thompson, and H. Sun, "A singular value-based adaptive modulation and cooperation scheme for virtual-MIMO systems." IEEE Trans. Vehicular Technology, to appear.

[16] D. Tse and P. Viswanath, *Fundamentals of Wireless Communication*. New York, NY, USA: Cambridge University Press, 2005.

[17] T. S. Rappaport, *Wireless Communications: Principles and Practice, 2nd Ed.* Prentice-Hall: Upper Saddle River, 2001.

[18] A. N. Akansu, P. Duhamel, X. Lin, and M. de Courville, "Orthogonal transmultiplexers in communication: a review," *IEEE Trans. on Signal Processing*, vol. 46, pp. 979–995, Apr 1998.

[19] X. Zhou, T. Lamahewa, P. Sadeghi, and S. Durrani, "Two-way training: optimal power allocation for pilot and data transmission," *IEEE Trans. Wireless Commun.*, vol. 9, pp. 564–569, Feb. 2010.

[20] M. Sharif and B. Hassibi, "On the capacity of MIMO broadcast channels with partial side information," *IEEE Trans. Information Theory*, vol. 51, pp. 506 – 522, Feb. 2005.

[21] M. Jankiraman, *Space-Time Codes and MIMO Systems*. Norwood, MA, USA: Artech House, Inc., 2004.

[22] H. Bölcskei and A. J. Paulraj, "Multiple-input multiple-output (MIMO) wireless systems," *Chapter in The Communications Handbook, 2nd edition*, pp. 90.1–90.14, 2002.

[23] S. Alamouti, "A simple transmit diversity technique for wireless communications," *IEEE Journal on Selected Areas in Communications*, vol. 16, pp. 1451–1458, Oct. 1998.

[24] V. Tarokh, H. Jafarkhani, and A. R. Calderbank, "Space-time block codes from orthogonal designs," *IEEE Trans. Inform. Theory*, vol. 45, pp. 1456–1467, Jul. 1999.

[25] L. Zheng and D. Tse, "Diversity and multiplexing: a fundamental tradeoff in multiple-antenna channels," *IEEE Trans. Inform. Theory*, vol. 49, pp. 1073–1096, May 2003.

[26] G. J. Foschini and M. J. Gans, "On limits of wireless communications in a fading environment when using multiple antennas," *Wireless Personal Communications*, vol. 6, pp. 311–335, 1998.

[27] I. E. Telatar, "Capacity of multiantenna Gaussian channels," *Euro. Trans. Commun.*, vol. 10, no. 6, pp. 585–595, 1999.

[28] A. J. Paulraj, D. A. Gore, and R. U. Nabar, *Introduction to Space-Time Wireless Communications*. Cambridge, UK: Cambridge University Press, 2003.

[29] D. Gesbert, M. Shafi, D.-S. Shiu, P. J. Smith, and A. Naguib, "From theory to practice: an overview of MIMO space-time coded wireless systems," *IEEE Journal on Selected Areas in Communications*, vol. 21, pp. 281–302, Apr 2003.

[30] F. R. Farrokhi, G. J. Foschini, and A. Lozano, "Link-optimal space-time processing with multiple transmit and receive antennas," *IEEE Communications Letters*, vol. 5, pp. 85–87, Mar. 2001.

[31] A. Nosratinia, T. E. Hunter, and A. Hedayat, "Cooperative communication in wireless networks," *IEEE Communications Magazine*, vol. 42, pp. 74 –80, Oct. 2004.

[32] A. Scaglione, D. L. Goeckel, and J. N. Laneman, "Cooperative communications in mobile ad hoc networks," *IEEE Signal Processing Magazine*, vol. 23, pp. 18–29, sept. 2006.

[33] A. Sendonaris, E. Erkip, and B. Aazhang, "User cooperation diversity. Part I. system description," *IEEE Trans. Commun.*, vol. 51, pp. 1927–1938, Nov. 2003.

[34] A. Sendonaris, E. Erkip, and B. Aazhang, "User cooperation diversity. Part II. implementation aspects and performance analysis," *IEEE Trans. Commun.*, vol. 51, pp. 1939 –1948, Nov. 2003.

[35] T. Cover and A. Gamal, "Capacity theorems for the relay channel," *IEEE Trans. Inform. Theory*, vol. 25, pp. 572–584, Sep 1979.

[36] L. Lai, K. Liu, and H. El Gamal, "The three-node wireless network: achievable rates and cooperation strategies," *IEEE Trans. Inform. Theory*, vol. 52, pp. 805–828, Mar. 2006.

[37] S. Vishwanath, N. Jindal, and A. Goldsmith, "Duality, achievable rates, and sum-rate capacity of Gaussian MIMO broadcast channels," *IEEE Trans. Information Theory*, vol. 49, pp. 2658 – 2668, Oct. 2003.

[38] R. U. Nabar, H. Bolcskei, and F. W. Kneubuhler, "Fading relay channels: performance limits and space-time signal design," *IEEE Journal on Selected Areas in Communications*, vol. 22, pp. 1099 –1109, aug. 2004.

[39] J. N. Laneman, D. N. C. Tse, and G. W. Wornell, "Cooperative diversity in wireless networks: Efficient protocols and outage behavior," *IEEE Trans. Inform. Theory*, vol. 50, pp. 3062–3080, Dec. 2004.

[40] R. U. Nabar and H. Bolcskei, "Space-time signal design for fading relay channels," in *IEEE Global Telecommunications Conference (GLOBECOM)*, vol. 4, (San Francisco, USA), pp. 1952–1956, Dec. 2003.

[41] J. N. Laneman and G. W. Wornell, "Distributed space-time-coded protocols for exploiting cooperative diversity in wireless networks," *IEEE Trans. Inform. Theory*, vol. 49, pp. 2415–2425, Oct. 2003.

[42] A. Host-Madsen, "Capacity bounds for cooperative diversity," *IEEE Trans. Inform. Theory*, vol. 52, pp. 1522–1544, April 2006.

[43] A. Wyner and J. Ziv, "The rate-distortion function for source coding with side information at the decoder," *IEEE Trans. Inform. Theory*, vol. 22, pp. 1–10, Jan 1976.

[44] J. Jiang, J. S. Thompson, P. M. Grant, and N. Goertz, "Practical compress-and-forward cooperation for the classical relay network," in *European Signal Processing Conference*, (Glasgow, Scotland), pp. 2421–2425, Aug. 2009.

[45] T. Cover and J. Thomas, *Elements of Information Theory (Second Edition)*. John Wiley and Sons, New York, 2005.

[46] A. Bletsas, A. Khisti, D. P. Reed, and A. Lippman, "A simple cooperative diversity method based on network path selection," *IEEE Journal on Selected Areas in Communications*, vol. 24, pp. 659–672, Mar. 2006.

[47] A. Bletsas, H. Shin, and M. Win, "Cooperative communications with outage-optimal opportunistic relaying," *IEEE Trans. Wireless Commun.*, vol. 6, pp. 3450–3460, Sep. 2007.

[48] N. Jindal, U. Mitra, and A. Goldsmith, "Capacity of ad-hoc networks with node cooperation," in *IEEE Int. Symp. Inform. Theory*, (Chicago, IL, USA), p. 271, Jun. 2004.

[49] H. Sato, "The capacity of the Gaussian interference channel under strong interference (Corresp.)," *IEEE Trans. Information Theory*, vol. 27, pp. 786–788, Nov 1981.

[50] C. Huppert and J. Klotz, "Required transmit power applying Tomlinson-Harashima-precoding in scalar and MIMO broadcast systems," *IEEE Trans. Commun.*, vol. 58, pp. 3011–3020, Oct. 2010.

[51] Y. Fan and J. S. Thompson, "MIMO configurations for relay channels: Theory and practice," *IEEE Trans. Wireless Commun.*, vol. 6, pp. 1774–1786, may 2007.

[52] S. Cui, A. Goldsmith, and A. Bahai, "Energy-efficiency of MIMO and cooperative MIMO techniques in sensor networks," *IEEE Journal on Selected Areas in Communications*, vol. 22, pp. 1089 –1098, Aug. 2004.

[53] S. Jayaweera, "Virtual MIMO-based cooperative communication for energy-constrained wireless sensor networks," *IEEE Trans. Wireless Commun.*, vol. 5, pp. 984–989, May 2006.

[54] P. Viswanath and D. N. C. Tse, "Sum capacity of the vector Gaussian broadcast channel and uplink-downlink duality," *IEEE Trans. Inform. Theory*, vol. 49, no. 8, pp. 1912 – 1921, 2003.

[55] G. Caire, G. Taricco, and E. Biglieri, "Bit-interleaved coded modulation," *IEEE Trans. Inform. Theory*, vol. 44, no. 3, pp. 927–946, 1998.

[56] A. Steiner, A. Sanderovich, and S. Shamai, "Broadcast cooperation strategies for two colocated users," *IEEE Trans. Inform. Theory*, vol. 53, no. 10, pp. 3394 – 3412, 2007.

[57] M. Katz and S. Shamai, "Relaying protocols for two colocated users," *IEEE Trans. Inform. Theory*, vol. 52, pp. 2329–2344, June 2006.

[58] C. T. K. Ng, I. Maric, A. J. Goldsmith, S. Shamai, and R. D. Yates, "Iterative and one-shot conferencing in relay channels," in *IEEE Information Theory Workshop*, (Punta del Este, Uruguay), pp. 193–197, March 2006.

[59] J. Lee, S. Kim, H. Suman, T. Kwon, Y. Choi, J. Shin, and A. Park, "Downlink node cooperation with node selection diversity," in *IEEE VTC 2005-Spring.*, vol. 3, (Stockholm, Sweden), pp. 1494–1498 Vol. 3, May-1 June 2005.

[60] H. Kwon and J. M. Cioffi, "Multi-user MISO broadcast channel with user-cooperating decoder," in *IEEE Vehicular Technology Conference (VTC)*, (Calgary, Canada), pp. 1–5, Sept. 2008.

[61] H. Kwon and J. M. Cioffi, "MISO broadcast channel with user-cooperation and limited feedback," in *IEEE International Symposium on Information Theory*, (Seoul, Korea), pp. 1694 – 1698, June 2009.

[62] A. Guillen I Fabregas and G. Caire, "Coded modulation in the block-fading channel: coding theorems and code construction," *IEEE Trans. Inform. Theory*, vol. 52, pp. 91–114, Jan. 2006.

[63] R. Dabora and S. D. Servetto, "On the role of estimate-and-forward with time sharing in cooperative communication," *IEEE Trans. Inform. Theory*, vol. 54, no. 10, pp. 4409 – 4431, 2008.

[64] S. C. Draper, B. J. Frey, and F. R. Kschischang, "Iterative decoding of a broadcast message," in *Proc. Allerton Conf. on Communication, Control, and Computing*, (Monticello, USA), 2003.

[65] Z. Bai, D. Yuan, and K. Kwak, "Performance evaluation of STBC based cooperative systems over slow Rayleigh fading channel," *Computer Communications*, vol. 31, pp. 4206 – 4211, November 2008.

[66] A. Gersho and R. M. Gray, *Vector Quantization and Signal Compression*. Kluwer Academic Publisher, 1992.

[67] R. M. Gray and D. L. Neuhoff, "Quantization," *IEEE Trans. Inform. Theory*, vol. 44, pp. 2325–2383, Oct 1998.

[68] M. Kuhn, J. Wagner, and A. Wittneben, "Cooperative processing for the WLAN uplink," in *IEEE WCNC*, (Las Vegas, USA), pp. 1294–1299, March 2008.

[69] E. Biglieri, R. Calderbank, A. Constantinides, A. Goldsmith, A. Paulraj, and H. V. Poor, *MIMO Wireless Communication*. Cambridge University Press, 2007.

[70] M. R. McKay and I. B. Collings, "Capacity and performance of MIMO-BICM with zero-forcing receivers," *IEEE Trans. Commun.*, vol. 53, pp. 74–83, Jan. 2005.

[71] A. Martinez, A. Guillen I Fabregas, and G. Caire, "Error probability analysis of bit-interleaved coded modulation," *IEEE Trans. Inform. Theory*, vol. 52, pp. 262–271, Jan. 2006.

[72] P. Frenger, P. Orten, and T. Ottosson, "Convolutional codes with optimum distance spectrum," *IEEE Commun. Lett.*, vol. 3, pp. 317–319, Nov 1999.

[73] E. Malkamaki and H. Leib, "Evaluating the performance of convolutional codes over block fading channels," *IEEE Trans. Inform. Theory*, vol. 45, pp. 1643–1646, July 1999.

[74] P.-C. Yeh, S. A. Zummo, and W. E. Stark, "Error probability of bit-interleaved coded modulation in wireless environments," *IEEE Trans. Vehicular Technology*, vol. 55, pp. 722–728, March 2006.

[75] A. Guillen I Fabregas, A. Martinez, and G. Caire, "Error probability of bit-interleaved coded modulation using the Gaussian approximation," in *2004 Conference on Information Sciences and Systems*, (Princeton, USA), pp. 1–4, March 2004.

[76] Y. Zhu, Y. Xin, and P.-Y. Kam, "Outage probability of Rician fading relay channels," *IEEE Trans. Vehicular Technology*, vol. 57, pp. 2648 – 2652, July 2008.

[77] W. Limpakom, Y.-D. Yao, and H. Man, "Outage probability analysis of wireless relay and cooperative networks in Rician fading channels with different K-factors," in *Proc. IEEE 69th VTC 2009-Spring*, (Barcelona, Spain), pp. 1 – 5, April 2009.

[78] K. Sayood, *Introduction to Data Compression, Third Edition (Morgan Kaufmann Series in Multimedia Information and Systems)*. San Francisco, CA, USA: Morgan Kaufmann Publishers Inc., 2005.

[79] J. Conway and N. Sloane, "Voronoi regions of lattices, second moments of polytopes, and quantization," *IEEE Trans. Inform. Theory*, vol. 28, pp. 211–226, Mar. 1982.

[80] M. Sabin and R. Gray, "Product code vector quantizers for waveform and voice coding," *IEEE Transactions on Acoustics, Speech and Signal Processing*, vol. 32, pp. 474–488, June 1984.

[81] A. Balamesh and D. Neuhoff, "A new fixed-rate quantization scheme based on arithmetic coding," in *IEEE International Symposium on Information Theory*, p. 435, Jan. 1993.

[82] N. Moayeri, "Some issues related to fixed-rate pruned tree-structured vector quantizers," *IEEE Trans. Inform. Theory*, vol. 41, pp. 1523–1531, Sep. 1995.

[83] M. Ghogho and A. Swami, "Training design for multipath channel and frequency-offset estimation in MIMO systems," *IEEE Trans. on Signal Processing*, vol. 54, pp. 3957–3965, Oct. 2006.

[84] M. A. McKeown, D. G. M. Cruickshank, I. A. B. Lindsay, J. S. Thompson, S. A. Farson, and Y. Hu, "Carrier frequency offset estimation in BLAST MIMO systems," *Electronics Letters*, vol. 39, pp. 1752–1753, Nov. 2003.

[85] Y. Sun, Z. Xiong, and X. Wang, "EM-based iterative receiver design with carrier-frequency offset estimation for MIMO OFDM systems," *IEEE Trans. on Commun.*, vol. 53, pp. 581–586, April 2005.

[86] K. Deng, Y. Tang, S. Shao, and S. Li, "Carrier frequency offset estimation for MIMO correlated fading channels," in *IEEE Wireless Communications and Networking Conference (WCNC)*, (Kowloon, Hong Kong), pp. 1035–1038, Mar. 2007.

[87] Y. Yao and G. B. Giannakis, "Blind carrier frequency offset estimation in SISO, MIMO, and multiuser OFDM systems," *IEEE Trans. on Communications*, vol. 53, pp. 173–183, Jan. 2005.

[88] J. Zhang, Y. R. Zheng, C. Xiao, and K. B. Letaief, "Channel equalization and symbol detection for single-carrier MIMO systems in the presence of multiple carrier frequency offsets," *IEEE Trans. on Vehicular Technology*, vol. 59, pp. 2021–2030, May 2010.

[89] Y.-J. Liang, J.-F. Chang, and D.-S. Shiu, "Joint carrier frequency offset estimation and signal detection in MIMO BLAST systems," *IEEE Trans. on Vehicular Technology*, vol. 58, pp. 2783–2792, July 2009.

[90] A. O. Yilmaz, "Cooperative diversity in carrier frequency offset," *IEEE Communications Letters*, vol. 11, pp. 307–309, April 2007.

[91] D. Veronesi and D. L. Goeckel, "Multiple frequency offset compensation in cooperative wireless systems," in *IEEE Global Telecommunications Conference (GLOBECOM)*, (San Francisco, CA USA), pp. 1–5, Nov. 27-Dec. 1 2006.

[92] A. Yadav, V. Tapio, M. Juntti, and J. Karjalainen, "Timing and frequency offsets compensation in relay transmission for 3GPP LTE uplink," in *IEEE International Conference on Communications (ICC)*, (Cape Town, South Africa), pp. 1–6, May 2010.

[93] J. Shanbehzadeh and P. O. Ogunbona, "On the computational complexity of the LBG and PNN algorithms," *IEEE Trans. on Image Processing*, vol. 6, pp. 614 –616, April 1997.

[94] Y.-C. Wu, Q. Chaudhari, and E. Serpedin, "Clock synchronization of wireless sensor networks," *IEEE Signal Processing Magazine*, vol. 28, pp. 124–138, Jan. 2011.

[95] M. Leng and Y.-C. Wu, "On clock synchronization algorithms for wireless sensor networks under unknown delay," *IEEE Trans. Vehicular Technology*, vol. 59, no. 1, pp. 182 –190, 2010.

[96] K.-L. Noh, Q. M. Chaudhari, E. Serpedin, and B. W. Suter, "Novel clock phase offset and skew estimation using two-way timing message exchanges for wireless sensor networks," *IEEE Trans. Commun.*, vol. 55, pp. 766–777, April 2007.

[97] "ETSI TS 125 104 V8.7.0 Technical Specification Universal Mobile Telecommunications System (UMTS); Base Station (BS) radio transmission and reception (FDD) (3GPP TS 25.104 version 8.7.0 Release 8)," July 2009.

[98] "3GPP TS 36.211 V8.5.0, Technical Specification Group Radio Access Network; Evolved Universal Terrestrial Radio Access (E-UTRA); Physical Channels and Modulation (Release 8)," Dec. 2008.

[99] R. van Nee, A. van Zelst, and G. Awater, "Maximum likelihood decoding in a space division multiplexing system," in *IEEE 51st Vehicular Technology Conference Proceedings (VTC 2000-Spring)*, vol. 1, (Tokyo, Japan), pp. 6–10, May 2000.

[100] I. B. Collings, M. R. G. Butler, and M. McKay, "Low complexity receiver design for MIMO bit-interleaved coded modulation," in *IEEE ISSSTA*, (Sydney, Australia), pp. 12–16, Aug. 2004.

[101] M. R. G. Butler and I. B. Collings, "A zero-forcing approximate log-likelihood receiver for MIMO bit-interleaved coded modulation," *IEEE Communications Letters*, vol. 8, pp. 105–107, Feb. 2004.

[102] S. Catreux, V. Erceg, D. Gesbert, and J. Heath, R. W., "Adaptive modulation and MIMO coding for broadband wireless data networks," *IEEE Communications Magazine*, vol. 40, pp. 108–115, Jun. 2002.

[103] C.-B. Chae, A. Forenza, R. W. Heath, M. McKay, and I. Collings, "Adaptive MIMO transmission techniques for broadband wireless communication systems," *IEEE Communications Magazine*, vol. 48, pp. 112–118, May 2010.

[104] Z. Zhou, B. Vucetic, M. Dohler, and Y. Li, "MIMO systems with adaptive modulation," *IEEE Trans. on Vehicular Technology*, vol. 54, no. 5, pp. 1828–1842, 2005.

[105] Z. Zhou and B. Vucetic, "Design of adaptive modulation using imperfect CSI in MIMO systems," *Electronics Letters*, vol. 40, pp. 1073–1075, Aug. 2004.

[106] U. Fernandez-Plazaola, E. Martos-Naya, J. Paris, and A. J. Goldsmith, "Adaptive modulation for MIMO systems with channel prediction errors," *IEEE Trans. Wireless Commun.*, vol. 9, pp. 2516–2527, Aug. 2010.

[107] A. Forenza, M. R. McKay, A. Pandharipande, R. W. Heath, and I. B. Collings, "Adaptive MIMO transmission for exploiting the capacity of spatially correlated channels," *IEEE Trans. Vehicular Technology*, vol. 56, no. 2, pp. 619–630, 2007.

[108] D. Seethaler, G. Matz, and F. Hlawatsch, "An efficient MMSE-based demodulator for MIMO bit-interleaved coded modulation," in *IEEE GLOBECOM '04.*, vol. 4, (Dallas, Texas USA), pp. 2455–2459, 29 Nov. 2004.

[109] D. Haccoun and G. Begin, "High-rate punctured convolutional codes for Viterbi and sequential decoding," *IEEE Trans. Commun.*, vol. 37, pp. 1113 –1125, Nov. 1989.

[110] R. Narasimhan, "Spatial multiplexing with transmit antenna and constellation selection for correlated MIMO fading channels," *IEEE Trans. on Signal Processing*, vol. 51, pp. 2829–2838, Nov 2003.

[111] E. Dahlman, S. Parkvall, J. Skold, and P. Beming, *3G Evolution: HSPA and LTE for Mobile Broadband*. Elsevier Academic Press, 2 ed., 2008.

[112] P. Dharmawansa and M. R. McKay, "Exact minimum eigenvalue distribution of a correlated complex non-central wishart matrix," in *IEEE GLOBECOM 2008*, (New Orleans, USA), pp. 1–5, Nov. 2008.